

**Development and Application of Reversed Phase Liquid
Chromatography Based Techniques for Automated
Purification of Biologically Active Ingredients from Plant
Extracts and for Characterization of Plant Extracts and
Environmental Pollutants**

Dissertation

zur Erlangung des Grades
des Doktors der Naturwissenschaften
der Naturwissenschaftlich-Technischen Fakultät III
Chemie, Pharmazie, Bio- und Werkstoffwissenschaften
der Universität des Saarlandes

von

Anis H. Mahsunah

Saarbrücken

2006

Tag des Kolloquiums: 14. März 2007

Dekan: Prof. Dr. K. Hegetschweiler

Berichtserstatter: Prof. Dr. Christian Huber

PD Dr. Frank Steiner

Danksagung

Die vorliegende Dissertation entstand am Institut für Instrumentelle Analytik und Bioanalytik der Universität des Saarlandes unter Leitung von PD Dr. Frank Steiner.

Daher bedanke ich mich herzlich bei

Herrn PD Dr. Frank Steiner für die ausgezeichnete Betreuung, für die wertvollen Diskussionen und dafür, dass er jederzeit ein offenes Ohr für meine Probleme hatte,

Herrn Univ. Prof. Dr. Christian Huber für die Stellung des Themas sowie für die finanzielle und hervorragende fachliche Unterstützung bei der Durchführung dieser Arbeit,

Herrn Prof. Dr. Dr. h. c. Heinz Engelhardt für die zahlreiche Anregungen im theoretischen Bereich,

Herrn Reiner Wintringer (Windy) für die wertvollen Gespräche und die praktischen Hilfestellungen, die mir den Laboralltag sehr erleichtert haben,

Frau Christa Göllen für die Unterstützung in bürokratischen Angelegenheiten und für die freundlichen Gespräche,

den Mitarbeitern der Werkstatt für das schnelle Beheben apparativer Probleme, und der gesamten Gruppe im Arbeitskreis für das gute Arbeitsklima, die ständige Hilfsbereitschaft und gute Zusammenarbeit. Besonderer Dank gilt Dr. Markus Martin, Manuela Hügel und Verena Fraaß für die Unterstützung in der Endphase dieser Arbeit.

Für die finanzielle und materielle Unterstützung sowie für die gute Zusammenarbeit bedanke ich mich bei der Firma Dionex Softron, vornehmlich vertreten durch Herrn Frank Arnold und Herrn Thomas Piecha.

Ganz besonders danke ich meinen Eltern, meinem Mann und meinen Kindern Ismail und Rahmah für ihre Liebe, Unterstützung und Geduld, die das Gelingen dieser Arbeit erst möglich machten.

Alles Lob und alle Dankbarkeit gebühren dem Herrn der Welten.

Table of Contents

Danksagung	ii	
Table of Contents	iii	
Summary	viii	
Zusammenfassung	xi	
 Part 1: Development and Application of Automated HPLC Purification System with Photometric and Mass spectrometric Trigger		
Chapter 1: Introduction	3	
References	5	
 Chapter 2: Instrumental Setup for Automated Purification System with Mass Spectrometric and Photometric Fraction Collection Trigger		7
2.1 Introduction	7	
2.2 Experimental	9	
2.2.1 Chemicals and Materials	9	
2.2.2 Instrumental Setups	10	
2.2.3 Determination of peak dispersion.....	11	
2.2.4 Determination of the Delay Times at Different Make-up Flows and Synchronization.....	11	
2.2.5 Determination of Fraction Purity and Compound Recovery	12	
2.2.6 Mass Spectrometric Conditions and Mass-directed Fraction Collection Settings	12	
2.3 Results and Discussion	12	
2.3.1 Setup of an Automated HPLC Purification System Using a Commercial Splitting Device	12	
2.3.1.1 Commercial Split System for Preparative Flow of 10 to 50 mL/min.....	13	
2.3.1.2 Commercial Split System with Analytical Flow of 1-10 mL/min	17	
2.3.2 Theoretical Modeling and Experimental Setup for Fast Automated Purification with Mass Spectrometric and Photometric Fraction Collection	20	
2.3.2.1 Optimization of Delay Capillary Dimensions for Minimal Dispersion	20	
2.3.2.2 Theoretical Modeling and Experimental Evaluation of Splitter Setup for Mass Directed Fraction Collection	24	

2.3.2.3	Influence of the Make-up Flow Rate on Mass Spectrometric Signal Quality	31
2.3.2.4	Synchronization for UV- and Mass Spectrometric Trigger.....	33
2.3.2.5	Evaluation of Fraction Purity and Recovery with the Optimized System	36
2.4	Conclusions.....	39
	References	40
Chapter 3: Characterization and Loadability Study of RP-HPLC Columns for Automated Purification System		43
3.1	Stationary Phase Characterization	43
3.1.1	Introduction	43
3.1.2	Experimental	44
3.1.2.1	Columns	44
3.1.2.2	Instrumental Setup	45
3.1.2.3	Conditions for the Engelhardt Test.....	45
3.1.2.4	Conditions for Standard Tests with Amitriptyline	46
3.1.3	Results and Discussion	47
3.1.3.1	Engelhardt Test.....	47
3.1.3.2	Standard Test with the Strong Base Amitriptyline	51
3.1.3.3	Variation of Conditions from the Standard Base Test Procedure	52
3.1.4	Conclusions of Stationary Phase Characterization	61
3.2	Column Loadability Study.....	63
3.2.1	Introduction	63
3.2.2	Experimental	65
3.2.2.1	Chromatographic conditions.....	65
3.2.3	Results and Discussion	66
3.2.3.1	Loading Capacity Study for Acetylsalicylic Acid	66
3.2.3.2	Loading Capacity Study for Amitriptyline.....	82
3.2.3.3	Loading Capacity Study for Phenol	95
3.2.3.4	Loading Capacity Study for Rutin.....	96
3.3	Conclusions.....	98
	References	99

Chapter 4: Application of Automated Purification System for Fractionation of Biologically Active Ingredients from Plant Extracts Applying Photometric and Targeted Mass Spectrometric Trigger.....	103
4.1 Introduction	103
4.2 Automated Fractionation of Biologically Active Ingredients from St. John's Wort Extract (<i>Hypericum perforatum</i> L.).....	103
4.2.1 Introduction and Tasks.....	103
4.2.2 Experimental	105
4.2.2.1 Chemicals and Materials	105
4.2.2.2 Instrumental setups.....	105
4.2.2.3 Conditions for Fractionation	105
4.2.3 Results and Discussion.....	108
4.2.3.1 Fractionation of St. John's Wort Extract from Accelerated Solvent Extraction (ASE)	108
4.2.3.2 Fractionation of commercial St. John's wort extract	114
4.2.4 Conclusion	120
4.3 Fractionation of degradation products from active ingredients in a transdermal delivery system drug	121
4.3.1 Introduction	121
4.3.2 Experimental	121
4.3.2.1 Chemicals and materials	121
4.3.2.2 Instrumental Setups	121
4.3.2.3 Sample preparation and conditions for HPLC separation and fractionation	121
4.3.3 Results and discussions.....	122
4.3.3.1 Optimization of the separation.....	122
4.3.3.2 Fraction collection and determination of purity and recovery	124
4.3.4 Conclusions.....	126
4.4 Fractionation of toxic gliadin from European wheat extract.....	127
4.4.1 Introduction	127
4.4.2 Experimental	127
4.4.2.1 Instrumental setup.....	127
4.4.2.2 Chemicals and materials	128
4.4.2.3 Conditions for HPLC separation and fractionation of gliadins	129

4.4.3	Results and discussion.....	129
4.4.4	Conclusion	130
4.5	Conclusions of APS applications.....	130
	References	131

Part 2: Characterization of Plant Extracts and Environmental Pollutants

Chapter 5: Characterization of St. John's Wort Extracts from Accelerated Solvent Extraction (ASE)..... 135

5.1	Introduction	135
5.2	Experimental	135
5.2.1	Instrumental Setup	135
5.2.2	Columns	136
5.2.3	Sample preparation.....	136
5.2.3.1	Extraction procedures	136
5.2.3.2	Preparation for the analysis by HPLC–UV–MS	138
5.2.3.3	Conditions for the analysis by HPLC–UV–MS.....	138
5.3	Results and discussion.....	139
5.3.1	Identification of Constituents in St. John's Wort ASE Extracts	139
5.3.2	Characterization of ASE Extraction Methods	141
5.3.3	Quantification of the extraction yields.....	146
5.3.4	Comparison of the Luna and Acclaim columns	155
5.4	Conclusions.....	156
	References	157

Chapter 6: Method Development for the Analysis and Quantification of Polycyclic Aromatic Hydrocarbons (PAHs) and Small Phenols in Road Asphalts Containing Tar..... 159

6.1	Introduction	159
6.2	Experimental	160
6.2.1	Materials and Chemicals	160
6.2.2	HPLC Apparatus and Elution Conditions.....	160
6.2.3	Procedure of Extraction by Sonication of the Raw Sample for Phenol Analysis.....	161
6.2.4	Procedure for the Sample Preparation for Phenols prior to HPLC Analysis	161

6.3	Results and Discussion	162
6.3.1	Analysis of PAHs.....	162
6.3.1.1	Development of the Gradient HPLC Method for PAH Analysis	162
6.3.1.2	PAH Detection	163
6.3.1.3	Calibration for PAH Analysis	164
6.3.1.4	Extraction Procedure for Asphalts Containing Tar	164
6.3.1.5	Sample Preparation for HPLC	166
6.3.1.6	Recovery of the Sample	167
6.3.1.7	HPLC Analysis of the Sample for PAH Content	168
6.3.1.8	Comparison of the Powder and Coarse Sample Extraction Kinetics	170
6.3.1.9	Optimization of Detection Wavelength for HPLC Analysis of PAHs	171
6.3.2	Analysis of Phenols.....	175
6.3.2.1	Development of the HPLC Method for Phenol Analysis	176
6.3.2.2	Calibration for Phenol Analysis	177
6.3.2.3	Sample Preparation for Phenols and Recovery Rate of Alkaline Aqueous Extraction from CH ₂ Cl ₂	178
6.3.2.4	HPLC Analysis for Phenol Content	181
6.3.2.5	Batch Extraction of the Raw Sample for Phenol Analysis Applying Sonication	184
6.3.2.6	Comparison of Liquid-liquid Extraction into Alkaline Aqueous Solution and SPE Clean-up of CH ₂ Cl ₂ Extracts for Sample Preparation Prior to Phenol Analysis.....	186
6.3.2.7	Phenol Analysis from Cold Batch Extraction on the Sample	187
6.4	Conclusions.....	189
	References	190
	Appendix	191

Summary

Automated preparative HPLC purification systems are an important and useful technology in pharmaceutical and chemical development. The systems have been applied to high-throughput purification of products from combinatorial compound synthesis for drug discovery, single compound isolation for further structure elucidation and activity screening, as well as fractionation of active compounds from plant extracts.

Fraction collection in automated HPLC purification system can be triggered by less selective UV detection or by highly selective mass spectrometry (MS) for target-oriented trigger or simultaneously by both detection systems. Unlike UV detection, mass spectrometry is a destructive detection technique. Therefore, a post-column split must be applied to send a small fraction of the column main flow to the mass spectrometer. A passive splitting device for an automated semi-preparative HPLC system using a column dimension of 10 mm i.d. was constructed and its design was optimized by theoretical modeling and experimental evaluation for both photometric- and mass spectrometric fraction collection trigger. The challenges in the implementation of automatic triggers are proper synchronization of peak detection and peak collection as well as minimization of band dispersion in the connection tubing between detectors and fraction collector. These could be verified with the optimized system. Both modeling and experiments using a standard mixture of parabens showed that compound transfer in the capillary connection both to fraction collector and mass spectrometer is the most critical part for the adjustment of delay time. The optimized instrumental setup was synchronized and characterized with both a microparticulate column operated at 5 mL/min and a silica-based monolithic C18-column (Monolith) of the same dimension performed at 10 mL/min for further increasing the speed of fractionation. Since the fast mode using a monolithic column can be accomplished on exactly the same instrumental setup, it represents an ideal alternative to the standard mode for high throughput purification of simple crude mixtures.

Since the cost of isolated compounds depends strongly on their loadability on the column, maximizing loading capacity is of utmost importance. It is also known that the loadability may vary widely with the nature of the compound. Therefore, volume loading capacity for acetylsalicylic acid and mass loadability for some pharmaceutically relevant compounds (acetylsalicylic acid, amitriptyline, phenol and

rutin) on some RP-HPLC columns in semi-preparative dimension (10 mm i.d.) compared to their analytical dimension (4.6 mm i.d.) was studied extensively. In order to characterize the column properties and to obtain the optimum chromatographic conditions for the loadability study, the columns were first evaluated with the Engelhardt test and with different tests using amitriptyline as representative of a strongly basic drug. The Engelhardt test revealed similar properties for Luna 5 μ m columns in both dimensions as well as for Luna and Acclaim in semi-preparative dimension. The column properties between three tested Acclaim columns were markedly different. Retention studies showed different influence on the retention of strong organic bases like amitriptyline using methanol and acetonitrile as eluent at different pH. The volume loading capacity obtained with Luna and Acclaim semi-preparative columns was similar, whilst the Monolith exhibited 66% more volume loading capacity than both packed columns. This can be attributed to the higher total porosity and thus higher column void volume of the monolithic column. The semi-preparative columns were generally more loadable (column volume normalized values) than the analytical ones, even for columns with identical properties like Luna. Mass loadability for acetylsalicylic acid on the semi-preparative Acclaim was 3.3 fold higher than on the respective analytical dimension, whilst semi-preparative Luna exhibited 2 fold loadability compared to the analytical one. Furthermore, plots of the peak shape parameters revealed unusual behavior for both Luna columns. Semi-preparative Acclaim was superior in term of peak shape and loadability for acetylsalicylic acid. The Luna semi-preparative column exhibited a 3.3-fold mass loading capacity relative to the analytical one for amitriptyline, whilst the Acclaim semi-preparative scale was 2.5-fold more loadable than the analytical column. The best results for amitriptyline mass loadability were achieved with an acetonitrile-water eluent at pH 7.0. Luna columns exhibited better performance and loadability than Acclaim columns for this compound. The loading capacity for phenol and rutin on both Luna and Acclaim semi-preparative columns was similar. However, the peak shapes obtained with the Luna were slightly better. The mass loading capacity of Monolith was generally less than the packed columns in the same dimension.

The optimized automated purification system (APS) was successfully applied to the fully automated fraction collection of pharmacologically and medically relevant components from plant extracts. The APS was utilized for fractionation of precious ingredients in St. John's wort (*Hypericum perforatum* L.) extracts, minor degradation products from active ingredients in a thermal stressed drug, and for isolation of the

toxic protein gliadin which can cause a so-called coeliac disease.

In the second part of this work, St. John's wort extracts obtained from Accelerated Solvent Extraction (ASE) applying different extraction procedures were characterized. Moreover, asphalt samples containing tar were extracted, prepared and analyzed for polycyclic aromatic hydrocarbons (PAHs) and small phenols contents.

Nine samples from dried St. John's wort plant material were extracted either by one single extraction step or several times applying a sequence of extraction methods. Accelerated solvent extraction carried out with the protocol of group extraction 4 applying four consecutive extractions using hexane, methylene chloride, ethyl acetate, and acetonitrile gave the best results. The dried ASE extracts should be re-constituted in methanol for analysis using HPLC or for fractionation applying APS.

The most of main ingredients in St. John's wort could be identified by HPLC analysis using UV and MS detectors. However, hyperforin was not found in the extracts. Comparing Acclaim and Luna analytical columns for analysis of St. John's wort extracts under identical conditions, both columns were generally comparable.

For the analysis of environmental pollutants in road asphalt samples, two individual HPLC methods with photodiode array detection and individual foregoing sample preparation procedures aligned to the demands of the present matrix were developed. The first was for the analysis of PAHs, the second for small phenols in tar asphalt samples. The extraction of PAHs and phenols were performed with CH_2Cl_2 by Soxhlet and by cold extraction. The extraction of the phenols was additionally evaluated for a triple batch extraction under sonication. The sample preparation for the analysis of PAHs pursued a cleaning up of the CH_2Cl_2 extract by liquid chromatography on silica followed by a transfer to a methanol solution to inject into reversed phase HPLC. Two individual ways of sample preparation were developed for the phenol analysis. One comprised a liquid-liquid extraction from the methylene chloride extract into alkaline aqueous solution at pH 13, the other was carried out in a similar way by liquid chromatography on silica. The developed analysis methods were applied to a coarsely and a finely milled aliquot of the sample. From the coarse sample, lower amounts of PAHs could be extracted and analyzed under the same conditions. A total content of 3500 mg PAHs/kg asphalt sample was determined in the finely milled aliquot for 4h Soxhlet extraction. The phenol analysis resulted in a total content of small phenols at approx. 17 ppm. The Soxhlet CH_2Cl_2 extraction with following alkaline aqueous extraction turned out to be the preferred way.

Zusammenfassung

Automatisierte preparative HPLC-Purification-Systeme mit UV- und/oder MS-Trigger sind eine wichtige Methodik im Bereich pharmazeutischer und chemischer Entwicklung. Das System wird bei der Hochdurchsatzfraktionierung in der kombinatorischen Synthese für die Suche nach neuen Wirkstoffen, der Einzelsubstanzisolierung für Strukturaufklärung und Aktivitäts-Screening, als auch bei der Fraktionierung von aktiven Substanzen aus Pflanzenextrakten eingesetzt.

Im Gegensatz zur UV-Detektion ist die Massenspektrometrie keine zerstörungsfreie Detektionstechnik. Deshalb muss ein Post-Column-Split implementiert werden. Ein passives Splitsystem für ein automatisiertes HPLC Purification System sowohl mit UV- als auch MS-Trigger für Säulen mit der Dimension von 10 mm i.d. wurde konstruiert, mit Hilfe eines mathematischen Modells optimiert und experimentell evaluiert. Die Herausforderungen bei der Implementierung von automatischem Trigger sind Synchronisierung zwischen Peakdetektion und -fraktionierung sowie Minimierung der Bandenverbreiterung in den Verbindungskapillaren zwischen Detektor und Fraktionssammler. Diese konnten mit dem optimierten System verifiziert werden. Theoretische Modellierung und experimentelle Versuche mit einer Standardmischung von Parabenen zeigten, dass der Zonentransport zum Fraktionssammler und zum Massenspektrometer die wichtigsten Parameter bei der Einstellung der Delayzeit sind. Das optimierte System wurde mittels einer mit 5 μm Material gepackten Säule mit Flussrate 5 mL/min sowie einer Monolith-Säule bei gleicher Dimension mit Flussrate 10 mL/min synchronisiert und charakterisiert. Da die Erhöhung der Fraktionierungsgeschwindigkeit mit einer Monolith-Säule bei gleichem Instrumenten-Setup erreicht wird, kann es als eine ideale Alternative zu einer Standardmethode für Hochdurchsatzreinigung von einfachen Substanzgemischen eingesetzt werden.

Die mit der Isolierung von Substanzen verbundenen Kosten sind stark abhängig von der Beladbarkeit der Säule. Deshalb ist die Maximierung der Beladbarkeit der Säule von großer Bedeutung. Zudem ist bekannt, dass die Beladbarkeit von der chemischen Natur der Proben abhängig ist. Aus diesem Grund wurden Volumenbeladbarkeit für Acetylsalicylsäure und Massenbeladbarkeit für einige Pharmazeutika auf verschiedene RP-HPLC-Säulen in semi-preparativer Dimension (10 mm i.d.) verglichen mit der analytischen Dimension (4,6 mm i.d.) umfassend untersucht. Die Säulen wurden zunächst mit dem Engelhardt-Test und mit

verschiedenen Test-Methoden unter Einbeziehung einer starken Base (Amitriptylin) untersucht, um die Säuleneigenschaften zu charakterisieren und um die optimalen chromatographischen Bedingungen für die Beladbarkeitsstudie zu erhalten.

Der Engelhardt-Test zeigte ähnliche Eigenschaften für 5 µm Luna-Säulen in beiden Dimensionen sowie für die semi-preparativen Luna- und Acclaim-Säulen. Die Eigenschaften der drei Acclaim-Säulen waren allerdings sehr unterschiedlich. Retentionstudien zeigten verschiedene Einflüsse von Methanol und Acetonitril als Eluenten bei unterschiedlichen pH-Werten auf der Retention der starken Basen wie Amitriptylin.

Semi-preparative Luna und Acclaim Säulen besitzen gleiche Volumenbeladbarkeit, während die Volumenbeladbarkeit auf der Monolith-Säule 66% höher als auf die beiden gepackten Säulen ist. Dies kann durch höhere Totalporosität und somit höheres Durchflussvolumen der Monolith-Säule erklärt werden. Semi-preparative Säulen waren im Allgemeinen mehr beladbar als die analytischen, auch für Säulen mit gleichen Eigenschaften wie Luna. Die Massenbeladbarkeit für Acetylsalicylsäure auf die semi-preparative Acclaim war um einen Faktor 3,3 höher als auf der analytischen Säule, während die semi-preparative Luna nur 2-fach mehr beladbar (normiert auf Säulenvolumina) war als die analytische. Weiterhin waren die Plots der Peakparameter bei Luna-Säulen ungewöhnlich. Die besten Ergebnisse für die Massenbeladbarkeit von Amitriptylin wurden mit Acetonitril-Wasser-Eluent bei pH 7 erreicht. Die Luna-Säulen zeigten bessere Performance und Beladbarkeit für diese Probe als die Acclaim-Säulen. Die semi-preparative Luna war um Faktor 3,3 mehr beladbar als die analytische, während die Beladbarkeit auf der semi-preparativen Acclaim Säule 2,5-fach höher war als für die analytische. Die semi-preparativen Luna- und Acclaim-Säulen zeigten ähnliche Beladbarkeit für Phenol und Rutin. Allerdings zeigte die Luna-Säule bessere Peakform für diese Proben. Die Massenbeladbarkeit auf der Monolith-Säule war im Allgemeinen geringer als auf den gepackten Säulen gleicher Dimension.

Das optimierte Automatisierte Purification System (APS) konnte erfolgreich für vollautomatische Fraktionierung von pharmakologisch und medizinisch relevanten Inhaltsstoffen aus Pflanzenextrakten angewandt werden. Das APS wurde für Fraktionierung wertvoller Inhaltsstoffe in Johanniskraut-Extrakten (*Hypericum perforatum* L.), zur Isolierung von Abbauprodukten aus aktiven Inhaltsstoffen in einem pharmazeutischen Präparat und für die Isolierung des toxischen Proteins

Gliadine, die eine so genannte Zöliakie-Krankheit verursachen kann, eingesetzt.

Der zweite Teil dieser Arbeit beschreibt die Charakterisierung von durch Accelerated Solvent Extraction (ASE) erhaltenen Johanniskraut-Extrakten sowie die Bestimmung von polyzyklischen aromatischen Kohlenwasserstoffen (PAKs) und Phenolen in teerhaltigem Straßenasphalt.

Neun Proben von getrocknetem Johanniskraut-Pflanzenmaterial wurde entweder in einem Schritt oder in mehreren Schritten in einer Sequenz von Extraktionsmethoden extrahiert. Die ASE-Extraktion mit vier aufeinander folgenden Extraktionsschritten mit den Solventien Hexan, Dichlormethan, Ethylacetat und Acetonitril, ergab die beste Ausbeute. Die getrockneten ASE-Extrakte sollten für die weitere Analyse mittels HPLC oder für Fraktionierung mittels APS in Methanol überführt werden.

Die meisten Hauptinhaltsstoffe in Johanniskraut konnten mittels HPLC-UV-MS identifiziert werden. Hyperforin konnte jedoch nicht bestimmt werden. Vergleich man die zwei für die Analytik benutzten analytischen Säulen Luna und Acclaim, waren die beiden unter gleichen chromatographischen Bedingungen vergleichbar.

Zwei individuelle HPLC-Methoden und vorhergehende Prozeduren für die Probenvorbereitung von sehr komplexer Asphalt-Matrix wurden für die Bestimmung von PAKs und Phenolen entwickelt. Die Extraktion wurde in Dichlormethan mit zwei verschiedenen Methoden durchgeführt, der Soxhlet-Extraktion und der Kaltextraktion, und zusätzlich für Phenol einer Ultraschallextraktion. Für die anschließende PAK-Analyse wurde die Probe auf einer kleinen Kieselgelsäule mit Dichlormethan als Elutionsmittel chromatographisch aufgereinigt und in ein RP-HPLC-kompatibles Lösemittel (Methanol) überführt. Zwei individuelle Probenvorbereitungs-Methoden wurden für die Phenol-Analyse entwickelt. Eine war die Flüssig-Flüssig-Extraktion des Dichlormethanextraktes in eine alkalische wässrige Lösung bei pH 13, die andere war die chromatographische Aufreinigung entsprechend der Probenvorbereitung für die PAKs. Mit den entwickelten Analysemethoden wurden grob und fein gemahlene Proben untersucht. Die grob gemahlene Probe ergab einen geringeren Gehalt an PAKs. Eine Gesamtbelastung von ca. 3500 mg PAKs/kg Asphalt wurde in fein gemahlener Probe nach 4-stündiger Soxhlet-Extraktion ermittelt. Die Phenolanalyse zeigte eine Gesamtbelastung durch kleine Phenole von nur ca. 17 mg/kg. Soxhlet-Extraktion mit anschließender alkalischer Flüssig-Flüssig-Extraktion erwies sich als die beste Methode.

PART 1:

**Development and Application of Automated
HPLC Purification System with Photometric
and Mass Spectrometric Trigger**

Chapter 1

Introduction

Both pharmaceutical and biotechnological industries have raised the demand for the development of novel, faster, and more efficient ways to discover and isolate pharmacologically active compounds [1]. The purification of natural and synthetic compounds by fully automated preparative HPLC using gradient elution and real-time, data-dependent fractionation triggering is becoming an increasingly important and useful technology in chemical and pharmaceutical development [2-6]. Typical applications include the high-throughput purification of products from combinatorial syntheses [7-13] or even manual single compound synthesis [4] for further structure elucidation and activity screening, as well as the fractionation of extracts of active ingredients from medicinal plants [14].

A variety of instrumental solutions, which are in many cases equipped with dedicated software control, is commercially available and frequently termed "*automated purification system*" (APS). The most commonly employed chromatographic modes include normal-phase- [4], reversed-phase- [6,7], or supercritical-fluid chromatography [3]. The elution of the separated components may be monitored by a photometric detector and, alternatively or additionally, by a mass spectrometer, usually interfaced by means of an electrospray- or atmospheric pressure chemical ionization interface. Unattended fraction collection based on real-time photometric [4] or mass-selective triggering [2] has considerably increased the productivity of preparative fractionation, facilitating full automation of the process of compound separation and targeted fraction collection. High-speed and throughput are realized by means of a combination of automation [2], parallelization [5,15], and rapid separations in short columns packed with small particles (sub-2- μm particles) [16,17]. The latter approach is, however, frequently compromised by the pressure limitations of several preparative HPLC pumping systems. The common solution is either the use of short columns packed with larger, 5-10 μm particles at the cost of lower column efficiency [12] or of highly permeable monolithic columns that provide high efficiency at fast linear velocities and very moderate column back pressures [18].

In this work, an automated HPLC purification system applying both photometric and mass spectrometric fraction collection trigger in semi-preparative dimension using 10 mm i.d. columns was implemented and optimized. The system was optimized by

theoretical modeling and evaluated with a packed microparticulate 5 μm C18 column. Moreover, a prototype silica-based monolithic column of the same dimensions was utilized to investigate the performance of the setup under high-throughput conditions. Particular focus was laid on minimized peak dispersion and compatibility with a range of flow rates from 5 to 10 mL/min.

In APS applications, a certain amount of purified compounds is desired. The cost of preparing this quantity depends strongly on the loadability of the compound on the column. Therefore, maximizing loadability is of utmost importance in preparative chromatography, since both the cost of the equipment and the operation increase with the size of the column. However, it is also known that the column loadability may vary widely with the nature of the compound [19]. For this reason, different types of column loading capacity were studied for an acidic pharmaceutical compound (acetyl salicylic acid) on a set of RP-HPLC columns in a semi-preparative dimension and in an analytical dimension as comparison. Furthermore, mass loadability for a strongly basic drug (amitriptyline) on the same columns was extensively studied. In order to compare the loading capacity of the columns for different solutes, the loadability of a polar weakly acidic compound phenol and a neutral compound rutin was also investigated. In order to characterize the column properties, the freshly purchased unused columns were characterized prior to the loadability studies. The characterization of different column properties was performed using the Engelhardt test. Because of higher silanol activity obtained with some RP-columns, and in order to find the optimum chromatographic conditions for the loadability study, an extensive study using different mobile phases for a strongly basic probe compound (amitriptyline) was carried out.

The optimized APS utilizing both photometric- and mass spectrometric trigger was applied to fractionation of pharmacologically and medicinally relevant compounds from plant extracts. The fractionation of precious compounds in St. John's wort (*Hypericum perforatum* L.) extracts by UV and MS trigger is described in detail. Moreover, fractionation of degradation products from 2 active ingredients in a thermal stressed pharmaceutical formulation was performed for structural elucidation by NMR spectroscopy. Furthermore, fraction collection of toxic gliadin from wheat extract was carried out.

References

- [1] Ripka, W.C., Barker, G. and Krakover, J. (2001) High-throughput purification of compound libraries. *Drug Discov. Today*, **6**, 471-477.
- [2] Zeng, L., Wang, X., Wang, T. and Kassel, D.B. (1998) New developments in automated PrepLCMS extends the robustness and utility of the method for compound library analysis and purification. *Comb. Chem. High Throughput Screen.*, **1**, 101-111.
- [3] Wang, T., Barber, M., Hardt, I., and Kassel, D.B. (2001) Mass-directed fractionation and isolation of pharmaceutical compounds by packed-column supercritical fluid chromatography/mass spectrometry. *Rapid Commun. Mass Spectrom.*, **15**, 2067-2075.
- [4] Renold, P., Madero, E., and Maetzke, T. (2001) Automated normal-phase preparative high-performance liquid chromatography as a substitute for flash chromatography in the synthetic research laboratory. *J. Chromatogr. A*, **908**, 143-148.
- [5] Fang, L., Cournoyer, J., Demee, M., Zhao, J., Tokushige, D. and Yan, B. (2002) High-throughput liquid chromatography ultraviolet/mass spectrometric analysis of combinatorial libraries using an eight-channel multiplexed electrospray time-of-light mass spectrometer. *Rapid Commun. Mass Spectrom.*, **16**, 1440.
- [6] Goetzinger, W., Zhang, X., Bi, G., Towle, M., Cherrak, D. and Kyranos, J.N. (2004) High-throughput HPLC/MS purification in support of drug discovery. *Jnt. J. Mass Spectrom.*, **238**, 153.
- [7] Zeng, L., Burton, L., Yung, K., Shushan, B., and Kassel, D.B. (1998) Automated analytical/preparative HPLC/MS system for the rapid characterization and purification of compound libraries. *J Chromatogr. A*, **794**, 3-13.
- [8] Zeng, L. and Kassel, D.B. (1998) Developments of a Fully Automated Parallel HPLC/Mass Spectrometry System for the Analytical Characterization and Preparative Purification of Combinatorial Libraries. *Anal. Chem.*, **20**, 4380-4388.
- [9] Edwards, C. and Hunter, D.J. (2003) High-throughput purification of combinatorial arrays. *J. Comb. Chem.*, **5**, 61-66.
- [10] Kyranos, J.N., Cai, H., Zhang, B., and Goetzinger, W.K. (2001) High-throughput high-performance liquid chromatography/mass spectrometry for modern drug discovery . *Curr. Opin. Biotechnol.*, **12**, 105-111.
- [11] Isbell, J., Xu, R., Cai, Z., and Kassel, D.B. (2002) Realities of high-throughput LC/MS purification of large combinatorial libraries: a report on overall sample throughput using parallel purification. *J. Comb. Chem.*, **4**, 600-611.

- [12] Bauser, M. (2002) Preparative HPLC-MS for the high-throughput purification of combinatorial libraries. *J. Chrom. Sci.*, **40**, 292-296.
- [13] Searle, P.A. and Hochlowski, J.E. (2004) Comparison of preparative HPLC/MS and preparative SFC techniques for the high-throughput purification of compound library. *J. Comb. Chem.*, **6**, 175-180.
- [14] Wolfender, J.L., Terreaux, C. and Hostettmann, K. (1999) The important of LC-MS and LC-NMR in the discovery of new lead compounds from plants. *Pharm. Biol.*, **38**, Suppl. 1, 41-54.
- [15] Edwards, C., Liu, J., Smith, T.J., Brooke, D., Hunter, D.J., Organ, A. and Coffey, P. (2003) Parallel preparative high-performance liquid chromatography with on-line molecular mass characterization. *Rapid Commun. Mass Spectrom.*, **17**, 2027.
- [16] Heinig, K. and Henion, J. (1999) Fast liquid chromatographic-mass spectrometric determination of pharmaceutical compounds. *J. Chromatogr. B*, **732**, 445.
- [17] Leroy, F., Presle, B., Verillon F. and Verette, E. (2001) Fast generic gradient Reversed-Phase High Performance Liquid Chromatography using short narrow-bore columns packed with small nonporous silica particles for the analysis of combinatorial libraries. *J. Chromatogr. Sci.*, **39**, 487-490.
- [18] Svec, F. and Huber, C.G. (2006) Monolithic materials: Promises, challenges, achievements. *Anal. Chem.*, **78**, 2101-2107.
- [19] Neue, U.D., Wheat, Th.E., Mazzeo, J.R., Mazza, C.B., Cavanaugh, J.Y., Xia, F. and Diehl, M. (2004) Differences in preparative loadability between the charged and uncharged forms of ionizable compounds. *J. Chromatogr. A*, **1030**, 123-134.

Chapter 2

Instrumental Setup for Automated Purification System with Mass Spectrometric and Photometric Fraction Collection Trigger

2.1 Introduction

Automated HPLC purification is a method of choice for the fractionation of high purity single compounds from a mixture running a single chromatographic separation. The important applications of the system are high-throughput purification of compounds from combinatorial chemistry [1-7], and fractionation of the impurities or degradation products from parent compounds [8,9]. A sufficient quantity of the fractions is necessary for further identification of their chemical structure or for toxicity tests [8].

Formerly, the automated HPLC purification system was triggered by less selective UV detection [10]. Consequently, every UV-active compound with UV intensity above a certain threshold was collected [11]. This is regarded as an advantage if every fraction is considered to be a target. However, this turns into a problem when only one fraction is desired, such as in combinatorial chemistry [6]. The advantages of UV-based systems are its ruggedness, low price, optimal signal-to-noise ratio and easy handling [6].

Since the implementation of mass spectrometry (MS) for target-oriented fraction trigger, it is gaining recognition [2]. The main advantage is that only the desired target molecule will be collected. This results in advantages, such as online identification, easy-to-handle logistics, and less demand on fraction collector capacity [11]. Because the splitting and the nature of the MS detector, peak broadening is sometimes observed [6]. This can lead to impure samples especially when fast chromatography is applied. The principle of UV-based and MS-based fraction collection is shown in Figure 2.1.

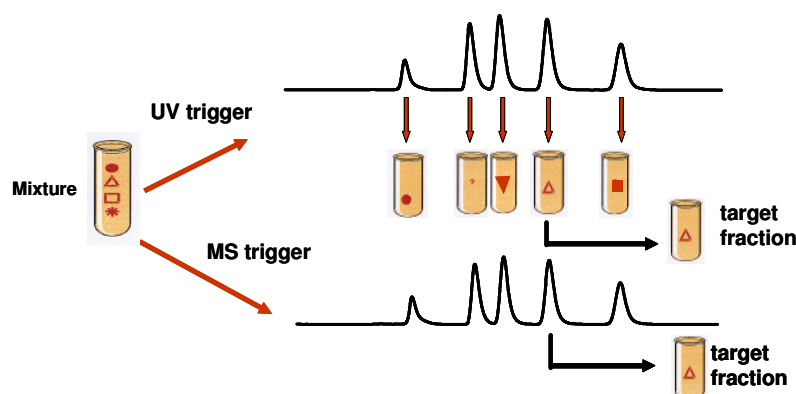


Figure 2.1: Principle of photometric and mass-based fractionation

General issues in the implementation of automatic triggers for fractionation are proper synchronization of peak detection and peak collection as well as minimization of band dispersion in the connecting tubing between detector(s) and fraction collector. Since mass spectrometry (MS) is a destructive detection technique, a selective mass spectrometric fraction collection trigger requires splitting of the column effluent between mass spectrometer and fraction collector. Moreover, ion sources are easily fouled by large amounts of analyte, necessitating a substantial reduction and dilution of the column effluent flow to the mass spectrometer. In passive splitting devices, the flows of column effluent to the fraction collector and mass spectrometer, respectively, are regulated by the permeabilities of suitably dimensioned flow restrictors [12]. A supplementary Tee-piece may be implemented into the stream flowing to the mass spectrometer to accommodate the addition of make-up flow for dilution and to speed up the analyte zone. This configuration results in two parallel liquid paths flowing from column outlet to fraction collector and from make-up pump to mass spectrometer. Both flows are interconnected by means of the two Tee-pieces, allowing the transfer of solution from one flow to the other (see Figure 2.8). Active splitters on the other hand, based upon a rapidly switched valve that transfers a small portion of the column effluent to a second flow of solvent directed to the mass spectrometer, have been shown to offer high flexibility and a broad range of splitting ratios independently of column permeability. Both active and passive splitting devices have been successfully incorporated into instrumental setups for mass-triggered fractionation [6,11,13,14]. A comparison of active and passive splitters for preparative HPLC has shown that active splitting devices (also called mass rate attenuators) offer minimal peak broadening and easy adaptation to a broad range of flow rates, split

ratios, and make-up flows [15]. Nevertheless, due to abrasion of the rapidly moving parts, rotor seals have to be exchanged on a regular basis. Moreover, peak profiles need to be smoothed by suitable averaging because of the discontinuous transfer of liquid between the donor and acceptor stream [15]. Passive splitters, on the other hand, are more difficult to optimize but hold the advantage of zero maintenance apart from the clogging risk and continuous transfer of liquid from one effluent stream to the other.

Optimization of the split ratios, the time delays between the analytes passing the detector(s) and fraction collector, and the tubing dimensions in passive splitting devices is considerably complex on an empirical basis. A review of the current literature on automatic purification systems reveals that detailed descriptions of the setup of passive splitting devices and synchronization have not yet been published. Although the optimal settings are usually pre-installed from the factory, changes in column dimensions and/or flow rates may require modification of preset parameters. In this chapter, the set-up and characterization of automated HPLC purification systems with commercial passive splitters are reported. Because the tested commercially available splitters could not satisfy the requirements for high speed purification using flow rates typical for 10 mm i.d. columns, a passive splitting device was constructed and its design was optimized by theoretical modeling and step by step experimental evaluation for both photometric- and mass spectrometric fraction collection trigger.

The system is evaluated with 100 x 10 mm i.d. columns packed with a microparticulate 5 μm octadecyl-stationary phase. Moreover, a prototype octadecylated silica-monolith of the same dimensions was utilized for the first time in a semi-preparative setup to investigate the performance of the setup under high-throughput conditions. Particular focus was laid on minimized peak dispersion and compatibility with a range of flow rates from 5 to 10 mL/min.

2.2 Experimental

2.2.1 Chemicals and Materials

All reagents used were of analytical grade. Methyl paraben, ethyl paraben, propyl paraben and butyl paraben were purchased from Fluka (Buchs, Switzerland), uracil

from Serva (Heidelberg, Germany), acetonitrile from Sigma-Aldrich (Steinheim, Germany). High-purity water was obtained from a Purelab Ultra system (ELGA, Celle, Germany). Preparative HPLC separations were performed either in a Luna C18(2) microparticulate column (100 Å, 5 µm, 100 x 10 mm i.d., Phenomenex, Torrance, CA, column #1), a prototype microparticulate column (120 Å, 5 µm, 100 x 10 mm i.d., Dionex, Sunnyvale, USA, column #2) or a silica-based, C18-derivatized monolithic research column (100 x 10 mm i.d., Merck, Darmstadt, Germany, column #3). Analytical HPLC separations were carried out on a Luna C18(2) column (100 Å, 5 µm column 150 x 4.6 mm i.d., Phenomenex).

2.2.2 Instrumental Setups

Preparative HPLC-UV-MS separations and fractionations were performed using a preparative HPLC system (Dionex Summit, Dionex, Germering, Germany) consisting of a binary semi-preparative high-pressure gradient pump (Model P680P HPG-2), a helium degassing unit, a semi-preparative autosampler (Model ASI-100P), a diode array detector (Model UVD340U PDA) with a semi-preparative detector cell (6 µl cell volume, 2 mm path length), a quadrupole mass spectrometer with an electrospray interface (Model MSQ), a high-pressure pump for delivering make-up flow (Model AXP-MS), and a fraction collector holding 7 mL tubes (Model Foxy Jr., Isco, Los Angeles, CA, USA). The fraction collector features a switching valve, which can be set to either direct the column effluent to an array of 144 sampling tubes or to a waste reservoir. The splitting system used for fractionation applying mass spectrometry was either a commercial splitting device (Accurate 1/1000, LCPackings, Amsterdam) or a home-made splitting system.

The home-made splitting system was assembled from Tee-pieces and capillary tubing from Valco (Houston, TX) or Upchurch (Oak Harbor, WA) and polyimide-coated fused silica capillaries of different inner diameters (Polymicro Technologies, Phoenix, AZ). The system was fully controlled through the Chromeleon Chromatography Management System (version 6.6, SP2, Dionex). Figure 2.8 shows a schematic of the set-up of the purification system incorporating the home-made splitting assembly. The dimensions of the capillaries were as follows: capillary 1 (PTFE) 10,000 x 0.50 mm i.d., capillary 2 (fused silica) 400 x 0.05 mm i.d., capillary 3 (PEEK) 300 x 0.13 mm i.d.

Analytical HPLC separations were performed on a system comprising a binary analytical high-pressure gradient pump (Model Summit P680A HPG-2, Dionex), a degassing unit (Model Degasys DG-1210, Dionex), an analytical auto-sampler with integrated temperature control (Model Summit ASI-100T, Dionex), and a dual wavelength UV detector (Model 2487, Waters, Milford, MA). The analytical system was also fully controlled by Chromeleon software.

2.2.3 Determination of peak dispersion

Peak dispersion was determined by analyzing a solution of four parabens (methyl-, ethyl-, propyl-, and butylparaben) or three parabens (methyl-, propyl-, and butylparaben) 100 mg/L each dissolved in mobile phase, using column #1 or column #2. Elution was accomplished with acetonitrile-water (60/40, v/v) at a flow rate of 5 mLmin⁻¹. The injection volume was 100 µL and the detection wavelength was 254 nm. In order to keep the volumes constant when the detector was installed at the end of the delay capillaries, a dummy detection cell was mounted in place of the original detector position. The peak widths at half height were calculated by Chromeleon.

2.2.4 Determination of the Delay Times at Different Make-up Flows and Synchronization

The delay times at different make-up flows were determined by injecting 100 µL of a solution containing methyl-, propyl-, and butylparaben, 1 g/L each, dissolved in mobile phase using column #2. Mobile phase and make-up solvent were water/acetonitrile (40/60 v/v). MS conditions are given in section 2.2.6.

The system was characterized and synchronized by injection of 50 µL of a solution containing methyl-, propyl-, and butylparaben, 1 g/L each. The mobile phase and make-up solvent were water/acetonitrile (40/60 v/v) for the microparticulate column (column #1) and water/acetonitrile (50/50 v/v) for the monolithic column (column #3). The flow rates through the columns were 5 mL/min for column #1 and 10 mL/min for the column #3. The make-up flow was 200 µL/min in both cases. UV-detection was performed at 254 nm, and MS conditions are given in section 2.2.6.

2.2.5 Determination of Fraction Purity and Compound Recovery

The recovery was evaluated by injecting a solution containing methyl-, propyl-, and butylparaben, 1 g/L each dissolved in mobile phase, onto the 10 mm i.d. columns (#1 and #3). The injection volume was 50 μ L and the mixture was separated under the chromatographic conditions given in section 2.2.4. Fractions were automatically collected and subsequently diluted to 5.00 mL with eluent. A second 100 μ L-aliquot of the original paraben solution was diluted to 5.00 mL as well. Aliquots of 10 μ L of both solutions were analyzed on the analytical HPLC-UV system at a flow rate of 2 mL/min with an eluent comprising acetonitrile-water (60/40, v/v). The ratio of areas from these two analyses was utilized to calculate the recovery of parabens from the 10 mm i.d. columns during automated fractionation.

2.2.6 Mass Spectrometric Conditions and Mass-directed Fraction Collection Settings

The electrospray source was operated at 3 kV needle voltage and 300 $^{\circ}$ C probe temperature. The cone voltage was -50 V (negative mode). Full scan acquisition between m/z 100-250 with a scan time of 0.5 sec was performed. Mass traces were on-line extracted for m/z 151 \pm 0.5 (methylparaben), 179 \pm 0.5 (propylparaben), and 193 \pm 0.5 (butylparaben) and used as data for peak detection and automated triggering. The threshold settings for the fraction collection were 20,000 counts for column #1 and 35,000 for column #3.

2.3 Results and Discussion

2.3.1 Setup of an Automated HPLC Purification System Using a Commercial Splitting Device

The set-up of the semi-prep purification system with MS triggered fraction collection using a commercial splitting device Accurate 1/1000 from LCPackings (Amsterdam) is shown in Figure 2.2.

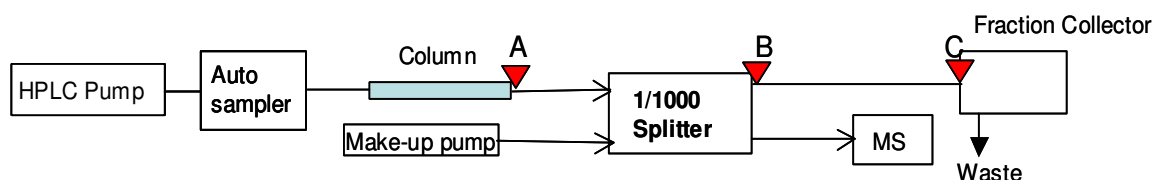


Figure 2.2: Scheme of purification system with commercial splitter

The LCPackings 1/1000 Accurate Split configuration comprises two T-connections T1 and T2 (Figure 2.3). The split-T-connection T1 receives the HPLC flow from the column and divides it into the two exit lines. The main flow exits along the delay tubing into the fraction collector (or waste), depending on the position of the fraction collector valve. The split flow transfers a minor aliquot from the main stream to the MS detector for mass selective trigger of fraction collection. A second T-connection (T2) is used to incorporate a make-up flow of an MS-friendly solution into the split flow in order to dilute the concentrated bands from the prep column, to speed up the transfer of the peak to the MS detector and to deliver an appropriate flow to the MS source to generate a stable pneumatically assisted electrospray.

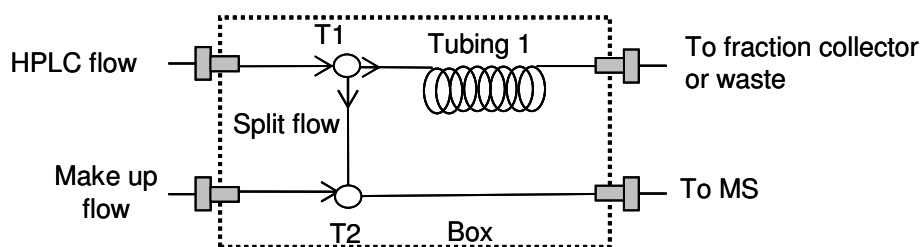


Figure 2.3: Schematic diagram of the commercial splitter (LCPackings 1/1000 Accurate).

In order to select the suitable splitting device for the automated purification system, two commercially available splitters for two different column flow ranges (1-10 mL/min and 10-50 mL/min) were investigated.

2.3.1.1 Commercial Split System for Preparative Flow of 10 to 50 mL/min

The assembly of the Accurate splitting device Accurate 1/1000, specified for flow rate 10-50 mL/min is as follows (Figure 2.3): the length of the stainless steel capillary of

the Tubing 1 was measured to be 5900 mm and the volume was 2600 μL . From these figures, the i.d. of this capillary was calculated to be 0.75 mm. The fused silica capillary that represents the split flow restrictor had a length of 620 mm. Considering the specified split ratio of 1:1000, the i.d. of this restrictor was calculated to be 0.075 mm.

To implement the commercial splitter in the purification system, the original tubing from splitter to fraction collector was a stainless steel capillary with dimensions 1010 x 1.0 mm, the ESI source was connected to the splitter via a fused silica capillary of 980 x 0.20 mm. With this set-up (established by Dionex for a larger scale system) and the recommended make-up flow of 1 mL/min (make-up solution identical to mobile phase $\text{H}_2\text{O}/\text{ACN}$: 40/60), 100 μL of the mixture of 3 parabens (methyl-, propyl-, butylparaben) at a concentration of 10 g/L each were injected into column #2, but no signal could be observed at the MS detector.

A further optimization of the connection capillaries with respect to dispersion minimization was carried out while maintaining the use of the commercial splitter. The original steel capillary (1010 x 1.0 mm) to connect the fraction collector was replaced by a PTFE tubing with the dimensions 5600 x 0.5 mm i.d. The former connection to ESI source (980 x 0.20 mm) was replaced by a PEEK capillary of 1000 x 0.13 mm i.d., thus reducing its volume to achieve faster signal transport at the given make-up flow rate.

2.3.1.1.1 Characterization of the slightly modified system for peak dispersion

To systematically characterize this slightly modified system, a solution of methyl-, propyl- and butylparaben were injected onto the column #2. The eluted peaks were recorded with a UV detector at 254 nm (UVD 340, Dionex) at 3 different positions: (A) behind the column, (B) behind the splitter, (C) at the fraction collector switching-valve (Figure 2.2).

Figure 2.4 compares the chromatograms of the paraben mixture separation recorded directly behind the column (Figure 2.2, position A) and behind the splitter (Figure 2.2, position B). As can be seen, a pronounced peak dispersion occurred in the splitting device. This could be related to the wide-bore tubing 1 (Figure 2.3), which was originally selected with respect to a column flow rate between 10 to 50 mL/min, specified for this splitting device.

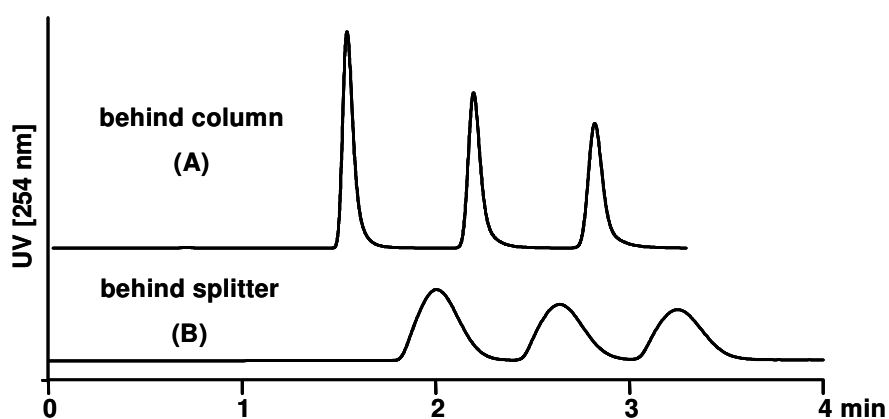


Figure 2.4: Chromatograms of methylparaben, propylparaben and butylparaben (100 mg/L each) using column #2 recorded behind column (A) and behind splitter for column flow 10-50 mL/min (B). (A) and (B) refer to positions in Figure 2.2. Experimental conditions are given in section 2.2.3.

The corresponding peak widths at 50% peak height and the HETP's are given in Table 2.1. The peak widths at 50% peak height of the zones eluting from the main stream line of the splitter are 3-times larger than the zones entering this device (measured behind the column) and the HETP's were 10-times lower (square function for calculation). No measurable additional band broadening in the PTFE connection tubing (5600 x 0.5 mm i.d.) to the fraction collector switching valve was encountered when detection was carried out at position C (Figure 2.2).

Table 2.1: Peak width at 50% peak height (min) and HETP recorded with UV detector at different positions according to Figure 2.2 (Accurate 1/1000 for column flow 10-50 mL/min).

	Peak width at 50% peak height (additional dispersion in %)			HETP	
	behind column (A)	behind splitter (B)	at fraction collector switching valve (C)	behind column	behind splitter
Methylparaben	0.12	0.41 (242%)	0.46 (12%)	3588	373
Propylparaben	0.14	0.43 (207%)	0.48 (12%)	5393	567
Butylparaben	0.17	0.45 (165%)	0.51 (13%)	6517	798

2.3.1.1.2 Characterization of split and signal generation in the MS detector

A first experiment was carried out with the set-up described in Figures 2.2 and 2.3 applying a make-up flow of 1 mL/min (make-up solution identical to mobile phase at H₂O/ACN: 40/60) and injecting 100 μ L of a paraben mixture (10 g/L each) into the column #2 running at a flow rate of 5 mL/min. Under these conditions, no signal was obtained in the MS detector, as already experienced with the unmodified set-up.

To study the cause of this observation, the MS detector was replaced by a simpler and more robust UV detector (Waters 2487). This was done, because it could not be initially verified that both the splitting/make-up system and the ESI-MS detector operated properly under the given conditions. The UV detector was installed in place of the MS to unambiguously approve the transfer of sample into the split restrictor, which could possibly to be suppressed by an overpressure generated at T2 (Figure 2.3), due to a high make-up flow through the restrictive narrow connection capillary to the MS (Figure 2.2). At a make-up flow rate of 1 mL/min, no peaks could be monitored with the UV detector as well. This clearly proves a mal-operation of the splitter. Since this effect could be related to an overpressure at T2 resulting from the pronounced make-up flow through the narrow bore connection capillary to the MS detector, the make-up flow was varied in a subsequent experiment.

Figure 2.5 shows the influence of the make-up flow on the chromatograms recorded with a UV detector at the position of the MS detector. The higher the make-up flow the lower was the signal. Eventually at a make-up flow of 1 mL/min the split flow was completely suppressed (or inverted), obviously since the pressure at T2 was higher than that at T1.

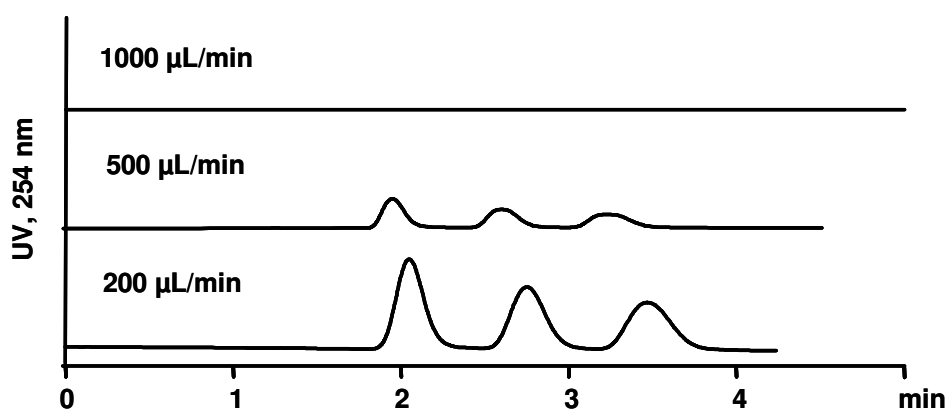


Figure 2.5: Peaks of MS flow line at different make-up flow detected with a UV detector.

Due to the obvious band dispersion in this commercial splitter, another commercial splitter specified for column flow of 1 to 10 mL/min was investigated. The results are described in the following section.

2.3.1.2 Commercial Split System with Analytical Flow of 1-10 mL/min

The dimension of the LCPackings Accurate splitting device 1/1000, specified for flow rate 1-10 mL/min is as follows (Figure 2.3): Tubing 1 consists of a long stainless steel capillary with inner diameter of 0.50 mm and a yellow PEEK capillary with inner diameter of 0.18 mm. The volume of Tubing 1 was measured to be 930 μ L. The fused silica capillary that represents the split flow restrictor had a length of 350 mm and i.d. of 25 μ m.

To integrate the commercial splitter in the purification system, the original tubing from splitter to fraction collector was a PEEK capillary with dimensions 1006 x 0.50 mm. The ESI source was connected to the splitter via a PEEK capillary of 1086 x 0.13 mm.

The system was characterized at 2 different positions by injection of a solution three parabens using column #2. Figure 2.6 compares the chromatograms of the paraben mixture separation recorded directly behind the column (Figure 2.2, position A) and behind the splitter (Figure 2.2, position B). As can be seen, obvious peak dispersion occurred in the splitting device, however, less pronounced than obtained with the splitting device for column flow rate 10-50 mL/min.

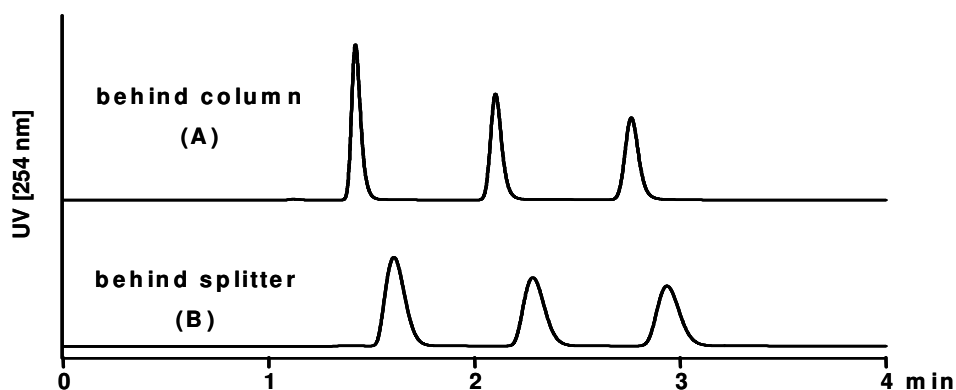


Figure: 2.6: Chromatograms of methylparaben, propylparaben and butylparaben (100 mg/L each) recorded behind column (A) and behind splitter for column flow 1-10 mL/min (B). (A) and (B) refer to positions in Figure 2.2. Experimental conditions are given in section 2.2.3.

The corresponding peak widths at 50% peak height and the HETP's are depicted in Table 2.2. The peak widths at 50% peak height of the peaks measured behind the splitter are almost two times larger than the zones measured behind the column. The HETP's were more than 2-times lower.

Table 2.2: Peak width at 50% peak height (min) and HETP recorded with UV detector at different positions according to Figure 2.2.

	peak width at 10% peak height (additional dispersion in %)		HETP	
	behind column	behind splitter	behind column	behind splitter
	(A)	(B)	(A)	(B)
Methylparaben	0.06	0.11 (83%)	3640	1290
Propylparaben	0.07	0.12 (71%)	5030	2150
Butylparaben	0.09	0.13 (44%)	5825	2990

In a flow splitting setup, a delay volume is generally required between the point where the flow is split to the mass spectrometer and the fraction collector. The delay volume serves to compensate for the time delay due to the transfer of components from the splitting Tee-piece to the mass spectrometer. Moreover, it must allow for

sufficient computation time for data handling and processing before data-dependent instrument control can make a decision to collect a fraction or to send the column effluent to waste. In this instrumental and computational setup, a delay time of at least 8 sec was mandatory to guarantee uncompromised fraction collection. A further investigation was carried out in order to verify if the delay time is suitable for the operation. To characterize this system, 100 μL of a test solution of methylparaben, propylparaben and butylparaben (1 g/L each, diluted in mobile phase) were injected onto the column. The mobile phase and the make-up mobile phase were $\text{H}_2\text{O}/\text{ACN}$: 40/60 with a column flow rate of 5 mL/min. To detect the arrival of the substance at the fraction collector, the end of the capillary from the splitting device to the fraction collector was connected directly (without additional dead volume) with a UV detector (UVD 340, Dionex).

Figure 2.7 compares the measured and the calculated delay time depending on the make-up flow (equations for the calculation see next section). It is obvious that the calculated and especially the measured delay time were much lower than the required (8 sec).

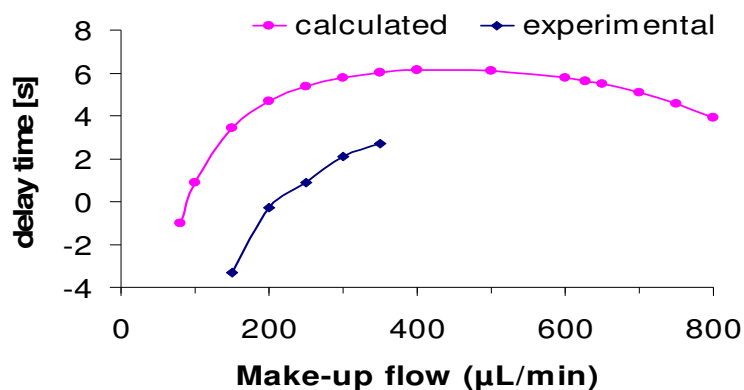


Figure 2.7: Measured and calculated delay time dependence on the make-up flow with column flow rate 5 mL/min.

2.3.2 Theoretical Modeling and Experimental Setup for Fast Automated Purification with Mass Spectrometric and Photometric Fraction Collection

Due to the requirement of the minimum delay time of 8 sec and the obvious band dispersion in the commercial splitter, it was necessary to replace the commercial splitter by a home-made splitting system with a configuration similar to the commercial one, but with capillaries of smaller bore and the smallest possible number of connectors. The development of this setup is described in this section.

2.3.2.1 Optimization of Delay Capillary Dimensions for Minimal Dispersion

Figure 2.8 gives an overview of the setup of the automated purification system used in this study. The major part of the column effluent, pumped at a flow rate of 5-10 mL/min, is directed through a UV detector to the fraction collector. An additional UV-detector is placed between the splitting point and fraction collector. In this case, the volumes of detection cell and tubing are a part of the delay volume.

The delay capillary is referred to as capillary 1 (actually a combination of capillary 1a and 1b, with the UV detection cell in between) in Figure 2.8. Its total volume determines the time delay at a given flow rate, while its length and inner diameter control the generated zone dispersion and back pressure. A continuous flow is directed through capillary 3 to the mass spectrometer by a make-up pump operated at 200 μ L/min. The transfer of sample components from the column effluent to the flow to the mass spectrometer is effected by two Tee-pieces and a small inner diameter fused silica capillary (capillary 2), which interconnects both flows to fraction collector and mass spectrometer, respectively. Optimization of the dimensions of capillary 2 is discussed later.

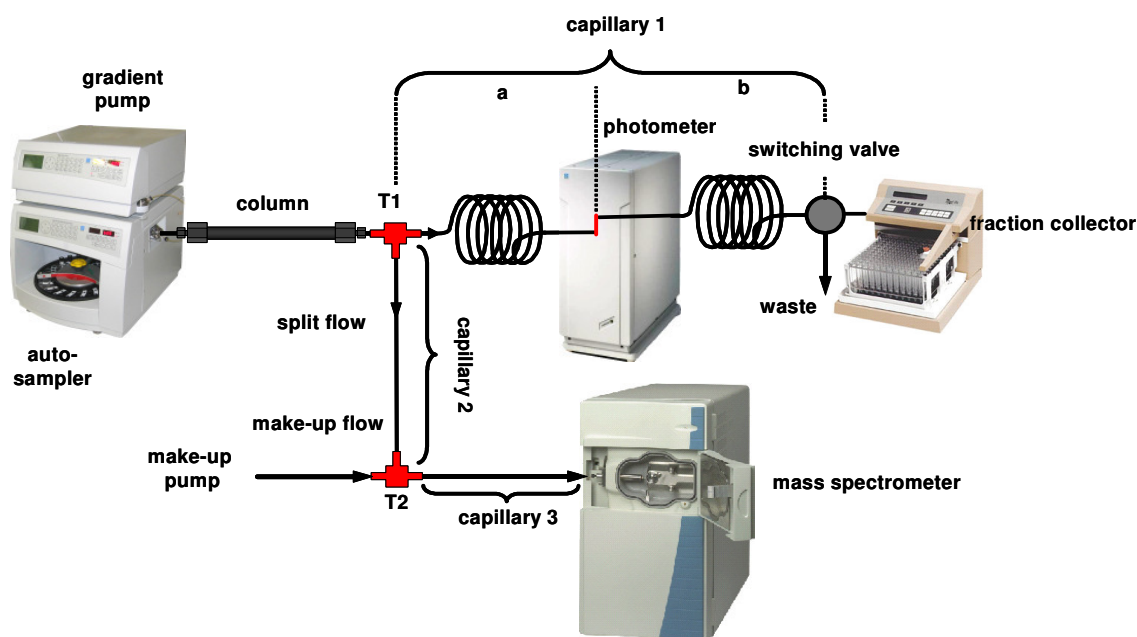


Figure 2.8: set-up of HPLC purification system with home made splitting system. Schematic diagram of the optimized instrumental setup for photometric and mass spectrometric trigger. Capillary 1 (PTFE) 10,000 x 0.5 mm i.d., UV detector positioned at 4,000 mm from T1, capillary 2 (fused silica) 400 x 0.05 mm i.d., capillary 3 (PEEK) 300 x 0.13 mm i.d.

The delay volume necessary to adequately synchronize the mass spectrometric trigger may be estimated based on the following assumptions. At a flow rate of 5 mL/min characteristic for a packed column with 10 mm i.d., a delay volume of 670 μ L is required to generate an 8 sec time delay. This volume, however, needs to be increased with columns operated at higher flow rates, such as monolithic columns. For instance, the envisaged 10 mL/min flow rate would require 1340 μ L delay volume. Moreover, the volume of the delay capillary in front of the fraction collector additionally has to compensate for any time delay generated in the split connection in front of the mass spectrometer. For these reasons, it was decided to implement a delay volume of approximately 2,000 μ L between splitting point and fraction collector. Such a volume is generated by a 2.5 m piece of a 1.0 mm i.d. capillary or a 10 m piece of a 0.5 mm i.d. capillary. Smaller capillary i.d.s cause lower peak dispersion, since the parabolic zone profile generated in all open tubes will be more rapidly counterbalanced by diffusion. However, capillary length must be increased to the power of two with decreasing capillary i.d., generating considerably high back

pressures. This additional backpressure influences the split ratio and can limit the available column inlet pressure.

Band dispersion in both capillaries of 1.0 and 0.5 mm i.d. was evaluated by using the microparticulate column #1 operated at 5 mLmin⁻¹ and placing the detector cell directly behind the column outlet or at the end of the respective delay capillaries. Figure 2.9 overlays the chromatograms of the standard mixture of alkyl parabens measured directly behind the separation column (Figure 2.9a) and at the outlet of delay capillaries of 2,500 x 1.0 mm i.d. (Figure 2.9b) or 10,000 x 0.5 mm i.d. (Figure 2.9c). Both delay capillaries featured identical delay volumes (1,960 µL). As expected, the 1.0 mm i.d. capillary caused markedly more pronounced band broadening relative to that with 0.5 mm i.d. From Table 2.3 can be deduced that the average increases in peak widths with the 1.0 mm and 0.50 mm i.d. delay capillaries were 129% and 75%, respectively. On the other hand, the system pressure drop of approximately 50 bar using acetonitrile eluent was obtained with the 0.50 mm i.d. delay capillary, which prevented the use of even smaller i.d. capillaries to further reduce band dispersion, since pressure 4th potent to the radius of the capillary. A capillary having an inner diameter of 0.50 mm was taken as a base for optimization of the splitter design.

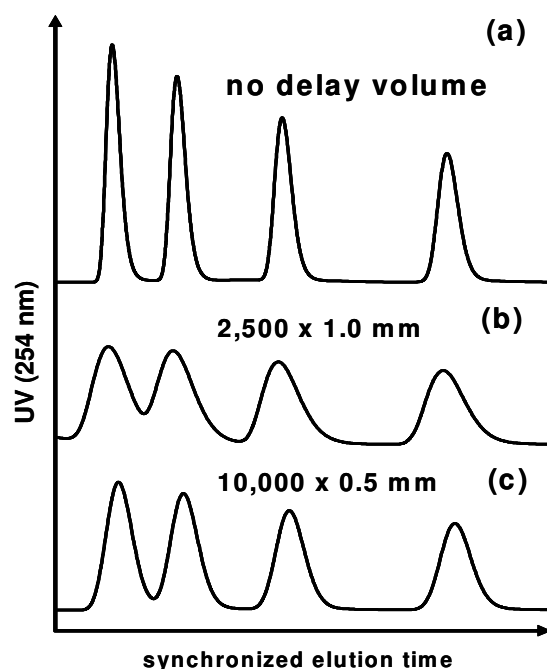


Figure 2.9: Chromatograms for determination of peak dispersion using the microparticulate column operated at 5 mL/min. Detection cell installed (a) behind the separation column, (b) behind the delay capillary 2,500 x 1.0 mm i.d., (c) behind the delay capillary 10,000 x 0.50 mm i.d.; sample, mixture of 4 parabens. Experimental conditions are given in section 2.2.3.

Table 2.3: Peak widths at half height directly behind column #1 and behind two different delay capillaries of the same volume (1,960 μ L).

Substance	$w_{0.5}$ [s]		
	behind column	behind tubing 2,500 x 1.0 mm	behind tubing 10,000 x 0.5 mm
Methylparaben	3.8	9.8	7.4
Ethylparaben	4.1	10.6	7.7
Propylparaben	4.7	10.4	8.0
Butylparaben	5.6	10.9	8.6
Average	4.55	10.43	7.93

2.3.2.2 Theoretical Modeling and Experimental Evaluation of Splitter Setup for Mass Directed Fraction Collection

Four requirements were defined for the splitter setup:

- I. Suitability for operation at 5-10 mL/min column flow,
- II. Band dispersion between trigger detector (either photometer or mass spectrometer) and fraction collector below 30%,
- III. Split ratio between 1:400 and 1:1,000,
- IV. Delay time for mass spectrometric trigger minimum 8 sec.

The column flow was selected for optimized flow rates with both the microparticulate (column #1) and monolithic (column #3) columns. A realistic maximum band broadening requirement was based on the results obtained with *capillary 1* having an i.d. of 0.50 mm. The selected split ratio range was considered to be a good compromise between minimum loss of substance to the mass spectrometer and sufficient ESI-MS detection performance under the make-up flow rates suitable for the given instrument. The system delay time was a requirement defined by the utilized software control. The setup was based on two Tee-pieces (T1 and T2) connected by a flow bridge (capillary 2). Inlet and outlet of the first Tee were connected to the column outlet and delay capillary 1, whereas the second Tee accommodated the connections to the pump delivering make-up flow and to the mass spectrometer, respectively (see Figure 2.8).

Aim of the optimization was to determine the best combination of capillary dimensions in the common configuration depicted in Figure 2.8. In the following descriptions, the 2 Tee-pieces and the 3 (variable) capillaries will be assigned as in Figure 2.8. The pressure gradient between T1 and T2 and the dimension of capillary 2 (between both Tee-pieces) directly control the split flow and thus the split ratio. Another important aspect of this part of the setup is the influence of both the length of and the linear velocity in capillary 2 connecting the two Tee-pieces. These variables mainly determine the time to transfer a peak from T1 to the mass spectrometer. This is because of a much higher linear velocity in capillary 3 (which is predominantly controlled by the magnitude of make-up flow), resulting in minor contribution of this second part to the total transfer time to the mass spectrometer. To calculate the so-called system delay time for mass spectrometric trigger, the time to transport the detection zone from T1 to the mass spectrometer has to be subtracted from the time taken for the main peak zone to travel from T1 to the fraction collector valve.

As all the above mentioned criteria (capillary dimensions and magnitude of make-up flow) are strictly interrelated, optimization by empirical design is very difficult. Therefore, the influence of the different parameters on theoretical split ratio and system delay time was modeled. All calculations were based on the assumption that the pressure at T1 is determined by column flow rate and the permeability of capillary 1 (sum of 1a and 1b in Figure 2.8), whilst the pressure at T2 is solely controlled by the make-up flow and the permeability of capillary 3. The influence of the flow through capillary 2 (only 5 – 20 $\mu\text{L}/\text{min}$) was considered negligible for the calculation of the pressure drop between T1 and T2.

The pressure drop in all capillaries was calculated by using the integrated Hagen-Poiseuille equation for laminar flow following Equation 1 and 2. Considering the pressures at the fraction collector valve and at the sprayer of the electrospray ion source to be zero, $p(\text{T1})$ and $p(\text{T2})$ directly refer to the pressures at T1 and T2, while F_1 and F_3 indicate column flow rate, and make-up flow rate; η the viscosity; R_1 and R_3 the tubing radii of capillary 1 and 3; L_1 and L_3 the lengths of capillary 1 and 3.

$$p(\text{T1}) = \frac{8\eta}{\pi} \cdot \frac{F_1 \cdot L_1}{R_1^4} \quad (\text{Eq. 1})$$

$$p(\text{T2}) = \frac{8\eta}{\pi} \cdot \frac{F_3 \cdot L_3}{R_3^4} \quad (\text{Eq. 2})$$

The split flow rate between T1 and T2 was calculated from the pressure difference $p(\text{T1}) - p(\text{T2})$ according to Eq. 3, where F_2 indicates the split flow rate; η the viscosity; R_2 the tubing radius of capillary 2; and L_2 the length capillary 2:

$$F_2 = \frac{\pi}{8\eta} \cdot \frac{(p(\text{T1}) - p(\text{T2}))}{L_2} \cdot R_2^4 \quad (\text{Eq. 3})$$

Dividing the column flow rate by the split flow rate, the split ratio was calculated. The theoretical delay time Δt was calculated by means of Eq.4 which is based on the information obtained from Eqs. 1 – 3 (V_1 , V_2 and V_3 indicate the volumes of capillary 1, 2 and 3, calculated from their nominal dimensions):

$$\Delta t = V_1/F_1 - V_2/F_2 - V_3/(F_2+F_3) \quad (\text{Eq. 4})$$

The optimized setup was developed in a step by step variation of the four parameters length of capillary 1 (i.d. is already defined to be 0.5 mm), length of capillary 2 (considering standardized available narrow bore diameters of fused silica like 75 and 50 μm), i.d. of capillary 3 (minimum length was determined by instrument design to be 300 mm) and the magnitude of the make-up flow. The influence of these four important system parameters on the pressure gradient between T1 and T2, split flow, split ratio and system delay time is illustrated in Figures 2.10 to 2.13. All modeling was performed for column flow rates of both 5 mL/min (column #1) and 10 mL/min (column #3).

With a make-up flow of 200 $\mu\text{L}/\text{min}$ (calculations regarding make-up flow are reported in detail in section 1.3.4) and using the predefined parameters for capillary 2 (400 mm x 50 μm) and capillary 3 (300 mm x 130 μm) the influence of the length of capillary 1 considering an i.d. of 0.5 mm was modeled for the pressure gradient between T1 and T2 (Figure 2.10a), the split flow (Figure 2.10b), the split ratio (Figure 2.10c) and the system delay time. It can be seen that the curves of the pressure gradient and the split flow run linear with the length of capillary 1 (Figure 2.10a and 2.10b). From Figure 2.10c it can be deduced that the length must be between 6,600 mm and 11,000 mm to fulfill the requirement of a split ratio between 400 and 1,000 with both flow rates. Figure 2.10d clearly shows that delay time was a bigger issue at higher column flow rates, since the curve for 10 mL/min showed a much shallower slope and reached the required 8 sec level at a capillary length of approx. 9,700 mm. In consequence, it is recommended to adjust a relatively low split ratio of approx. 500, because the setup generated sufficient time delay at higher column flow rates. In order to have a little reserve in the delay time, a length of 10,000 mm was considered as optimal for capillary 1.

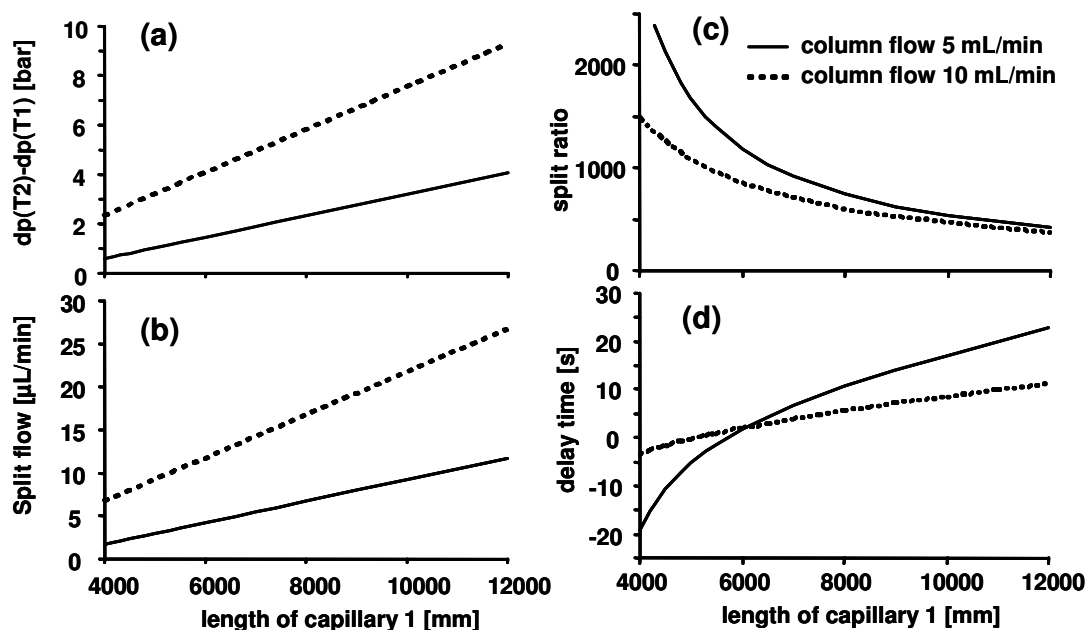


Figure 2.10: Modeling of the influence of the system parameter length of capillary 1) on (a) pressure gradient between T1 and T2, (b) split flow, (c) split ratio and (d) delay time (for capillary denotation refer to Figure 2.8).

Figure 2.11 shows the influence of the i.d. of capillary 3 at a fixed length of 300 mm (capillary 1 is 10,000 mm x 0.5 mm, capillary 2 is 400 mm x 50 μm) on the pressure gradient between T1 and T2, the split flow, the split ratio and the system delay time. Here, the split ratio was more critical with smaller column flow rates. Split ratios smaller than 1,000 were modeled for 5 mL/min flow and for capillaries having an i.d. of more than 106 μm . Moreover, the split ratio did not fall below 470 from an i.d. of 150 μm both for 5 and 10 mL/min flow rates (Figure 2.11c). Once more, the bigger issue was system delay time, especially with higher column flow rates (Figure 2.11d). It became obvious that the i.d. of capillary 3 must be 106-170 μm to guarantee a delay of 8 sec. Reducing the i.d. of capillary 3 at a given make-up flow significantly increased the pressure at T2 and thus reduced the linear velocity in capillary 2, as shown in the plot of the pressure gradient (Figure 2.11a) and the split flow (Figure 2.11b) with the diameter of capillary 3. In fact, the velocity in capillary 2 mainly determined the system delay time. This is clearly proven by the calculations presented in Figure 2.11d. As a further increase would only be of minimal effect on the split flow, the optimal i.d. of capillary 3 was defined to be 130 μm , which is readily available in PEEK material.

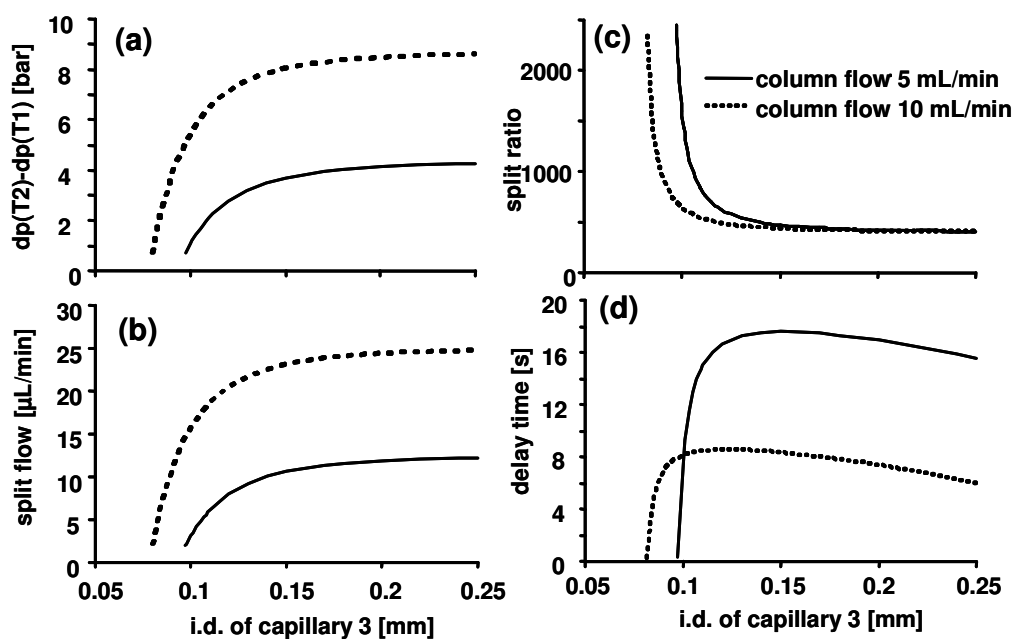


Figure 2.11: Modeling of the influence of the system parameter length of diameter of capillary 3 on (a) pressure gradient between T1 and T2, (b) split flow, (c) split ratio and (d) delay time (for capillary denotation refers to Figure 2.8).

The most critical parameter in the splitter design was the dimension of capillary 2. Figure 2.12a shows the influence of its length on the split ratio, Figure 2.12b on the system delay time. The modeling was made for variable capillary lengths having an i.d. of 50 μm or 75 μm . It can be seen from the plot in Figure 2.12a that the split ratio with the 75 μm capillary is much lower, due to its smaller restriction effect relative to capillary 1. This is most critical at a flow rate of 10 mL/min, where the split ratio adopted values below 100 at practical capillary lengths of less than 1,000 mm. Considering the influence on the delay time (modeled in Figure 2.12b), it is obvious that under such conditions a delay of less than 6 sec was generated, which prevents the applicability of 75 μm i.d. tubing for capillary 2. For a 50 μm i.d. capillary a length of more than 350 mm resulted in split ratios greater than 400 for both 5 and 10 mL/min column flow rates. Figure 2.12b shows, however, that a length of 420 mm must not be exceeded to guarantee at least 8 sec delay time for the more critical flow rate of 10 mL/min. Hence, a length of 400 mm and an i.d. of 50 μm were defined as optimal for capillary 2. The modeling of capillary dimensions as presented above resulted in the following capillary dimensions for an optimal splitter setup: *capillary 1*, 10,000 mm x 0.5 mm; *capillary 2*, 400 mm x 0.050 mm; *capillary 3*, 300 mm x 0.13 mm.

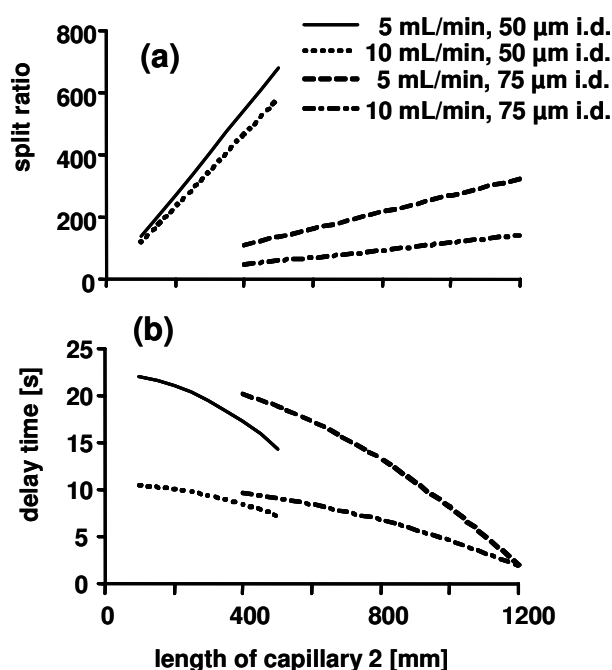


Figure 2.12: Modeling of the influence of the system parameter length of capillary 2 on (a) split ratio and (b) delay time (for capillary denotation refers to Figure 2.8).

Finally, the influence of make-up flow in the optimized setup on pressure gradient between T1 and T2, split flow, split ratio and system delay time was modeled (Figure 2.13). When the make-up flow was increased, the pressure at T2 increased linearly and thus the pressure gradient and the split flow decreased linearly (Figure 2.13 a and b). This induced a hyperbolic increase in the split ratio with increasing make-up flow. The split ratio rose above 1,000 when the make-up flow exceeded 450 $\mu\text{L}/\text{min}$ for a column flow of 5 mL/min.

The dependence of delay time on make-up flow rate turned out to be rather complex, as can be seen in Figure 2.13d. Up to a make-up flow rate of approx. 50 $\mu\text{L}/\text{min}$, the increase in linear velocity through capillary 3 mainly determined the time elapsing for a zone migrating from T1 to the mass spectrometer. As this time was reduced, the delay time increased. At higher flow rates, however, a marked back pressure was generated at T2 which dramatically decreased the linear velocity in capillary 2. This was the reason for the plateau at make-up flow rates larger than 100 $\mu\text{L}/\text{min}$, as the opposite effects on the flow through capillary 2 and capillary 3 compensated each other. The plateau was largely extended at a column flow rate of 10 mL/min, as can be deduced from the dotted line in Figure 2.13d. At a column flow rate of 5 mL/min, a

lower pressure was built up at T1. Hence, the pressure generated at T2 by the make-up flow contributed more strongly to the pressure difference between T1 and T2 (see solid line in Figure 2.13d). For this reason, the system delay time showed a pronounced decrease when the make-up flow rate exceeded 400 $\mu\text{L}/\text{min}$. It was derived from the modeling that a make-up flow rate between 150 and 450 $\mu\text{L}/\text{min}$ is compatible with the required minimum system delay time of 8 sec and split ratio smaller than 1:1000 for both 5 and 10 mL/min column flow rates.

The optimal splitter setup as derived above was assembled and the experimental delay times were measured for different make-up flow rates. For this experiment, the UV-detector was positioned at the outlet of capillary 1 in order to detect the effective arrival of the peak zone at the fraction collector switching valve. The obtained experimental delay times for both column flow rates are included in Figure 2.13d together with the modeled curves. The deviations from the theoretical values were minimal and can be explained by deviations of the effective capillary i.d.s. from the specified values. According to the power of 4 in Hagen-Poiseuille's law (Eq. 1), this effect is very significant.

The plateau-like behavior for the delay time within a certain range of make-up flow rates could be experimentally verified (Figure 2.13d), so that a make-up flow rate between 150 and 300 $\mu\text{L}/\text{min}$ can be selected for required dilution of the substance zone to MS without adjusting the delay time. The dilution of the substance zone is due to reduction of split flow with make-up flow and on the other hand due to dilution of the substance zone with the make-up flow.

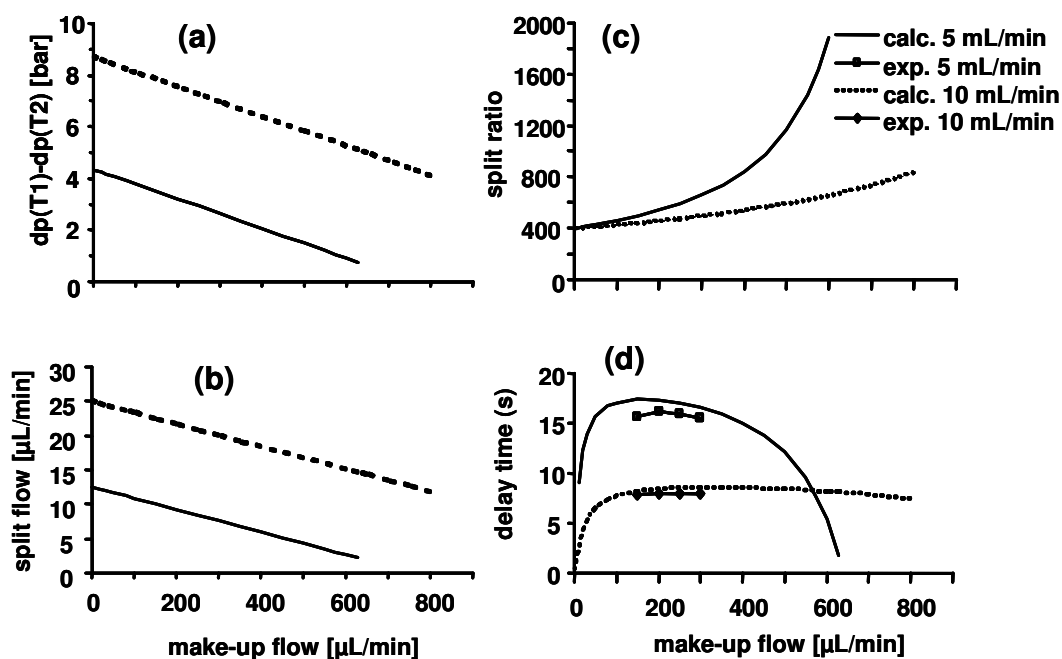


Figure 2.13: Modeling and experimental verification of the influence of the system parameter make-up flow rate on (a) pressure gradient between T1 and T2, (b) split flow, (c) split ratio and (d) delay time. Experimental conditions are given in section 2.2.4.

2.3.2.3 Influence of the Make-up Flow Rate on Mass Spectrometric Signal Quality

According to the manufacturer, the linear quadrupole mass spectrometer applied in this study is optimized for robust routine operation at flow rates between 0.2 and 1 mL/min. The range for adjusting the flows of nebulizing gas and drying gas of the electrospray ion source are rather limited and moreover, both flows may not be regulated independently. Before connecting the mass spectrometer to the split-system, it was tuned by direct infusion of a solution of parabens (10 ng/ μL) at a flow rate of 200 $\mu\text{L}/\text{min}$. Using the optimized tuning parameters and the instrumental setup described above (Figure 2.8), the separation and detection of a mixture of methyl paraben, propyl paraben and butyl paraben (1 g/L each, 100 μL injected) were evaluated. Figure 2.14 illustrates an overlay of the reconstructed total ion current chromatograms obtained with different make-up flow rates without any smoothing of the signal to critically assess signal stability. The peaks were generated on the microparticulate column (column #1) at a flow rate of 5 mL/min. With make-up

flows in the range of 100-300 $\mu\text{L}/\text{min}$, the elution times of all parabens matched almost perfectly, which is a clear proof of the independence of delay time on make-up flow in this range.

Considering the peak shapes and peak sizes, a strong influence of the make-up flow rate could be deduced. At 80 and 100 $\mu\text{L}/\text{min}$, the observed signals were unstable and noisy. This is an indication for unstable electrospray. Lacking the possibility to adjust the nitrogen flows independently, it was not possible to optimize the electrospray conditions for that flow rate range. At a make-up flow rate of 150 $\mu\text{L}/\text{min}$ or higher, stable and well-shaped signals were observed. With further increasing make-up flow rates a simultaneous decrease in the peak intensities was observed. This is due to the dilution of the peak zones, as ESI-MS is a (pseudo-)concentration dependent process. Increased dilution is not only a consequence of the larger volume of make-up-flow added to the column effluent, but also due to a reduction in the flow through capillary 2 because of a higher backpressure at T2 (see Figure 2.13).

The independence of the system delay time and the pronounced dilution effect with increasing make-up flow made this an ideal variable to control the concentration of the detection zones at the mass spectrometer without the need to correct system synchronization. A make-up flow of 200 $\mu\text{L}/\text{min}$ proved to be suited for most of the applications and was selected for the system characterization as described below.

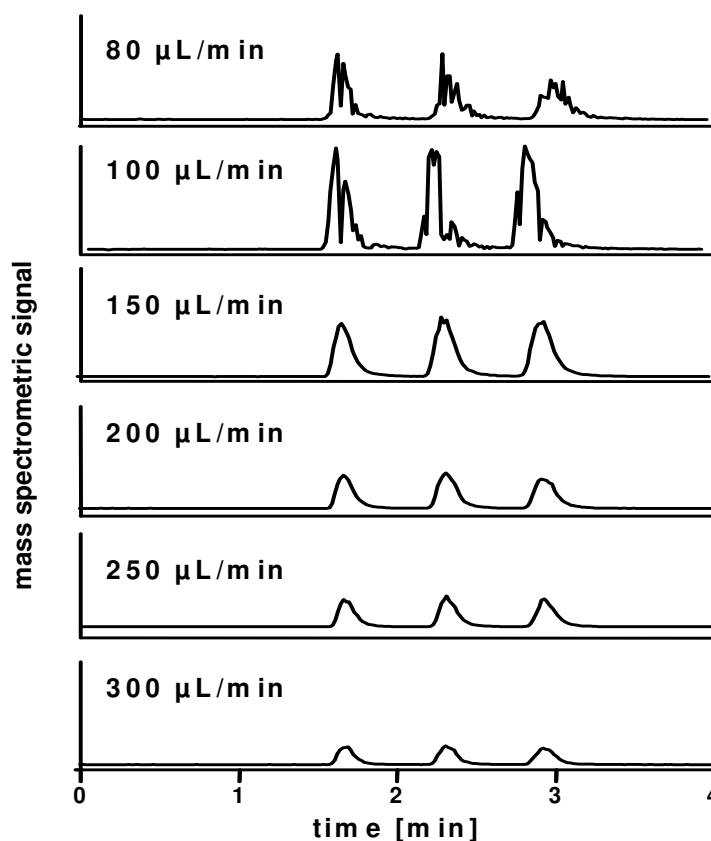


Figure 2.14: Influence of the make-up flow rate on the mass spectrometric signal quality. Experimental conditions are given in sections 2.2.4 and 2.2.6.

2.3.2.4 Synchronization for UV- and Mass Spectrometric Trigger

Combined photometric and mass spectrometric triggers are common practice for purification in high-throughput mode. The UV-detector is placed in-line between Tee 1 and fraction collector, as depicted in Figure 2.8. For synchronization of the system, the actual delay times for both photometric- and mass spectrometric trigger were determined and subsequently entered into the software for correct fractionation trigger. To record the relevant chromatograms, the UV detector was positioned at the outlet of capillary 1 in order to determine peak arrival time and peak shape at the fraction collector, whilst a dummy detection cell was mounted at the original detection position in order to keep the delay volume constant.

Figure 2.15 depicts the separation of three parabens in the microparticulate column at a flow rate of 5 mL/min. The uppermost and middle trace show the signal at the synchronized UV-detector (Figure 2.15a) and at the mass spectrometer (Figure 2.15b), respectively. The lower trace represents the compound zones arriving at the

fraction collector. In order to measure the time delays, the zone dispersion in the connecting capillaries, and the synchronization of the band widths between the detectors and the fraction collector, the elution times and peak widths at half height were extracted from the chromatograms (Table 2.4). It can be seen that the peak zones pass both detectors simultaneously, while they arrive at the fraction collector with a delay of 16 s, offering sufficient time for real-time peak detection and valve switching. Because of the additional connecting capillary between UV detector and fraction collector, the band widths at the fraction collector were slightly higher than those at the UV detector. Moreover, peak widths recorded by the mass spectrometer were larger because of the comparatively large time constant of mass spectrometric detection (2 spectra per s). Synchronization was completed by entering the time delays and signal threshold for collection as parameters into the software for correct peak collection.

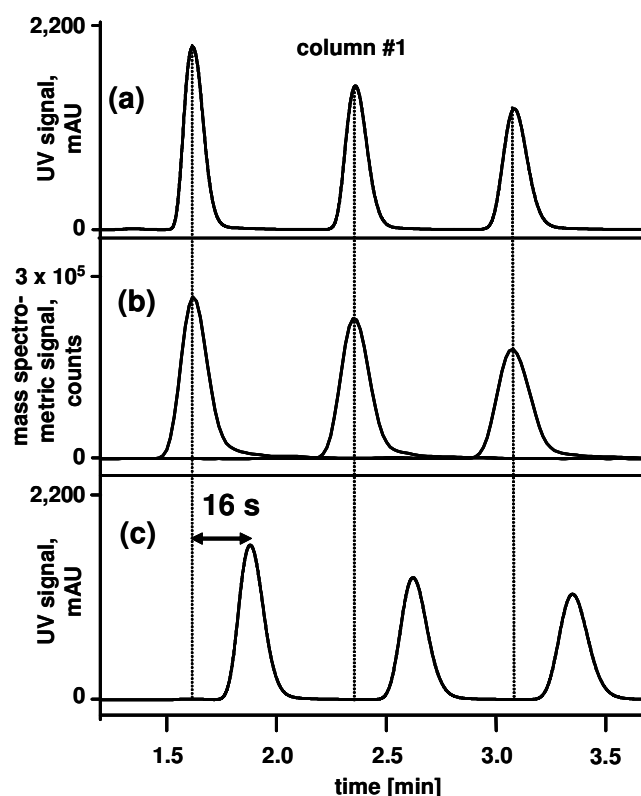


Figure 2.15: Synchronization and characterization of the optimized setup with the microparticulate column operated at 5 mL/min. Chromatograms recorded at the following positions: (a) at the synchronized UV detector, (b) at the mass spectrometer, (c) at the fraction collector. Experimental conditions are given in section 2.2.4.

The synchronization of the purification system with a semi-preparative monolithic column operated at a flow rate of 10 mL/min is illustrated in Figure 2.16. Although the monolithic column was eluted with a weaker eluent, the generated retention factors were 2-3-fold smaller than those with the microparticulate column. Compared to the microparticulate column, the resolution was lower with the monolithic column, which enabled the separation of the paraben mixture exactly with baseline resolution. This decrease in resolution is mostly due to lower phase ratio and a slight peak tailing in the monolithic column. The elution profiles recorded by the mass spectrometer even showed partial peak overlap. Nevertheless, the parameters derived from this experiment were suitable for proper synchronization of the system and enabled the fractionation of the paraben mixture at the fraction collector with resolution to baseline. It can be seen from the time shift in the elution profiles at the detectors and the fraction collectors that the delay time decreased to 8 sec with a column flow rate of 10 mL/min.

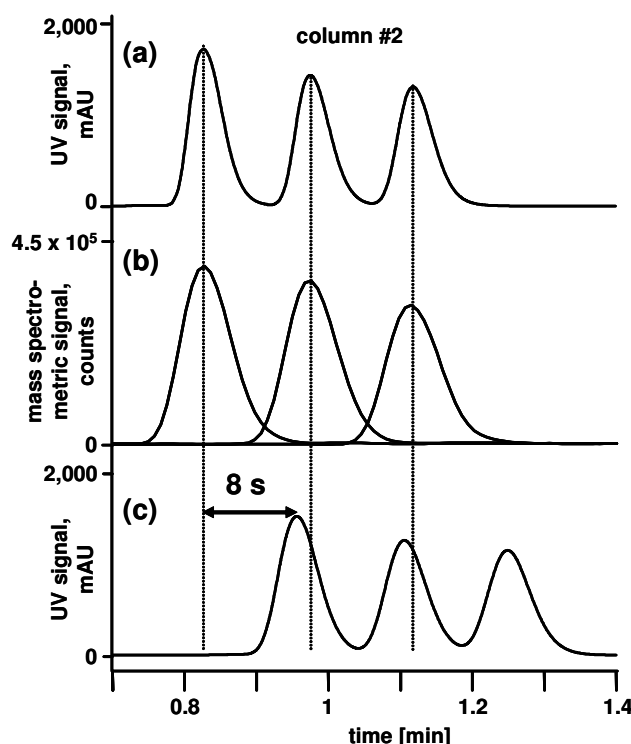


Figure 2.16: Synchronization and characterization of the optimized setup with the monolithic column operated at 10 mL/min. Chromatograms were recorded at the following positions: (a) at the synchronized UV detector, (b) at the mass spectrometer, (c) at the fraction collector. Experimental conditions are given in section 2.2.4.

Table 2.4: Peak widths at half height $w_{0.5}$ and elution times t_R in the optimized system at both trigger detectors and at the fraction collector for column #1 and column #3.

Substance	$w_{0.5}$, column #1 [s]			t_R , column #1 [min]		
	UV- detector	MS- detector	fraction collector	UV- detector	MS- detector	fraction collector
Methyl – paraben	6.0	8.3	7.6	1.62	1.62	1.88
Propyl – paraben	6.6	9.0	8.2	2.36	2.35	2.62
Butyl – paraben	7.5	9.5	8.9	3.09	3.09	3.35
Substance	$w_{0.5}$, column #3 [s]			t_R , column #3 [min]		
	UV- detector	MS- detector	fraction collector	UV- detector	MS- detector	fraction collector
Methyl – paraben	3.1	4.9	3.8	0.83	0.83	0.96
Propyl – paraben	3.2	4.9	3.9	0.98	0.98	1.11
Butyl – paraben	3.4	5.2	4.1	1.12	1.12	1.25

2.3.2.5 Evaluation of Fraction Purity and Recovery with the Optimized System

The test mixture of parabens was also applied to evaluate the performance of fractionation with the optimized setup for both the microparticulate and the monolithic column. Only the fractionation with the monolithic column is shown in Figure 2.17, as this fractionation was more challenging than that with the packed column, due to the higher separation velocity and the reduced resolution between the sample zones. Figure 2.17a shows the UV chromatogram, which was utilized as a control in this experiment but not as a trigger for fractionation. The expected m/z values of the three parabens were entered as target values for mass spectrometric fraction trigger. Figure 2.17b depicts the chromatographic traces of the three channels, on which

single-ion monitoring was performed to detect the three parabens. Begin and end of the eluting bands were defined when the signal passed a given threshold value and those parts of the peak profile that were selected for collection by the software are indicated in Figure 2.17b by solid rectangles. Moreover, grid lines indicate the corresponding time intervals, shifted by the delay time, during which the eluting compounds were collected in the fraction collector.

Re-injections of the fractions into an analytical HPLC system equipped with a microparticulate column (Luna C18(2), 5 μm , same stationary phase as used in semi-preparative column #1) were carried out to assess fractionation quality by quantifying the recovered amount of substance and its purity. The chromatograms of these re-injections are depicted in Figure 2.17c. Peak purity was calculated as area% in the chromatograms. To determine recovery, a differential quantification was carried out, as described in the experimental section. The obtained purity and recovery values for both the microparticulate and monolithic column are summarized in Table 2.5. With both columns the purities for peak one are 100%. Slight carryover in the following fractions stems from a tiny volume of previous fraction stored in a short piece of tubing between the switching valve and the outlet or the robotic arm used to fill the fraction tubes (see arrows in Figure 2.17c). This problem could be readily alleviated by using a fraction collector having a minimal dead volume between switching valve and capillary outlet or by an additional feature allowing the purging of the tubing in between the fractionation intervals. The recoveries obtained with the microparticulate column were close to 100%, demonstrating the high yield of pure substance feasible with very well resolved compounds. In the case of the more critical separation on the monolithic column, the recovery was around 95%, which reflects the loss of material due to decreased peak resolution in the very fast fractionation.

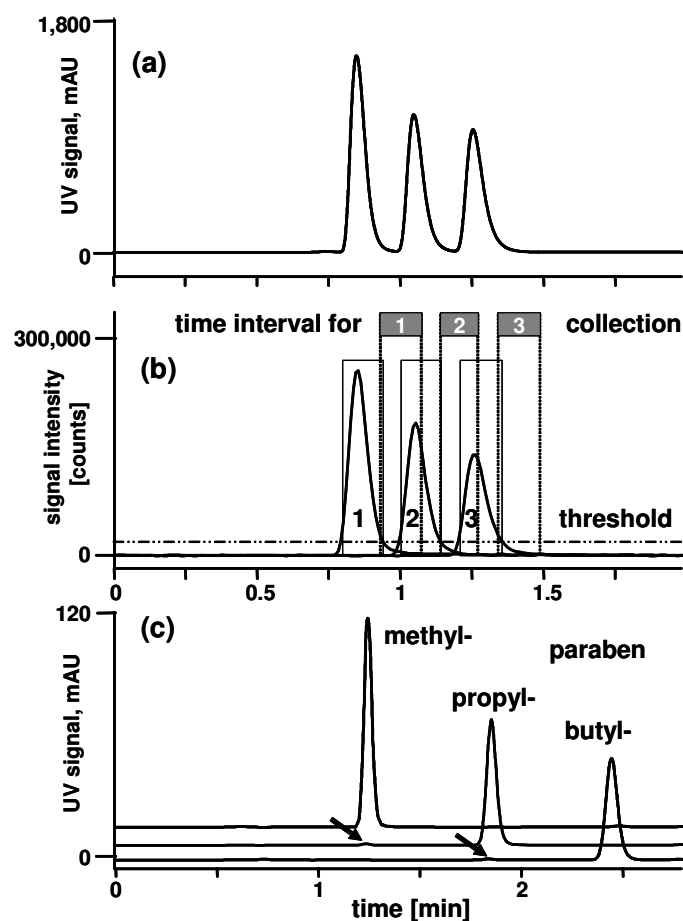


Figure 2.17: Semi-preparative fractionation with mass spectrometric fractionation trigger (column #3) and re-analysis of the fractions using an analytical column. The chromatograms recorded at (a) 254 nm, and (b) at m/z 150.5-151.5 for methylparaben (1), m/z 178.5-179.5 for propylparaben (2), and m/z 192.5-193.5 for butylparaben (3) are shown. The chromatograms of the re-injected fractions are illustrated in (c); arrows indicate slight carryover from previous fractions. Experimental conditions are given in section 2.2.5 and 2.2.6.

Table 2.5: Recovery and purity of the fractions determined with analytical HPLC.

Substance	Column #1	Column #1	Column #3	Column #3
	Recovery (%)	Purity (%)	Recovery (%)	Purity (%)
Methylparaben	104	100	97	100
Propylparaben	102	99.3	92	99.1
Butylparaben	101	99.3	95	99.1

2.4 Conclusions

Two tested commercially available split systems could not fulfill the requirements for high speed purification using flow rates typical for 10 mm i.d. columns. Hence, a passive splitting device was constructed and its design was optimized by theoretical modeling and step by step experimental evaluation for both photometric- and mass spectrometric fraction collection trigger.

Mathematical modeling of the critical parameters of a passive splitting device facilitates the efficient optimization of tubing dimensions suitable for automated photometric and mass spectrometric triggering of peak fractionation in semi-preparative HPLC with good predictive accuracy. Using a standard mixture of parabens, peak dispersion and synchronization may be experimentally evaluated in order to validate system performance. Both modeling and experiment show that compound transfer in the capillary connecting flow to fraction collector and mass spectrometer is the most critical parameter in the adjustment of delay time.

In standard mode, operation of a 100 x 10 mm i.d. column packed with 5 μm particles at a pressure of 60-70 bar with water/acetonitrile eluents generates 2,500-3,500 theoretical plates. Adjusting a gradient volume of 5 column flow through volumes, purification in gradient mode including column regeneration using this setup takes 5-6 min per run.

A silica-based monolithic C18-column of the same dimensions performed at 10 mL/min is suitable for further increasing the speed of fractionation. In spite of the higher flow rate utilized with the monolithic column, only 35-40 bar operating pressure is required. The separation efficiency is slightly lower but in the same order of magnitude as with the packed column (1,500-2,500 theoretical plates). Additionally, the plates were generated in less than half the time and at one quarter of the backpressure. The fast mode enables gradient purification in 2-2.5 min per run at the cost of a decrease in resolution. Since the fast mode can be accomplished on exactly the same instrumental setup, it represents an ideal alternative to the standard mode for high throughput purification of simple crude mixtures.

References

- [1] Zeng, L., Burton, L., Yung, K., Shushan, B., and Kassel, D.B. (1998) Automated analytical/preparative HPLC/MS system for the rapid characterization and purification of compound libraries. *J Chromatogr. A*, **794**, 3-13.
- [2] Zeng, L. and Kassel, D.B. (1998) Developments of a Fully Automated Parallel HPLC/Mass Spectrometry System for the Analytical Characterization and Preparative Purification of Combinatorial Libraries. *Anal. Chem.*, **20**, 4380-4388.
- [3] Edwards, C. and Hunter, D.J. (2003) High-throughput purification of combinatorial arrays. *J. Comb. Chem.*, **5**, 61-66.
- [4] Kyranos, J.N., Cai, H., Zhang, B., and Goetzinger, W.K. (2001) High-throughput high-performance liquid chromatography/mass spectrometry for modern drug discovery. *Curr. Opin. Biotechnol.*, **12**, 105-111.
- [5] Isbell, J., Xu, R., Cai, Z., and Kassel, D.B. (2002) Realities of high-throughput LC/MS purification of large combinatorial libraries: a report on overall sample throughput using parallel purification. *J. Comb. Chem.*, **4**, 600-611.
- [6] Bauser, M. (2002) Preparative HPLC-MS for the high-throughput purification of combinatorial libraries. *J. Chrom. Sci.*, **40**, 292-296.
- [7] Searle, P.A. and Hochlowski, J.E. (2004) Comparison of preparative HPLC/MS and preparative SFC techniques for the high-throughput purification of compound library. *J. Comb. Chem.*, **6**, 175-180.
- [8] Neue, U.D., Wheat, T.E., Mazzeo, J.R., Mazza, C.B., Cavanaugh, J.Y., Xia, F., Diehl, D.M. (2004) Differences in preparative loadability between the charged and uncharged forms of ionizable compounds. *J. Chromatogr. A*, **1030**, 123-134.
- [9] Wilfried, M.A., Niessen, W.M.A., Lin, J., Bondoux, G.C. (2002) Developing strategies for isolation of minor impurities with mass spectrometry-directed fractionation. *J. Chromatogr. A*, **970**, 131-140.
- [10] Renold, P., Madero, E., and Maetzke, T. (2001) Automated normal-phase preparative high-performance liquid chromatography as a substitute for flash chromatography in the synthetic research laboratory. *J. Chromatogr. A*, **908**, 143-148.
- [11] Moritz, R. and O'Reilly, N. (2003) Mass-based fraction collection of crude synthetic peptides in analytical and preparative scale. *J. Biomol. Techn.*, **14**, 136-142.
- [12] Chervet, J. P (1991) Micro flow processor, *European Patent*, 0495255A1.

-
- [13] Wang, T., Barber, M., Hardt, I., and Kassel, D.B. (2001) Mass-directed fractionation and isolation of pharmaceutical compounds by packed-column supercritical fluid chromatography/mass spectrometry. *Rapid Commun. Mass Spectrom.*, **15**, 2067-2075.
- [14] Leister, W., Strauss, K., Wlśnoski, D., Zhao, Z., and Lindsley, C. (2003) Development of a custom high-throughput preparative liquid chromatography/mass spectrometer platform for the preparative purification and analytical analysis of compound libraries. *J. Comb. Chem.*, **5**, 322-329.
- [15] Cai, H., Kiplinger, J.P., Goetzinger, W.K., Cole, R.O., Laws, K.A., Foster, M., and Schrock, A. (2002) A straightforward means of coupling preparative high-performance liquid chromatography and mass spectrometry. *Rapid Commun. Mass Spectrom.*, **16**, 544-554.

Chapter 3

Characterization and Loadability Study of RP-HPLC Columns for Automated Purification System

3.1 Stationary Phase Characterization

3.1.1 Introduction

The column is the heart of the HPLC system, because in the column the physicochemical processes resulting in retention selectivity, take place [1,2]. In HPLC, the most widely used columns are from the reversed-phase (RP) type [3,4]. The wide variety of the presently available RP-HPLC phases, fortunately, facilitates the solution of a multitude of different separation problems via stationary phase selection. However, this leaves the analyst with the difficult problem of a proper column selection for a specific problem [5]. Although reversed-phase columns differ in a variety of ways, three attributes can be identified as most relevant for its retention properties [6,7]. One is the retentivity of a column towards non-polar solutes that has been described as “hydrophobicity”. This property is correlated with stationary phase alkyl length, bonding density, and substrate surface area, and is related to the quantity of hydrocarbon contained within the column. The second column property is the “silanol activity”. The third property is the “shape selectivity”. This may differ among columns with similar hydrophobicity and silanol activity.

Silanols cannot be completely eliminated from the silica surface even after extensive silanization and end-capping [3]. The “silanol activity” includes cation exchange with strong bases, hydrogen bonding with polar solutes, both as a donor and an acceptor, as well as anion exclusion [3,6]. Cation exchange depends both on the number of exchange sites as well as on the pK_a of these sites. In addition, anion exchange is possible, if for example amino groups are bonded to a packing to mask its silanol activity [6]. The study of silanol activity is usually based on asymmetric peak shapes often obtained with the analysis of ionized basic compounds [7,9]. The particular interest in this area is due to the large number of important pharmaceuticals and other biomedically relevant compounds which possess basic groups [10]. Because peak tailing is the most objectionable characteristic associated with silanol activity,

peak asymmetry (A_s) is commonly used as a figure of merit for this property [7]. Tests for silanol activity have been reported for buffered and unbuffered mobile phases. The presence of buffer ions suppresses some of the interaction with basic analytes [3]. If weak bases such as anilines are used, even a low concentration of buffer ions can suppress the influence of surface silanols [5,8]. Engelhardt and coworkers have developed such a test based on the retention and peak shape of p-ethylaniline in a mobile phase containing water-methanol [2,11,12]. Neue and Jerowik [8] and Sander et al. [7] have utilized amitriptyline as a probe for silanol activity, in a buffered mobile phase environment. The buffered mobile phase is thought to provide a more robust and more reproducible test [8,13]. McCalley performed a number of experiments concerned with elution behaviour of basic solutes on RP-stationary phases [10,13-22].

A variety of test procedures have been developed to evaluate and characterize hydrophobicity, silanol activity, and other aspects of column performance in a single chromatographic test [6,7,11]. These methods are simple, but nevertheless several significant properties of HPLC packings can be derived [2,6]. The Engelhardt test is the most cited and used method [2]. Neue et al. have developed a test similar to the Engelhardt test [3]. Another new single run testing method has been developed by Sander et al., common by known NIST test [7]. The selection of the components in this test was based on published testing protocols [8,11] and commercial column literature.

In this study some RP-HPLC columns in semi-preparative dimension (10 mm i.d.) were characterized and compared to their respective analytical dimension (150 x 4.6 mm i.d.). The characterization of different column properties was performed using the Engelhardt test. Because of higher silanol activity obtained with some RP-columns, an extensive study using different mobile phases for a strongly basic probe amitriptyline was carried out.

3.1.2 Experimental

3.1.2.1 Columns

The columns tested are listed in Table 3.1. All columns were tested using the Engelhardt test. Monolith is a silica-based monolithic research column from Merck (Darmstadt, Germany). The Acclaim C18 5 μm in semi-preparative dimension

(100x10 mm i.d.) was also a prototype.

Table 3.1: Characteristics of 8 columns used in this work

	Acclaim C18			Luna C18(2)		Synergi Polar-RP		Monolith
Pore size [Å]	120			100		80		-
Surface area [m ² /g]	300			400		475		-
Carbon load [%]	18			17.5		11		-
pH range	2-8			1.5-10		1.5-7		-
Particle size [µm]	3	5	5	5	5	4	4	-
Column i.d. (mm)	4.6	4.6	10	4.6	10	4.6	10	10
Column length (mm)	150	150	100	150	100	150	150	100
Manufacturer	Dionex			Phenomenex		Phenomenex		Merck

3.1.2.2 Instrumental Setup

Preparative HPLC-UV runs were performed using a preparative HPLC system (Dionex, Germering, Germany) consisting of a binary semi-preparative high-pressure gradient pump (Model P680P HPG-2), a helium degassing unit, a semi-preparative autosampler (Model ASI-100P), and a diode array detector (Model UVD340U PDA) with a semi-preparative detector cell (6 µl cell volume, 2 mm path length).

Analytical HPLC runs were performed on an analytical HPLC system comprising a binary analytical high-pressure gradient pump (Model Summit P680A HPG-2), a degassing unit (Model Degasys DG-1210), an analytical auto-sampler with integrated temperature control (Model Summit ASI-100T), and a diode array detector (Model UVD340U PDA) with an analytical detector cell (10 µl cell volume, 9 mm path length). Both HPLC systems were fully controlled by Chromeleon software.

3.1.2.3 Conditions for the Engelhardt Test

The substances of the simplified Engelhardt test and their concentration are as follows: uracil (20 mg/L), phenol (200 mg/L), p-ethylaniline (160 mg/L), toluene (1500 mg/L) and ethylbenzene (1500 mg/L). The following conditions were used: eluent methanol/water 49:51 (w/w), flow rate 1.0 mL/min for analytical columns (4.6 mm i.d.)

and 4.7 ml/min for semi-preparative columns (10 mm i.d.), temperature 40 °C using a column oven for analytical columns or 23 °C using room temperature control for semi-preparative columns, injection 10 µL for analytical columns and 47 µl for semi-preparative column, detection at 254 nm.

Peak asymmetries were calculated according to USP at 5% peak height using the following formula: $A_s=(a+b)/2a$, where a and b are the left and right peak widths at 5% peak height.

3.1.2.4 Conditions for Standard Tests with Amitriptyline

Conditions for Dionex column specification test:

Sample solution: amitriptyline at 240 mg/L dissolved in mobile phase, injection: 5 µL for analytical column; 25 µL for semi-prep column, mobile phase: 80% methanol, 20% phosphate buffer 0.03 M, pH 6.0 (v/v), flow rate: 1 mL/min for analytical scale; 4.7 mL/min for semi-preparative scale, temperature: 30 °C, detection: 220 nm.

Conditions for NIST test:

Chromatographic conditions in this modified NIST test is described elsewhere [7]. Injection: amitriptyline at 2800 mg/L dissolved in mobile phase; 2 µL analyte for analytical column; 10 µL analyte for semi-prep column, mobile phase: 80% methanol, 20% phosphate buffer 0.02 M, pH 7.0 (v/v), flow rate: 1 mL/min for analytical scale; 4.7 mL/min for semi-preparative scale, temperature: 23 °C, detection: 210 nm.

Conditions for Waters test:

Injection: 5 µL amitriptyline at 100 mg/L dissolved in mobile phase, mobile phase: 65% methanol, 35% phosphate buffer 0.02 M, pH 7, flow rate: 1 mL/min, column oven temperature: 23 °C, detection: 254 nm

Retention study for amitriptyline using different mobile phases

Buffers were prepared for pH 6.0, 7.0 and 8.0 using phosphate, pH 3.0 using either TFA or phosphate, pH 4.0 and 5.0 using either phosphate or acetate, and for pH 9.0 using bicarbonate. The pH measurements were performed in the aqueous solution. The mobile phases used were methanol/buffer: 80/20 v/v or acetonitrile/buffer at different volumetric concentration. Amitriptyline was dissolved in the mobile phase. The separations were performed at 23 °C for analytical column using a column oven and for semi-preparative column at room temperature. The flow rates were set to 1 mL/min for the analytical and 4.7 mL/min for the semi-preparative column dimension.

3.1.3 Results and Discussion

3.1.3.1 Engelhardt Test

The test mixture according to the Engelhardt test contained the substances uracil (inert marker), phenol (probing polar properties), p-ethyl aniline (weak base probing silanol properties, is commonly used to determine peak asymmetry as a measure for silanol activity), toluene (hydrophobic properties), ethyl benzene (hydrophobic properties, in combination with toluene used to determine methylene group selectivity). Peak symmetry was determined according to USP at 5% peak height.

To assess the chromatographic performance of the columns in detail, the results of Engelhardt are listed in Table 3.2. The analytical columns were tested at 40°C and the semi-preparative columns at 23°C. The Luna analytical column was evaluated at 40°C and 23°C, in order to compare the values at both temperatures and with the Luna semi-preparative column.

Results obtained for tests at 40°C shows that the retention factors of phenol (hydrophilic compound) were similar except on the polar column Synergi Polar-RP (Table 3.2). The hydrophobic compounds toluene and ethylbenzene eluted earlier on Luna 5 µm analytical than on Acclaim 5 µm analytical column. This indicated that the Luna analytical column exhibited less hydrophobicity than the Acclaim 5 µm. The retention factor on Acclaim 3 µm analytical column was also smaller (i.e. less hydrophobicity) than the 5 µm analytical. The difference between these two Acclaim columns could be due to different bonding density, carbon load and packing density. On both polar Synergi Polar-RP columns, all compounds eluted earlier than on other packed columns. This could be attributed to reduction of the hydrophobicity by the embedded polar group [13,23].

The retention factors of the hydrophobic compounds (toluene and ethylbenzene) at 23°C on both analytical and semi-preparative Luna columns were identical. The retention factor of these compounds on the Acclaim 5 µm semi-preparative column was smaller than on the Luna columns. However, the analytical Acclaim 5 µm column exhibited more hydrophobicity than the Luna analytical column (measured at 40°C). This means that the Acclaim 5 µm analytical column exhibited more hydrophobicity than the semi-preparative dimension. It indicated that both columns were packed from different batches. This is also demonstrated by different peak asymmetries of p-ethylaniline of both columns. However, the methylene selectivity ($\alpha_{EB/T}$) of all Luna and Acclaim columns was similar.

The peak asymmetry of p-ethylaniline with both Luna columns and Synergi analytical column was similar (Table 3.2). Peak asymmetry values of p-ethylaniline <1.3 qualify these phases as a material with low silanol activity. However, peak asymmetry with Synergi semi-preparative column was pronounced, though the manufacturing date revealed that both Synergi columns were packed from the same batch. The peak asymmetry obtained with both Acclaim analytical columns was also remarkably higher than the other analytical columns, indicating a higher residual silanol activity of Acclaim analytical columns. The value obtained with the 5 μm material column was slightly higher than that of the 3 μm material. This is remarkable, as generally 3 μm materials exhibited higher sensitivity (peak asymmetries) against bases like p-ethylaniline [2].

The value of separation factor $\alpha_{P/T}$ (the k ratio of phenol and toluene) is a measure for the polar selectivity of stationary phases. It is obvious that the polar selectivity of both Acclaim analytical columns was similar and smaller than the polar property of the Luna analytical column (Table 3.2). As expected, the Synergi Polar-RP columns exhibited the highest polar selectivity. The methylene selectivity ($\alpha_{EB/T}$ - the k ratio of ethylbenzene and toluene) with all columns was identical (1.9) except for Synergi columns.

The semi-preparative silica-based monolithic RP-column (Monolith) exhibited lower retention for all compounds compared to packed columns due to its higher column porosity. However, the polarity and the methylene selectivity were comparable to other classical RP-columns.

Concerning peak efficiency, the substances with small or no retention exhibited lower plate numbers which indicates extra column band broadening. This evidently accounted for almost all columns. The effect was more pronounced on the semi-preparative setup than on the analytical. The peak of p-ethylaniline of both analytical Acclaim columns shows a remarkably low efficiency compared to the other analytical columns, due to the high peak asymmetry. The plate number ratio between both materials, however, follows exactly the theoretical prediction (theoretical: $N_{3\mu\text{m}}/N_{5\mu\text{m}} = 5/3=1.67$, obtained value: 1.65). With all peaks of higher retention (toluene and ethylbenzene), where the instrumental influence should be negligible, the 3 μm is more efficient than theoretically expected ($N_{3\mu\text{m}}/N_{5\mu\text{m}} > 1.82$). From these relations it is obvious that the 3 μm material is packed more efficiently. The plate numbers on the Luna analytical column are generally slightly higher than on Acclaim 5 μm . In the

semi-prep scale, however, Acclaim showed better efficiency than Luna for late eluting peaks.

In terms of efficiency for later eluting purely hydrophobic substances (toluene in Engelhardt test), good properties ($H/dp < 3.5$) were found for all columns tested (see reduced plate heights in Table 3.2). However, the 5 μm analytical column showed a slightly smaller efficiency.

Figure 3.1 shows chromatograms of the Engelhardt test applied to the columns (only test from 2 RP columns are shown).

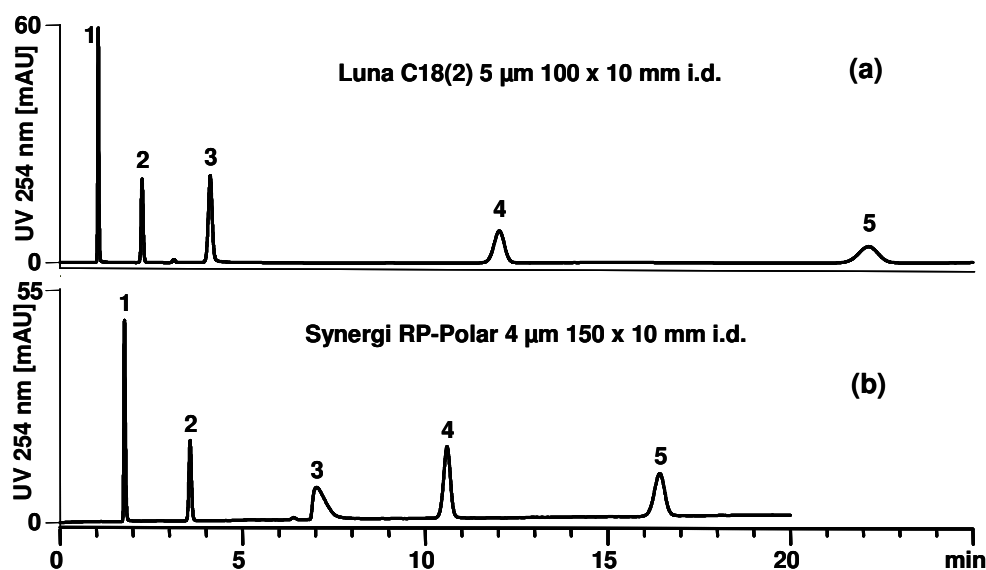


Figure 3.1: Chromatograms of Engelhardt mixture on (a) Luna C18(2) 5 μm 100 x 10 mm i.d. column, (b) Synergi Polar-RP 4 μm 150 x 10 mm i.d. column; mobile phase: water/methanol 51/49 (w/w); temperature 24°C. Peak identification: 1, uracil; 2, phenol; 3, p-ethylaniline; 4, toluene; 5, ethylbenzene.

Table 3.2: Engelhardt test at 40 °C and 25 °C

Column	k_{phenol}	k_{Toluene}	k_{EB}	$\alpha_{\text{P/T}}$	$\alpha_{\text{EB/T}}$	A_s (p-EA)
Synergi Polar-RP 4.6 mm i.d., 40 °C	0.7	3.4	5.4	0.21	1.6	1.2
Acclaim 3 μm 4.6 mm i.d; 40 °C	0.9	8.3	15.4	0.11	1.9	2.2
Acclaim 5 μm 4.6 mm i.d; 40 °C	0.9	9.1	16.9	0.10	1.9	2.4
Luna 2 5 μm 4.6 mm i.d; 40 °C	0.9	7.8	14.5	0.12	1.9	1.1
Luna 2 5 μm 4.6 mm i.d; 25 °C	1.0	10.5	20.0	0.10	1.9	1.2
Luna 2 5 μm 10 mm i.d; 25 °C	1.1	10.4	20.2	0.11	1.9	1.1
Acclaim 5 μm 10 mm i.d; 25 °C	1.0	10.1	19.2	0.10	1.9	1.5
Synergi Polar-RP 10 mm i.d.; 25 °C	1.0	5.0	8.3	0.20	1.7	2.7
Monolith 10 mm i.d.; 25 °C	0.4	3.8	7.1	0.11	1.9	1.6
	Plate number per meter column					Efficiency (H/dp)_T
	Uracil	Phenol	p-EA	Toluene	EB	
Synergi Polar-RP 4.6 mm i.d., 40 °C	39,373	69,493	76,700	91,593	87,553	2.7
Acclaim 3 μm 4.6 mm i.d; 40 °C	29,349	77,987	48,168	122,159	110,959	2.7
Acclaim 5 μm 4.6 mm i.d; 40 °C	38,613	73,427	29,253	67,173	59,487	3.0
Luna 2 5 μm 4.6 mm i.d; 40 °C	29,240	64,813	77,047	86,847	79,173	2.3
Luna 2 5 μm 4.6 mm i.d; 25 °C	30,053	61,693	53,400	90,153	84,607	2.2
Luna 2 5 μm 10 mm i.d; 25 °C	16,310	44,840	33,480	76,070	69,300	2.6
Acclaim 5 μm 10 mm i.d; 25 °C	16,910	39,320	43,230	77,780	77,000	2.6
Synergi Polar-RP 10 mm i.d., 25 °C	57,907	82,040	12,207	100,720	100,160	2.5
Monolith 10 mm i.d.; 25 °C	17,470	27,720	50,880	100,170	109,060	-

EB=ethylbenzene, P=phenol, T=toluene, p-EA=p-ethylaniline

3.1.3.2 Standard Test with the Strong Base Amitriptyline

Amitriptyline is a strongly basic (tertiary amine) antidepressant drug with aqueous pK_a of 9.4 [24]. This compound is a representative of basic pharmaceutical which is widely used for column test purposes. The elution characteristics of amitriptyline represent the column activity towards organic bases. Elution of organic bases with severe peak tailing is often associated with high silanol activity [6,7,21]. However, the elution of such compounds with symmetrical peak shape is considered indicative of silanol deactivation [7]. Because peak tailing is the characteristic associated with silanol activity, asymmetry factor A_s is a measure of this property [7]. Unlike the conditions in the Engelhardt test, the tests using amitriptyline (NIST, Dionex, Waters) require a buffered eluent.

The pronounced p-ethyl aniline peak asymmetry of the tested Acclaim analytical columns in the Engelhardt silanol test gave rise to further studies on the behavior of the Acclaim and Luna columns with the basic compound amitriptyline.

With the Waters test, no elution of amitriptyline was observed up to a retention factor of 10 for Acclaim and Luna columns. A gradient program following the isocratic step (Waters conditions) enabled elution at 80 % methanol. A reasonable explanation for this late elution can be found in strong hydrophobic interactions, which is in good agreement with results of the Engelhardt test. Hence, the Waters test cannot be considered for the discussion of column base behavior.

The most important results obtained by Dionex and NIST tests compared to the Engelhardt test are summarized in Table 3.3. The reported results from the Engelhardt test monitor column efficiency (reduced plate height of toluene) and the silanol activity (asymmetry of p-ethylaniline).

For all columns, the peak asymmetries obtained with the Dionex test were satisfying. It did not reveal significant silanol activity with the Acclaim columns. The peak asymmetry obtained with the NIST test for 5 μm Acclaim and Luna material columns was satisfying. These columns could be classified as columns with low silanol activity towards organic bases. Under NIST and Dionex conditions, the 3 μm analytical Acclaim column showed higher asymmetry than the 5 μm column (in case of NIST highly significant) which is in contradiction to the results obtained with the Engelhardt test. When the ratios of the $A_{s\text{amitriptyline}}$ for all Acclaim columns are considered, they are not consistent between Dionex and NIST conditions. This can most likely be related to different pH behaviour of the 3 materials. The excellent behaviour of the

Acclaim 5 μm semi-prep column exhibited in the Engelhardt test could not be confirmed with tests using the strong base amitriptyline.

The results obtained with Luna columns under Engelhardt, DIONEX and NIST tests were consistent and comparable between both dimensions. Both materials provided identical chromatographic properties. It appears that the columns were packed from the same batch, as also claimed by the manufacturer.

Table 3.3: Comparison of the results of standard column tests for Acclaim and Luna columns.

	Acclaim 3 μ 4.6 mm	Acclaim 5 μ 4.6 mm	Acclaim 5 μ 10 mm	Luna 5 μ 4.6 mm	Luna 5 μ 10 mm
Asymmetry (AMI)					
DIONEX	1.4	1.3	1.4	1.2	1.2
NIST	2.1	1.4	1.4	1.4	1.3
Engelhardt Test					
Efficiency: (H/dp) _{toluene}	2.7	3.0	2.8	2.4	2.6
Asymmetry p-ethylaniline	2.2	2.4	1.5	1.1	1.1

3.1.3.3 Variation of Conditions from the Standard Base Test Procedure

Methanol and acetonitrile are the common mobile phases used in RP-HPLC [2]. The retention of basic compounds is highly dependent on the mobile phase and the buffer pH [16,25]. Therefore, retention of amitriptyline was investigated extensively in both mobile phases at different pH values. The study of pH influence should enable an interpretation of the different test results and moreover provide data to find optimum conditions for the application of the column materials in a semi-preparative purification system.

3.1.3.3.1 Variation of pH values in methanol eluent

To give an impression of the peak shape at low and increased sample loading and

the retention shift with differing pH values adjusted with phosphate and TFA, all chromatograms are overlaid in Figure 3.2 and Figure 3.3. The pH was measured in the aqueous buffer prior to addition of the organic solvent. Figure 3.2a shows the chromatogram for the Acclaim 3 μm column at low sample loading (1.2 μg). It shows the pronounced decrease of retention when the pH was reduced from 7.0 to 5.0. The peak heights differ markedly, due to the altering peak shape. Between pH 7.0 and 6.0, no marked difference in peak shape occurred at low sample load. At pH 5.0, the poorest peak shape with fronting asymmetry was encountered. The sharpest and most symmetrical peaks were obtained at pH 4.0 and pH 3.0, however at very low retention ($k < 1$). The retention at pH 3.0 and pH 4.0 with phosphate buffer was identical. At low sample load (1.2 μg), the retention decreased upon a change from phosphate to TFA and the peaks mutated from tailing to leading, but became sharper at half peak height.

Figure 3.2b shows the same set of experiments and additionally with 5 mM phosphate buffer performed at higher sample load of 14 μg for all pH values, except 5 μg for pH 5.0. At this sample load, a regular peak shape was achieved at pH 7.0 with 20 mM phosphate buffer. However, at buffer concentration lower by factor of 4 and at 20 mM phosphate pH 6.0, a fronting shoulder was observed at this high sample load. The peaks obtained at pH 5.0 and 4.0 exhibited extreme leading and very low efficiency, even at sample load of 5.0 μg . With phosphate at pH 3.0, a decrease of retention with increasing loading occurred, whilst with TFA retention increased weakly and a front shoulder appeared.

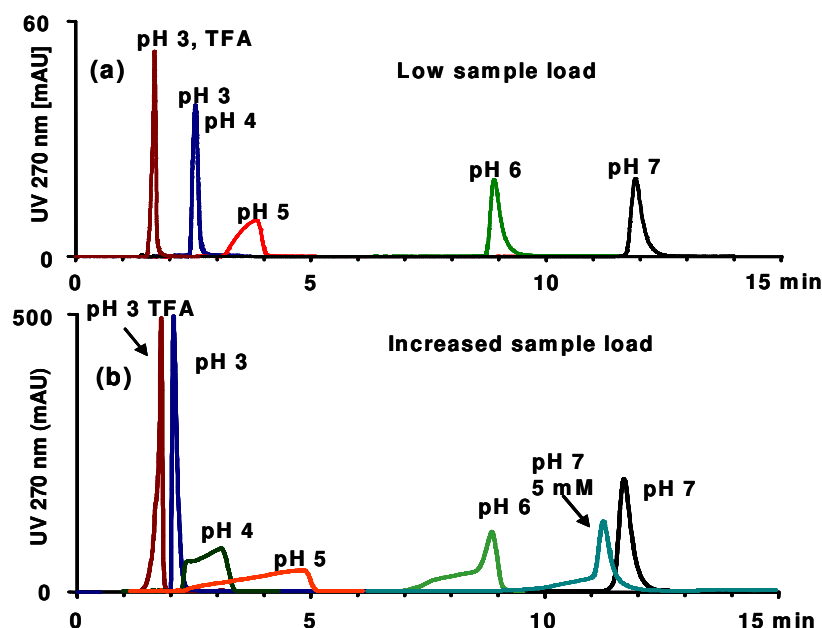


Figure 3.2: Overlay of amitriptyline peaks on the Acclaim 3 µm column at different pH values. Influence of eluent pH on amitriptyline retention and peak shape (a) At low sample load (1.2 µg), eluent: 20% phosphate buffer at 20 mM pH 3.0-7.0 and TFA pH 3.0 and 80 % methanol, (b) At increased sample load (14 µg or 5 µg for pH 5.0), eluent: 20% phosphate buffer 20 mM at pH 3.0-7.0, phosphate buffer 5 mM at pH 7.0 and TFA pH 3.0, 80 % methanol.

Figure 3.3 illustrates the peak shape under low sample load for the Luna 5 µm analytical column (Figure 3.3a) and the semi-preparative column (Figure 3.3b). The elution conditions for the analytical column were 80% methanol and 20 mM phosphate buffer at pH 4.0 to 7.0 and 23°C. The peak shapes were similar to the results obtained with Acclaim 3 µm column material. The difference was only found at pH 6.0. On the Luna, the peak moved to fronting.

The elution conditions for amitriptyline on the Luna semi-preparative column were 80% methanol and 20% either phosphate buffer for pH 3.0, 6.0 and 7.0 or acetate buffer for pH 4.0 and 5.0 or bicarbonate buffer for pH 9.0 (Figure 3.3b). The peak shape obtained for all pH values was excellent. However, the retention for pH 3.0-5.0 was very low ($k < 1$), similar to the results with other columns. The peak at pH 6.0 shows a fronting, as observed in the Luna analytical column, indicating the presence of ionic interaction besides hydrophobic interaction. The retention behavior at pH 7.0 and 9.0 was nearly identical. This indicates similar retention mechanisms occurring at both pH values. At pH 9.0, a small part of amitriptyline exists charged and the

residual silanols exist mostly charged, both retention mechanisms (hydrophobic and ionic interactions) could occur. Much stronger hydrophobic interactions can be expected with the uncharged species.

As can be seen in Figure 3.3b, elution of low mass amitriptyline at pH 4.0 and 5.0 using acetate buffer showed symmetrical peaks. The distorted peaks observed on both Luna and Acclaim columns with phosphate buffer at these pH values (Figure 3.2a and Figure 3.3a) can be attributed to insufficient buffering ability of phosphate at these pH values, since the $pK_{a,1}=2.0$ and $pK_{a,2}=7.1$, whilst buffering capacity is in the range of $pK_{a}\pm 1$ with the highest buffer capacity at pH equal to pK_{a} .

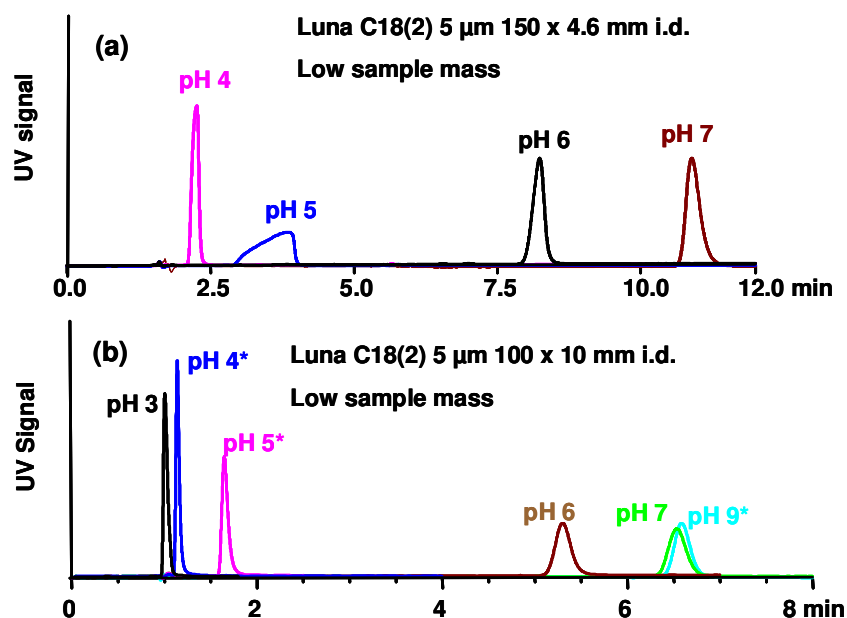


Figure 3.3: Overlay of amitriptyline peaks on the Luna 5µm columns at different pH values. Influence of eluent pH on amitriptyline retention and peak shape (a) On Luna 5 µm analytical column at low sample load (1.2 µg), eluent: 20% phosphate buffer at 20 mM pH 4.0-7.0 and 80 % methanol, (b) On Luna 5 µm semi-preparative column at low sample load (10 µg), eluent: 20% phosphate buffer at 20 mM for pH 3.0, 6.0 and 7.0 or acetate buffer for pH 4.0 and 5.0 and 80 % methanol. (*) Acetate buffer.

Figure 3.4 shows the plot of the retention factor depending on the pH values for aqueous methanol (20 mM buffer/methanol: 20/80) on the Luna semi-preparative column, Luna analytical and Acclaim 3 µm analytical column. This plot showed the

common retention mechanism of a basic compound on Type B RP columns [8]. On all three columns, it exhibited no or small retention at pH 3.0 to 5.0. The decrease in retention with decreasing pH can be attributed to suppression of silanol dissociation (pK_a silanol ~ 7) and thus smaller contribution of cation exchange to retention. At the same time the degree of analyte protonation increases and its hydrophobic retention becomes smaller. The pK_a of amitriptyline in water should be 9.4 [24]. Under purely aqueous conditions, less than 1% of amitriptyline should exist as free base at pH 7, which will not be alike at the given 80 % methanol content. The concept of pH and pK_a in aqueous–organic mixtures has become better understood. In general, the pK_a of acids increases as the organic solvent concentration increases whilst the pK_a of bases decreases compared with their values in aqueous solution [26,27,28]. Thus, in phosphate buffers the pH of aqueous–organic mixtures is raised, while the pK_a of basic solutes is lowered which both lead to less solute protonation than would be expected in a purely aqueous solution. To understand the retention mechanisms of basic compounds, it is necessary to know the pH of mobile phase, the pK_a of the compound in the mobile phase, and the pK_a of the residual silanols in the mobile phase [29].

The retention on Luna semi-preparative column at pH 7.0 to 9.0 is identical. It evidenced a sigmoidal plot with inflection point at pH 5.6. This inflection point is the so-called apparent pK_a [8] or chromatographic pK_a ($pK_{a,chrom}$) [30]. At a pH value equal to the inflection point the solute is to 50% dissociated (under this given chromatographic condition). The $pK_{a,chrom}$ depends on the pK_a of the buffer and of the solute in mobile phase [30].

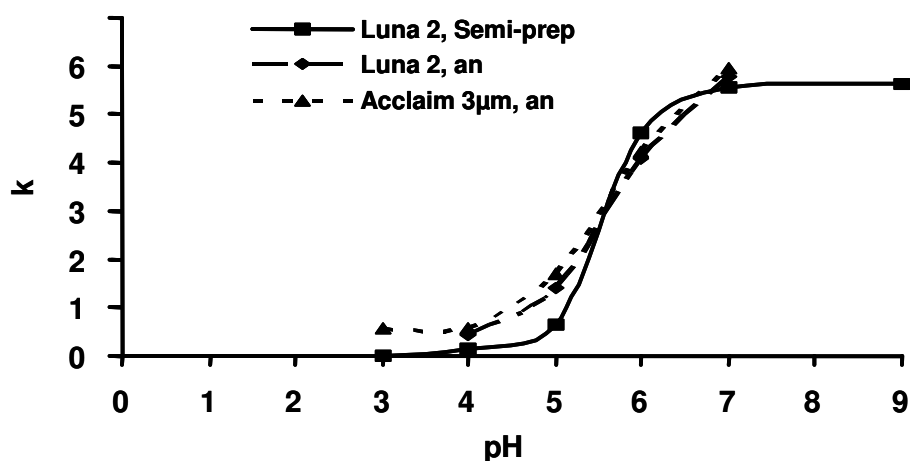


Figure 3.4: Dependence of the retention on the pH values

3.1.3.3.2 Retention behavior and peak shape for amitriptyline with acetonitrile eluents

Obviously, the solvating properties of the eluent have a significant influence on the chromatographic behavior of amitriptyline. As acetonitrile has several properties which differ from methanol – it is aprotic, has no hydrogen donor capacity and is less polar – the investigation of the retention of amitriptyline using acetonitrile as organic solvent is another point of interest. Moreover, acetonitrile eluent could be favorable particularly in preparative HPLC with APS due to its lower viscosity. In order to compare the results obtained with methanol eluent to those with acetonitrile and to optimize the elution conditions for loading capacity studies, the retention factors of the strong base amitriptyline were measured on Acclaim 3 μm analytical column at different eluent pH values and different acetonitrile concentrations and on Luna 5 μm semi-preparative column at different acetonitrile concentrations at pH 7.0. This pH is in the region of the average pKa of silanol groups on silica-based phases [31].

The results obtained with the Acclaim column are shown in Figure 3.5. Figure 3.5a shows the dependence of $\ln k$ on the acetonitrile content for different pH values. Using a 10 mM phosphate buffer, the deviation from a linear correlation of $\ln k$ versus % ACN was more pronounced at lower pH values. At the same time the slope of the fit increased significantly from pH 7.0 to pH 6.0. With 20 mM acetate buffer at pH 5.5 the strongest deviation from linearity was observed. Figure 3.5b depicts the dependence of $\ln k$ on eluent pH for different ACN percentages. At pH 7.0 with 30% acetonitrile the retention factor was higher than 8. The curves at 40 % and 50 % represent a pronounced increase in retention from pH 6.0 to pH 7.0.

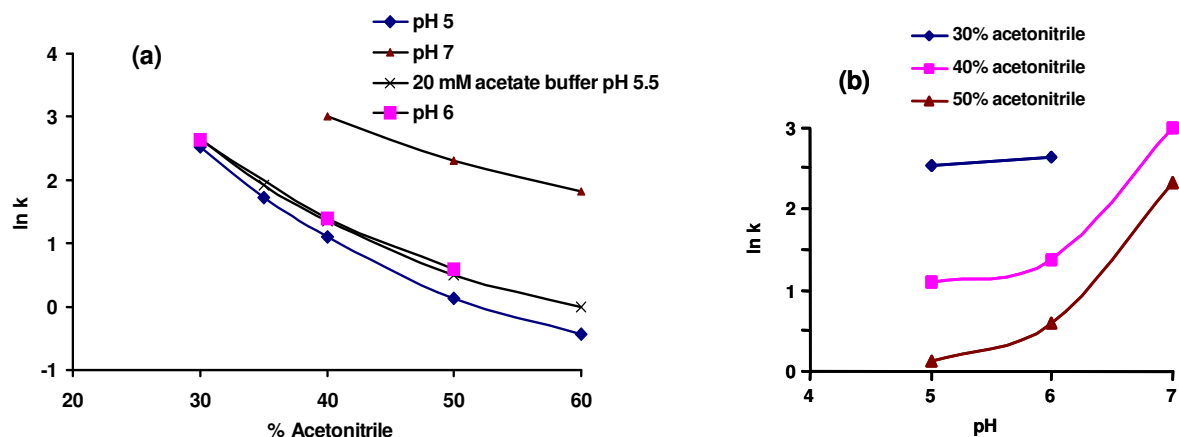


Figure 3.5: Dependence of amitriptyline retention on acetonitrile content for different eluent pH values on Acclaim 3 μm analytical column. Column oven temperature was set to 38 $^{\circ}\text{C}$, flow rate at 1 mL/min.

Figure 3.6a demonstrates the retention of amitriptyline in 20 mM phosphate buffer pH 7.0 – acetonitrile in different acetonitrile content measured on the Luna 5 μm semi-preparative column. Similar retention behavior as on the Acclaim 3 μm analytical column was observed, as depicted in Figure 3.5a. The curve of purely hydrophobic retention in logarithmic scale vs. organic modifier contents should exhibit linear plot for k values between 1 and 15 [32]. A non-linear curve can be attributed to the presence of ionic interactions of the analyte with the residual silanols of the stationary phase at pH 7.0. At this pH, the basic solute amitriptyline exists partly protonated and partly as free base. Heinisch et al. reported similar results performed on a XTerra-MS column [30]. However, they suggested that the ionic interaction of the protonated solute with residual silanols is not the reason for this phenomenon. They explained this rather with a compensation of two effects, the decrease of retention due to lower hydrophobic interaction on the one hand and an increase in retention due to a reducing dissociation rate of the solute on the other hand [30].

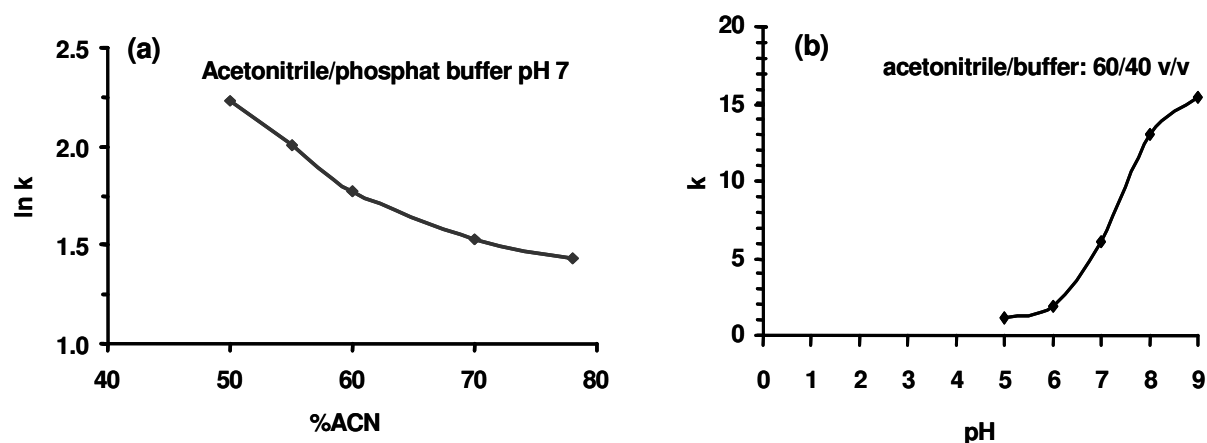


Figure 3.6: Dependence of amitriptyline retention on pH at different ACN concentrations measured on Luna 5 μm semi-preparative column.

The retention behavior of amitriptyline in the acetonitrile-aqueous mobile phase (Figure 3.6b) is different from that in the methanol mobile phase (Figure 3.4). With the acetonitrile mobile phase at pH 9, the retention increased up to 3-fold compared to that with the methanol mobile phase. The inflection point was determined to be at pH 7.3 (calculated by Origin) compared to this with methanol at pH 5.6 (Figure 3.4). The difference could be due to different nature of the organic modifiers and also its different concentration in the mobile phase, since these can have different effects on the mobile phase pH and thus different protonation of the compound.

IUPAC recommended three definitions of the pH scales: ^w_pH (the pH is measured in the aqueous buffer before mixing it with the organic modifier), ^s_pH (the pH is measured after mixing the aqueous buffer with the organic modifier, but the pH calibration is performed with the common aqueous reference buffers), and ^s_pH (the pH is measured in the mobile phase solvent with the pH electrode calibrated with the buffer from the same solvent composition), respectively [33]. The measured ^s_pH for a mobile phase containing aqueous phosphate buffer pH 7.0 – methanol: 20/80 v/v was 9.0 and for aqueous phosphate buffer pH 7.0 – acetonitrile: 40/60 v/v was 8.0. These values are in accordance with the values obtained by Rosés et al. [26,27,28] and Heinisch et al. [30].

Table 3.4 lists the retention data, the theoretical plates in peak half height (N), the peak width at 10% peak height ($w_{0.1}$), and the asymmetry factor at 10% peak height (A_s) at low sample loading (10 μg) with methanol and acetonitrile eluents measured

on the Luna 5 μm semi-preparative column. With methanol eluent, the best efficiency was obtained at pH 7.0 and pH 9.0. The 80% methanol-phosphate buffer pH 7.0 eluent was isoelutrop to the 60% acetonitrile-phosphate buffer eluent for amitriptyline. The normal range for isoelutropic condition between aqueous acetonitrile and methanol is approx. 10% [2]. It is obvious that the peak parameters with methanol mobile phase were generally superior to that with acetonitrile. The asymmetry factors obtained with acetonitrile were higher. This is in accordance with the results reported by McCalley et al. [13]. The peak parameters at pH 9.0 with 60% acetonitrile mobile phase were better than at pH 8.0. This might be due to the dominance of hydrophobic retention at pH 9.0, because amitriptyline is mostly unprotonated. However, the retention factor obtained with pH > 7 was higher than 10.

Table 3.4: Peak shape parameter for amitriptyline on the Luna semi-preparative column at low sample load with methanol and acetonitrile eluents.

	k	N	w_{0,1}(min)	As₀ at 10% pw
Methanol/ 20 mM buffer:				
80/20 v/v				
pH 3	0.0	2430	0.10	2.6
pH 4	0.2	4820	0.08	1.8
pH 5	0.7	3020	0.15	1.9
pH 6	4.6	4600	0.35	1.3
pH 7	5.6	6440	0.36	1.4
pH 9	5.6	6563	0.36	1.2
Acetonitrile/20 mM buffer				
pH 7 50% ACN	9.5	1645	1.12	3.2
pH 7 55% ACN	7.4	1998	0.83	3.4
pH 7 60% ACN	5.9	2328	0.64	3.5
pH 7 70% ACN	4.6	3478	0.43	3.6
pH 8 60% ACN	13.1	3099	1.17	5.1
pH 9 60% ACN	15.4	5768	0.86	2.0

The efficiency and peak shape obtained on the Acclaim analytical column with acetonitrile eluent are plotted in Figure 3.7. The plate numbers at different eluent conditions are depicted in Figure 3.7a, the peak asymmetry values in Figure 3.7b. A trend towards improved peak shape with increased organic content is obvious. This behavior was not observed with Luna (Table 3.4). Increasing pH values also enhance plate numbers and asymmetry factors in most cases. At pH < 6, no acceptable peak efficiency could be obtained, no matter which ACN content was used. At pH 6.0, a tremendous increase of plate number (factor 10) occurred between 40 and 60% ACN. At pH 7.0, the efficiencies are generally high. In spite of the higher plate number with acetate buffer relative to the results with phosphate at pH 5, the peak asymmetry values using acetate were not acceptable (smallest value higher than 4).

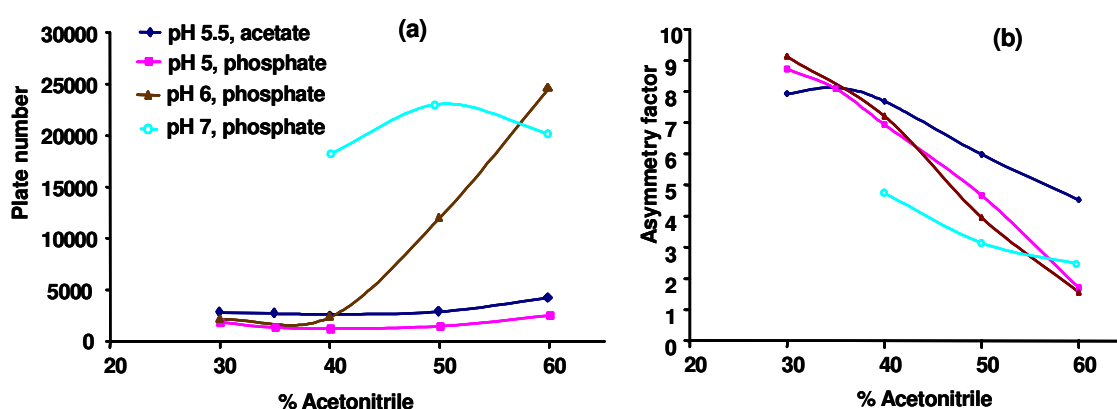


Figure 3.7: Peak efficiencies for amitriptyline under different eluent conditions

3.1.4 Conclusions of Stationary Phase Characterization

The comparative standardized column tests proved a similar performance of the semi-prep Acclaim column relative to the semi-prep Luna column. Acclaim was slightly superior in plate numbers, Luna was slightly superior with respect to overall peak symmetry. The retention factors were very similar with both columns. Luna semi-prep was slightly advantageous for silanol activity, both columns showed nevertheless satisfying properties with all three different tests (Engelhardt, NIST, Dionex tests).

Luna analytical and semi-preparative columns provided similar chromatographic

properties, as shown in the results obtained with all three different tests. However, marked differences in retention factors and silanol activity were encountered between the analytical and semi-prep columns for Acclaim columns. This would hamper a straightforward method scale-up due to resulting difference in selectivity. Furthermore, the silanol activity results obtained with three different tests were inconsistent.

Retention studies show the different influence on the retention of strong organic bases like amitriptyline using methanol and acetonitrile as eluent. This could be due to the nature of the organic modifier or due to different content of aqueous buffer in both eluents, which are 20% in methanol mobile phase and 40% in acetonitrile mobile phase. At pH 7.0, both eluents were iso-elutrope with respect to amitriptyline. From the results of the variation of acetonitrile concentration, a pronounced advantage of higher organic content and neutral pH values can be deduced with respect to peak shape parameters for amitriptyline. At pH 7, lower ACN contents than 60 % also enable reasonable chromatographic conditions, but as the retention factor was quite high, these conditions are not favorable for experiments with the purification system.

3.2 Column Loadability Study

3.2.1 Introduction

The primary goal of the separation in analytical chromatography is identification and quantification of compounds, whilst preparative chromatography aims at the production of a single purified compound and using it for a further goal [34, 35]. The most preferred approach is to maximize the preparative load without a compromise in the purity of the collected fractions [36].

There are two different types of column loadability, namely volume overloading and mass overloading [36]. Volume overloading is normally applied for compounds with lower solubility. At low injected sample volume, the peak shapes are symmetrical. With increasing sample volume the peak becomes broader and forms a rectangle whilst the peak shape remains symmetrical. Under overloading condition the peak height remains constant and therefore forms a plateau.

The column mass loadability varies widely with the nature of the compound [34]. Different loadability was found between the non-ionic and the ionic form of an ionizable compound [34]. The loadability depends also on the physicochemical parameters of the chromatographic system, such as the chemical nature of the mobile and stationary phases [1]. A traditional way to optimize the load of a multi compound mixture is to increase the injected sample mass until the two peaks touch. This is so called touching-band optimization.

The mass loadability of a non-ionized compound can be described by simple adsorption isotherms such as the Langmuir isotherm [34,36]. Figure 3.8 shows the Langmuir isotherm and the changes of the peak shape with increasing sample load. As can be seen in Figure 3.8 a, at low sample load, the isotherm is linear, refers to the range of so-called linear chromatography. Under this condition, the peak shapes are symmetrical, and the retention factor, the band width, and therefore the column efficiency remain unaffected by concentration changes [36]. With increasing sample load the plot becomes curved and forms a plateau at high concentration. The plateau indicates the presence of a maximum concentration on the stationary phase (saturation capacity). The slope of the isotherm is equal to the capacity factor or retention factor k of the solute at a given mobile phase concentration. Under overloading condition the retention factor decreases with increasing sample load and

the peak maximum moves to shorter retention time, leading to right-angled triangle shapes and the end of the peak always appears at the same time (Figure 3.8b) [1,36]. The saturation capacity depends on the retention factor of the solute. This value is smaller for higher k factors, because the slope of the isotherm is steeper.

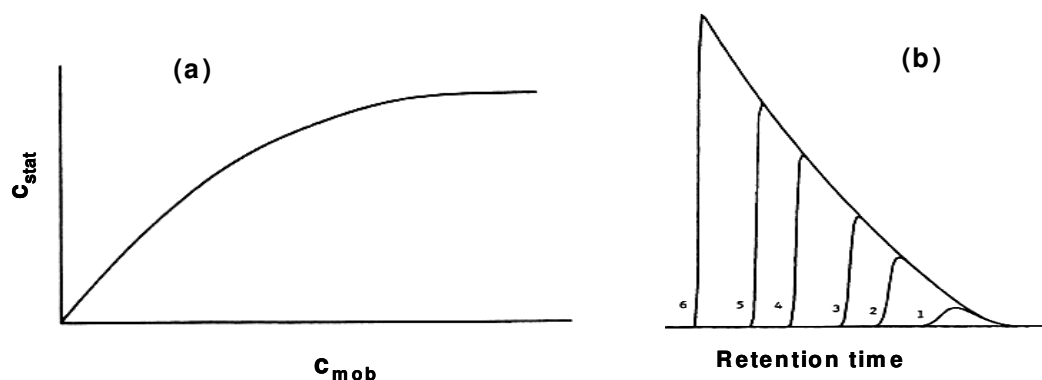


Figure 3.8: Langmuir isotherm (a) and changes of peak shape with increasing sample load (b).

The loadability of ionized compounds such as basic compounds on RP stationary phases is reported up to 50 times lower than that of the non-ionized compounds [34]. At low pH values (pH 3.0 or less) the basic compounds are fully ionized. At this pH values the ionization of silanol groups in Type B packings (columns with ultrapure silica which do not contain acidic silanols) can be suppressed. Therefore, silanol interaction cannot occur. However, rapid peak shape deterioration with increasing sample load and overloading of the stationary phase in sub microgram sample load were observed [37]. It was reported that overloading was caused by mutual repulsion of ions of the same charge on the phase surface [19,34,38].

The overloading of a variety of charged and uncharged compounds using highly inert modern RP materials was also studied by Gritti and Guiochon [39,40]. They measured the adsorption isotherm data of the compounds by frontal analysis. These data were modeled and used to calculate the adsorption energy distribution (AED). Based on these data they showed that these phases were still definitely heterogeneous, consisting of weak (type 1), intermediate (type 2), and strong (type 1) adsorption energy sites with the amount ratio 400:4:1, which could be accessed by different types of analyte. They found similar saturation capacity for charged and uncharged compounds. The overloading by very small amounts of ionized bases

reported by McCalley could be explained by the overloading of the strongest sites, while the continuing high total saturation capacity of the phase for these analytes measured by frontal analysis was due to the filling of weak sites [40]. However, results at very high loadings of ionized bases obtained by frontal analysis, which are typically 100 times higher than the empirical results, are not relevant to practitioners who require high column peak capacity (good resolution) [10]. Since the loss of efficiency occurs already at much lower mass of ionized solute [10].

To avoid overloading at low sample load, strongly basic solutes ($pK_a > 8$) can be separated at a mobile phase pH above that of their pK_a , where they exist as neutral molecules. However, the most silica-based columns are not stable for extended use above pH of 7.5 due to possible hydrolysis of the bonded phase [41].

In this part of the work, different types of the column loadability were studied for an acidic pharmaceutical compound acetylsalicylic acid. Moreover, the mass loadability for a strongly basic compound such as amitriptyline on the RP columns in semi-preparative dimension compared to the analytical dimension was studied extensively using different mobile phases. Furthermore, the mass loadability of a polar weakly acidic compound (phenol) and a neutral compound (rutin) on semi-preparative columns was also investigated in order to compare the loading capacity of the columns for different solutes.

3.2.2 Experimental

The Columns and instrumental setup used in these experiments are as described in section 3.1.2.

3.2.2.1 Chromatographic conditions

Loading capacity study for acetylsalicylic acid

The analyte was dissolved in the mobile phase. The mobile phase was 30 % acetonitrile, 70 % water titrated with formic acid to pH 3.0 (v/v). The temperature was set to 23°C. The flow rates were set to 1.3 mL/min for the analytical and 5.0 mL/min for the semi-preparative column dimension. All chromatograms were recorded at detection wavelength of 258 nm and 295 nm.

Loading capacity study for amitriptyline

Phosphate buffers (20 mM) were prepared using $\text{NaH}_2\text{PO}_4/\text{Na}_2\text{HPO}_4$. 20 mM carbonate buffer pH 9.0 was prepared using ammonium carbonate. The pH values were measured in the aqueous phase prior to addition of the organic modifier.

Loading capacity study for phenol

The analyte was dissolved in the mobile phase. The mobile phase was 30 % acetonitrile, 70 % water titrated with formic acid to pH 3.0 (v/v). The temperature was set to 23°C. The flow rate was set to 5.0 mL/min. All chromatograms were recorded at detection wavelength of 254 nm.

Loading capacity study for rutin

The mobile phase was 20 % acetonitrile/methanol (9/1 v/v), 80 % water with 0.1% formic acid. The analyte was dissolved in methanol/water with 0.1% formic acid in 50/50 v/v. The temperature was set to 23°C. The flow rate was set to 5.0 mL/min. All chromatograms were recorded at detection wavelength of 270 nm.

3.2.3 Results and Discussion

3.2.3.1 Loading Capacity Study for Acetylsalicylic Acid

Acetylsalicylic acid is a representative for acidic pharmaceutical compound. The pK_a value of this weak acid in water is 3.5. The loadability study with this compound was performed using a mobile phase containing water at pH 3 (70%) and acetonitrile (30%). At this condition, the pK_a of the compound in the mobile phase is slightly higher than the pK_a in water, since higher organic solvent concentration increases the pK_a value of acidic compounds [26,27,28]. However, organic phase content up to 20% does not change the pH of the mobile phase and the pK_a of the compound [3]. In aqueous solution at pH 3.0, 32% of acetylsalicylic acid are dissociated. In the applied mobile phase (water pH 3.0-acetonitrile 70:30 v/v) this compound is less dissociated than in water.

The aim of this work was to investigate systematically the different overloading types in the semi-preparative HPLC, such as volume overloading at constant injection sample mass, mass overloading at constant injection volume, and volume overloading at constant sample concentration.

3.2.3.1.1 Selectivity of Acclaim columns for acetylsalicylic acid and salicylic acid

In the acetylsalicylic acid purchased from Sigma, an additional peak of salicylic acid (impurity) was obtained, which was significant at a detection wavelength of 295 nm, where the impurity compound is detected 38 times more sensitive than the main solute. The UV spectra of both compounds are shown in Figure 3.9.

As can be seen in Figure 3.10, the observed selectivity (α) of acetylsalicylic acid to salicylic acid is different on all Acclaim columns. Moreover, it varies in different directions with increasing sample load. With the 3 μm material (A), a slight increase in α from 1.31 to 1.35 was encountered with increasing amount of sample. Applying the analytical column with 5 μm material (B), a clearly smaller selectivity ($\alpha=1.03$) was observed and the peaks could no longer be resolved. When the sample load was increased, the selectivity was also increased to $\alpha=1.06$ and a clear shoulder of salicylic acid appeared. From the poor resolution between the peaks and a possible displacement effect (interpretation of increasing selectivity), an impact on the determination of the acetylsalicylic acid loading capacity with the 5 μm analytical column is to be expected. As shown in Figure 3.10c, the semi-preparative column (C) exhibited the greatest selectivity for the two acids. Unlike with column A and B, its α -value dropped from 1.94 to 1.78 when the sample load was increased.

Once more, these selectivity variations confirm the already described differences in the chromatographic behavior of the three Acclaim C18 materials.

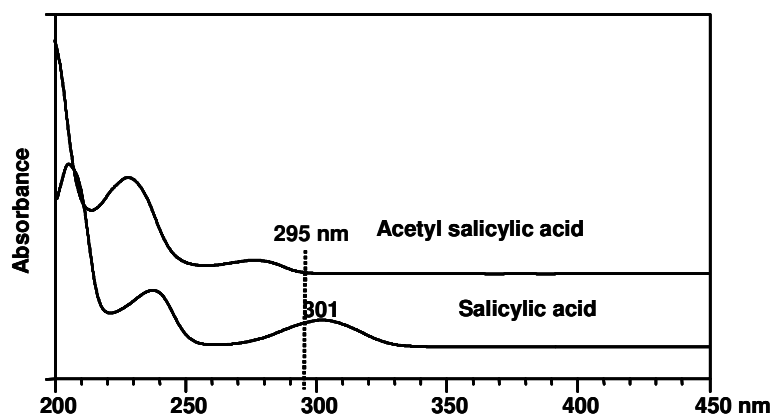


Figure 3.9: Overlay of UV spectra of acetylsalicylic acid (ASA) and the impurity salicylic acid (SA) in a solution containing 99.5% ASA and 0.5% SA

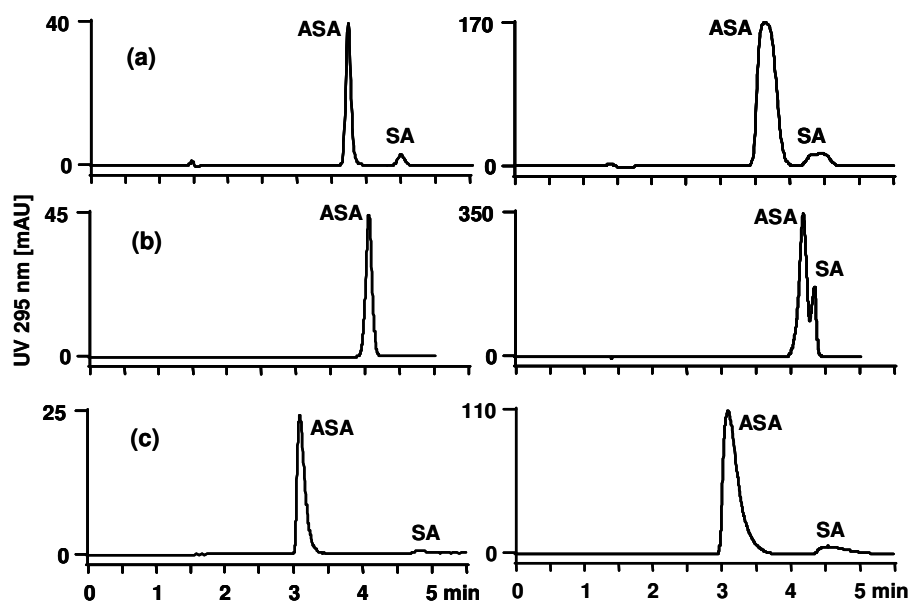


Figure 3.10: Chromatograms of acetylsalicylic acid (ASA, 1 g/L) and salicylic acid (SA) detected at 295 nm measured on three Acclaim columns, left: in non-overloading condition (10 μ L injection for analytical, 100 μ L for semi-preparative column), right: injection volume overloaded (120 μ L for analytical, 1200 μ L for semi-preparative column). (a) Acclaim 3 μ m analytical; (b) Acclaim 5 μ m analytical; (c) Acclaim 5 μ m semi-preparative dimension

3.2.3.1.2 Volume loading at constant sample mass

The aim of this study is the determination of the volume loading capacity by variation of injection volume at constant analyte mass injected on the column. The injected mass should be low in order to avoid mass overloading. This study was carried out on all three Acclaim columns, on both Luna columns and on the silica-based monolithic column (Monolith).

For attempts on the analytical 3 μ m Acclaim column, the sample mass was set to 50 μ g and 100 μ g absolute injection on column. It was verified independently that no mass overloading occurs at these levels. Since the volume loading capacity for both sample masses was similar, the study on other analytical columns was performed at sample mass of 100 μ g corresponding to 40 μ g per mL column bed. The sample mass for semi-preparative columns was set to 500 μ g absolute injection on column

corresponding to 63.7 μg per mL column bed. This is by 50 % higher than the normalized injected mass was on the analytical columns (40 $\mu\text{g}/\text{mL}$ bed). When the protocol was modified to the semi-preparative scale, the injected sample mass was adopted to the increase of the column cross sectional area (approx. factor 5) and the influence of the column length was neglected.

Overlays of the peaks are depicted in Figure 3.11 to Figure 3.13. The injection volume is indicated in the chromatogram overlays. The interpretation was made from the chromatograms detected at 258 nm, although for study on the analytical columns the extinction exceeded the common linear range of UV detectors. From the peak shapes, however, no serious detector overloading could be deduced. The areas of the peaks were equal due to the same solute mass injected on the column. The peaks started at the same point, because the start zones of the injection system in the loading and inject position are identical. With increasing volume loading, peaks became broader and therefore the peak maximum shifted to higher retention times. With the Acclaim 5 μm analytical column, the peaks at low injection volumes showed significant fronting (Figure 3.11a). This could be due to a competitive effect with the closely eluted impurity compound salicylic acid.

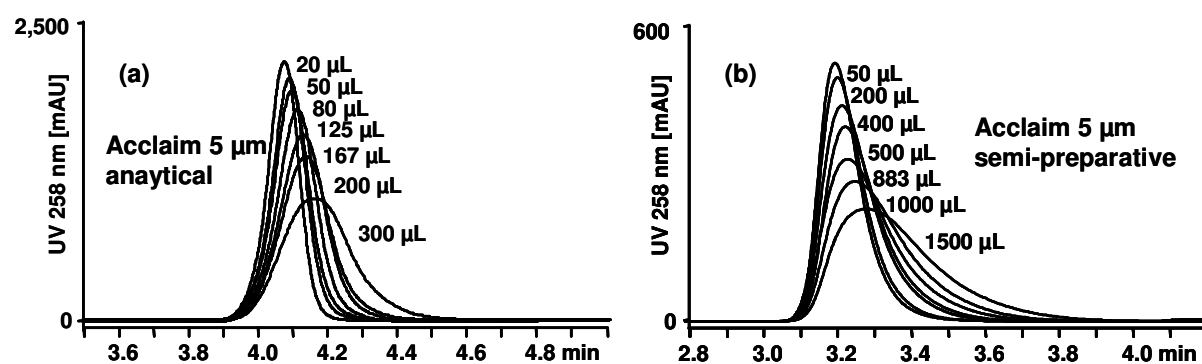


Figure 3.11: Peak overlays of 100 μg acetylsalicylic acid injected at different volumes on the Acclaim 5 μm columns.

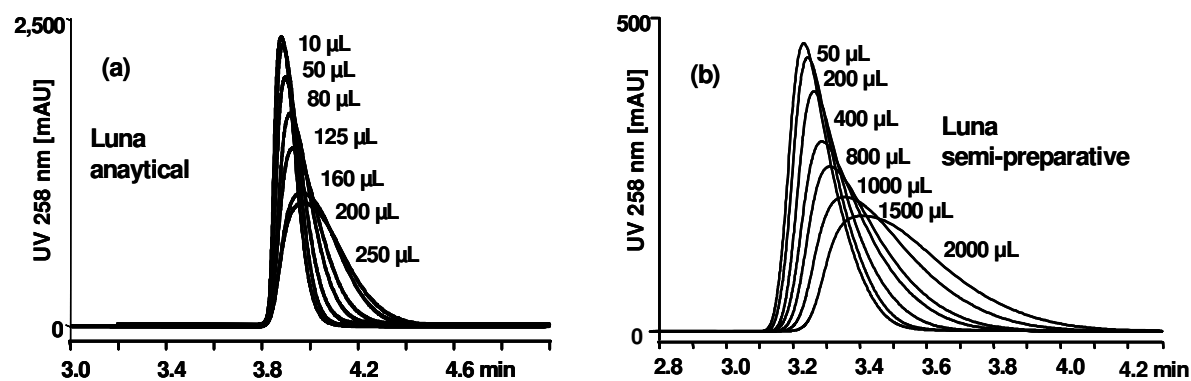


Figure 3.12: Peak overlays of 100 µg acetylsalicylic acid injected at different volumes on the Luna 5 µm columns.

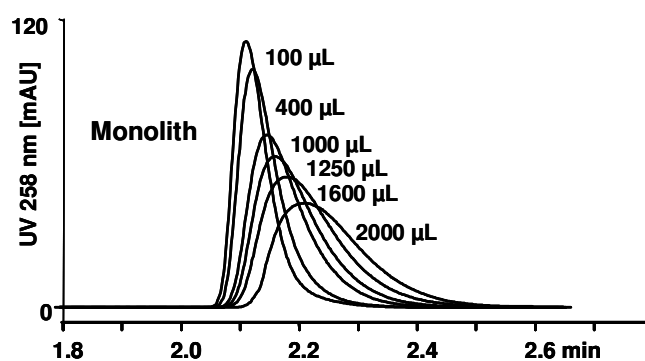


Figure 3.13: Peak overlay of 100 µg acetylsalicylic acid injected at different volumes on the silica based monolithic column (Monolith).

To interpret the results with regard to optimum volume loadability, the most critical peak shape parameter, the peak width at 10 % peak height ($w_{0.1}$), is plotted versus the normalized injection volume. The selected unit per bed volume ($\mu\text{L}/\text{mL}$) is used to compare loading capacities between different column dimensions and different stationary phase densities. The geometrical column void volume is considered as the bed volume. The optimum volume loading capacity was obtained at the volume giving a 10% increase of peak width at 10% peak height ($w_{0.1}$) compared to the value at low injection volume ($w_{0.1}$), as $w_{0.1} = 1.1 w_{0.1,0}$. The $w_{0.1}$ value is described in length unit (mm) instead of in time unit (sec or min). This unit is independent of the column flow rate and dimension.

The plots of $w_{0.1}$ depending on the injection volume for the Acclaim columns are shown in Figure 3.14a. As can be seen, the $w_{0.1}$ value at low injection volume for the

3 μm was better than for other Acclaim columns. However, the overloading occurred earlier and its slope was higher. The optimum volume loading capacity for the 3 μm Acclaim column at 50 μg sample mass was determined to be 8 μL per mL bed. This corresponds to the injection on column of 20 μL . This value did not vary when increasing the injected mass from 50 μg to the limit mass capacity of 100 μg . The optimum volume loading for the 5 μm analytical column was determined to be 16 $\mu\text{L}/\text{mL}$ bed corresponding to 40 μL absolute injection on column. For the respective semi-preparative column, the optimum volume loading capacity was determined to be 31 μL per mL bed corresponding to 243 μL absolute injection volume on column. The volume loading capacity for the 5 μm analytical column relative to that of the 3 μm one is significantly higher than chromatographic theory would predict. The theoretical ratio would be a factor of 1.3 ($\sqrt{(5/3)}$) instead a factor of 2. The value with the semi-preparative column was by 100% higher than that on the analytical dimension.

Figure 3.14b shows the dependency of $w_{0.1}$ on the injection volume for the Luna columns. The slope of overloading range for the semi-preparative column was much flatter. The optimum volume loading for the analytical column was determined to be 20 $\mu\text{L}/\text{mL}$ bed corresponding to an absolute injection volume of 50 μL . This volume is by 25% higher than that determined for the Acclaim 5 μm analytical column. The value for the semi-preparative column was 32 μL per mL bed corresponding to 251 μL absolute injection volume, similar to the value with the Acclaim semi-preparative column.

The plot of $w_{0.1}$ value dependent on the injection volume for the Monolith is shown in Figure 3.14c. The optimum volume loading capacity obtained with Monolith was 51 $\mu\text{L}/\text{mL}$ bed corresponding to 400 μL injection volume on column. This is higher than that obtained with both packed semi-preparative columns, which can be attributed to the higher porosity of the monolithic column.

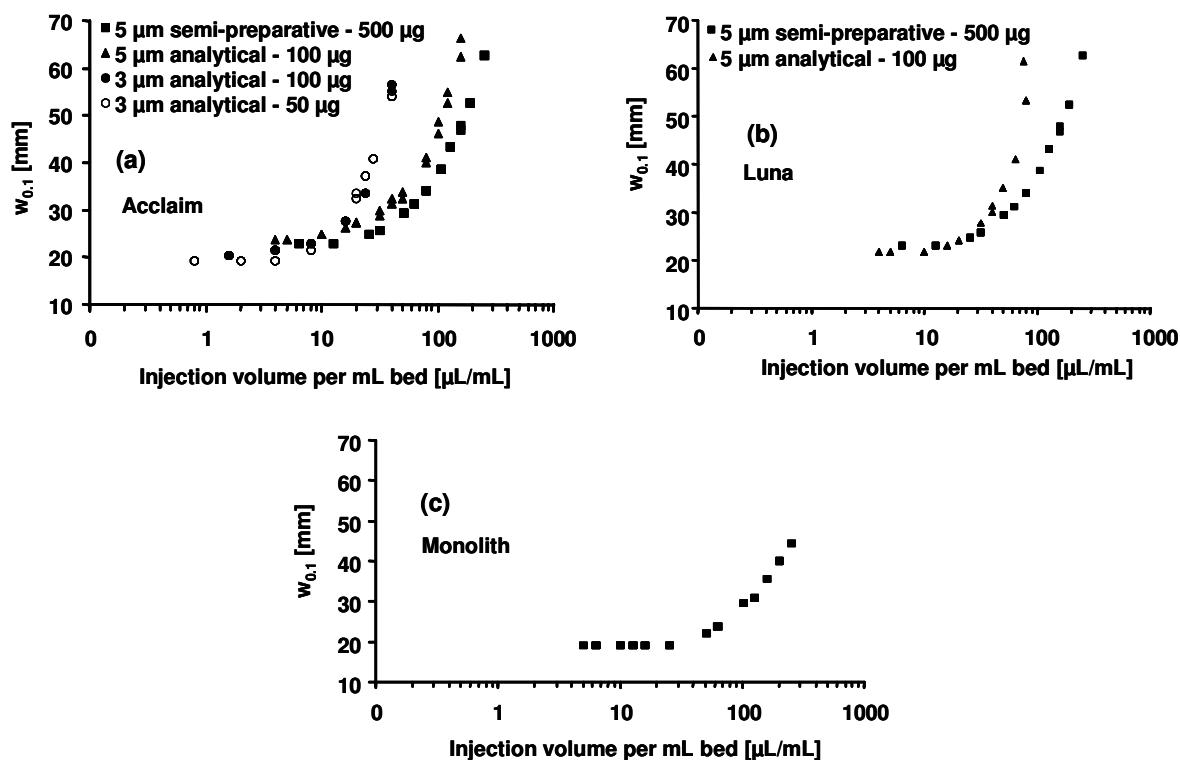


Figure 3.14: Dependency of peak shape parameter $w_{0.1}$ on the injection volumes

3.2.3.1.3 Mass loading at constant injection volume

The aim of this study is the determination of mass loading capacity at constant injection volume. This study was carried out on all 3 Acclaim columns, on both Luna columns and on the silica-based monolithic column (Monolith). The injection volume was 10 μL or 20 μL for the analytical columns and 100 μL or 200 μL for the semi-preparative columns. As investigated in the previous section, these injection volumes are far away from the overloading range.

Overlays of the peaks are depicted in Figure 3.15 to Figure 3.17. The corresponding injected sample mass is depicted in the respective chromatogram overlays. Since the UV absorptions at 258 nm clearly exceeded the dynamic range of the UV detector, the peaks detected at 295 nm were considered for interpretation. At this wavelength the peak height of salicylic acid is less than 10% that of acetylsalicylic acid. The increasing sample mass injected on column caused increasing peak tailing and a decreasing retention factor, except for peak shapes on the analytical 5 μm Acclaim column due to the interference of salicylic acid. On this column the peaks at low sample mass showed fronting (Figure 3.15a) and with increasing mass loading the

retention factor decreased and the interference of salicylic acid became noticeable.

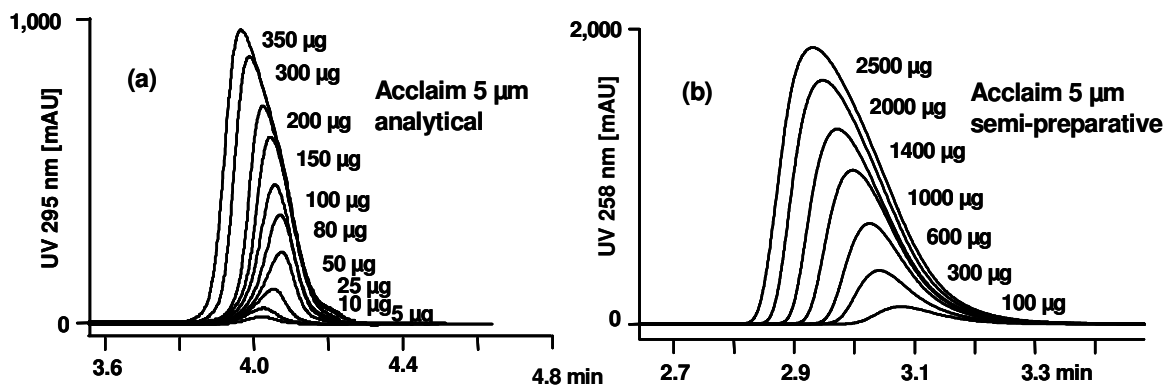


Figure 3.15: Peak overlays at different masses injected on the 5 µm Acclaim columns. The injection volume was 10 µL for the analytical column and 100 µL for the semi-preparative. Legend shows absolute mass injected.

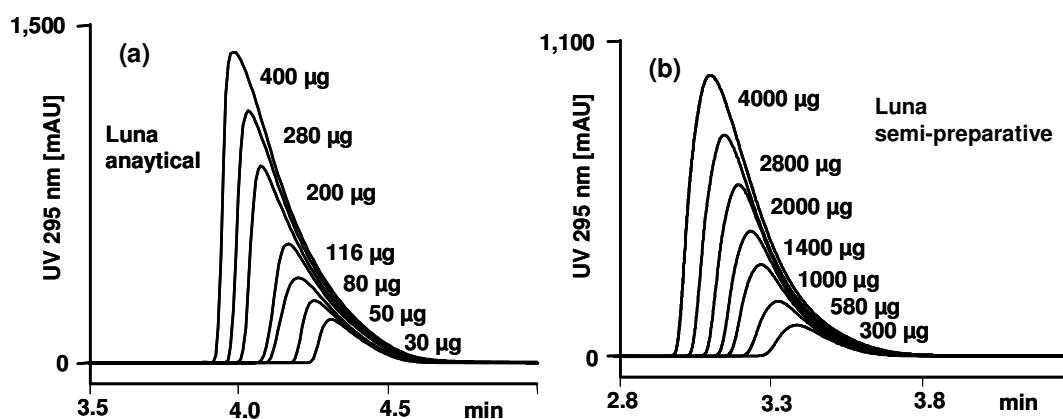


Figure 3.16: Peak overlays at different masses injected on the Luna analytical column (a) and semi-preparative column (b). The injection volume was 20 µL for the analytical column and 200 µL for the semi-preparative. Legend shows absolute mass injected.

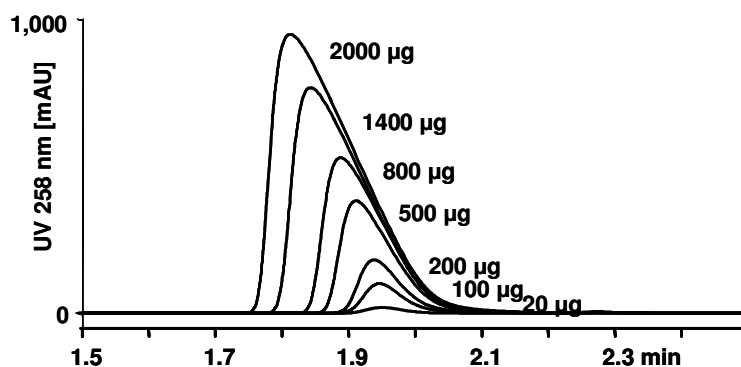


Figure 3.17: Peak overlay at different masses injected on Monolith. The injection volume was 100 μL . Legend shows absolute mass injected.

The same peak shape parameter as considered previously were plotted versus the absolute mass injected on column (Figure 3.18) in order to determine the optimum mass loading capacity. Increase of $w_{0.1}$ value by 10% to the value in non-overloading range is used as a measure for the optimum mass loading.

Figure 3.18a shows the plots of $w_{0.1}$ depending on the injection volume for the Acclaim column. The $w_{0.1}$ value in the non-overloading range for the 3 μm was excellent. Furthermore, this value on the semi-preparative 5 μm column was better than on the analytical one. This can be attributed to the competitive effect of salicylic acid on the analytical column. The curves for both analytical Acclaim columns run parallel, therefore the optimum mass loading capacity for both columns was similar, determined to be 42 μg per mL bed (corresponding to 105 μg sample mass on column). The optimum mass loading for the 5 μm semi-preparative column was determined to be 138 $\mu\text{g}/\text{mL}$ bed corresponding to 1083 μg absolute injection on column. This value is more than 3-fold higher than that on the analytical column dimension.

Figure 3.18b shows the dependency of $w_{0.1}$ value on the sample mass for the Luna columns. The plots show unusual behavior for both columns. The $w_{0.1}$ value increased gradually with increasing sample mass, even at low sample mass. The optimum mass loading was determined to be 4 $\mu\text{g}/\text{mL}$ bed (corresponding to 10 μg) for the analytical column and 8 $\mu\text{g}/\text{mL}$ (corresponding to 63 μg) for the semi-preparative column. This unusual behavior could be related to the interaction of acetylsalicylic acid with the functionality in the stationary phase that is used to extend its stability at higher pH values.

The plot of $w_{0.1}$ value for Monolith is shown in Figure 3.18c. The optimum mass loading capacity obtained with Monolith was 27 $\mu\text{g/mL}$ bed corresponding to 212 μg sample mass injected on column. This lower value compared to the mass loading capacity obtained with the Acclaim column can be attributed to the lower amount of stationary phase in the monolithic column.

Comparing the relative retention factor on Luna columns to that of the Acclaim 5 μm columns (k/k_0) (Figure 3.19), it can be seen that the plot for the Acclaim columns was as expected (e.g. remaining constant over a certain range), whilst the k values on the Luna decreased continuously. The relative $w_{0.1}$ value ($w_{0.1}$ value divided by the value at low sample mass, $w_{0.1}/w_{0.1,0}$) for these four columns are plotted in Figure 3.19b. The plot characteristic was similar for both Luna columns, however, on the semi-preparative column exhibited three sections.

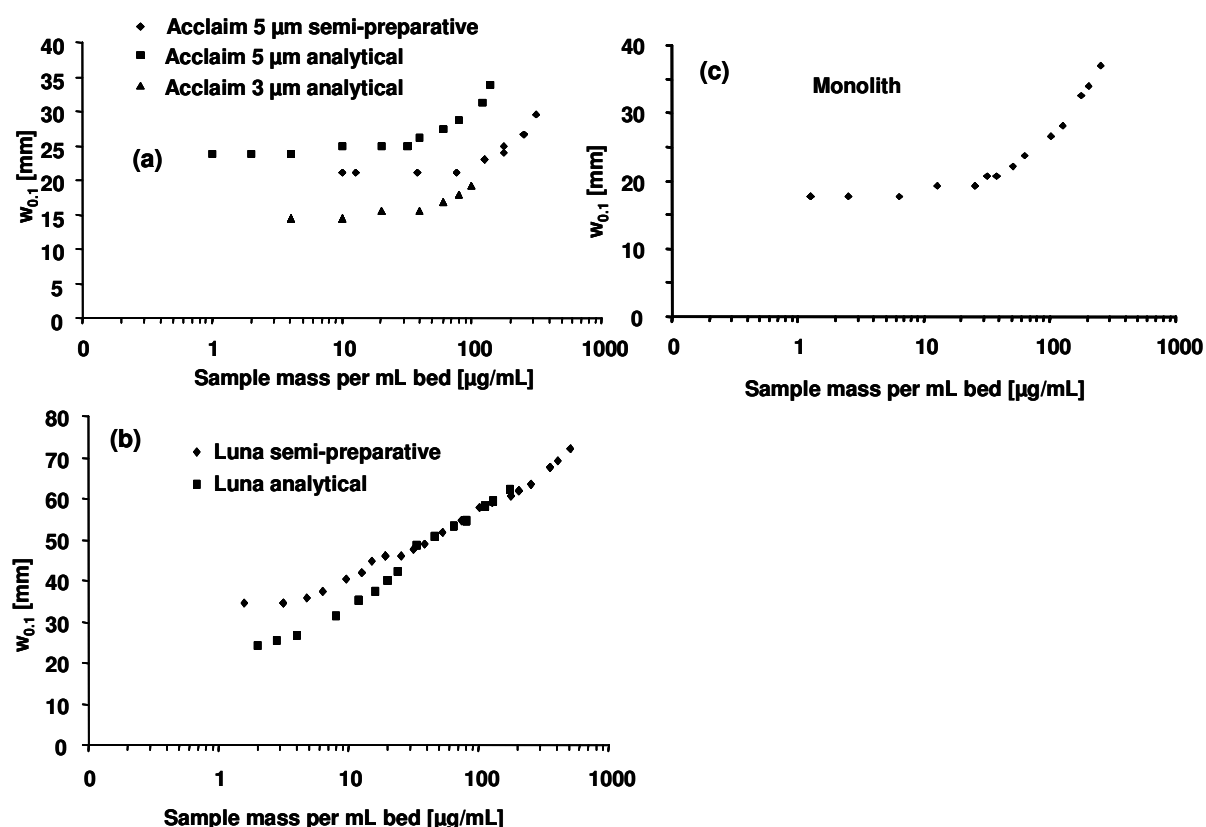


Figure 3.18: Peak shape parameter depending on the sample mass of acetylsalicylic acid

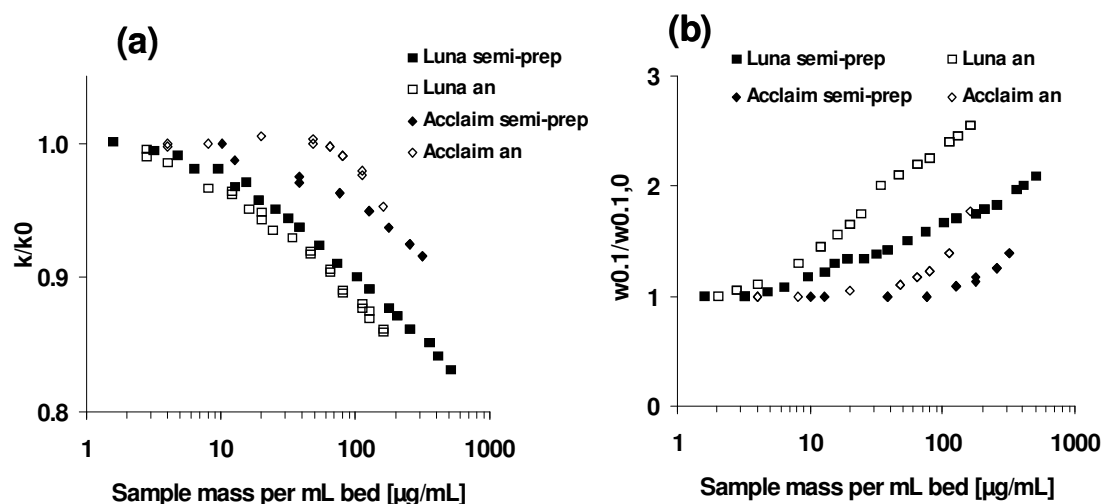


Figure 3.19: Relative retention factor and peak shape parameter depending on sample mass on the Luna and Acclaim columns. (a) Relative retention factor, (b) relative peak width at 10% peak height

To compare the results of the mass overloading experiments carried out with the Luna and Acclaim columns, the determined values for peak shape parameter are depicted in Table 3.5. N_0 and $w_{0.1,0}$ are peak efficiency and peak width at 10% peak height for low sample load, respectively. The table shows the peak shape parameter values in theoretical plate number (N) equal to 90% of N value at low sample load ($N = 0.9N_0$) and $w_{0.1}$ equal to 110% of $w_{0.1}$ value at low sample load ($w_{0.1} = 1.1w_{0.1,0}$). The value $w_{0.1} = 1.1w_{0.1,0}$ was used as a measure for the optimum loading capacity, since the values of $w_{0.1} = 1.1w_{0.1,0}$ are higher than that of $N = 0.9N_0$. Moreover, at $w_{0.1} = 1.1w_{0.1,0}$ the peaks were not yet distorted. In contrast, McCalley used $N = 0.9N_0$ as a measure for the optimum loading capacity [37].

Table 3.5: Values of peak shape parameters for acetylsalicylic acid on the Luna and Acclaim columns

Column	N=0.9N ₀		w _{0.1} =1.1 w _{0.1,0}	
	µg	µg/mL bed	µg	µg/mL bed
Luna semi-prep	30	3.8	63	8
Luna analytical	7.5	3.0	10	4
Acclaim semi-prep	725	92.4	1083	138
Acclaim analytical 5 µm	88	35.3	105	42
Acclaim analytical 3 µm	88	35.3	105	42

3.2.3.1.4 Variation of injection volume at constant sample concentration

The aim of this work was to investigate peak characteristics under increasing volume load at a constant sample concentration of 1 g/L.

Overlays of the peaks with increasing sample load are depicted in Figure 3.20 to Figure 3.22. The corresponding injection volume is depicted in the respective chromatogram overlays. As shown in Figure 3.9 (section 3.2.3.1.1), the absorbance of acetylsalicylic acid at 258 nm is much higher than that at 295 nm. However, the interpretation was done at 258 nm, since on the Acclaim 5 µm analytical column the peak of salicylic acid strongly interfered with that of acetylsalicylic acid at detection wavelength 295 nm (Figure 3.20b). As can be seen in Figure 3.20b, a systematic increase in selectivity with increasing volume load can be observed. This must be due to a displacement effect which takes place in the wide sample zone at the head of the column. This is surprising, since the amount of the impurity should be in the range of 0.5% (according to the manufacturer Sigma). From the increasing second peak it must be deduced that an ongoing conversion (hydrolysis) of acetylsalicylic acid takes place in the acidic sample solution at ambient temperature. From the peak height ratio observed in the run with 250 µL injection volume, a salicylic acid concentration of ca. 1.5% can be determined.

The peaks shapes obtained on the Acclaim 5 µm analytical column at 258 nm (Figure 3.20a) were similar to that obtained with the volume loading capacity study (Figure 3.11a). With other columns, peak tailing occurred with increasing sample load. In the overloading range, peak plateau was observed (Figure 3.21 and Figure 3.22).

Furthermore, the peaks on Monolith exhibited tri-angled shape with increased volume loading (Figure 3.22).

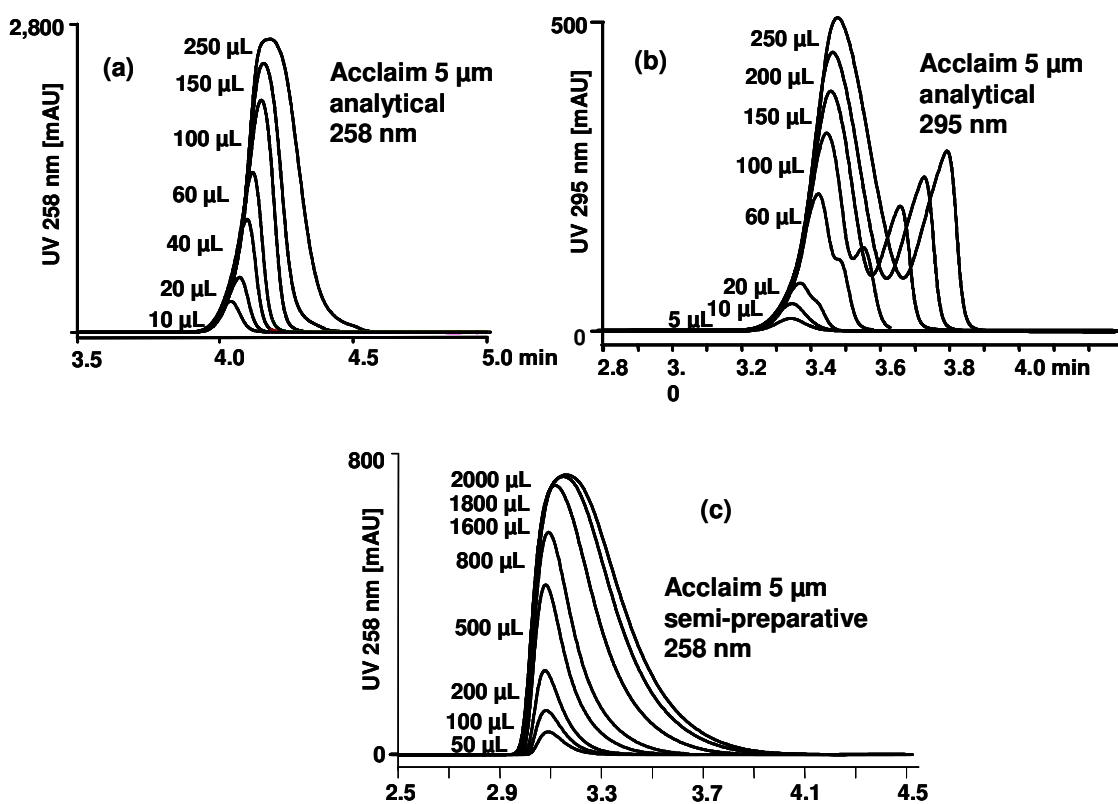


Figure 3.20: Increase of acetylsalicylic acid sample load by varying injection volume at constant sample concentration of 1 g/L on the 5 μm analytical column (a) at 258 nm, and (b) at 295 nm and (c) on semi-preparative Acclaim column at 258 nm.

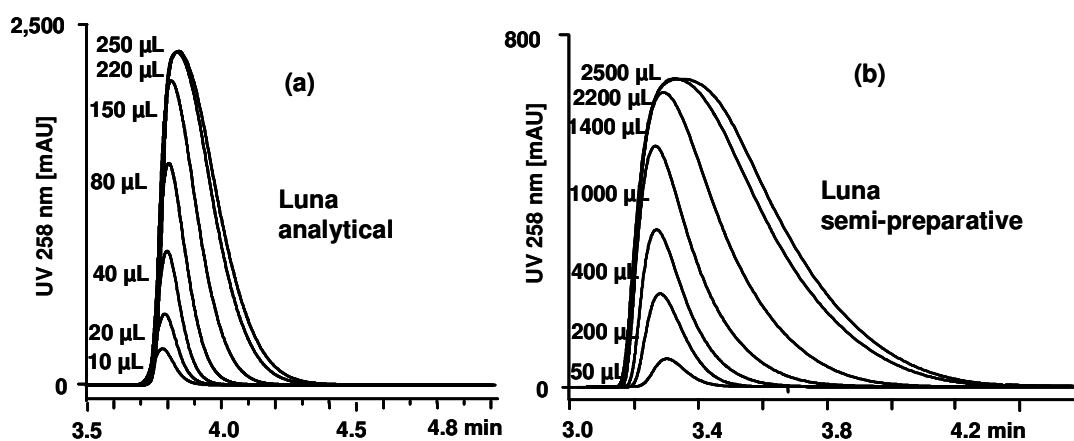


Figure 3.21: Peak shapes of acetylsalicylic acid sample load by varying injection volume at constant sample concentration of 1 g/L on the Luna columns.

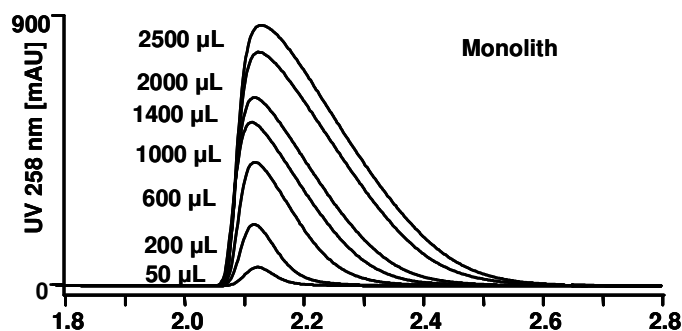


Figure 3.22: Peak shapes of acetylsalicylic acid sample load on Monolith.

The plot for the peak shape parameter $w_{0.1}$ of this experimental series is shown in Figure 3.23. The plot behavior obtained in this experiment (volume loading at constant sample concentration of 1 g/L) was different from the study with increasing volume loading at constant sample mass. The results are a combination of both both overloading effects (volume loading and mass loading), since the sample mass injected on the column increased with increasing volume loading.

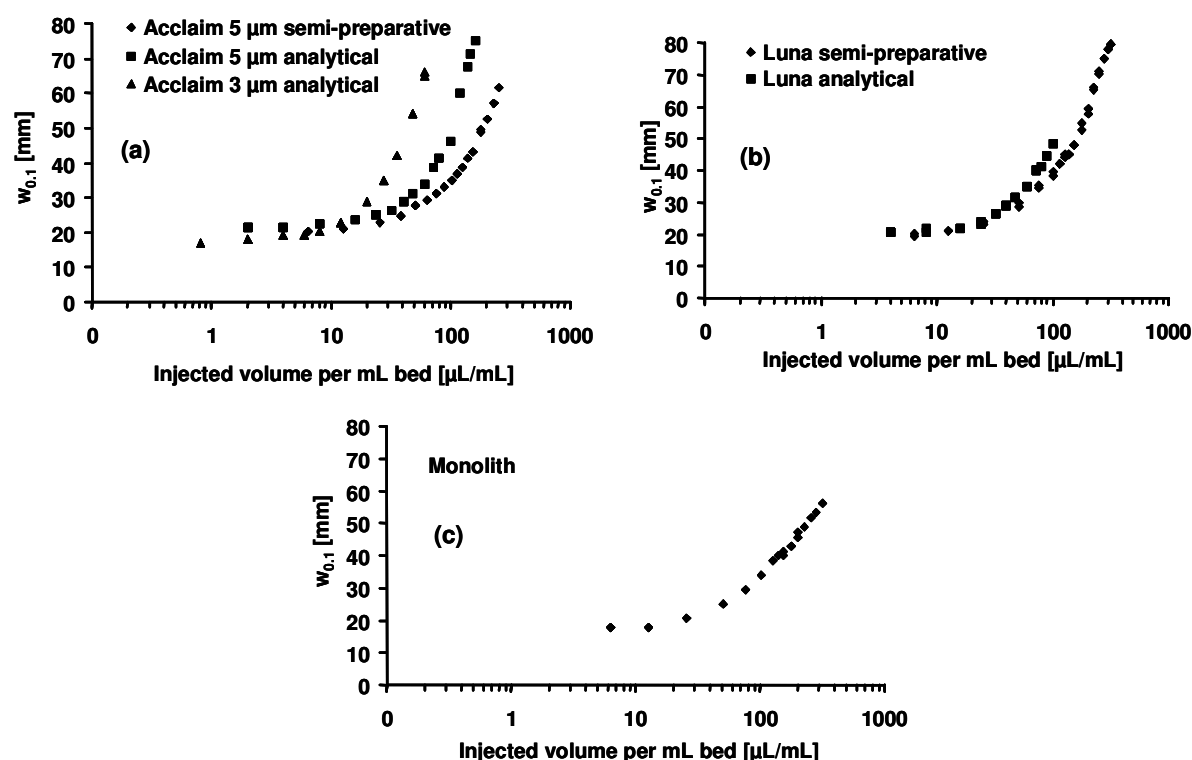


Figure 3.23: Peak shape parameter of acetylsalicylic acid sample load by varying injection volume at constant sample concentration of 1 g/L on different columns.

3.2.3.1.5 Conclusion from overloading experiment with acetylsalicylic acid

To compare the results of the volume and mass loading capacity experiments carried out with the Acclaim columns, Luna columns and Monolith, the determined loading capacities are depicted in Figure 3.24. The loading capacity was calculated by 10% increase of peak width at 10% peak height ($w_{0.1}$).

Volume loading capacity is in general a parameter, which strongly depends on the instrumental set-up. Moreover, it decreases with the column plate number ($\sim 1/\sqrt{N}$) and strongly increases with the retention factor ($\sim(1+k)$) and both parameters varied with the columns (Table 3.6). The result of volume loading capacity for Luna columns, which showed similar retention factors for both columns, is in good accordance with theory (theory 1.63, results 1.60). However, the results varied significantly with other columns, when the retention factors were different. Therefore, to perform a scale-up for volume loading capacity, it is necessary to set similar retention factors for both column dimensions.

The volume loading capacity obtained with Monolith was obviously higher than that with both packed columns in the same dimension. This can be attributed to the higher total porosity and thus higher column void volume of the monolithic column. The retention factor of acetylsalicylic acid on the Monolith was similar to that on the Acclaim semi-preparative column (Table 3.6), although the organic phase content with Monolith was lower (20% acetonitrile).

The data for the mass loading capacity (normalized for the column bed volumes) varied considerably with almost all columns, except between the Acclaim 3 μm and 5 μm analytical columns. The mass loading capacity difference between analytical and semi-prep columns with the Acclaim columns was pronounced (3.3-fold). This could be due to differences in the chromatographic properties of the three materials, which is in accordance with the standard test results and the selectivities between the two carboxylic acids. The mass loading capacity on the Luna columns for acetylsalicylic acid was very low. The value obtained with the semi-preparative Acclaim was 17-fold and 5-fold higher than that with the semi-preparative Luna and Monolith, respectively. Furthermore, plots of the peak shape parameters revealed unusual behavior for both Luna columns.

The loading capacity difference between analytical and semi-prep columns was more pronounced with the Acclaim than with the Luna columns. For the purpose of APS, the Acclaim semi-prep column appeared clearly advantageous over the respective

Luna column for acetylsalicylic acid.

Table 3.6: Retention factor and peak shape parameters of acetylsalicylic acid at low injection mass and volume for different columns.

Column	k_0	$w_{0.1,0}$ (mm)	N_0	$1/\sqrt{N_0}$
Acclaim 3 μm	1.3	14.4	11,000	0.0095
Acclaim 5 μm analytical	2.4	23.8	10,500	0.0098
Luna analytical	2.5	24.2	9,000	0.0105
Acclaim 5 μm semi-prep	1.8	23.8	4,000	0.0158
Luna semi-prep	2.4	41.8	3,200	0.0177
Monolith	1.9	17.7	5,500	0.0135

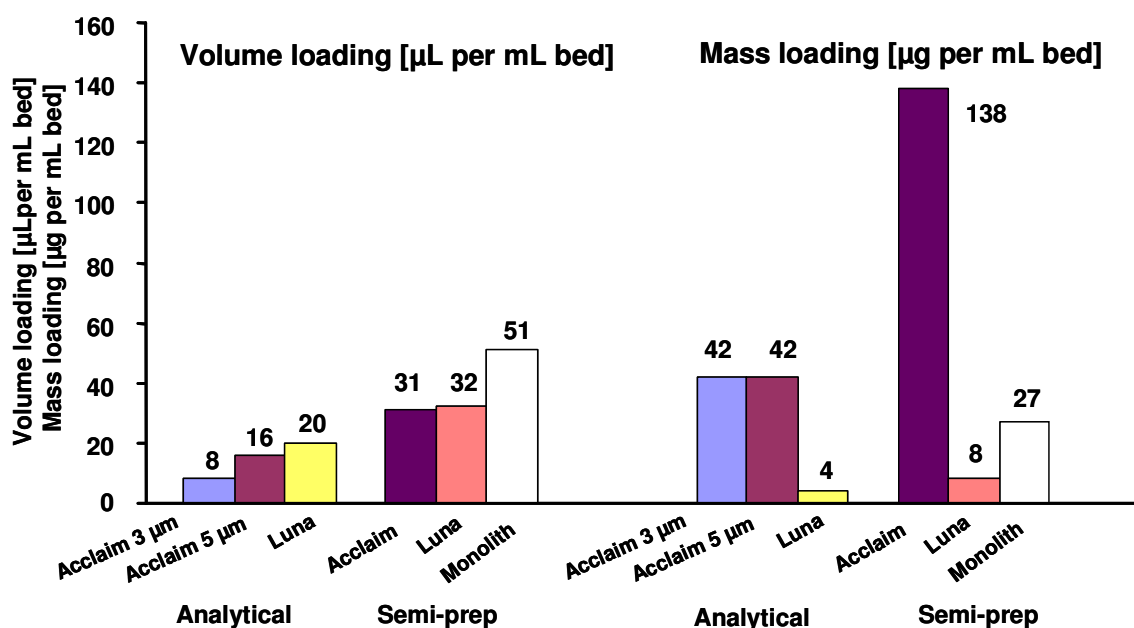


Figure 3.24: Volume and mass loading capacity for acetylsalicylic acid obtained with Acclaim, Luna and Monolith columns. Values are normalized for the column bed volumes.

3.2.3.2 Loading Capacity Study for Amitriptyline

APS systems are mostly applied in the pharmaceutical industry. Furthermore, large numbers of pharmaceuticals and biomedically relevant compounds contain basic groups. Amitriptyline is a strongly basic (tertiary amine) antidepressant drug with aqueous pK_a of 9.4 [24]. This compound is a representative of basic pharmaceutical which is widely used for column test purposes. Based on the results obtained in standard test and retention studies using amitriptyline (see section 3.1.3.2 and 3.1.3.3), this study was designed to investigate the loading capacity for amitriptyline using buffered aqueous methanol eluent at pH 6.0, 7.0 and 9.0 as well as using acetonitrile eluent at pH 7.0. The study was performed on packed RP-columns (Luna and Acclams) in analytical and semi-preparative dimensions, and on semi-preparative silica-based RP monolithic column (the Monolith).

3.2.3.2.1 Loading capacity for amitriptyline on the Luna columns

Figure 3.25 shows overlays of the peaks obtained with the Luna analytical column at pH 6.0 and pH 7.0 with phosphate buffer 20 mM -methanol (20/80) and at pH 7.0 with phosphate buffer 20 mM- acetonitrile (40/60). At pH 7.0 with phosphate buffer 20 mM -methanol (20/80) (Figure 3.25a), the retention decreased with increasing mass loading. Severe peak distortion including a pronounced front shoulder appeared at injected analyte amounts higher than 28 μg . This could be attributed to silanol overloading at high sample mass loading.

An overlay of amitriptyline chromatograms at pH 6.0 with methanol eluent for different solute mass loading is shown in Figure 3.25b. The retention increased with increasing mass loading. The peak distortion with pronounced front shoulder appeared already at injected analyte amounts 14 μg . At this pH, silanol overloading appeared earlier. This could be due to insufficient buffering capacity of phosphate at this pH.

Figure 3.25c shows an overlay of chromatograms at different mass loading obtained with phosphate buffer 20 mM- acetonitrile (40/60) at pH 7.0. The peak obtained with ACN eluent at low sample load showed a pronounced peak tailing, as also observed in earlier study (section 3.1.3.3.2). This can be considered a further indication for a marked contribution of cation exchange to amitriptyline retention due to the increase

of overall buffer concentration resulting from the higher amount of the aqueous component.

Unlike observed with the methanol eluent at this pH, the retention increased with increasing mass loading. Furthermore, the peak shape observed under overloading conditions was different from that with methanol eluents. With ACN, the peak shape moves to fronting and the retention increased, but no peak shoulder was observed up to 60 μg loading. This can be explained by a higher degree of silanol dissociation (more aqueous mobile phase and overall buffer concentration 8 mM) and thus no silanol overloading.

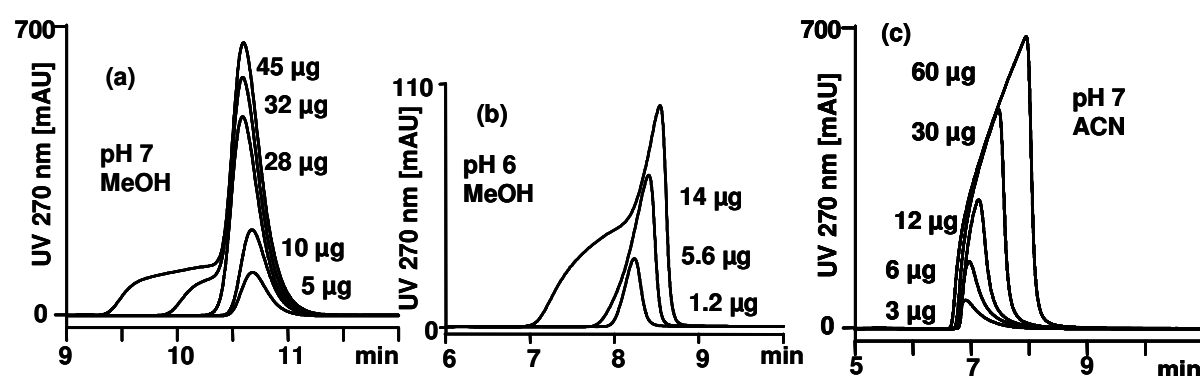


Figure 3.25: Amitriptyline peaks at different sample mass loadings on the Luna analytical column. (a) 20 mM phosphate buffer pH 7– methanol (20/80), (b) 20 mM phosphate buffer pH 6 – methanol (20/80), (c) 20 mM phosphate buffer pH 7– acetonitrile (40/60); flow rate 1 mL/min; temperature 23 °C; detection: 270 nm

Figure 3.26 shows overlays of the peaks obtained with the Luna semi-preparative column at pH 6.0 to 9.0 with phosphate buffer 20 mM -methanol (20/80) and at pH 7 with phosphate buffer 20 mM- acetonitrile (40/60). Loadability study was also carried out at pH 9. Since the Luna C18(2) column is specified for working at pH 2 to 10, it was of interest to extend the study to alkaline media.

An overlay of amitriptyline chromatograms at pH 6.0 for different solute mass loading is shown in Figure 3.26a. The retention increased with increasing mass loading. The peak distortion with pronounced front shoulder as observed with the Luna analytical column, appeared at injected analyte amounts higher than 24 μg .

At pH 7.0 with methanol eluent (Figure 3.26b) the front shoulders appeared at injected analyte amounts higher than 150 μg sample load, corresponding to 19

$\mu\text{g/mL}$ column bed. With the analytical column, at an injected solute mass of $32 \mu\text{g}$ ($12.9 \mu\text{g/mL}$ bed) the peak was already distorted. In contrast to pH 6.0, the retention decreased with increasing mass loading (typical column overloading). As mentioned in the analytical scale, the peak distortion with pronounced front shoulder can be considered due to silanol overloading.

At pH 9.0 the amitriptyline solute is largely uncharged and the surface silanols are fully ionized. The peak shape under overloading conditions (Figure 3.26c) was much better than at other pH values, as even in the highest loading range studied, the peaks were not distorted. At overloading conditions, the peaks appeared like a double peak. This could be due to the interaction of charged amitriptyline with the silanols. The retention time of the main peak maximum remained constant.

The peaks of amitriptyline obtained for different mass loadings with the acetonitrile eluent at pH 7.0 are overlaid in Figure 3.26d. The zone profiles encountered using this eluent were similar to those with the analytical scale column. No peak shoulder was observed up to $300 \mu\text{g}$ ($38 \mu\text{g/mL}$ bed) loading. At injection of $420 \mu\text{g}$ ($53 \mu\text{g/mL}$ bed) a plateau like front shoulder appeared under overloading conditions, but smaller than obtained with methanol eluents. The loadability study at analytical scale was done up to $60 \mu\text{g}$ loading corresponding to $24 \mu\text{g/mL}$ bed, no front shoulder was observed under these conditions.

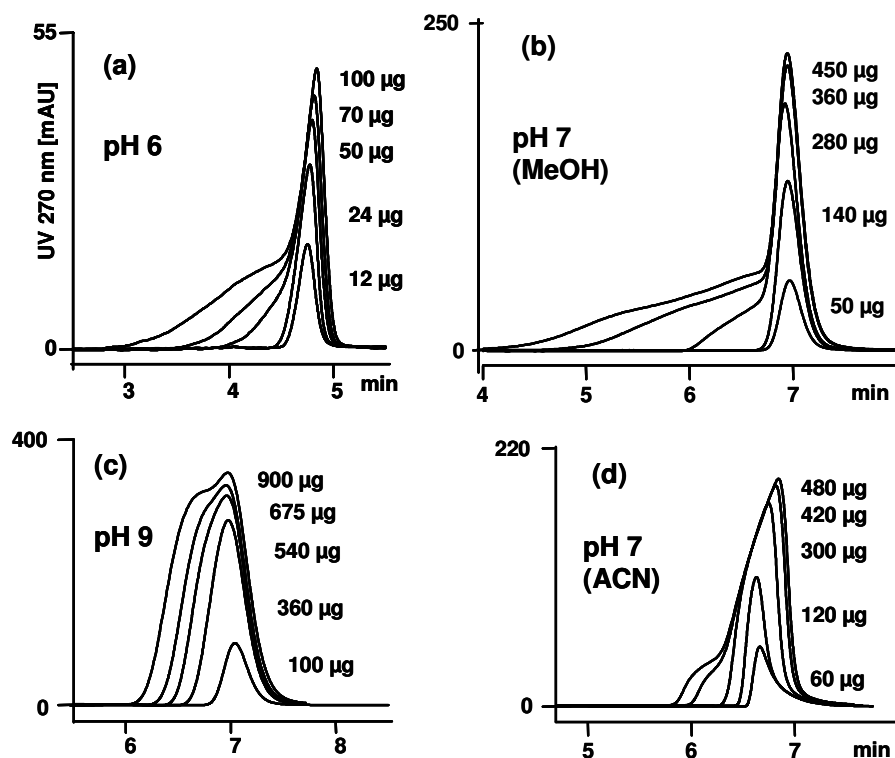


Figure 3.26: Amitryptiline peaks at different sample mass loadings on the Luna semi-preparative column. (a) 20 mM phosphate buffer pH 6.0–methanol (20/80), (b) 20 mM phosphate buffer pH 7.0–methanol (20/80), (c) 20 mM carbonate buffer pH 9.0–methanol (20/80) (d) 20 mM phosphate buffer pH 7.0–acetonitrile (40/60); flow rate 5 mL/min; temperature 23 °C; detection: 270 nm

The relative peak shape parameters are plotted as a logarithmic function of sample mass loading (Figure 3.27). To obtain this, the measured peak shape parameter value was divided by the value at small sample mass load, e.g. 10 µg. The horizontal lines indicate the peak shapes in the non-overloading range. In this condition, the values remain constant with the loading. Overloading occurs with increasing sample mass loading. In this overloading range the peak width increases gradually and therefore the efficiency decreases. With methanol eluents (Figure 3.27a, c, and d), the values of asymmetry and retention factors are not critical. The value of peak width at 10% peak height was most critical for investigations at pH 7.0, since pronounced peak shoulder appeared at high loading. The theoretical plates were also critical values. Unusual behavior of theoretical plate plots is shown with the acetonitrile mobile phase (Figure 3.27b and 3.27e), as also indicated unusual peak shapes at both low loading and under overloading conditions (Figure 3.25c and

Figure 3.26d).

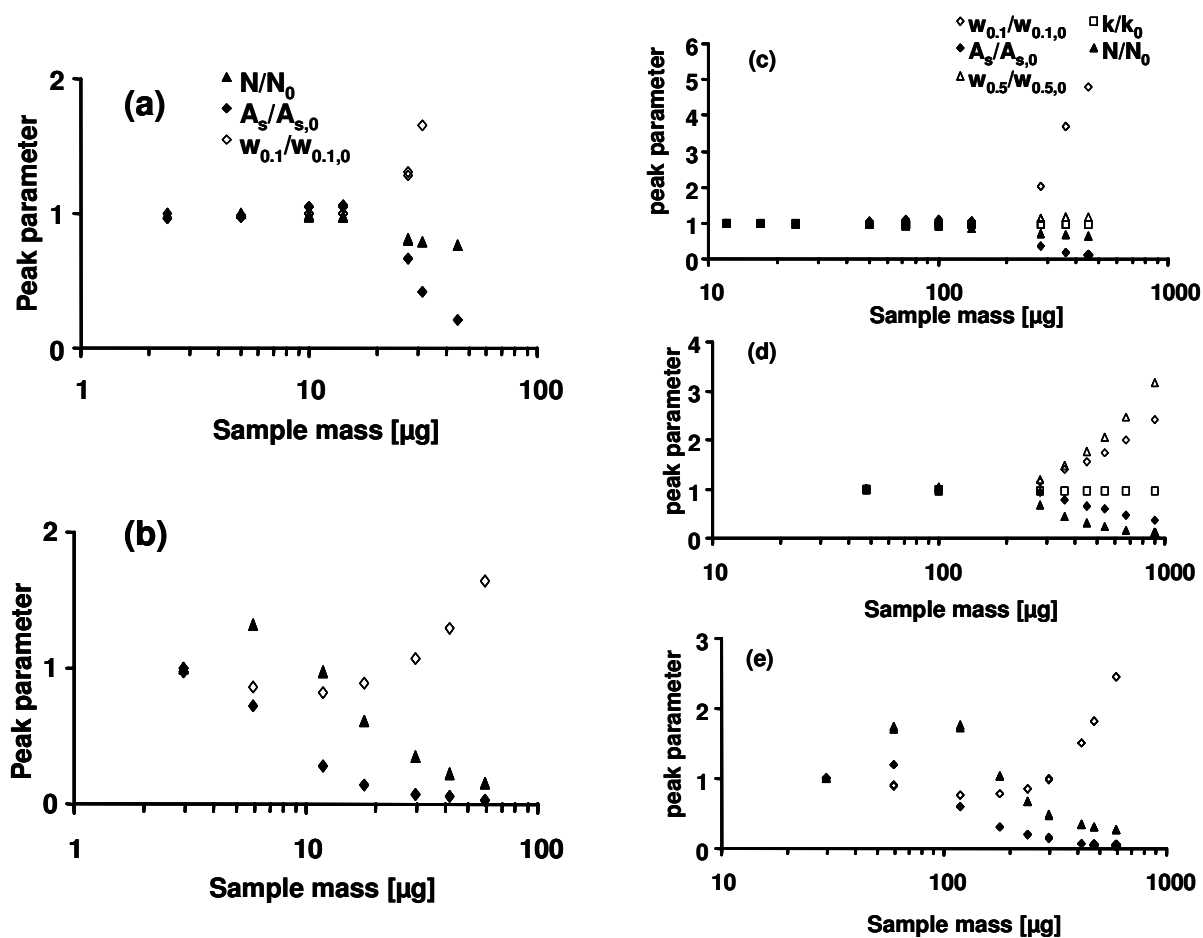


Figure 3.27: Plot of relative peak shape parameters for amitriptyline (efficiency, asymmetry, $w_{0.1}$, $w_{0.5}$ and k) dependent on logarithmic sample mass. (a) On the Luna analytical column using 20 mM phosphate buffer pH 7.0–methanol (20/80); (b) on the Luna analytical column using 20 mM phosphate buffer pH 7.0–acetonitrile (40/60), (c) on the Luna semi-preparative column using 20 mM phosphate buffer pH 7.0–methanol (20/80); (d) on the Luna semi-preparative column using 20 mM carbonate buffer pH 9.0–methanol (20/80); (e) on the Luna semi-preparative column using 20 mM phosphate buffer pH 7.0–acetonitrile (40/60); flow rate 5 mL/min; column oven temperature 23 °C; detection: 270 nm.

The most critical peak shape parameter (width at 10 % peak height) for both Luna columns at different eluent conditions is plotted versus sample load in mg per mL bed volume. All results can be seen at one glance in Figure 3.28. One can see that the loading behavior markedly depends on the eluent pH. On the analytical column

(Figure 3.28a) the efficiency with acetonitrile in the non-overloading range was slightly better. At pH 7, the slope of the increase of peak distortion was much flatter with ACN than that obtained with methanol. Hence, the loading capacity with acetonitrile must be considered superior to methanol, because in the highest loading range studied, the peaks were markedly less distorted using acetonitrile eluent. In the semi-preparative column dimension, the peak shapes in different eluents in the non-overloading range were similar. As discussed previously, the amitriptyline loading with 60% ACN eluent at pH 7.0 was preferable to that with 80% MeOH eluent at the same pH and aqueous mobile phase. However, for the Luna columns, which are stable for working up to pH 10, the slope of the overloading range was much shallower in alkaline media (pH 9.0). Hence, the column could be more loaded than the optimum loading capacity without serious loss in efficiency.

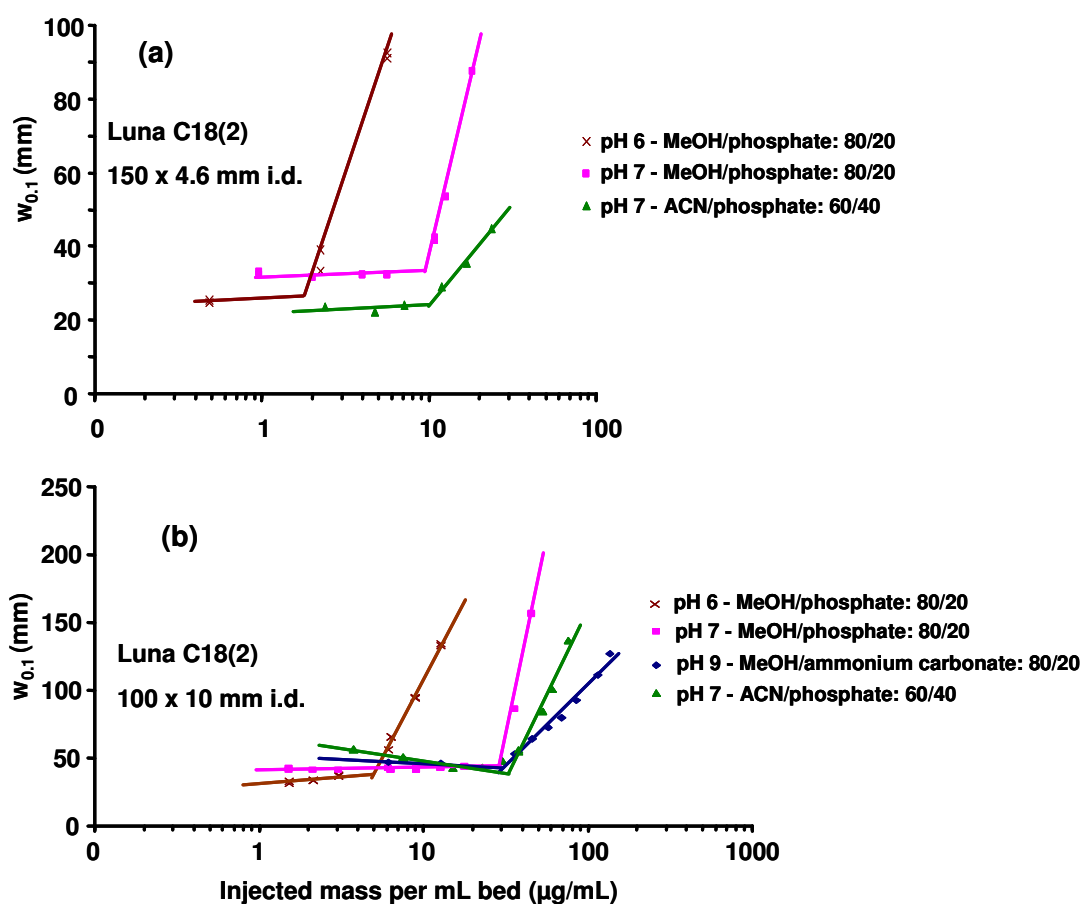


Figure 3.28: Plot of $w_{0.1}$ dependent on injected sample mass per mL bed using different eluents: (a) on the Luna analytical column, (b) on the Luna semi-preparative column.

Table 3.7 shows the peak shape parameter values in theoretical plate number (N) equal to 90% of N value at low sample load ($N = 0.9N_0$) and $w_{0.1}$ equal to 110% of $w_{0.1}$ value at low sample load ($w_{0.1} = 1.1w_{0.1,0}$) in μg sample load and μg per mL of bed volume. Similar loading capacity was obtained with the methanol eluent at pH 9.0 and acetonitrile eluent at pH 7.0. It is not understandable, because the solute should be mostly uncharged at pH 9.0 and exist partly ionized and partly as free base at pH 7.0 (Figure 3.4, section 3.1.3.3.1). Neue et al. reported that the loading capacity of un-ionized solute is higher than that of the ionized solute [34].

As apparent in Table 3.7, the loading capacity of amitriptyline on the semi-preparative column was surprisingly 3.3-fold higher than that on the analytical column dimension, although similar results with the Engelhardt test were obtained on both columns (Table 3.2, section 3.1.3.1). On the one hand this is advantageous, because the column enables high sample throughput in preparative chromatography. On the other hand it is difficult to predict the loading capacity within a scale-up process (with the same stationary phases) without performing the solvent consuming loadability study on the semi-prep column.

Table 3.7: Loading capacity for amitriptyline on the Luna columns

Mobile phase	$N=0.9N_0$		$w_{0.1}=1.1w_{0.1,0}$	
	μg	$\mu\text{g/mL bed}$	μg	$\mu\text{g/mL bed}$
Luna 100x10 mm i.d.				
pH 7 buffer-MeOH: 20/80	106	13.5	235	30
pH 9 buffer-MeOH: 20/80	131	16.7	290	37
pH 7 buffer-ACN: 40/60	200	25.5	320	41
Luna 150x4.6 mm i.d.				
pH 7 buffer-MeOH: 20/80	20	8.0	25	10
pH 7 buffer-ACN: 40/60	13	5.2	31	12.5

3.2.3.2.2 Loading capacity for amitriptyline on the Acclaim columns

Figure 3.29 shows overlays of amitriptyline peaks obtained with the Acclaim columns at pH 6.0. The peak shapes at overloading conditions obtained with both analytical

columns at the same elution conditions using 20 mM buffer were similar (Figure 3.29a and Figure 3.29b). Peaks distortion with front shoulder appeared, as also observed with the Luna columns. However, different peak shapes were obtained with the Acclaim semi-preparative column (Figure 3.29c).

At buffer concentration of 30 mM with the 5 μm analytical column (Figure 3.29d) at otherwise identical elution conditions, lower retention was achieved. Peak shoulder at overloading condition was also smaller. Mass loading of 5.6 μg gave non-distorted peak shape, compared to distorted peak with 20 mM buffer. The different overloading behavior at different buffer ionic strength indicated the contribution of ionic interaction at this pH. The shift of retention time to lower value is a further indication for this ionic interaction with the residual silanols in the stationary phase.

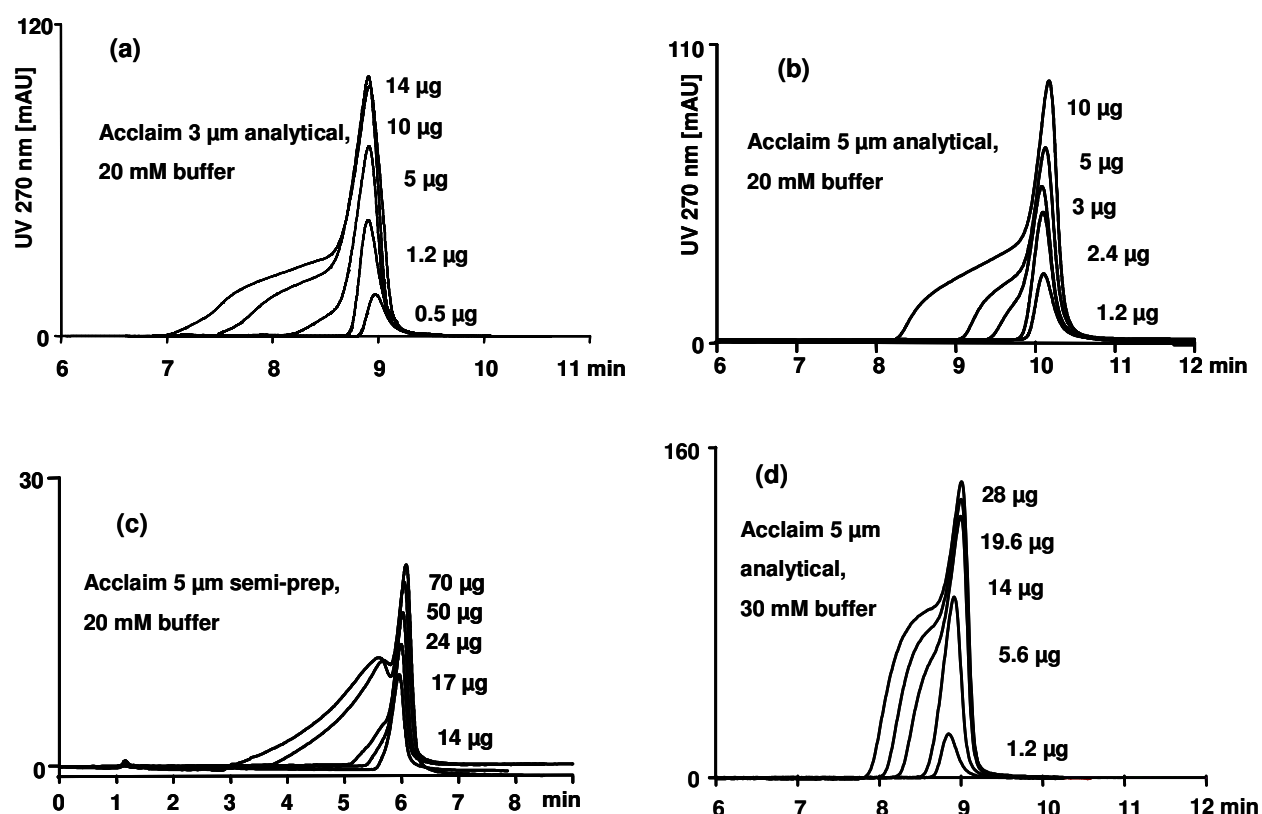


Figure 3.29: Amitriptyline peak shapes on the Acclaim columns at pH 6.0 using phosphate buffer-methanol: 20/80. (a) On the Acclaim 3 μm analytical column using 20 mM phosphate; (b) on the Acclaim 5 μm analytical column using 20 mM phosphate; (c) on the 5 μm semi-preparative column using 20 mM phosphate; (d) on the Acclaim 5 μm analytical column using 30 mM phosphate; temperature 23 $^{\circ}\text{C}$; detection: 270 nm; flow rate 5 mL/min for semi-preparative and 1.0 mL/min for analytical columns.

Figure 3.30 shows peak overlays of amitriptyline on Acclaim columns at pH 7.0 obtained with methanol eluent (upper side) and acetonitrile eluent (lower side). With methanol eluent the peak maximum moved to lower retention factors and the front shoulder was growing with a further increase of mass loading. The peak shape behavior obtained with the analytical columns were similar both for methanol and acetonitrile eluents. Such a behavior was also observed with the Luna columns at the same conditions. Unlike the zone profiles encountered with both analytical scale columns using acetonitrile eluent, a marked plateau like front shoulder appeared under overloading conditions, similar to the behavior in methanol eluents. At pH 7 peaks began to distort at higher mass loading than at pH 6. On the analytical columns, loading of 10 μg sample gave normal peak shape, whilst at pH 6 from 5 μg sample load the peaks were already distorted.

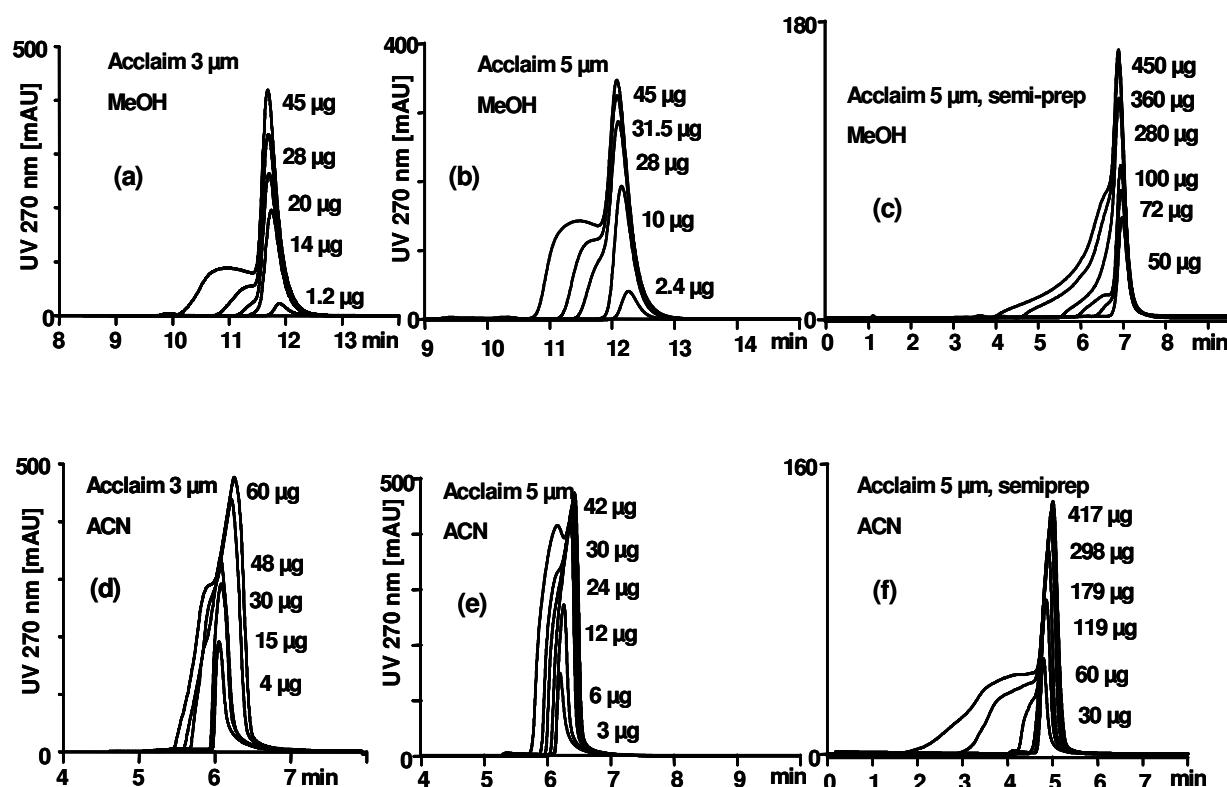


Figure 3.30: Amitriptyline peaks on Acclaim columns using 20 mM phosphate buffer pH 7.0 and methanol: 20/80 (upper chromatogram) and buffer – acetonitrile: 40/60 (lower chromatograms). (a) (b) on the 3 μm analytical column; (c) (d) on the 5 μm analytical column; (e) (f) on the 5 μm semi-preparative column.

Figure 3.31 depicts the mass loading capacity curves obtained with all Acclaim columns for the methanol and acetonitrile containing eluents in direct comparison. As also observed with the Luna columns, the loading capacity was markedly dependent on the pH values. Among the conditions applied for the study on the 5 μm analytical column, pH 7.0 provided a comparatively high loading ability of 8 μg per mL bed, whilst at pH 6.0 only 1 μg per mL bed could be loaded (Figure 3.31b). This trend was already observed with the 3 μm analytical column, where the ratio was, however, closer to 4 than to 8 (Figure 3.31a).

With the semi-preparative column, the only noticeable difference between the 2 eluents was the slightly better efficiency using acetonitrile in the non-overloading range. The overloading points were similar at about 20 $\mu\text{g}/\text{mL}$ bed volume. Fortunately, it is by 2.5-fold higher than that obtained with the 5 μm analytical column. The most remarkable fact, however, is the similar slope in the overloading range, which could be foreseen from the zone profiles (comparing Figure 3.30a and Figure 3.30f).

With both analytical columns at pH 7.0 the loading capacity revealed to be similar with both eluents. However, the slope of the increase of peak distortion was much flatter with acetonitrile than that observed with methanol. Hence, the loading capacity with acetonitrile must be considered superior to methanol, because in the highest loading range studied, the peaks were markedly less distorted using this eluent. Based on the results above it could be concluded that a mobile phase containing 60% acetonitrile was superior to that with 80% methanol, as the peaks were markedly less distorted in the highest loading range. The non-overloaded range ended with both eluents at approx. 7 $\mu\text{g}/\text{mL}$ bed. The overall behavior of the 5 μm analytical column for amitriptyline using both eluents mimicked that of the 3 μm column.

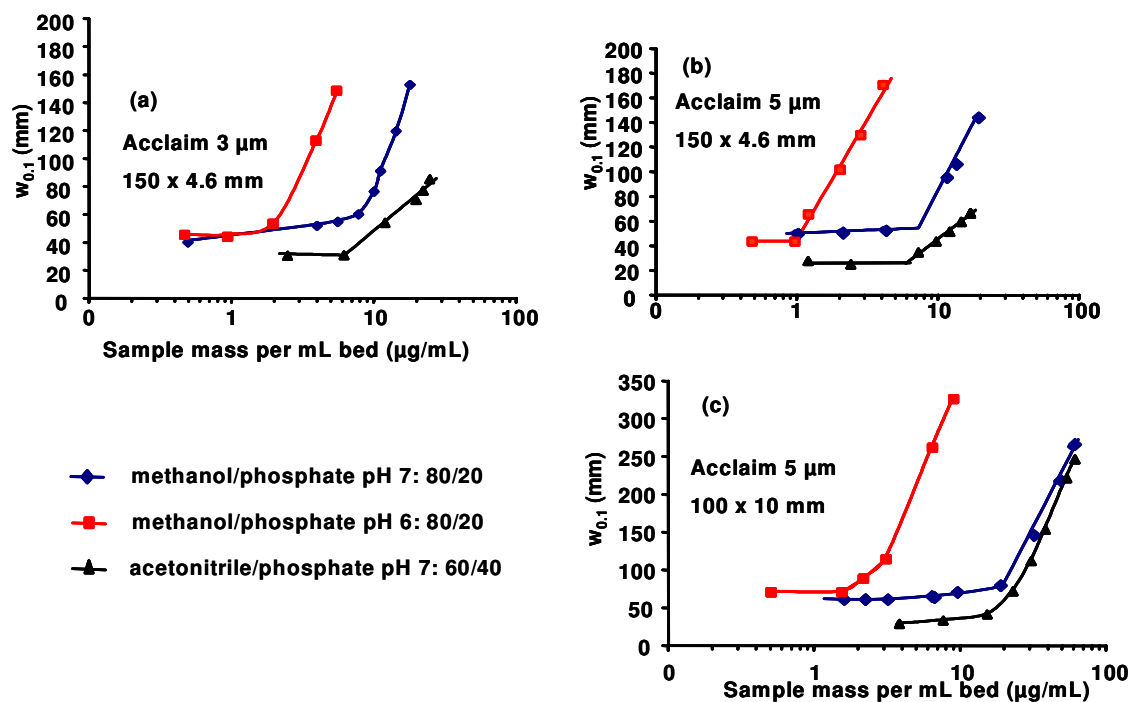


Figure 3.31: The plot of $w_{0.1}$ dependent on logarithmic sample mass per mL bed for amitriptyline on Acclaim columns with different eluents.

3.2.3.2.3 Loading capacity for amitriptyline on silica-based monolithic RP-column

Figure 3.32 depicts the peak overlays at different mass loading and the corresponding mass loading curve obtained with silica based monolithic RP-column (Monolith) at pH 7.0 using methanol and acetonitrile eluents. The peak shape behaviors obtained with this column were different from the packed columns. The peak shapes with both methanol and acetonitrile were similar. The only difference was the shape and width of the front shoulder. At low mass loading, the peaks were quite symmetrical, became broader and led to right-angled peaks with increasing sample mass. At higher mass loading it evidenced front shoulder, as also observed with other columns. This is due to silanol overloading, since at this pH hydrophobic and ionic interaction occurred simultaneously.

The $w_{0.1}$ plot behavior obtained with both eluents was slightly different. Using methanol eluent the value decreased slightly with increasing sample mass up to 400 μg (corresponding to 51 $\mu\text{g/mL}$ bed). Afterwards, as peak distortion with front shoulder appeared, the values increase rapidly and therefore formed a nearly vertical

plot. Using acetonitrile eluent the decrease of the $w_{0.1}$ value in the non-overloading condition (up to 500 μg) was more pronounced.

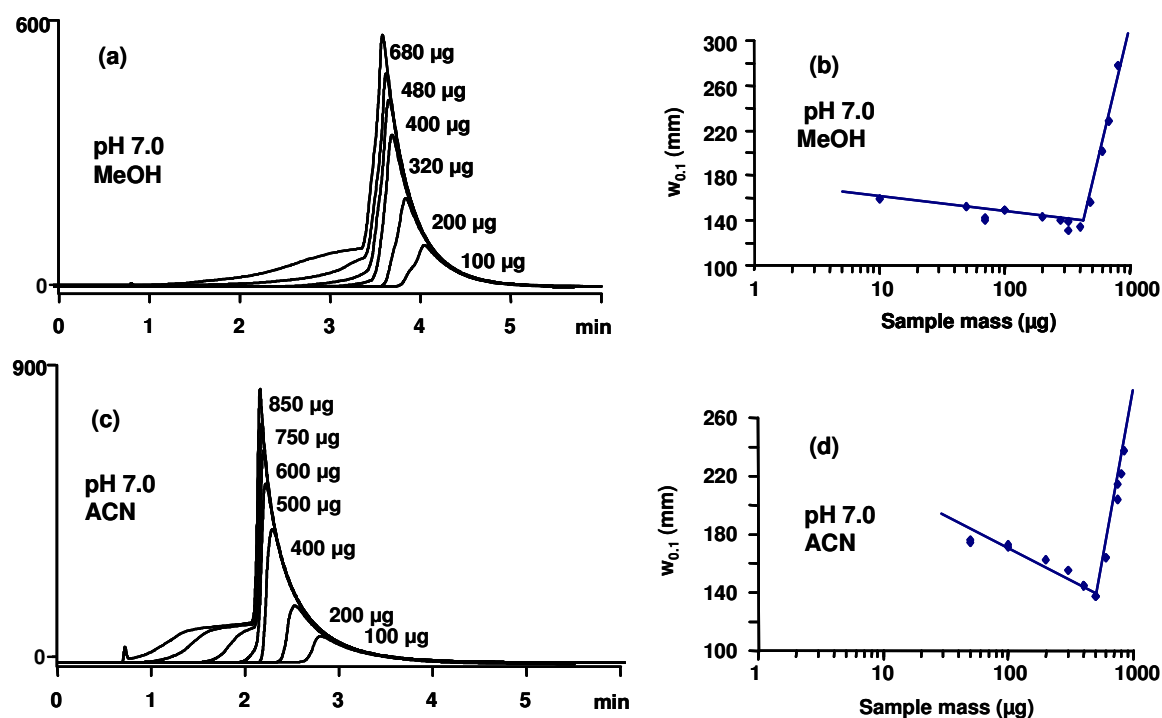


Figure 3.32: Peak overlays at different mass loading and the mass loading curve for amitriptyline on the Monolith. (a), (b) 20 mM phosphate buffer – methanol (26/74); (c), (d) 20 mM phosphate buffer – acetonitrile (40/60); temperature 23°C; detection: 270 nm; flow rate 10 mL/min.

3.2.3.2.4 Conclusions of loadability study for amitriptyline

The mass loadability study for amitriptyline was done on the Acclaim and Luna columns at both analytical and semi-preparative scales and on Monolith (in semi-preparative dimension). The normalized loadability of Luna and Acclaim columns for amitriptyline at different mobile phases is summarized in Table 3.8.

The loadability at pH 6.0 with methanol eluent was very low, due to insufficient buffering capacity of phosphate buffer at this pH value. The loadability at pH 7.0 with methanol and acetonitrile eluent was similar. However, the peak shapes under overloading conditions obtained with acetonitrile as eluent were better than with methanol at the same pH value. This could be due to the nature of the organic modifier or due to the difference in overall buffer concentration of both eluents (4 mM with methanol eluent and 8 mM with acetonitrile eluent). At pH 9.0 using carbonate

buffer and methanol eluent, the peak shapes under overloading conditions were superior. The loadability, however, was slightly lower than at pH 7.0.

Table 3.8: Loading capacity for amitriptyline on Luna and Acclaim columns

Column	Loading capacity [$\mu\text{g}/\text{mL}$ bed]			
	pH 6, MeOH	pH 7, MeOH	pH 7, ACN	pH 9, MeOH
Luna analytical	2	10	12.5	
Luna semi-prep	5	30	41	37
Acclaim 3 μm	2	8	7	
Acclaim 5 μm analytical	1	8	7	
Acclaim 5 μm semi-prep	2	20	20	

The poorer peak shape with the front shoulder under overloading conditions could be attributed to the surface silanol overloading due to insufficient silanol masking with the buffer ions at higher sample load. Blay [42] observed similar peak elution when he injected 14 μg amitriptyline on several columns using 5 mM phosphate buffer-methanol (20/80), as described in former NIST test [43]. When the overall buffer concentration increased to 20 mM, this front shoulder disappeared. McCalley used mobile phases containing overall buffer concentration of approx. 20 mM to perform the overloading study for strong bases (e.g. nortriptyline) [9,10,20,41]. Therefore, detrimental peak with front shoulder was not observed in his studies. However, in this work, higher buffer concentration cannot be used because of higher organic modifier content of mobile phase (80% methanol or 60% acetonitrile), which increases the risk of buffer precipitation.

The semi-preparative columns were generally more loadable than the analytical ones. At pH 7.0 the semi-preparative Acclaim is 2.5-fold more loadable than the analytical one, whilst the loadability of the Luna semi-preparative scale was 3.3-fold higher than the analytical scale.

The $w_{0.1}$ plot behavior obtained for Monolith with both methanol and acetonitrile eluents was unusual. In the non-overloading condition the value $w_{0.1}$ decreased with increasing sample mass. Afterwards, as peak distortion with front shoulder appeared, the values increase rapidly and therefore formed a nearly vertical plot.

3.2.3.3 Loading Capacity Study for Phenol

Phenol is a polar, weakly acidic compound with a pK_a value of 9.8 [24]. The elution of phenol on both semi-preparative Luna C18(2) and Acclaim C18 columns was performed at the identical condition as for acetylsalicylic acid (70% water titrated with formic acid pH 3.0 – 30% acetonitrile). At this given condition, phenol is in non-ionized form.

The overlays of phenol peaks obtained with the Luna C18(2) and Acclaim C18 semi-preparative columns are shown in Figure 3.33a and Figure 3.33c, respectively. With both columns, the retention decreased, as expected, with the increasing mass loading once the overloading conditions are reached. With increasing mass loading the peaks became triangle shaped, especially with the Luna column. The plots of peak shape parameters obtained with both columns are also depicted in Figure 3.33b and Figure 3.33d, respectively. The peak shapes of phenols were markedly better than that of acetylsalicylic acid.

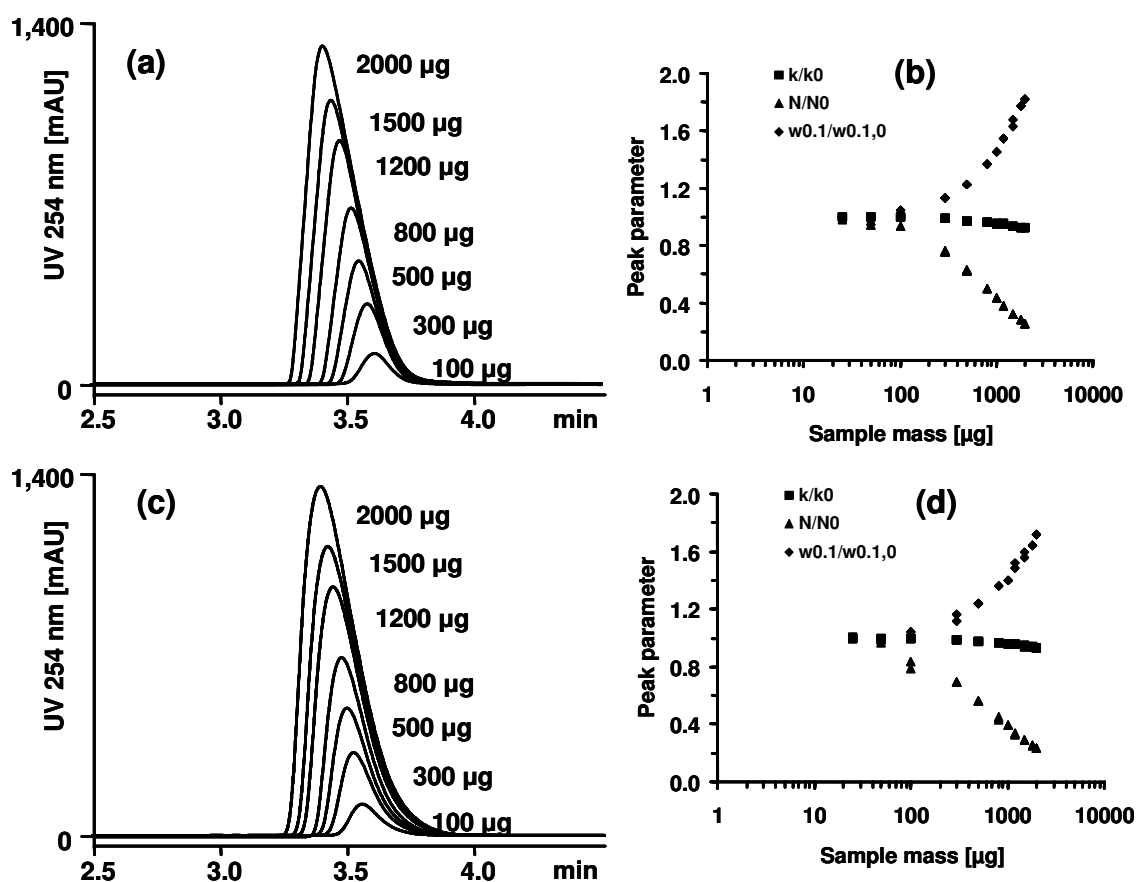


Figure 3.33: Overlays and the corresponding peak shape parameters of phenol on semi-prep Luna (a), (b), and semi-prep Acclaim (c) (d).

Table 3.9 shows the peak shape parameters at low sample loading and the mass loading capacity. The mass loading capacity ($w_{0.1} = 1.1w_{0.1,0}$) for both columns are similar, close to 225 μg (corresponding to 28.7 μg per mL bed volume). However, the peak shapes at non-overloading condition obtained with the Luna were slightly better than with the Acclaim. This could be attributed to the higher retention factor on Luna, despite of identical elution conditions for both columns. On the Acclaim semi-preparative column the loading capacity of phenol was much lower compared to the loading capacity of acetylsalicylic acid, although phenol eluted as non-ionized solute, with the molar loading capacity of approx. 0.3 and 0.8 $\mu\text{mol/mL}$ for phenol and acetylsalicylic acid, respectively. This could be due to the polar interaction of phenol with underivatized silanols.

Table 3.9: Peak shape parameters at low sample mass for phenol on the Luna and Acclaim semi-preparative column and their mass loading capacity

Column	k_0	N_0	$w_{0.1,0}$ (min)	$w_{0.1} = 1.1 w_{0.1,0}$	
				μg	$\mu\text{g/mL bed}$
Luna	3.6	5,000	33.7	225	28.7
Acclaim	2.4	4,900	36.1	220	28.0

3.2.3.4 Loading Capacity Study for Rutin

Rutin is a neutral compound with molecular weight of 610.51 and belongs to natural compound class of flavonoids. The elution of rutin on both packed semi-preparative columns Luna and Acclaim was performed in the mobile phase acetonitrile/methanol (9:1) 20% and water with 0.3% formic acid. This mobile phase was the initial condition for gradient separation of compounds in St. John's wort extract. Rutin was not dissolved in the mobile phase, but in methanol/aqueous formic acid (0.3%): 50/50, because of its low solubility. Its solubility in methanol is only 5 g/L and in water only 1g per 8 L water [24].

Figure 3.34 shows the overlay chromatograms obtained with the Luna, Acclaim and Monolith semi-preparative columns, respectively. The plots of peak shape parameters obtained with these columns are depicted in Figure 3.35. The retention

decreased with the injected mass, as expected. The peaks obtained with the Acclaim column were generally broader than with Luna. However, the mass loading capacity (Table 3.10) obtained with both columns revealed to be similar ($\sim 200 \mu\text{g}$). Monolith exhibited a lower loading capacity for rutin than the packed columns in the same dimension.

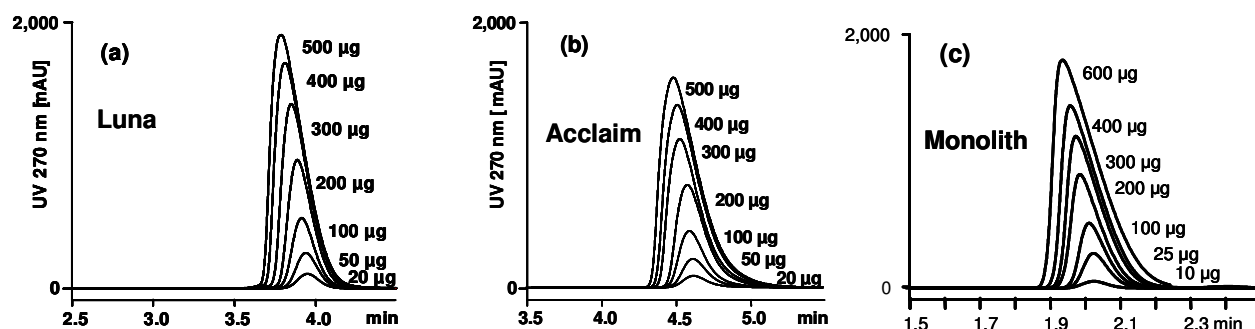


Figure 3.34: Overlaid peaks of rutin on three different stationary phases: On the semi-prep Luna (a), Acclaim (b): mobile phase: 80 % (A) water with 0.3% formic acid - 20 % (B) acetonitrile/methanol (9/1 v/v); temperature: 23°C; flow rate: 5.0 mL/min. On Monolith (c): mobile phase: 85 % (A) water with 0.3% formic acid - 15 % (B) acetonitrile/methanol (9/1 v/v); temperature: 23°C; flow rate: 10.0 mL/min. All chromatograms were recorded at detection wavelength of 270 nm.

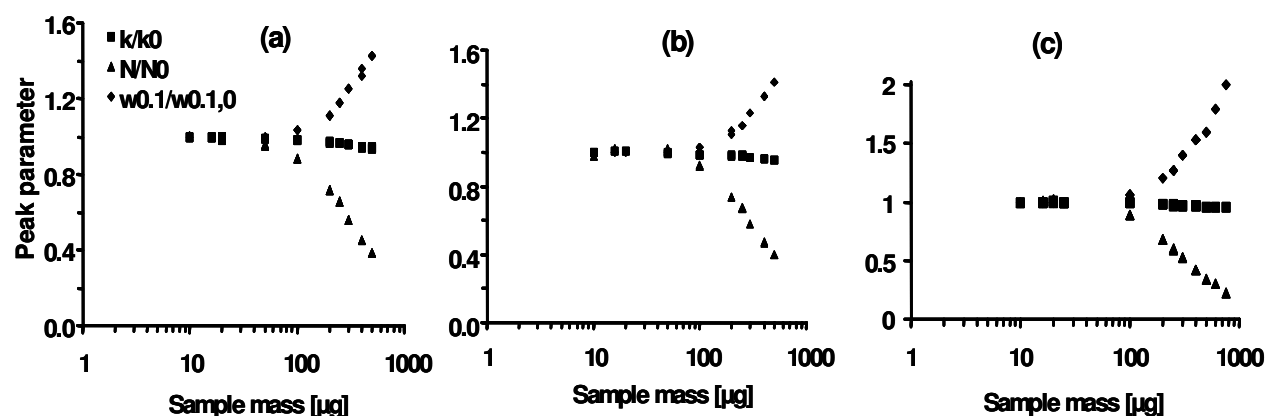


Figure 3.35: Peak shape parameters of rutin on semi-prep Luna (a), (b), and semi-prep Acclaim (c) (d). The mobile phase: 80 % water with 0.1% formic acid - 20 % acetonitrile/methanol (9/1 v/v); temperature: 23°C; flow rate: 5.0 mL/min. All chromatograms were recorded at detection wavelength of 270 nm.

Table 3.10: Peak shape parameters at low sample mass for rutin on the Luna, Acclaim and Monolith semi-preparative columns and the mass loading capacity.

Column	k_0	N_0	$w_{0.1,0}$ (mm)	$w_{0.1}=1.1 w_{0.1,0}$	
				μg	$\mu\text{g/mL bed}$
Luna	2.8	4,020	26.9	196	25.0
Acclaim	3.2	3,500	37.5	200	25.5
Monolith	2.0	3,600	22.2	124	16.8

3.3 Conclusions

The standard tests for silanol activity (NIST, Dionex specification, p-ethylaniline in Engelhardt test) revealed low residual silanol activity for both Luna C18(2) columns and for the semi-preparative Acclaim C18 5 μm column. The results of these tests applied to the corresponding analytical Acclaim C18 5 μm column were inconsistent. The markedly high silanol activity observed with the Engelhardt test from this column could not be confirmed with other tests. However, the methylene selectivity obtained with these columns was identical ($\alpha=1.9$).

The volume loading capacity obtained with Luna and Acclaim semi-preparative columns was similar, whilst Monolith exhibited 66% more volume loading capacity than both packed columns. This can be attributed to the higher total porosity and thus higher column void volume of the monolithic column. The volume loading capacity in the semi-preparative compared to the analytical dimension varied when the retention factors were different. Therefore, to perform a scale-up for volume loading capacity, it is necessary to set similar retention factors for both column dimensions.

In mass overloading experiments with the two compounds acetylsalicylic acid and amitriptyline on the semi-preparative and the analytical columns, different loading capacity for both scales was observed. The Acclaim semi-preparative column was 3.3-fold more loadable than the analytical column for acetylsalicylic acid, whilst semi-preparative Luna exhibited 2-fold loadability compared to the analytical one. Moreover, plots of the peak shape parameters ($w_{0.1}$ and k) of acetylsalicylic acid revealed unusual behavior for both Luna columns. However, the Acclaim 5 μm analytical column showed a clearly weaker selectivity for acetylsalicylic acid and the impurity salicylic acid than the semi-preparative column.

The Luna semi-preparative column exhibited a 3.3-fold mass loading capacity

relative to the analytical one for amitriptyline, whilst the Acclaim semi-preparative scale was 2.5-fold more loadable than the analytical column. Peak shapes for amitriptyline under overloading conditions obtained with both Luna columns measured in all mobile phases (MeOH and ACN) were similar. In contrast, different peak shapes were observed between the Acclaim 5 μm columns.

The loading capacity of phenol and rutin was similar for both Luna and Acclaim semi-preparative columns. However, the peak shapes obtained with the Luna were slightly better.

Based on the results above, it can be concluded that the overloading limits for solute mass of the semi-preparative columns cannot be easily scaled-up from the respective analytical columns. Optimization must be carried out with each specific set-up individually, even for the columns with similar chromatographic properties of their materials, such as both Luna columns, as verified in standard test results.

References

- [1] Ganetsos, G. and Barker, P.E. (Editors) (1992) Preparative and production scale chromatography. Marcel Dekker, Inc., New York.
- [2] Grüner, R. (2001) Charakterisierung und Anwendung stationärer Phasen in der Umkehrphasenchromatographie. *Dissertation*, Universität des Saarlandes, Saarbrücken.
- [3] Engelhardt, H., Blay, Ch. and Saar, J. (2005) Reversed phase chromatography – the mystery of surface silanols. *Chromatographia*, **62** Suppl., 19-29.
- [4] Neue, U.D. (1997) *HPLC columns, Theory, Technology, and Practice*. Wiley-VCH, New York.
- [5] Claessens, H.A., van Straten, M.A., Cramers, C.A., Jezierska, M. and Buszewskib, B. (1998) Comparative study of test methods for reversed-phase columns for high-performance liquid chromatography. *J. Chromatogr. A*, **826**, 136-156.
- [6] Neue, U.D., Tran, K., Iraneta, P.C. and Alden, B.A. (2003) Characterization of HPLC packings. *J. Sep. Sci.*, **26**, 174-186.
- [7] Sander, L.C. and Wise, S.A. (2003) A new standard reference material for column evaluation in reversed-phase liquid chromatography. *J. Sep. Sci.*, **26**, 283-294.

- [8] Neue, U.D., Serowik, E., Iraneta, P., Alden, B.A. and Walter, T.M. (1999) Universal procedure for the assessment of the reproducibility and the classification of silica-based reversed-phase packings: I. Assessment of the reproducibility of reversed-phase packings. *J. Chromatogr. A*, **849**, 87-100.
- [9] McCalley, D.V. (1998) Influence of sample mass on the performance of reversed-phase columns in the analysis of strongly basic compounds by high-performance liquid chromatography. *J. Chromatogr. A*, **793**, 31-46.
- [10] McCalley, D.V. (2006) Overload for ionized solutes in reversed-phase high-performance liquid chromatography. *Anal. Chem.*, **78**, 2532-2538
- [11] Grüner, R., Schwan, F., Engelhardt, H. (1998) Test zur Charakterisierung von RP-Phasen. *Laborpraxis*, **9**, 24-29.
- [12] Engelhardt, H., Grüner, R. (1999) Characterization of reversed-phase columns for efficiency, retention, and silanophilic activity. *Int. Lab.*, **29(5)**, 34-42.
- [13] McCalley, D.V. (1999) Comparison of the performance of conventional C phases with 18 others of alternative functionality for the analysis of basic compounds by reversed-phase high-performance liquid chromatography. *J. Chromatogr. A*, **844**, 23-38.
- [14] McCalley, D.V. (1996) Effect of organic solvent modifier and nature of solute on the performance of bonded silica reversed-phase columns for the analysis of strongly basic compounds by high-performance liquid chromatography. *J. Chromatogr. A*, **738**, 169-179.
- [15] McCalley, D.V. (1997) Comparative evaluation of bonded-silica reversed-phase columns for high-performance liquid chromatography using strongly basic compounds and alternative organic modifiers buffered at acid pH. *J. Chromatogr. A*, **769**, 169-178.
- [16] McCalley, D.V. and Brereton, R.G. (1998) High-performance liquid chromatography of basic compounds problems, possible solutions and tests of reversed-phase columns. *J. Chromatogr. A*, **828**, 407-420.
- [17] McCalley, D.V. (2000) Effect of temperature and flow-rate on analysis of basic compounds in high-performance liquid chromatography using a reversed-phase column. *J. Chromatogr. A*, **902**, 311-321.
- [18] McCalley, D.V. (2002) Comparison of conventional microparticulate and a monolithic reversed-phase column for high-efficiency fast liquid chromatography of basic compounds. *J. Chromatogr. A*, **965**, 51-64.
- [19] Buckenmaier, S.M.C. and McCalley, D.V. (2002) Overloading study of bases using polymeric RP-HPLC columns as an aid to rationalization of overloading on silica-ODS phases. *Anal. Chem.*, **74**, 4672-4681.

- [20] McCalley, D.V. (2003) Comparison of peak shapes obtained with volatile (mass spectrometry-compatible) buffers and conventional buffers in reversed-phase high-performance liquid chromatography of bases on particulate and monolithic columns *J. Chromatogr. A*, **987**, 17-28.
- [21] McCalley, D.V. (2003) Rationalization of retention and overloading behavior of basic compounds in reversed-phase HPLC using low ionic strength buffers suitable for mass spectrometric detection. *Anal. Chem.*, **75**, 3404-3410.
- [22] McCalley, D.V. (2003) Selection of suitable stationary phases and optimum conditions for their application in the separation of basic compounds by reversed-phase HPLC. *J. Sep. Sci.*, **26**, 187–200.
- [23] Engehardt, H., Grüner, R., Scherer, M. (2001) The polar selectivities of non-polar reversed phases. *Chromatographia*, **53** Suppl., 154-161.
- [24] Merck Index 11th edition
- [25] Neue, U.D., Trana, K., Méndez, A. and Carr, P.W. (2005) The combined effect of silanols and the reversed-phase ligand on the retention of positively charged analytes. *J. Chromatogr. A*, **1063**, 35-45.
- [26] Canals, I., Portal, J.A., Bosch, E. and Rosés, M. (2000) Retention of ionizable compounds on HPLC. 4. Mobile- phase pH measurement in methanol/water. *Anal. Chem.*, **72**, 1802-1809.
- [27] Espinosa, S., Bosch, E. and Rosés, M. (2002) Retention of ionizable compounds on HPLC. 12. the properties of liquid chromatography buffers in acetonitrile-water mobile phases that influence HPLC retention. *Anal. Chem.*, **74**, 3809-3818.
- [28] Rosés, M. (2004) Determination of the pH of binary mobile phases for reversed-phase liquid chromatography. *J. Chromatogr. A.*, **1037**, 283–298
- [29] Neue, U.D., Phoebe, C.H., Tran, K., Cheng, Y.F., Lu, Z. (2001) Dependence of reversed-phase retention of ionizable analytes on pH, concentration of organic solvent and silanol activity. *J. Chromatogr. A*, **925**, 49-67.
- [30] Heinisch, S. and Rocca, J.L. (2004) Effect of mobile phase composition, pH and buffer type on the retention of ionizable compounds in reversed-phase liquid chromatography: application to method development. *J. Chromatogr. A*, **1048**, 183-193.
- [31] Nawrocki, J. (1997) The silanol group and its role in liquid chromatography. *J. Chromatogr. A*, **779**, 29-71.
- [32] Snyder, L.R., Dolan, J.W. and Gant, J.R. (1979) Gradient eluent in highperformance liquid chromatography. *J. Chromatogr.*, **165**, 3-30
- [33] IUPAC (1998) *Compendium of Analytical Nomenclature. Definitive Rules 1997*, 3rd ed.; Blackwell: Oxford, U.K.

- [34] Neue, U.D., Wheat, T.E., Mazzeo, J.R., Mazza, C.B., Cavanaugh, J.Y., Xia, F. and Diehl, D.M. (2004) Differences in preparative loadability between the charged and uncharged forms of ionizable compounds. *J. Chromatogr. A*, **1030**, 123–134.
- [35] Guiochon, G. (2002) Preparative liquid chromatography. *J. Chromatogr. A*, **965**, 129-161.
- [36] Unger, K.K. (1992) *Handbuch der HPLC, Teil 2*, GIT Verlag, Darmstadt.
- [37] McCalley, D.V. (2005) Study of overloading of basic drugs and peptides in reversed-phase high-performance liquid chromatography using pH adjustment of weak acid mobile phases suitable for mass spectrometry. *J. Chromatogr. A*, **1075**, 57-64.
- [38] Häggglund, I. and Stahlberg, J. (1997) Ideal Model of Chromatography Applied to Charged Solutes in Reversed Phase Chromatography. *J. Chromatogr. A*, **761**, 3-11.
- [39] Gritti, F. and Guiochon, G. (2005) Effect of the surface heterogeneity of the stationary phase on the range of concentrations for linear chromatography. *Anal. Chem.*, **77**, 1020-1030.
- [40] Gritti, F. and Guiochon, G. (2005) The adsorption mechanism of nortryptiline on C18-bonded discovery. *J. Chromatogr. A*, **1095**, 27-39.
- [41] Davies, N.H., Euerby, M.R. and McCalley, D.V. (2006) Study of overload for basic compounds in reversed-phase high performance liquid chromatography as a function of mobile phase pH. *J. Chromatogr. A*, **1119**, 11–19.
- [42] Blay, Ch. (2003) Charakterisierung stationärer Phasen mit Hilfe der Chemometrik, in Hinsicht auf das Verhalten basischer Stoffe. *Dissertation*, Universität des Saarlandes, Saarbrücken.
- [43] National Institute of Standards & Technology, Certificate of Analysis, Gaithersburg, MD 20899.

Chapter 4

Application of Automated Purification System for Fractionation of Biologically Active Ingredients from Plant Extracts Applying Photometric and Targeted Mass Spectrometric Trigger

4.1 Introduction

The applications of the automated purification system utilizing both photometric- and mass spectrometric trigger is reported in this chapter. The challenge in developing effective procedures for automated purification system is balancing throughput, recovery and purity. The fractionation of precious compounds in St. John's wort extracts by UV and MS trigger is described in detail. Moreover, fractionation of minor degradation products in a thermal stressed pharmaceutical preparation was performed. Approximately 1 mg each of the fractions of these degradation products was required to further study their structure by nuclear magnetic resonance spectroscopy (NMR spectroscopy). Furthermore, fraction collection of toxic gliadin from wheat extract was carried out. The instrumental setup of the automated HPLC purification system is described in detail in Chapter 2.

4.2 Automated Fractionation of Biologically Active Ingredients from St. John's Wort Extract (*Hypericum perforatum* L.)

4.2.1 Introduction and Tasks

St. John's wort (*Hypericum perforatum* L.) is an herb indigenous to Europe, Western Asia, North America, and North Africa [1]. The plant has been used in Europe as a remedy against mood swings and to improve wound healing for many centuries [2]. St. John's wort extracts contain numerous biologically active substances including naphthodianthrones, such as hypericin and pseudohypericin, flavonoids and biflavons, such as amentoflavone, hyperin (hyperoside), rutin, quercitin, quercitrin and I3,II8-biapigenin, the phloroglucin derivates such as hyperforin and adhyperforin,

xanthenes and essential oil monoterpenes and sesquiterpenes [2, 3]. The main constituents and their structures are depicted in Figure 4.1.

Nowadays, the extract of the aerial part of the plant is becoming popular for the treatment of mild to moderate depression [4]. Hyperforin is indicated to be the major compound responsible for antidepressant activity [5]. However, it was further studied that the presence of rutin is mandatory [4]. Recently, it was also reported that flavonoids have antidepressant properties [3]. Furthermore, St. John's wort extract was investigated acting as anti-inflammatory, anti-viral, anti-bacterial, anti-tumour and hepato-protecting [2,5,6]. Although many studies in the phytochemical analysis and in the pharmacology have been done, the mechanisms of action are still under debate [4]. Therefore, further pharmacokinetic and pharmacodynamic studies of the main components and their metabolites are urgently needed to clarify the role of each constituent [7]. High purity fractions of these constituents are necessary.

Fractionation with UV and MS trigger of compounds in St. John's wort extracts from accelerated solvent extractor (ASE) as well as from commercial extracts using packed and monolithic columns was performed. Re-injection of the fractions into the analytical HPLC system with UV detector was carried out to control the purity of the fractions and to calculate the recovery.

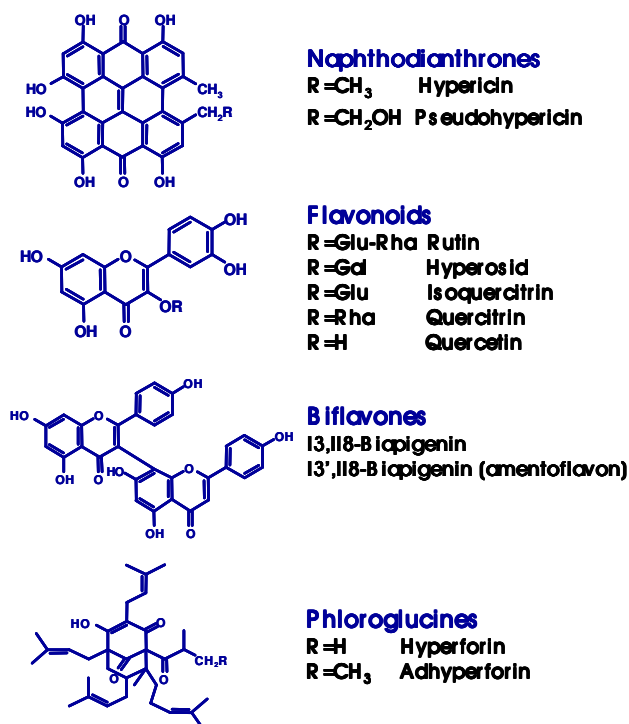


Figure 4.1: The main constituents of *Hypericum perforatum* L. and their structures

4.2.2 Experimental

4.2.2.1 Chemicals and Materials

All reagents used were of analytical grade. Acetonitrile and methanol were purchased from Sigma-Aldrich (Steinheim, Germany), formic acid from Merck (Darmstadt, Germany). High-purity water was obtained from a Purelab Ultra system (ELGA, Celle, Germany). Dried St. John's wort extracts from accelerated solvent extractor were obtained from Dionex (Sunnyvale). Commercial St. John's wort extracts Neuroplant 1x1 coating tablets brand Schwabe Arzneimittel (Karlsruhe) were obtained from a pharmacy.

The semi-preparative separation and fractionation were performed either in a Luna C18(2) column (100 Å, 5 µm, 100 x 10 mm i.d., Phenomenex, Torrance, CA), or a silica-based, C18-derivatized monolithic research column (100 x 10 mm i.d., Merck, Darmstadt, Germany).

Analytical HPLC separations or re-injection of the fractions were carried out on a Luna C18(2) column (100 Å, 5 µm column 150 x 4.6 mm i.d., Phenomenex).

4.2.2.2 Instrumental setups

The instrumental setups for fractionation using optimized APS and for re-injection of the fractions are described in Chapter 2.

4.2.2.3 Conditions for Fractionation

To trigger the fractionation, at least one so called detection channel is required. In this semi-preparative purification system two detection channels are available.

The fractionation can be triggered using one or both detection channels using command for channel selection options: ALL; fraction are collected if a peak is detected in all selected channels or ANY; if a peak is detected in at least one of selected channels).

In UV trigger the selected wavelength is defined as one detection channel, whilst in MS trigger the selected m/z should be extracted on-line. One on-line mass extraction is defined as a detection channel. Therefore, in the program, the detection channel name must be newly defined within the expected elution time. A Chromeleon

program for fractionation of 3 degradation products in a TDS sample using both UV and MS triggers (chromatogram in Figure 4.20) is represented in Appendix.

The substances to be collected and the corresponding m/z with the identification for the online mass extraction (MS_01 to MS_06) are collected in Table 4.1. The fractionation with UV trigger was performed at wavelength 270 nm.

Table 4.1: The substances to be collected with UV and MS trigger and the corresponding m/z values (peak identification in APS runs)

Peak number	Substance	m/z	Online mass extract
1	Rutin	609	MS_01
2	Hyperoside	463	MS_02
3	Isoquercitrin	463	MS_02
4	Astilbin	433	MS_03
5	Quercitrin	447	MS_04
6	Protohypericin	505	MS_05
7	Biapigenin	537	MS_06

4.2.2.3.1 Conditions for fractionation of St. John's wort extract from ASE

Conditions for fractionation and re-injection of fractions are following:

Conditions for fractionation:

Column: Luna semi-preparative column as described above.

Mobile phase: (A) H₂O + 0.3% formic acid, (B) ACN/MeOH:9/1+0.3% formic acid;

Gradient method: 0-3 min 20% B; 3-15 min 20-21% B; 15-17 min 21-45% B; 17-20 min 45-60% B; 20-23 min 60-100% B; injection 300 µL; flow rate: 5 mL/min; UV detection at 270 nm and UV spectra recorded.

Collect outside peaks: no.

MS: Block source temp: 300 °C; Cone voltage -100 V; scan time 1 sec (centroid);

TIC 200-700 m/z; Make up solvent: 0.3% formic acid in water/ACN: 60/40; make up flow 200 µL/min.

Conditions for re-injection into the analytical system:

Column: Luna analytical column as described above.

Mobile phase: (A) H₂O + 0.3% formic acid, (B) ACN/MeOH:9/1+0.3% formic acid;

Gradient program:

0-5 min 20% B, 5-17 min 20-21% B, 17-25 min 21-60% B, 25-27 min 60-100% B, 27-29 min 100% B, 29-31 min 100-20% B, 31-35 min 20% B;

injection 20 µL; flow rate: 1 mL/min; UV detection at 270 nm and UV spectra recorded.

4.2.2.3.2 Conditions for fractionation of commercial St. John's wort extract

HPLC conditions for fractionation were as follows:

The column used for fractionation was a Luna C18(2) column (100 Å, 5 µm, 100 x 10 mm i.d). The mobile phase was 0.3% formic acid in water (A) and ACN/MeOH: 90/10 v/v added with 0.3% formic acid; gradient method: 0-10 min: 20% B; 10-17 min: 20-60% B; flow rate: 5 mL/min; injection volume: 300 µL.

MS condition for fractionation:

The electrospray source was operated at 3 kV needle voltage and 300 °C probe temperature. The cone voltage was -100 V (negative mode). Make-up eluent was ACN/MeOH (9/1 v/v)/water/formic acid: 20/79.7/0.3 v/v, and make-up flow 200 µL/min. Full scan acquisition between m/z 100-700 with a scan time of 0.5 sec was performed.

HPLC condition for analytical separation and re-injection of fractions:

Mobile phase used was (A) H₂O + 0.3% formic acid and (B) ACN/MeOH: 9/1 +0.3% formic acid; flow rate 1 mL/min; temperature 25 °C, detection 3D spectra and 270 nm; gradient method: 0-10 min: 20% B; 10-25 min: 20-60% B; 25-27 min: 60-100% B.

4.2.3 Results and Discussion

4.2.3.1 Fractionation of St. John's Wort Extract from Accelerated Solvent Extraction (ASE)

The aim of this study was fractionations of 7 substances (Table 4.1) from St. John's wort extracts obtained by ASE. Fractionation was performed in 3 different modes: with non-selective UV trigger, with simultaneous UV and MS trigger, and with MS trigger.

4.2.3.1.1 Fractionation with UV trigger and determination of purity and recovery

The fraction collection was performed with UV trigger applying one detection channel at 270 nm. The parameters for the fractionation using detection channel 1 were set so that all of the desired peaks could be collected.

Figure 4.2 shows the UV chromatogram and the collected fractions (filled zones). The fractionation of the desired substances was successful. However, there were more fractions collected than expected, since UV is a non-selective trigger. Only the fractions of 7 substances listed in Table 4.1 were re-injected into the analytical system (Figure 4.4). The purity of the fractions determined from relative peak areas was satisfying, except for isoquercitrin (78%). The purity of rutin, astilbin, protohypericin and biapigenin was actually 100%. The reason for the impurities was the carry over from previous fractions. The high impurity of isoquercitrin is due to the poor resolution of the peaks of hyperoside and isoquercitrin using the semi-preparative set-up.

The recovery of the fraction was calculated from the peak areas of the respective substances in the re-injected fraction compared to these in the original ASE extract with consideration of the dilution factor (volume of fractions) and the injection volume. The so calculated recovery of rutin and biapigenin was determined to be 100% and 80%, respectively. Figure 4.3 shows an analytical run of St. John's wort ASE extract. As can be seen, the selectivity of the peaks on the analytical Luna C18(2) column is better than on the semi-preparative one. This could be due to the different column length between these columns (100 mm for semi-preparative, 150 mm for analytical column). Hence, the analytical column exhibited higher peak capacity.

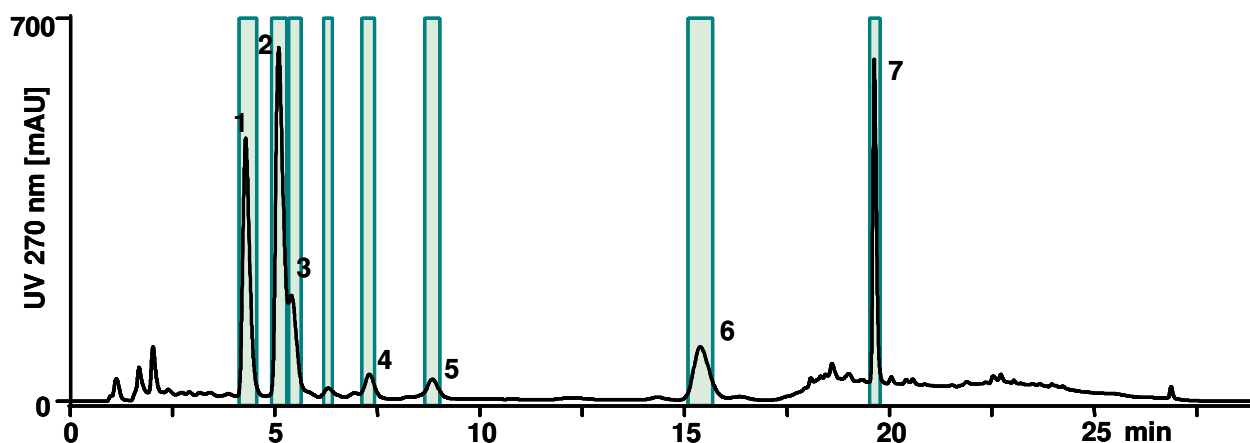


Figure 4.2: UV chromatogram of St. John's wort ASE extract and the collected fractions (filled zones). 1: rutin, 2: hyperoside, 3: isoquercitrin, 4: unknown peak with m/z 433, 5: quercitrin, 6: protohypericin, 7: biapigenin. Fraction collection parameters: Peak start slope: 3; peak end slope: -3; peak start threshold: 15; peak end threshold: 15; threshold no peak end: 500; threshold do not resolve: 200.

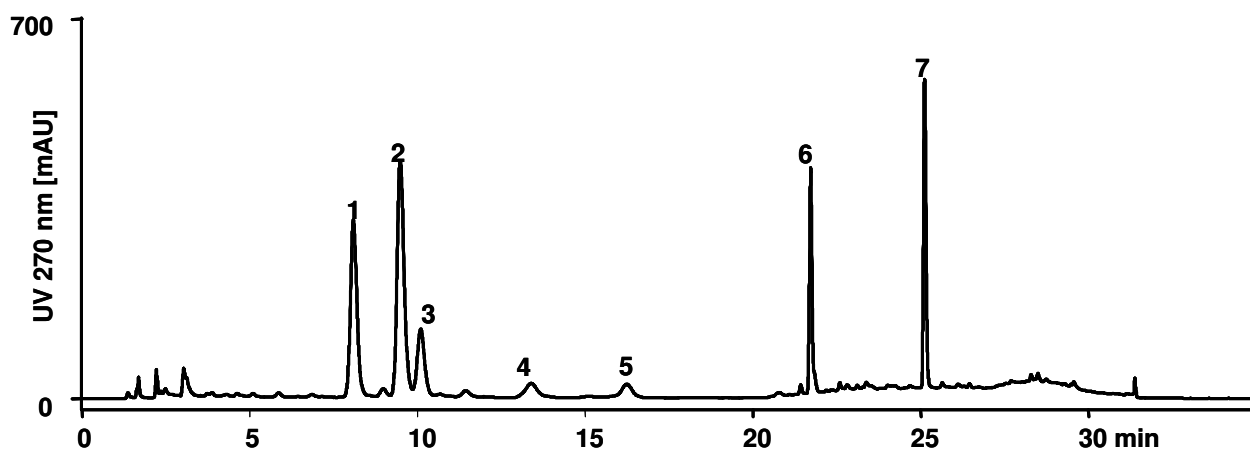


Figure 4.3: UV chromatogram of St. John's wort ASE extract analyzed using the gradient method for re-injection. Peak identification is listed in Table 7.

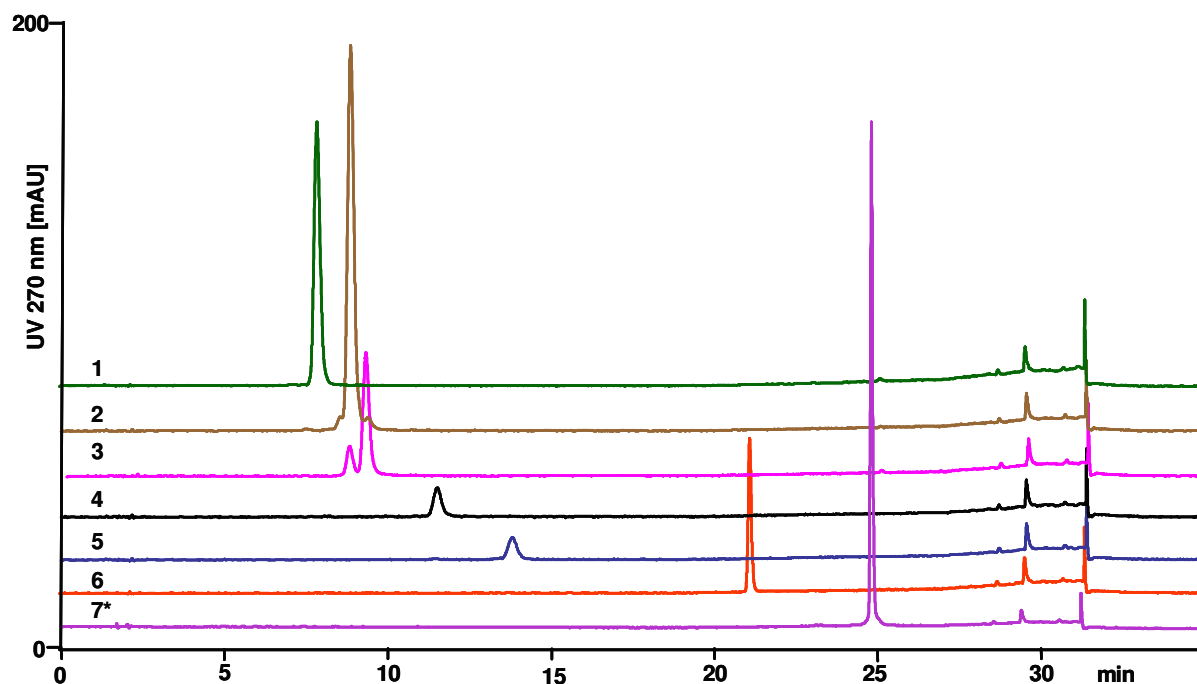


Figure 4.4: Re-injected fractions into the analytical system. (7*) The signal height of fraction 7 (biapigenin) was approx. 300 mAU.

4.2.3.1.2 Fractionation with simultaneous UV and MS trigger and the determination of purity and recovery

The following 4 substances in St. John's wort ASE extract were collected (Table 4.1, peak number 4-7): astilbin with m/z 433, quercitrin (m/z 447), protohypericin (m/z 505) and biapigenin (m/z 537). The fraction collection was performed with MS and UV trigger using 2 detection channels (channel evaluation: ALL). Detection channels 1 and 2 were used for MS trigger and for UV trigger at 270 nm, respectively. To perform the fractionation with MS trigger, extracting mass traces online is required. The m/z values of substances above were defined as MS_03 to MS_06 for the online mass extract as described in Table 4.1. Since each online mass extract needs a detection channel, the settings for detection channel 1 (MS trigger) are varied with the run time. Time program for detection channel 1: 0-8 min MS_03; 8-12 min MS_04; 12-17 min MS_05; 17-25 min MS_06.

In this experiment, the fractions were collected only when the conditions for fractionation were fulfilled in both detection channels. Figure 4.5 shows the UV chromatogram and the online mass extracts for four substances to be collected. As

shown in Figure 4.5b, the sensitivity of the mass spectrometric signals were very low, hence the signal-to-noise ratio was not satisfying. This could be due to fouling in the cone or block source. This resulted in lower fraction zones and therefore incomplete fractionation.

The chromatograms of re-injected fractions are shown in Figure 4.6. The obtained purity of the fractions (as relative peak areas) was 100% for astilbin (m/z 433), 91% for quercitrin, 100% for protohypericin, and 98% for biapigenin, respectively. The purity of quercitrin was quite low compared to other substances, since the previous peak was incompletely collected (Figure 4.5, fraction 1), so that a quite concentrated peak substance remained in the capillary between switching valve and droplet former of fraction collector. This resulted in high carry-over peak relatively to lower substance peak of quercitrin.

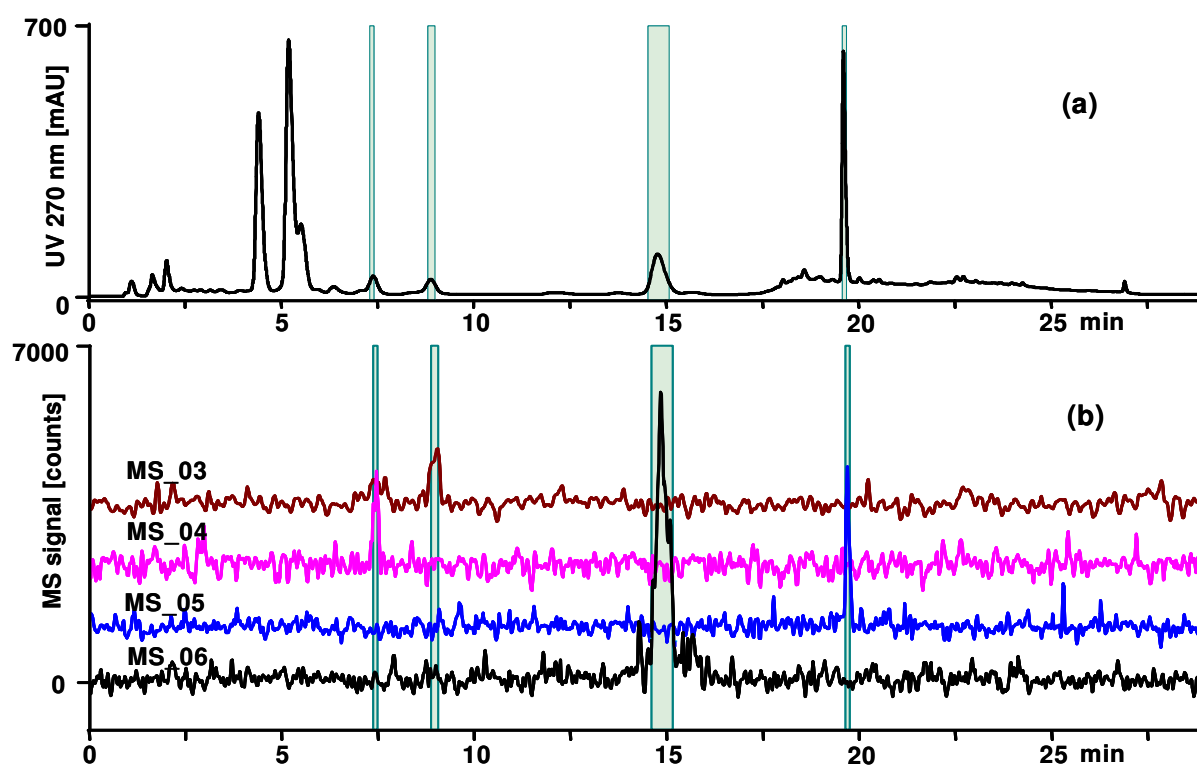


Figure 4.5: UV chromatogram (a) and online mass extract (b) for fractionation (filled zones) with simultaneous UV and MS trigger, 4: MS_03: m/z 433 (astilbin), 5: MS_04: m/z 447 (quercitrin), 6: MS_05 m/z 505 (protohypericin), 7: MS_06: m/z 537 (biapigenin). Fractionation parameters for detection channel 1 (MS trigger): Peak start threshold 1500; peak end threshold 1500; threshold no peak end 1500; threshold do not resolve 1500. Detection channel 2 (UV trigger): parameters as in previous section (fractionation with UV trigger).

The recovery of biapigenin was calculated to be 41%. This low recovery was also due to incompletely collected fraction (fraction volume of 680 μL , compared to 2000 μL with UV trigger) caused by lower signal to noise ratio of the mass spectrometric signals.

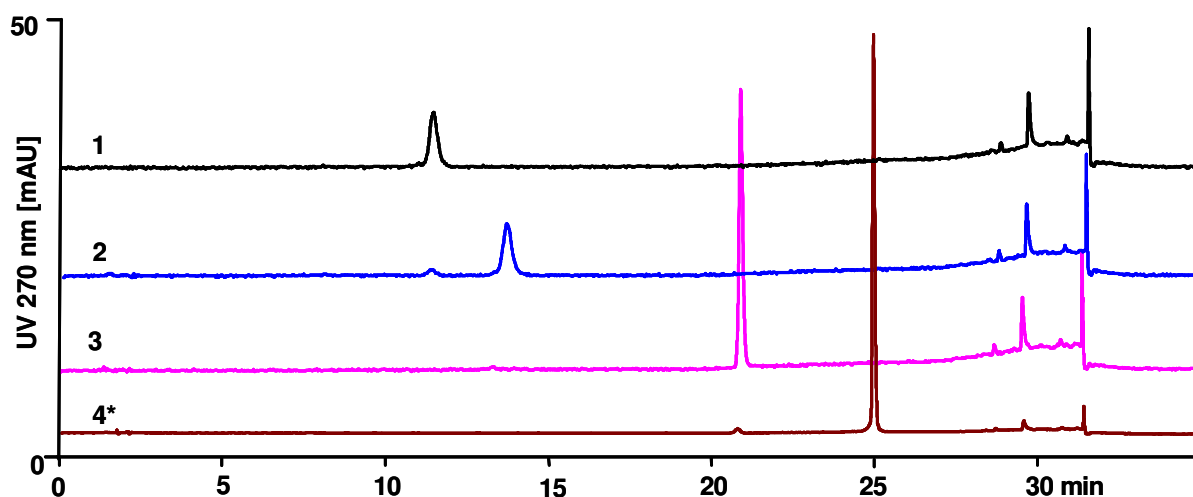


Figure 4.6: Re-injected fractions into the analytical system. (*) The signal height of fraction 7 (biapigenin) was approx. 300 mAU.

4.2.3.1.3 Fractionation with MS trigger and the determination of purity and recovery

The substances in St. John's wort ASE extract listed in Table 4.1 were collected: rutin (m/z 609), hyperoside and isoquercitrin (m/z 463), unknown substance with m/z 433, quercitrin (m/z 447), protohypericin (m/z 505) and biapigenin (m/z 537). The fraction collection was carried out with MS trigger.

Both detection channels were used for this fractionation (Channel evaluation: ANY). Detection channel 1 was used to trigger the fractionation of rutin (MS_01), hyperoside and isoquercitrin (MS_02) and biapigenin (MS_06), while detection channel 2 was used to trigger smaller peaks with m/z 433 (astilbin, MS_03), 447 (quercitrin, MS_04) and 505 (protohypericin, MS_05). The threshold for detection channel 1 was set higher than for channel 2. The time program for detection channel 1 was set as follows: 0-4.8 min MS_01; 4.8-10 min MS_02; 10-25 min MS_06. Time program for detection channel 2 was following: 0-8 min MS_03; 8-12 min MS_04; 12-25 min MS_05.

Figure 4.7 shows the online mass extracts for collected substances. The chromatograms of fractions re-injected into the analytical system are shown in Figure 4.8. The obtained purity of the fractions (as relative peak areas) was determined to be >98% for all fractions except for isoquercitrin and quercitrin. The calculated recovery was 100% for rutin and 44% for biapigenin, respectively. This low recovery was also due to incompletely collected fraction (fraction volume of 620 μL , compared to 2000 μL with UV trigger).

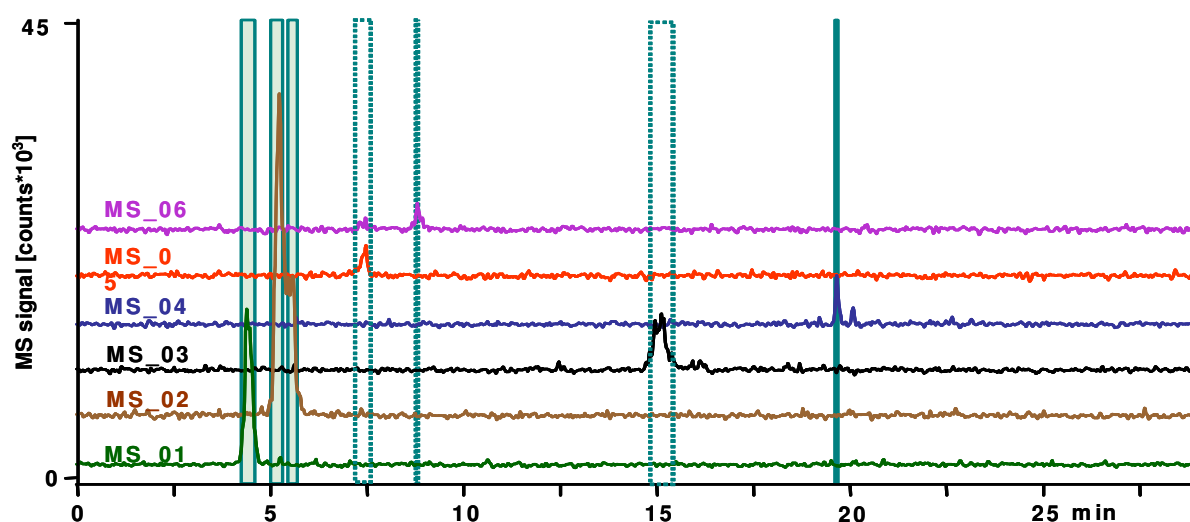


Figure 4.7: Online mass extracts for fractionation with MS trigger. Filled zones: triggering in detection channel 1, dashed zones: triggering in detection channel 2. Parameters for fractionation using detection channel 1: Peak start threshold 2000; peak end threshold 2000; threshold no peak end 13000; threshold do not resolve 12000. Parameters for detection channel 2: Peak start threshold 1500; peak end threshold 1500; threshold no peak end 1500; threshold do not resolve 1500.

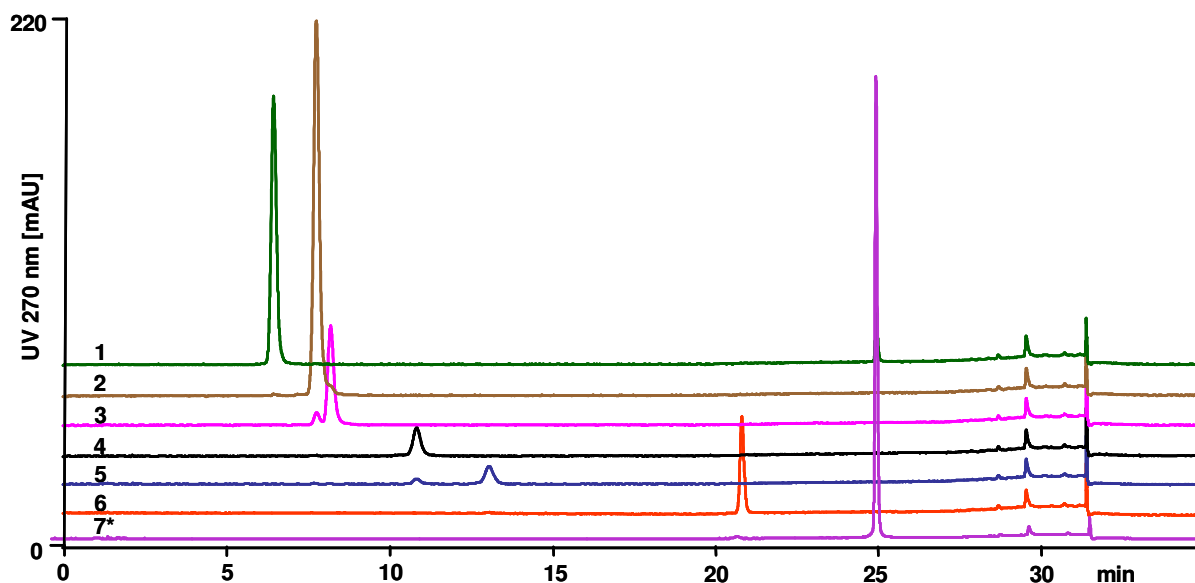


Figure 4.8: UV chromatogram of fractions re-injected into the analytical system. (*) The signal height of fraction 7 (biapigenin) was approx. 300 mAU.

4.2.3.2 Fractionation of commercial St. John's wort extract

The aim of the study described in this section was to fractionate the substances as depicted in Table 4.1 from a commercial St. John's wort coating tablet. The fractionation was carried out applying UV trigger and MS trigger. The gradient program for the HPLC separation was optimized from earlier runs (section 4.2.3.1). The separation time was shorter than that performed in the previous section.

4.2.3.2.1 Fractionation with UV trigger and determination of the purity and recovery

The fraction collection was performed with UV trigger applying one detection channel at 270 nm. Figure 4.9 shows the UV chromatogram and the collected fractions (filled zones) of St. John's wort commercial extract. The sample was prepared from 1 tablet dissolved with 20 mL eluent (extract from approximately 3 g of plant material). As can be seen, the UV signal intensity is 2-fold higher than that from ASE extract produced from 5 g plant material and dissolved in 10 mL eluent (Figure 4.2). Using the optimized gradient program, the separation time was 25% shorter than in earlier runs (section 4.2.3.1), however no significant decrease in resolution was observed.

The purity of 4 fractions re-injected (Figure 4.10) was determined to be 100% for

rutin, 94% for hyperoside, 82% for isoquercitrin and 100% for biapigenin. The low purity of isoquercitrin is also due to the carry over from previous fractions caused by the poor resolution of the peaks of hyperoside and isoquercitrin. The recovery of the fractions was calculated to be 83% for rutin, 74% for hyperoside, 63% for isoquercitrin and 73% for biapigenin.

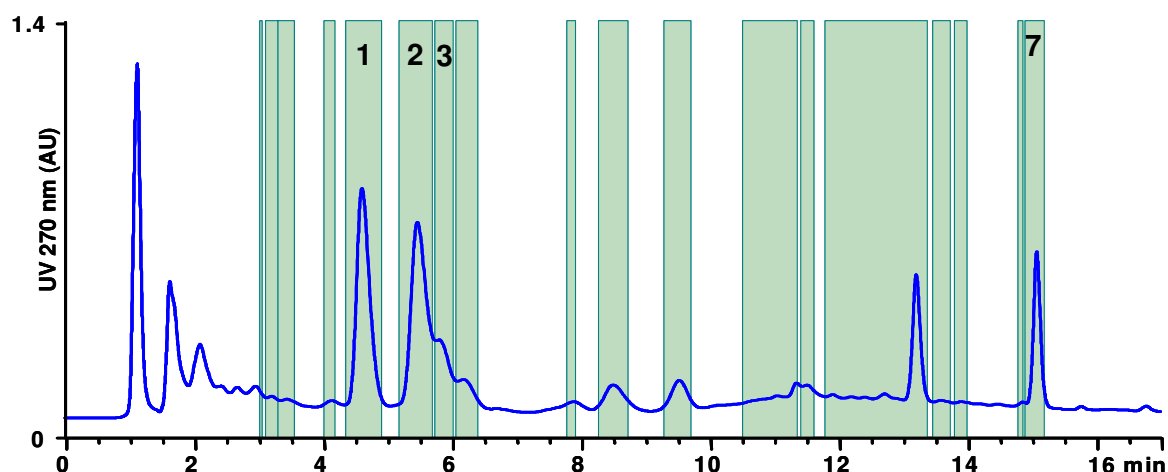


Figure 4.9: UV chromatogram of commercial St. John's wort extract and the collected fractions (filled zones). 1: rutin, 2: hyperoside, 3: isoquercitrin, 7: biapigenin. Fraction collection setting: peak start and end threshold 50 mAU, peak start slope 1, peak end slope -3; threshold no peak end: 600; threshold do not resolve: 400.

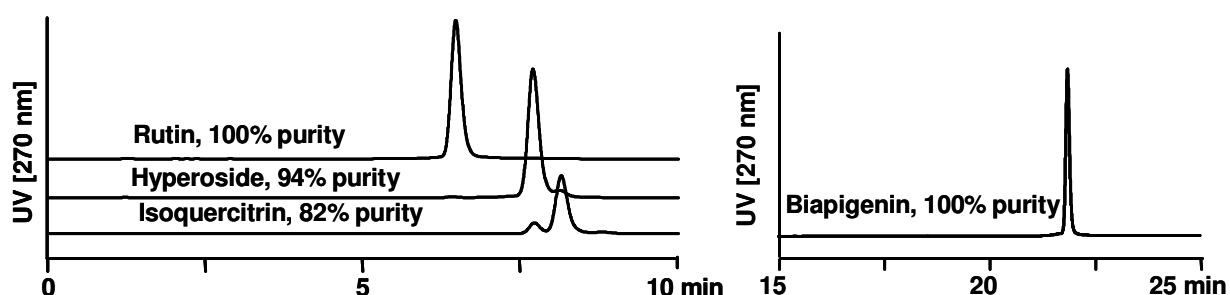


Figure 4.10: Re-injected fractions collected applying UV trigger into the analytical system.

4.2.3.2.2 Fractionation with MS trigger and the determination of purity and recovery

For mass targeted fraction collection, mass traces were on-line extracted for MS_01, MS_02, MS_03, MS_04 and MS_06 as listed in Table 1.

Figure 4.11 shows the online mass extracts of fractionation applying MS trigger

carried out with optimum conditions of mass spectrometer. The MS signals were 10-times higher than that in the previous experiment. The signal-to-noise ratio was satisfying. However, the resolution of the hyperoside and isoquercitrin peaks was lost due to band broadening in the splitter. Therefore, only one fraction of these substances was obtained.

The chromatograms of the fractions re-injected into the analytical system are shown in Figure 4.12. The fraction of hyperoside and isoquercitrin was well resolved by the analytical chromatography. The obtained purity of the fractions could be determined to be 97% for rutin and 86% for biapigenin. The calculated recovery was 24% for rutin and 59% for biapigenin.

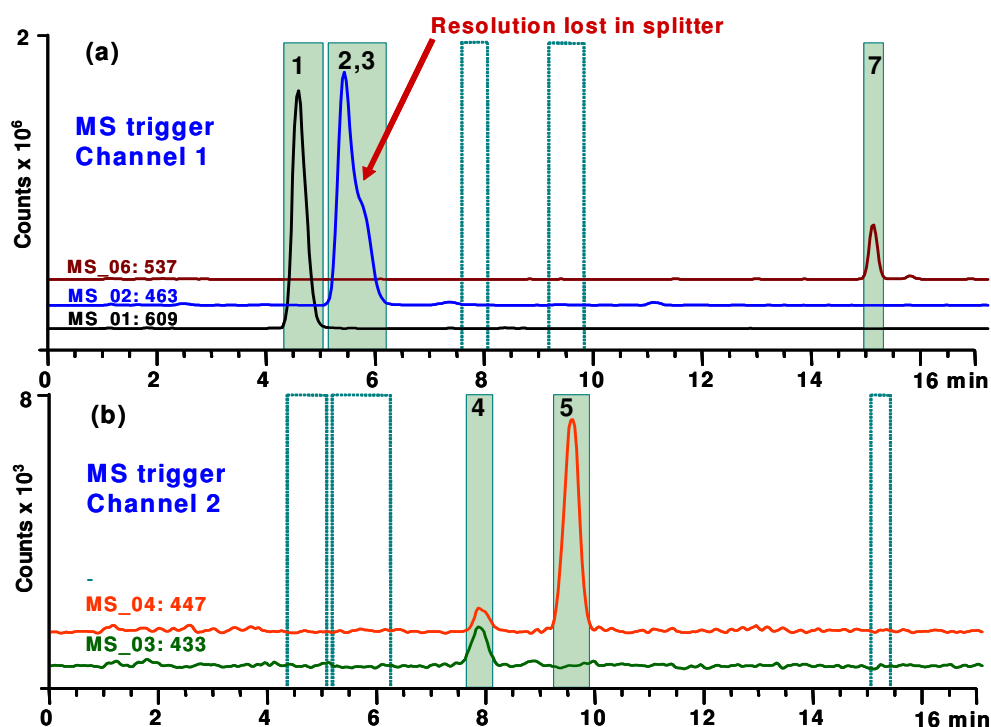


Figure 4.11: Online mass extract of commercial St. John's wort extract and the collected fractions (filled zones). (a) Detection channel 1, (b) Detection channel 2. Peaks 1: rutin, 2: hyperoside, 3: isoquercitrin, 4: astilbin, 5: quercitrin, 7: biapigenin. Fraction collection setting for detection channel 1: peak start and peak end thresholds 20,000 counts; for detection channel 2: peak start and peak end thresholds 2,000 counts

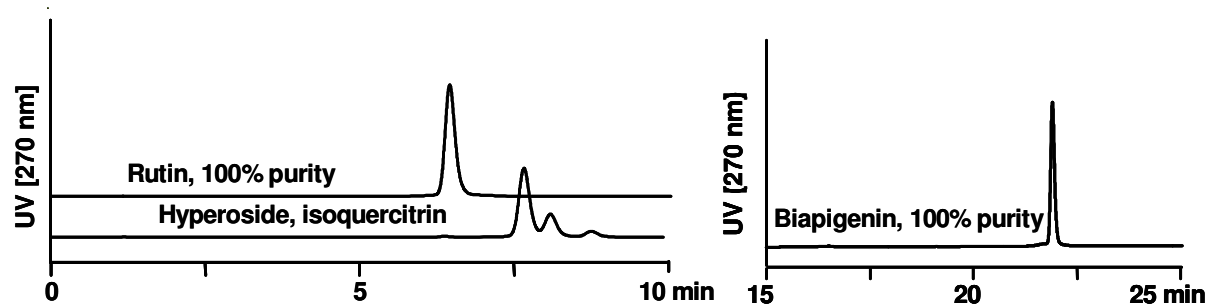


Figure 4.12: Re-injected fractions collected applying mass based trigger into the analytical system.

4.2.3.2.3 Fractionation with MS trigger using silica-based RP-monolithic column

Silica-based RP monolithic columns provide larger total porosity and thus higher permeability compared to packed RP columns. This allows operation at higher flow rates under moderate column back pressure. Therefore, it was expected that the use of this column for fractionation of St. John's wort extracts could increase throughput of samples with high purity.

Figure 4.13 depicts chromatograms of St. John's wort separation on Luna C18(2) and on a silica-based RP monolithic column (Monolith). At the same flow rate and elution conditions, the separation on Luna was superior compared to that on Monolith (Figure 4.13a). The resolution of the rutin and hyperosid peaks was 2.3 for Luna and 0.8 for Monolith. On Monolith, the resolution of these peaks decreased with increasing flow rate (Figure 4.13 b-d, gradient time was adapted to the flow rate).

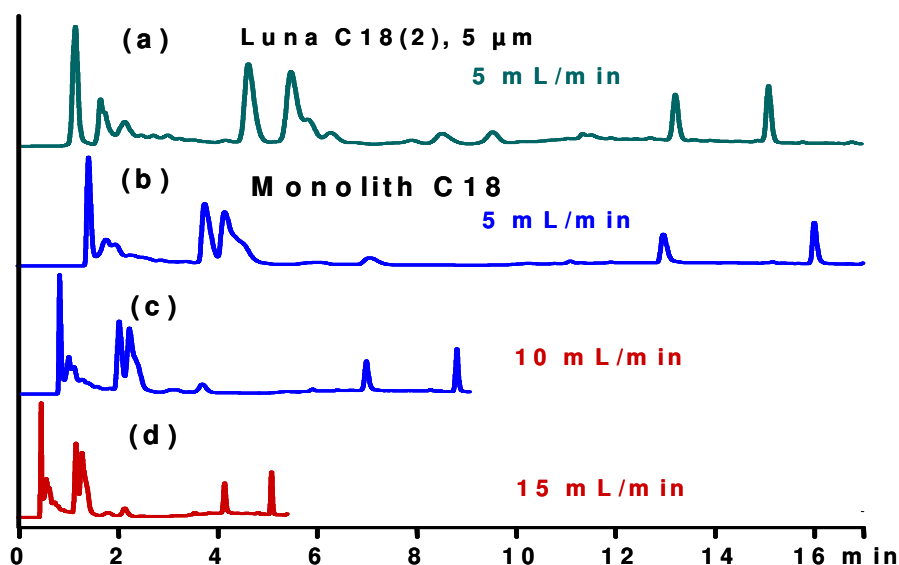


Figure 4.13: Separation of St. John's wort commercial extract (a) at 5 mL/min on Luna C18(2), (b) (c) (d) on Monolith at 5, 10 and 15 mL/min, respectively

Fractionation of St. John's wort extract on Monolith applying MS trigger is shown in Figure 4.14. As can be seen, the signals of online mass extracts were broader than the UV signal. The MS signal of peak 1 (rutin) overlapped partly with peak 2 (hyperoside). Because the peak end threshold for rutin peak was set at lower value, a part of hyperoside peak was collected with rutin. Therefore, the purity of rutin was quite low (94%), as shown in re-injected fractions in Figure 4.15. Hyperoside and isoquercitrin peaks co-eluted even in the main flow (peak 2 and 3 in Figure 4.14, UV signals). The re-injection was performed on the Luna analytical column, because a respective monolithic column in analytical dimension was not available. All peaks collected with MS_02 could be resolved by this analytical column, as shown in Figure 4.15. The purity of biapigenin was 100%. The recovery of rutin and biapigenin was determined to be both 100%.

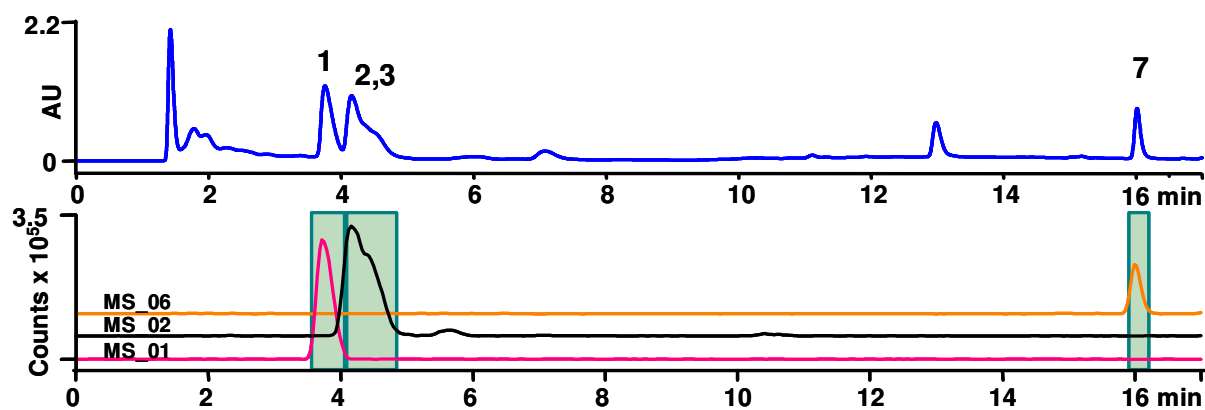


Figure 4.14: UV chromatogram and mass based fractionation separated on Monolith at 5 mL/min. Gradient: 0-10 min: 15% B; 10-17 min: 15-60% B. Fraction collection settings: detection channel 1 for MS_01 and MS_03, peak start and peak end thresholds 20,000 counts; detection channel 2 for MS_02, peak start threshold 200,000 and peak end thresholds 20,000 counts

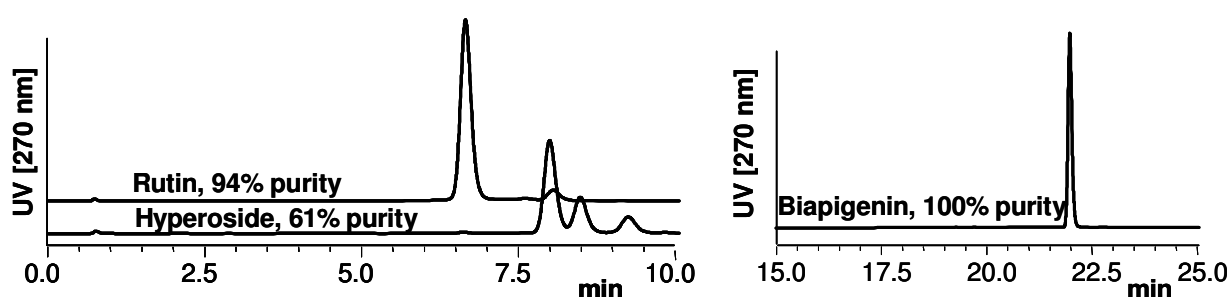


Figure 4.15: Re-injection of fractions collected as in Figure 4.15.

In order to increase the throughput, it was attempted to carry out fractionation at a column flow rate of 10 mL/min. The separation time was shortened to 6 min (Figure 4.16). The resolution of rutin and hyperoside was comparable to the separation with the same flow rate but was completed in 9 min run time, as depicted in Figure 4.14. The peak end threshold of rutin fractionation was set approximately 2/3 from peak maximum, so that contamination with the next peak could be avoided (Figure 4.16b). Therefore the purity of this fraction was 100% (Figure 4.16c), but the recovery was only 24%. The purity of biapigenin was only 86%, because a quite concentrated rutin peak remained in the capillary between the switching valve and drop former due to incomplete fractionation of the previous peak (carry-over effect). This problem could be solved, if the option in the fractionation parameter “collect outside peak yes” is

implemented. However, a large number of fraction collection tubes will be needed to collect the eluents between the rutin and biapigenin fraction and this complicates identification of the correct fractions.

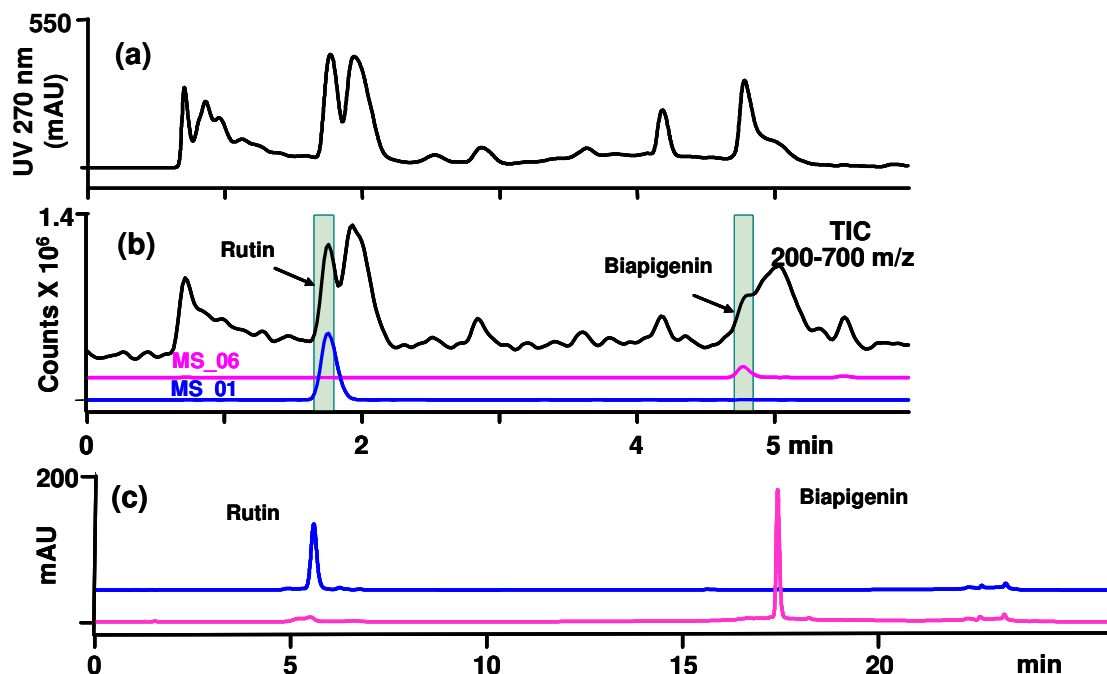


Figure 4.16: Fast chromatography and fractionation of St. John's wort extract on Monolith at 10 mL/min. (a) UV chromatogram, (b) TIC, online mass extract and collected fraction (filled zones), (c) re-injection of the fractions on Luna C18(2) analytical dimension at flow rate 1.7 mL/min. Gradient program for fractionation: 0-2.5 min 15% B; 2.5-6 min 60% B, fraction collection setting: detection channel 1 (MS_01) peak start threshold 20,000 counts, peak end threshold 500,000; detection channel 2 (MS_06) peak start and peak end threshold 20,000 counts.

4.2.4 Conclusion

The optimized APS is suitable for the fully automated fractionation of active ingredients of St. John's wort. Fractionation was carried out with UV trigger, MS trigger and simultaneous UV and MS trigger. Recoveries were in the range 63 to 100%, whilst the fraction purity was between 78 and 100%. For completely separated peaks, obtained purities approach 100%. Lower purity values are due to either incomplete chromatographic separation of the compounds (lower selectivity) or carry-over of previous peak caused by incomplete fraction collection.

4.3 Fractionation of degradation products from active ingredients in a transdermal delivery system drug

4.3.1 Introduction

This study was designed to implement automated fractionation of degradation products from the active ingredients present in a transdermal drug delivery system (TDS). The TDS contained 2 active ingredients at a markedly different content. Both active ingredients are natural substances, but their identity cannot be disclosed for the sake of the collaborator's interests. The related degradation products were formed during 13 month storage of this formulation at 40 °C. In order to identify the structures of the related degradation products by NMR, it was necessary to obtain a sufficient quantity of highly pure fractions of each substance.

4.3.2 Experimental

4.3.2.1 Chemicals and materials

All reagents used were of analytical grade. Acetonitrile and methanol were purchased from Sigma-Aldrich (Steinheim, Germany), trifluoroacetic acid (TFA) from Fluka (Buchs, Switzerland). High-purity water was obtained from a Purelab Ultra system (ELGA, Celle, Germany). TDS drugs containing active ingredients A and B were from Novosis (Munich, Germany)

The semi-preparative separation and fractionation were performed in a Synergi RP-Polar column (80 Å, 4 µm, 150 x 10 mm i.d., Phenomenex, Torrance, CA).

Analytical HPLC separations or re-injection of the fractions were carried out on a Synergi RP-Polar column (80 Å, 4 µm, 150 x 4.6 mm i.d., Phenomenex, Torrance, CA).

4.3.2.2 Instrumental Setups

The instrumental setups for fractionation using optimized APS and for re-injection of the fractions are described in Chapter 2.

4.3.2.3 Sample preparation and conditions for separation and fractionation

10 TDS samples, containing 0.4% active ingredient A and 11% active ingredient B

(identity of active ingredients confidential) were extracted in 250 mL acidic acetonitrile/ 0.10% hydrochloric acid by slow shaking overnight followed by 4 h sonication. This stock solution contained 0.17 mg mL⁻¹ active ingredient A and 4.62 mg mL⁻¹ active ingredient B. For HPLC injections, 12 mL of this solution were diluted with 88 mL water containing 0.025% TFA and then filtered through a 0.45 µm Teflon filter. The injection volume was 1000 µL. Purification using the 150 x 10 mm i.d. Synergy RP-polar column was performed by isocratic elution at 12% acetonitrile in 0.025% aqueous TFA for 5 min, followed by a gradient of 12-23% acetonitrile in 7 min, and finally 23-50% acetonitrile in 1.5 min at a flow-rate of 5.7 mL/min and 25 °C. Diode array spectra were recorded and the elution profile was monitored at 205 nm. The settings for mass spectrometric detection were as follows: block source temperature, 300 °C; needle voltage 2 kV; cone voltage 30 V (positive mode); scan time: 1 s; make-up flow, 200 µL min⁻¹, except from 9-11 min 300 µL min⁻¹; make-up eluent, 79.98% water/0.02% TFA/20% acetonitrile. The settings for fraction collection with photometric trigger were as follows: peak start threshold, 4 mAU; peak end threshold, 2 mAU; peak start slope 3 mAUs⁻¹; peak end slope, -2 mAUs⁻¹. The settings for MS trigger were: on-line extracted mass traces for m/z 218±0.5, 332±0.5, and 291±0.5.; peak start threshold, 250,000 counts; peak end threshold, 150,000 counts. The conditions for analytical re-chromatography on the 150 x 4.6 mm Synergy column were the same as for fractionation, except for the flow rate, which was 1.2 mL min⁻¹ and the injection volume, which was 50 µL.

4.3.3 Results and discussions

4.3.3.1 Optimization of the separation

To separate the substances in the TDS containing the 2 active ingredients as well as the degradation products, a semipreparative polar reversed-phase column was selected. The separation was carried out using the instrumental setup described above with an acetonitrile gradient in water containing 0.025% trifluoroacetic acid.

The separation of the sample was first carried out with eluent containing acetonitrile and water titrated with phosphoric acid at pH 2.5 and 5 mM TEA. Because this eluent is not suitable for detection by mass spectrometry (it builds a salt tri-ethylammonium phosphate), the use of TEA was then not considered. Furthermore, separation with eluent adjusted to pH 2.5 with commonly used additives in HPLC-MS such as formic

acid and TFA was carried out. No retention was observed by using formic acid as additive. Figure 4.17 compares the separation at pH 2.5 using phosphoric acid and TFA. It is apparent that useful selectivity difference could be obtained by changing the additive. Peaks 1, 2 and 3 were the degradation products to be collected. TFA was preferred, first because it is a volatile acid, second because the obtained peak shapes were superior and third because the substance to be collected (peak 2, degradation product 2) did not elute next to the major compound active ingredient B.

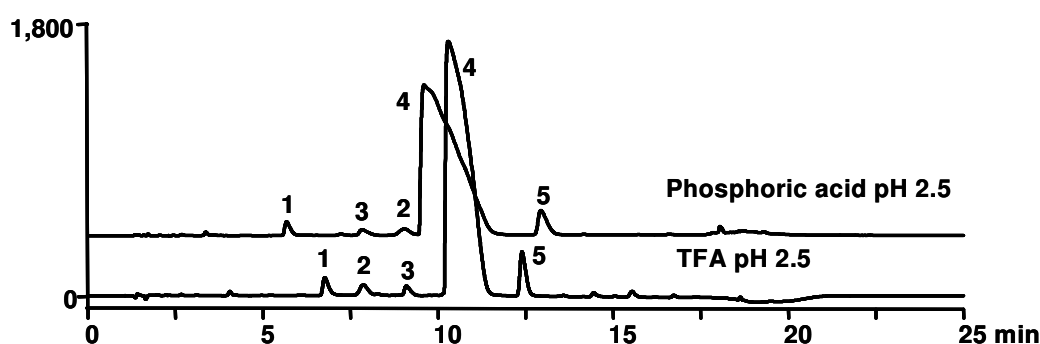


Figure 4.17: Separation of TDS sample on the analytical system using eluent containing phosphoric acid and TFA both at pH 2.5. Peak 1: degradation product (DP) 1, 2: DP2, 3: active ingredient A, 4: active ingredient B, 5: DP3.

Figure 4.18 shows separations performed on the semi-preparative Synergi RP-Polar column at different injection volumes. The resolution decreased with increasing injection volume. However, up to injection volume of 1000 μL , the resolution of peaks of degradation products was satisfying.

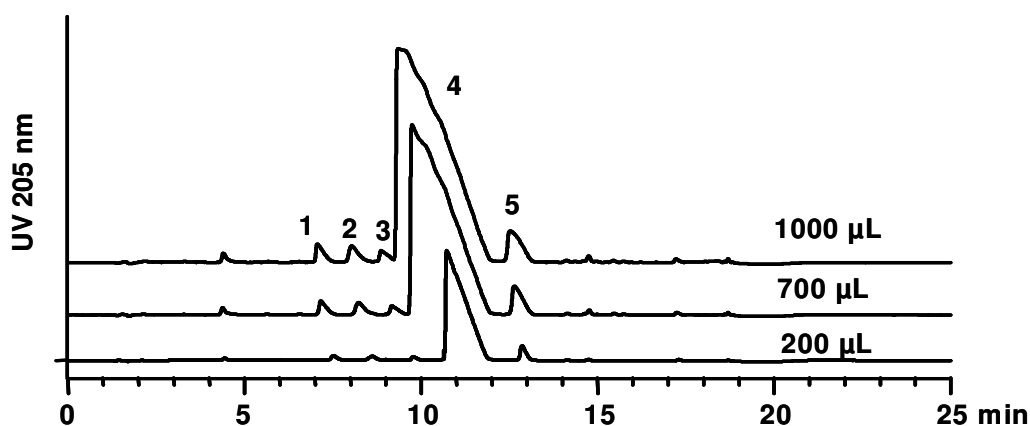


Figure 4.18: Separation of TDS sample on the semi-preparative APS at different injection volumes. Peak identifications see Figure 4.17.

4.3.3.2 Fraction collection and determination of purity and recovery

The fraction collection was performed with MS and UV trigger using 2 detection channels (channel evaluation: ALL). Therefore, only desired degradation products DP1, DP2 and DP3 were collected. Detection channels 1 and 2 were used for UV trigger at 205 nm and for MS trigger, respectively.

Figure 4.19 shows the UV chromatogram and the online mass extracts for 3 substances to be collected. As can be seen, the separation was excellent and the peaks of the three substances of interest were completely collected. Figure 4.20 shows the chromatogram from the injection of TDS sample into the analytical system and the re-injected fractions. The purity was determined to be 100% for DP1 and DP2 and 98.7% for DP3. It is not clear, why DP3 was contaminated with a small amount of active ingredient B. However, its purity was still >98%. The recovery of desired compounds was calculated to be 99.6% for DP1, 100% for DP2 and 97.8% for DP3.

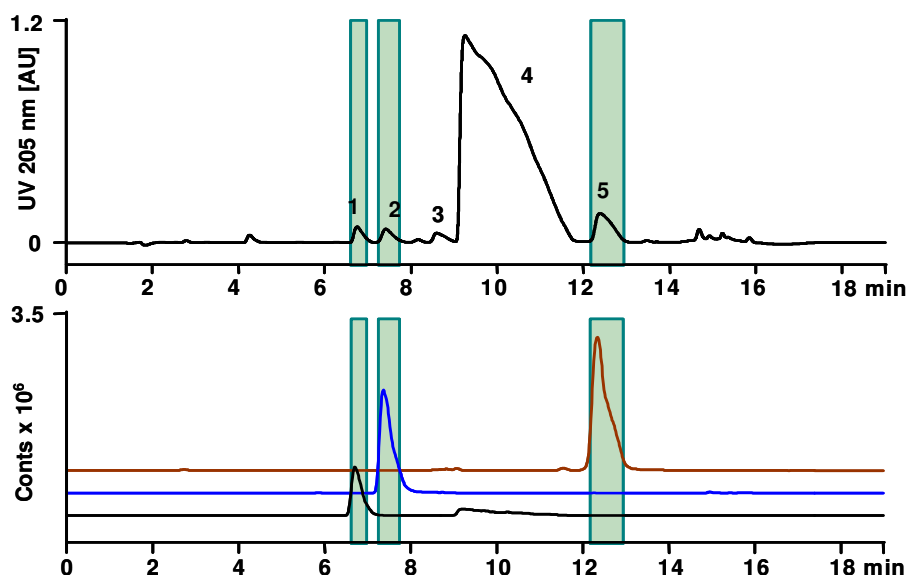


Figure 4.19: UV chromatogram and online mass extract for fractionation of degradation products in thermal stressed TDS sample containing 2 active ingredients with simultaneous UV and MS trigger (filled zones). Peak 1: degradation product 1 (DP1, m/z 219), 2: DP2 (m/z 333), 3: active ingredient A, 4: active ingredient B, 5: DP3 (m/z 292).

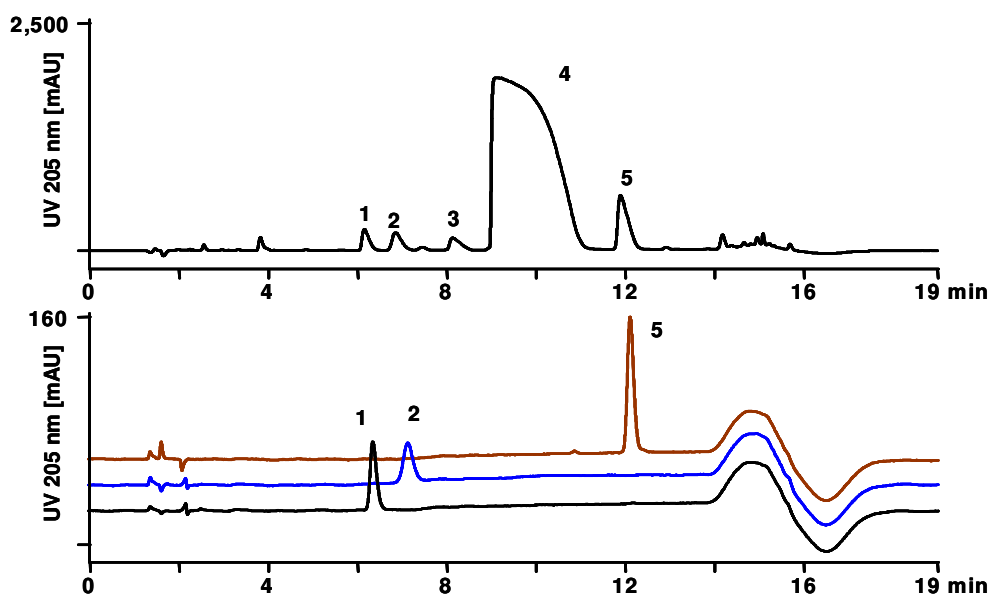


Figure 4.20: UV chromatograms of TDS sample injected into the analytical system and re-injected fractions of TDS sample. Injection volume was 50 μL each. Peak identifications see Figure 4.19.

Figure 4.21 shows the UV spectra of the compounds in TDS sample. It is evidenced that the UV spectra of DP1 and DP3 are similar to the UV spectrum of active ingredient B. However, it became obvious in the preliminary study that only DP2 and DP3 were observed in the TDS sample containing only active ingredient B. Degradation product DP1 could be a degradation product from active ingredient B in presence of active ingredient A, since their UV spectra were very similar.

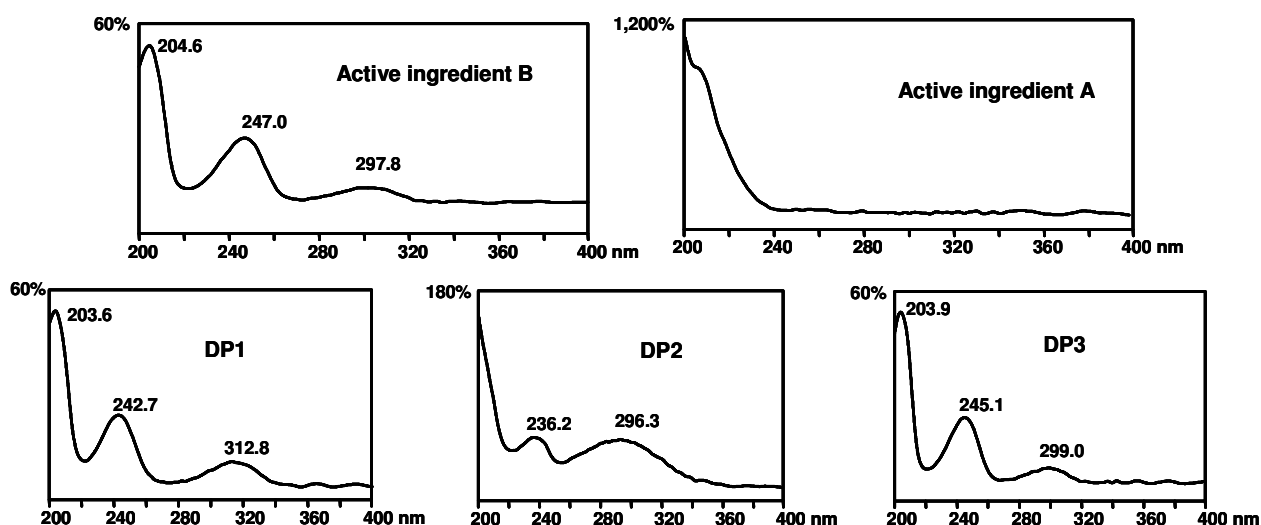


Figure 4.21: UV spectra of active ingredient B, active ingredient A and 3 degradation products (DP1, DP2, and DP3) formed in thermal stressed TDS samples.

Isolation of at least 1 mg each degradation products was necessary in order to study the structure of these substances by NMR spectroscopy. Table 4.2 describes how many injections were needed to obtain this amount. The calculation was based on the assumption that the peaks of these degradation products exhibited identical response factor as the peak of active ingredient B, since it is not possible to obtain reference standards for these substances. Injection of 1000 μL sample into APS contained 554 μg of active ingredient B. Considering the relative peak areas of active ingredient B and the degradation products, at least 1 mg of each degradation product was collected from 153 injections for DP1 and DP2 and from only 44 injections for DP3. Operation of the APS in for 7 days with 22 injections per day was required.

Table 4.2: Calculation of chromatographic runs needed to collect each 1 mg degradation products. Injection of 1000 μL sample contained 554 μg of active ingredient B.

	% area	μg substance per run	Injections for 1 mg substance	Volume fraction (mL)	Total volume (mL)
Active ingredient B	93.0	554			
DP 1	1.1	6.6	153	2.0	305
DP 2	1.1	6.6	153	2.7	412
DP 3	3.8	22.6	44	4.3	190

4.3.4 Conclusions

APS is applicable for the fully automated, unattended fraction collection from hundreds of injections using targeted UV and mass trigger. Minor components can be isolated from a large excess of major components using APS with purity and recovery higher than 98%. The isolated degradation products in the milligram range could be successfully applied for structural elucidation by NMR spectroscopy.

4.4 Fractionation of toxic gliadin from European wheat extract

4.4.1 Introduction

Gliadin is the ethanol soluble fraction of gluten. Another major protein fraction of gluten is glutenin [8]. Gluten is defined as the rubbery protein mass that remains when dough is washed to remove starch [8]. The soluble gliadin comprises mainly monomeric proteins, whilst the insoluble glutenin contains aggregated proteins [8]. Glutens are present in wheat, barley, and rye. Some people are sensitive to glutens due to the coeliac-active factor contained in gliadin. This causes the so called coeliac disease [9].

Coeliac disease is an immune-mediated disorder that affects primarily the gastrointestinal tract [9]. It is characterized by chronic inflammation of the small intestinal mucosa that may result in atrophy of intestinal villi, malabsorption, and a variety of clinical manifestations, which may begin in either childhood or adult life [9]. Intestinal symptoms can include diarrhea, abdominal cramping, pain, and distention, and untreated coeliac disease may lead to vitamin and mineral deficiencies, osteoporosis, and other extra-intestinal problems [9].

The aim of this study is to perform fractionation of γ -gliadin, one of the toxic gliadins. The fractionation was carried out utilizing the selective mass-based trigger.

4.4.2 Experimental

4.4.2.1 Instrumental setup

Fractionation and HPLC separations were performed on an analytical system comprising a binary analytical high-pressure gradient pump (Model Summit P680A HPG-2, Dionex), a degassing unit (Model Degasys DG-1210, Dionex), an analytical auto-sampler with integrated temperature control (Model Summit ASI-100T, Dionex), a dual wavelength UV detector (Model 2487, Waters, Milford, MA), a quadrupole mass spectrometer with an electrospray interface (Model MSQ), a high-pressure pump for delivering make-up flow (Model AXP-MS), and a fraction collector holding 7 mL tubes (Model Foxy Jr., Isco, Los Angeles, CA, USA). The system was fully controlled by Chromeleon software

The setup of the purification system incorporating the home-made splitting assembly is the same as depicted in Figure 1.7. However, the dimensions of the capillaries were optimized for fractionation using the analytical HPLC system. Since only columns in analytical dimension (4.6 mm i.d.) were available. The capillary dimensions were as follows: capillary 1 (PEEK) (a) 1,000 x 0.25 and (b) 2,500 x 0.38 mm i.d., capillary 2 (fused silica) 100 x 0.05 mm i.d., capillary 3 (PEEK) 200 x 0.13 mm i.d.

4.4.2.2 Chemicals and materials

All reagents used were of analytical grade. Acetonitrile and methanol were purchased from Sigma-Aldrich (Steinheim, Germany), trifluoroacetic acid (TFA) from Fluka (Buchs, Switzerland). High-purity water was obtained from a Purelab Ultra system (ELGA, Celle, Germany). Gliadin extract from European wheat IRRM-480 was obtained from Institute for Reference Materials and Measurements IRRM (Belgia).

The separation and fractionation were performed either in a Vydac C4 or C18 protein column (300 Å, 5 µm, 250 x 4.6 mm i.d., Grace, Hesperia, CA).

4.4.2.3 Conditions for HPLC separation and fractionation of gliadins

HPLC condition for fractionation and re-injection of the fraction:

Mobile phase (A) H₂O + 0.05% TFA and (B) ACN + 0.05% TFA; flow rate 2 mL/min; temperature 50 °C, detection 3D spectra and 210 nm, gradient for fractionation and re-injection 25-50% B in 20 min.

MS conditions for fractionation:

The electrospray source was operated at 3 kV needle voltage and 300 °C probe temperature. The cone voltage was +50 V. Make-up eluent was H₂O/ACN/TFA: 70/30/0.05, and make-up flow 150 µL/min. Full scan acquisition between m/z 200-2000 with a scan time of 1 sec was performed.

Fraction collection settings:

For mass targeted fraction collection, mass trace was on-line extracted for m/z 1381±0.5 and used as data for peak detection and automated triggering. Peak start threshold was 200,000 counts and end threshold 100,000 counts.

4.4.3 Results and discussion

Figure 4.22 shows the separation of gliadins in wheat extract on a C4 protein column 25 cm length (Vydac). The sample is quite complex, so that analysis time of 80 min was not sufficient to obtain adequate separation. The mass spectrum of γ -gliadin, one of the toxic gliadins, is shown in Figure 4.22b.

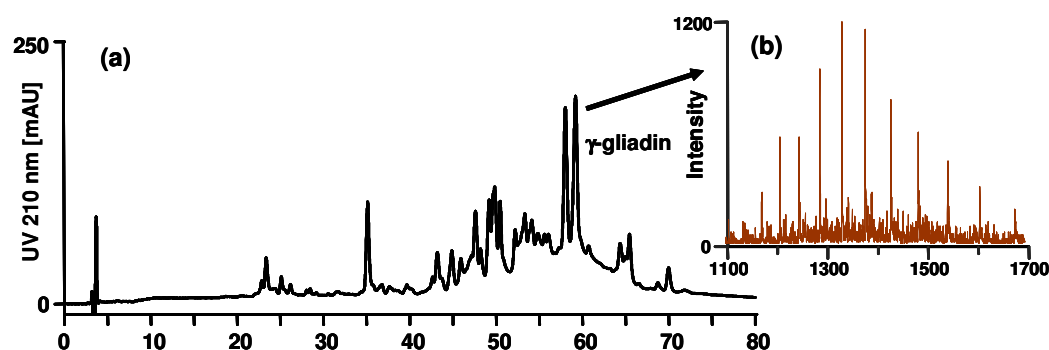


Figure 4.22: (a) UV chromatogram of gliadins from European wheat (IRRM-480); Vydac C4, 250 x 4.6 mm I.D. 5 μ m 300 Å; flow rate: 1 mL/min; gradient, A: H₂O + 0.05% TFA, B: ACN + 0.05% TFA, 20-50% B in 0-80 min, (b) Mass spectrum of γ -gliadin.

Fractionation of γ -gliadin was carried out using targeted mass trigger (Figure 4.23). One of the multiply charged masses (Figure 4.22b) could be selected as a mass target (1381 m/z). The separation was performed on a C18 protein column with 25 cm length, which exhibited inferior selectivity than the C4 column, at a flow rate of 2 mL/min and shorter time (20 min). The target peak co-eluted with the previous peak.

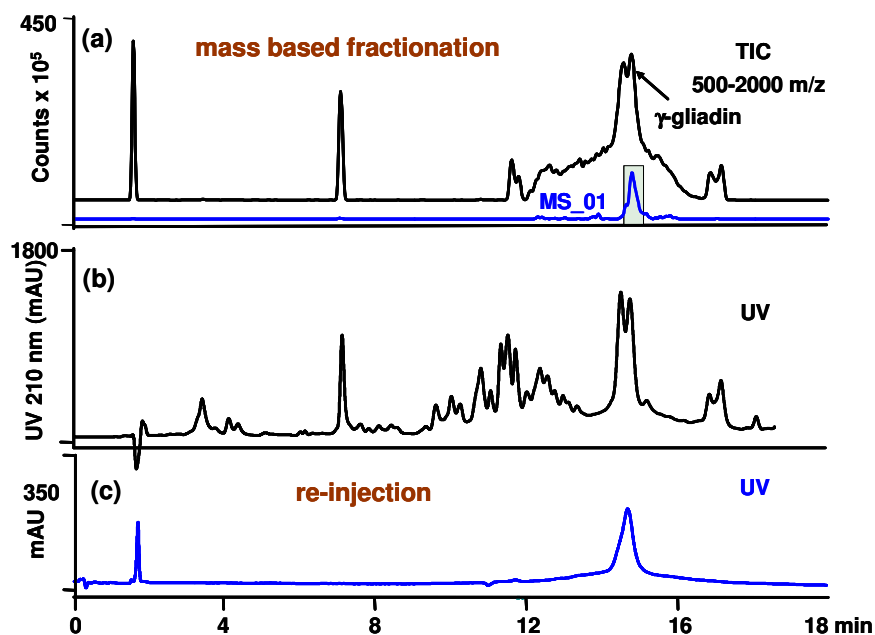


Figure 4.23: Fractionation of γ -gliadin. (a) TIC and on-line mass extract for fraction collection, (b) UV chromatogram, (c) re-injected fraction

4.4.4 Conclusion

Proteins, which exhibit series of multiply charged mass signals, can be successfully fractionated by targeted mass triggering. Mass triggering maximizes the recovery, however, the purity was low due to partly co-eluting peaks.

4.5 Conclusions of APS applications

The optimized automated purification system (APS) is applicable to the fully automated fraction collection of pharmacologically and medicinally relevant components from plant extracts. The fractionations were carried out applying non-selective photometric trigger or targeted mass spectrometric trigger or simultaneous photometric and mass spectrometric trigger. In this work, the APS system was utilized for fractionation of precious ingredients in St. John's wort extract, minor degradation products from 2 active compounds in a pharmaceutical formulation, and toxic protein gliadin.

The isolated ingredients in St. John's wort extract could be used to further study the biological activity of the compounds. The fractionated degradation products will be

used for structural elucidation by NMR spectroscopy. The isolated gliadins will be utilized for further identification by peptide fragment fingerprinting.

Sufficient peak resolution (≥ 1.5) allows for achieving 100% purity and recovery. Lower values are due to incomplete chromatographic separation of the compounds or incomplete fractionation of previous peaks, so that impurities due to carry-over are occurred.

References

- [1] Ganzera, M., Zhao, J. and Khan, I.A. (2002) *Hypericum perforatum* – Chemical profiling and quantitative results of St. John’s wort products by an improved HPLC method. *J. Pharm. Sci.*, **91**, 623-630.
- [2] Reichling, J., Hostanska, K., and Saller, K. (2001) Johanniskraut (*Hypericum perforatum* L.) – Vielstoffgemische kontra phyto gene Einzelstoffe. *Forsch Komplementärmed Klass Naturheilkd.*, **10**(suppl1), 28–32.
- [3] Butterweck, V., Jurgenliemk, G., Nahrstedt, A., and Winterhoff, H. (2000) Flavonoids from *Hypericum perforatum* show antidepressant activity in the forced swimming test. *Planta Med*, **66**, 3-6.
- [4] Butterweck, V. and Nahrstedt, A. (2003) Was ist bekannt über Johanniskraut? Phytochemie und Pharmakologie. *Pharm. Unserer Zeit*, **32**, 212-219.
- [5] Barnes, J., Anderson, L.A., and Phillipson, J.D. (2001) St John’s wort (*Hypericum perforatum* L.): a review of its chemistry, pharmacology and clinical properties. *J. Pharmacy and Pharmacology*, **53**, 583-600.
- [6] Avato, P., Raffo, F., Guglielmi, G., Vitali, C, and Rosato, A. (2004) Extracts from St John’s wort and their anti microbial activity. *Phytother. Res.*, **18**, 230–232.
- [7] Caccia, S. (2005) Antidepressant-like components of *Hypericum perforatum* extracts: An overview of their pharmacokinetics and metabolism. *Current Drug Metabolism*, **6**, 531-543.

-
- [8] Stern, M., Ciclitira, P.J., van Eckert, R., Feighery, C., Janssen, F.W., Méndez, E., Mothes, T., Troncone, R., and Wieser, H. (2001) Analysis and clinical effects of gluten in coeliac disease. *E. J. Gastroenterology and Hepatology*, **13**, 741-746.
- [9] National Institutes of Health (NIH) Consensus Development Conference on Celiac Disease, Conference Statement, June 28-30, 2004

PART 2:

Characterization of Plant Extracts and Environmental Pollutants

Chapter 5

Characterization of St. John's Wort Extracts from Accelerated Solvent Extraction (ASE)

5.1 Introduction

Several methods have been used to extract active compounds from St. John's wort (*Hypericum perforatum* L.) such as Soxhlet extraction [1], supercritical fluid extraction [2-5], pressured water extraction [6], ultrasonically assisted extraction [7] and accelerated solvent extraction [1, 7].

Comparisons of different extraction methods for the extraction of some active compounds from St. John's wort have already been reported [1, 7]. According to the authors the content of hypericins from St. John's wort obtained by ASE was little higher than that obtained by Soxhlet extraction or indirect sonication. The optimal conditions for ASE extraction were 40 °C and 100 bar, using methanol as the extraction solvent [1, 7]. These results are in agreement with a study on the optimization of extraction conditions for active components from St. John's wort using response surface methodology [8].

The aim of this work was characterization St. John's wort ASE extracts performed using different extraction procedures, identification of biological active constituents, analysis and quantification of the extracts.

5.2 Experimental

5.2.1 Instrumental Setup

HPLC-UV-MS analysis of the extracts was performed using a Dionex Summit analytical HPLC system (Dionex, Germering, Germany) with ASI 100T auto-sampler; pump P680; column oven TCC 100; UVD 340U with analytical detector cell; and weight spectrometer MSQ (ThermoFinnigan). Data acquisition and analysis were performed with Chromeleon version 6.60 SP2.

5.2.2 Columns

Luna C18(2) 100 Å 5 µm, 150 x 5.6 mm i.d. (Phenomenex, Torrance, CA) was used for identification and quantification of the extract (section 5.3.1 and 5.3.2). Acclaim 120 Å C18 5 µm, 150 x 5.6 mm i.d (Dionex, Sunnyvale, USA) was used for comparison with the Luna column (section 5.3.3).

5.2.3 Sample preparation

5.2.3.1 Extraction procedures

The ASE extracts of St. John's wort were obtained from Dionex ASE Group (Salt Lake City, USA). According to Dionex the extracts were prepared as follows: each 33 mL cell of the ASE was charged with 5 grams of plant material (refers to raw sample) mixed in hydromatrix. The cell was fitted with a cellulose filter. The extraction was performed using the methods described in Table 5.1.

Table 5.1: Methods for extraction of *Hypericum perforatum* by ASE.

	Method 1	Method 2	Method 3	Method 4
Pressure	1500 psi	1500 psi	1500 psi	1500 psi
Temp (C)	100	100	100	100
Static	5 min	5 min	5 min	5 min
Cycles	1	2	2	1
Flush	50%	50%	50%	50%
Purge	120 sec	120 sec	120 sec	120 sec
Solvent	CH ₂ Cl ₂	Ethyl acetate	Acetonitrile	Hexane

The list of obtained samples and the extraction methods are depicted in Table 5.2. Nine different samples of plant material were extracted either by one single extraction step (sample 1 and 2) or several times applying a sequence of extraction methods named group extraction (sample 3-9).

The obtained extracts were solvent free and dried. The weight of each dried extract (individual extraction steps and the sum) is depicted in Table 5.2. As several extraction procedures were repeated twice or three times, it can be seen that the repetition yielded varying amounts. The reason can be both sample in-homogeneity and experimental conditions. Further discussion will be mentioned in section 5.3.

Table 5.2: Extraction methods applied for the extraction of each sample of St. John's wort and the preparation for HPLC analysis. Method number refers to Table 5.1.

Sample	ASE extraction			Preparation for HPLC	
	Vial number	Method number	Extract weight (g)	Solvent	Filtration/ Centrifug.
Sample 1: extraction 1	12	3	0.2667	MeOH	C
Sample 2: extraction 1 repeated	21	3	0.8454	MeOH	C
Sample 3: group extraction 2	4	1	0.3137	MeOH	C
	5	3	0.1998	ACN	F
Sample 4: group extraction 2 repeated	10	1	0.2501	MeOH	C
	11	3	0.3044	MeOH	F
Sample 5: group extraction 3	1	1	0.2131	MeOH	C
	2	2	0.0684	MeOH	C
	3	3	0.1512	ACN	F
Sample 6: group extraction 3 repeated	7	1	0.2211	MeOH	C
	8	2	0.0597	MeOH	C
	9	3	0.1382	MeOH	F
Sample 7: group extraction 4	13	4	0.1212	MeOH	C
	14	1	0.0786	MeOH	C
	15	2	0.0522	MeOH	C
	16	3	0.1666	MeOH	C
Sample 8: group extraction 4 repeated	17	4	0,1558	MeOH	C
	18	1	0,0885	MeOH	C
	19	2	0,0671	MeOH	C
	20	3	0,1126	MeOH	C
Sample 9: group extraction 4 repeated in amber vials	22	4	0,2621	MeOH	C
	23	1	0,0789	MeOH	C
	24	2	0,0418	MeOH	C
	25	3	0,1506	MeOH	F

5.2.3.2 Preparation for the analysis by HPLC–UV–MS

Each extract from the sample of plant materials was re-constituted in 10 mL of MeOH (Table 5.2), except extracts from vial 3 and from vial 5, which were dissolved in 10 mL of acetonitrile (ACN).

After centrifugation and decantation, an aliquot of these solutions was diluted with 1 volume of water containing 0.1% formic acid and again filtered or centrifuged and decanted (Table 5.2, last column).

5.2.3.3 Conditions for the analysis by HPLC–UV–MS

In order to determine the optimal HPLC parameters, optimization of eluent composition and gradient profile was performed with sample 25 which was considered representative. The optimized conditions are as follows:

Mobile phase: (A) H₂O + 0.3% formic acid, (B) ACN/MeOH: 9/1 +0.3% formic acid;

Gradient method: see Table 5.3

Flow rate: 1mL/min.

Detection: 3D spectra and 270 nm.

MS: Block source temp: 500 °C; Cone voltage –100 V; weight spectrum in centroid, scan time 0.5 sec; TIC 100-700 m/z.

Table 5.3: Gradient profile for HPLC

Time (min)	B (%)
0	20
5	20
23	21
26	45
30	60
35	100
41	100
42	20
48	20

5.3 Results and discussion

5.3.1 Identification of Constituents in St. John's Wort ASE Extracts

For this experiment the St. John's wort ASE extract from vial 25 (Table 5.2, sample 9, group extraction 4 repeated in amber vial) prepared as described in Table 5.2 was selected.

Figure 5.1 shows the MS and UV chromatograms of the *Hypericum* extract from vial 25 (extraction solvent ACN) re-constituted in MeOH. The MS detection yielded more peaks than UV. Substances identified from the detected m/z are listed in Table 5.4. Hyperoside and isoquercitrin are two isomers (see Figure 5.1b). These two substances could not be sufficiently resolved with analytical HPLC.

The MS chromatogram (A) showed a peak with the molecular mass of hyperforin (m/z 535) at ca. 40 min retention time, where no peak was obtained in the UV chromatogram detected at 270 nm. This indicated that hyperforin could be present only in small amount in the extract, since hyperforin should be detectable at wavelength between 270 and 284 nm [9, 10]. The possible reason is the loss of this substance during extraction because it is sensitive against high temperature and light [11, 12, 13], since the extraction was performed at 100 °C. In a study it was reported that extraction of St. John's wort by ASE performed using extraction solvent methanol at temperature of 40 °C and 100 bar under light exclusion yielded 0.87 mg hyperforin per gram plant material [7].

Table 5.4: Substances identified in St. John's wort extract from vial 25 and the corresponding m/z values

Substance	m/z	Peak number
Rutin	609	1
Hyperoside	463	2
Isoquercitrin	463	3
Miquelianin	477	
Guaijaverin	449	
Astilbin	433	
Quercitrin	447	4
Protohypericin	505	5
Quercetin	301	6
Biapigenin	537	7

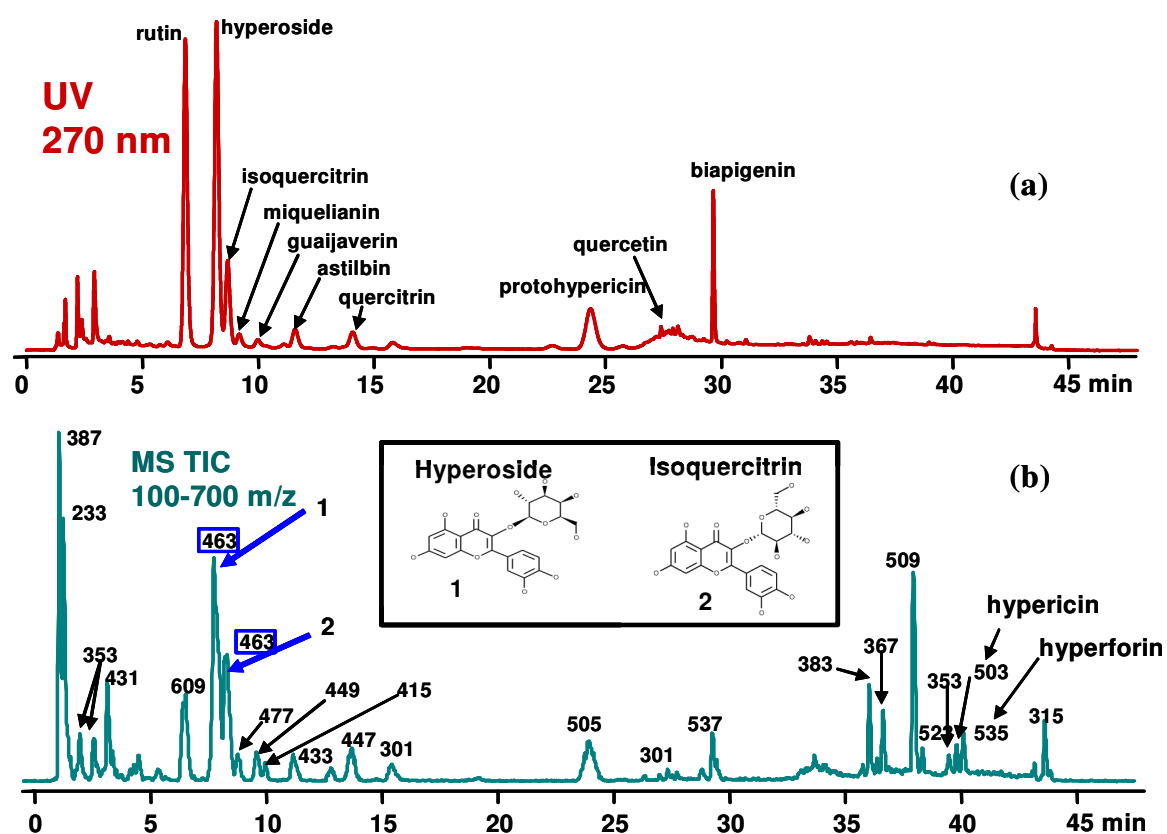


Figure 5.1: Identification of compounds in St. John's wort ASE extract. UV (a) and MS chromatograms (b) of sample 9 (vial 25, extraction solvent ACN) re-constituted in MeOH.

5.3.2 Characterization of ASE Extraction Methods

Figures 5.2 to 5.10 show the UV chromatograms of all nine *Hypericum* samples. Each chromatogram is labeled depending on the extraction method as given in Table 5.2. As listed in Table 5.2, most of the extracts were re-constituted in MeOH, except the extracts in vial 3 (sample 5, extraction method 3) and in vial 5 (sample 3, extraction method 3) which were re-constituted in acetonitrile. The quantitative yield of the ingredients will be further discussed in the following section.

Figure 5.2 and 5.3 show the analysis of two samples extracted by ASE under identical conditions (sample 1 and 2). The samples were extracted by one single step using acetonitrile and re-constituted in MeOH. Both plant material samples exhibited different pattern. The substance quercetin was found only in one sample (sample 1). Peaks of all other substances in sample 1 were generally smaller than that in sample 2.

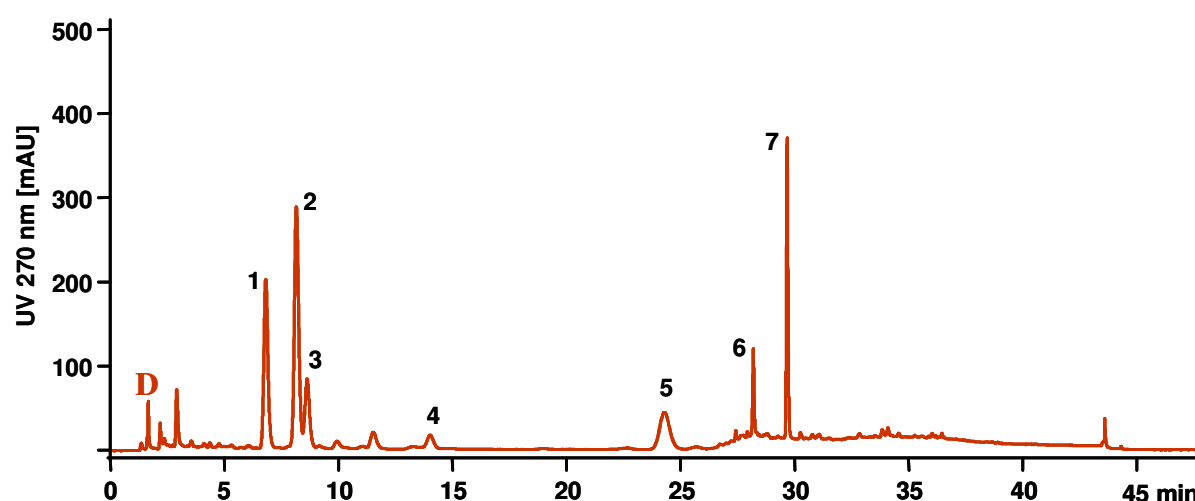


Figure 5.2: UV chromatogram of sample 1 (extraction 1). D refers to extraction method 3 with extraction solvent acetonitrile (Table 5.1). Peak identification: (1) rutin, (2) hyperoside, (3) isoquercitrin, (4) quercitrin, (5) protohypericin, (6) quercetin, (7) biapigenin.

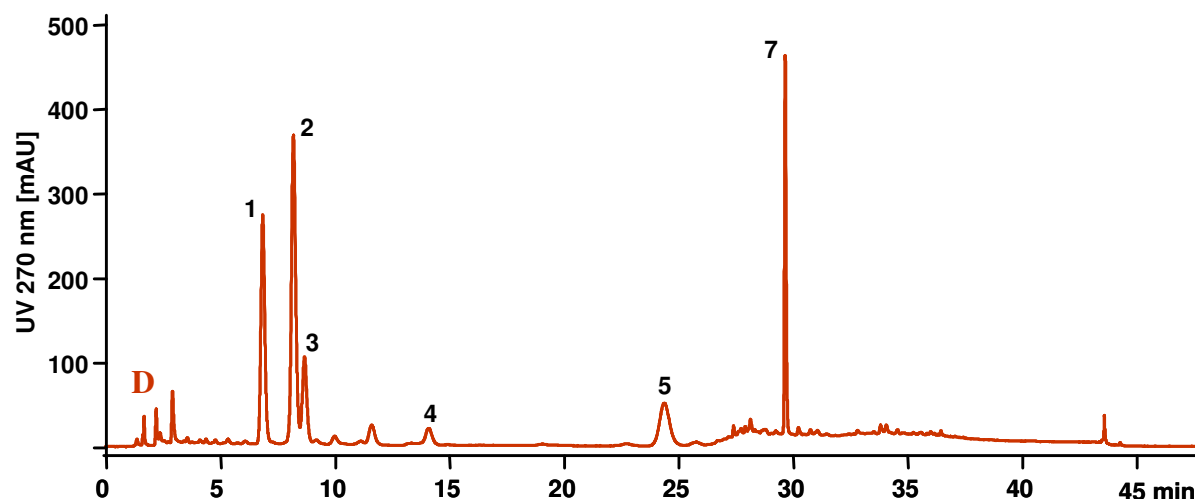


Figure 5.3: UV chromatogram of sample 2 (extraction 1 repeated). Identification of chromatograms and peaks refer to Figure 5.2.

The chromatograms of two samples extracted according to the protocol of group extraction 2 (Table 5.2) are shown in Figures 5.4 and 5.5. The samples were extracted first using dichloromethane (B) and then using acetonitrile (D). The ACN extract from sample 3 was re-constituted in ACN. Whilst the respective extract from sample 4 was re-constituted in MeOH.

As can be seen, no peak was found in the extract using a non-polar extraction solvent dichloromethane (Figure 5.4B and 5.5B). The extract re-constituted in ACN (Figure 5.4D) exhibited lower peak area, larger peak width and asymmetric peaks for early eluted substances than that re-constituted in MeOH (Figure 5.5D). A possible reason is poorer solubility of these hydrophilic substances in ACN relative to that in MeOH. It was observed that the extract re-constituted in ACN showed a turbid suspension. Whilst the extract re-constituted in MeOH yielded a clear solution. Surprisingly, peak of the hydrophobic substance biapigenin from the ACN solution was higher than from MeOH. It could be assumed that biapigenin is more soluble in ACN than in MeOH.

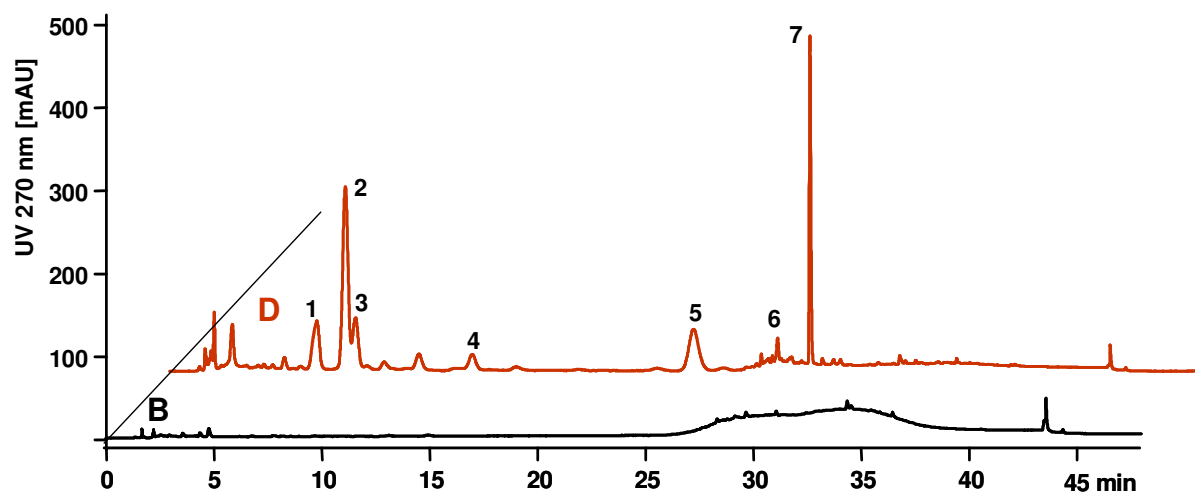


Figure 5.4: UV chromatograms of sample 3 (group extraction 2). Chromatogram D: the extract was re-constituted in ACN. B and D refer to extraction method 1 (dichloromethane) and 3 (acetonitrile), respectively (Table 5.1). Peak identification: (1) rutin, (2) hyperoside, (3) isoquercitrin, (4) quercitrin, (5) protohypericin, (6) quercetin, (7) biapigenin.

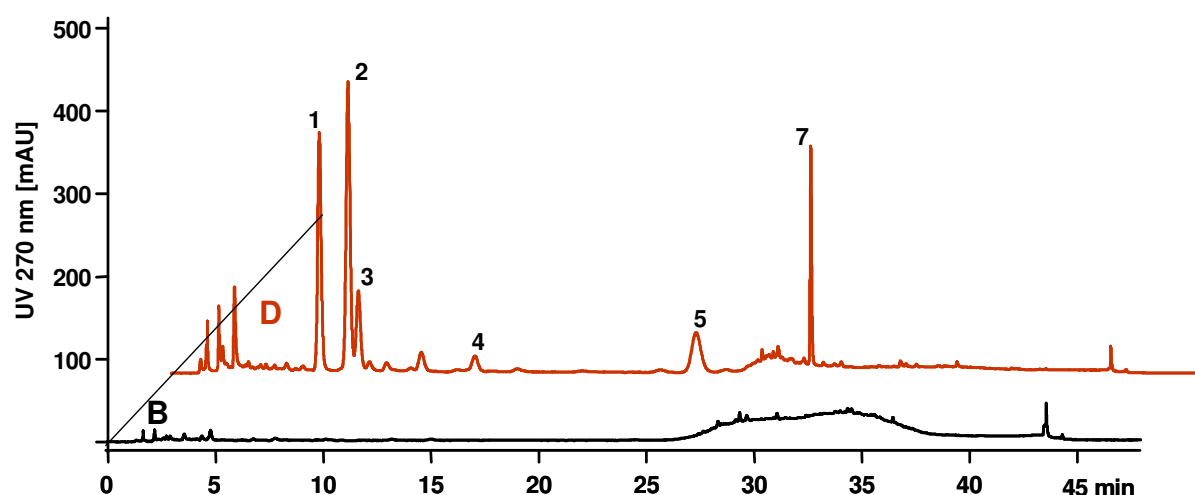


Figure 5.5: UV chromatograms of sample 4 (group extraction 2 repeated). Identification of chromatograms and peaks refer to Figure 5.4.

Figure 5.6 and 5.7 show the analysis of two samples (sample 5 and 6) extracted by ASE under identical conditions. Both samples were extracted in 3 steps consecutively using extraction solvents dichloromethane, ethyl acetate and acetonitrile, as listed in Table 5.2. The extracts were re-constituted in MeOH, except the acetonitrile extract from sample 5 was re-constituted in ACN (Figure 5.6D).

As also observed in sample 3 and 4, no peak was found in the extracts using dichloromethane. Chromatograms of both samples extracted using ethyl acetate

showed similar pattern (Figure 5.6C and 5.7C). However, the peaks of substances from the first sample are generally much higher than from the second sample. The peak shapes of substances in ACN extract re-constituted in ACN (Figure 5.6D) exhibited similar behavior as in previous extract (Figure 5.4D).

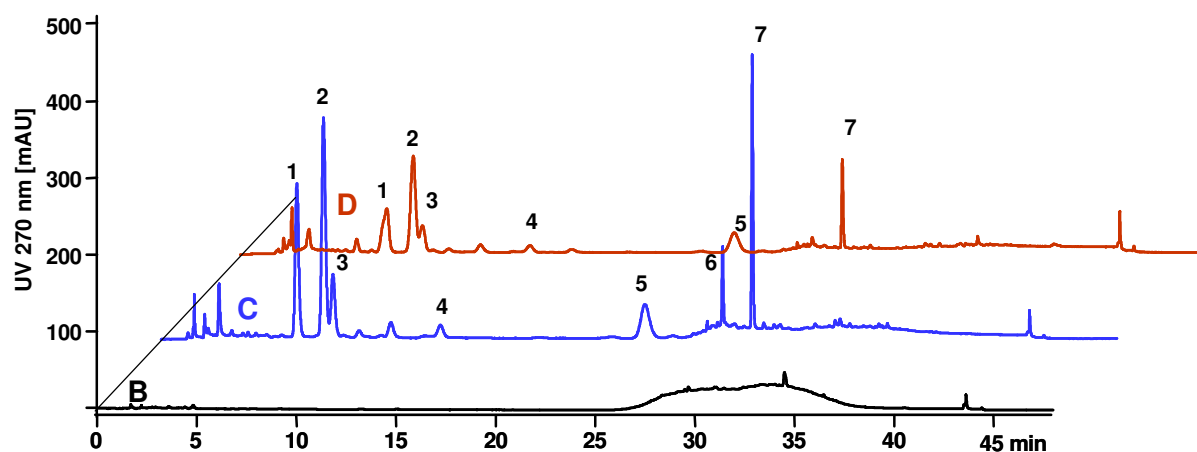


Figure 5.6: UV chromatograms of sample 5 (group extraction 3). B, C, and D refer to extraction method 1 (dichloromethane), 2 (ethyl acetate) and 3 (acetonitrile). Peak identification: (1) rutin, (2) hyperoside, (3) isoquercitrin, (4) quercitrin, (5) protohypericin, (6) quercetin, (7) biapigenin. Chromatogram D: the extract was re-constituted in ACN.

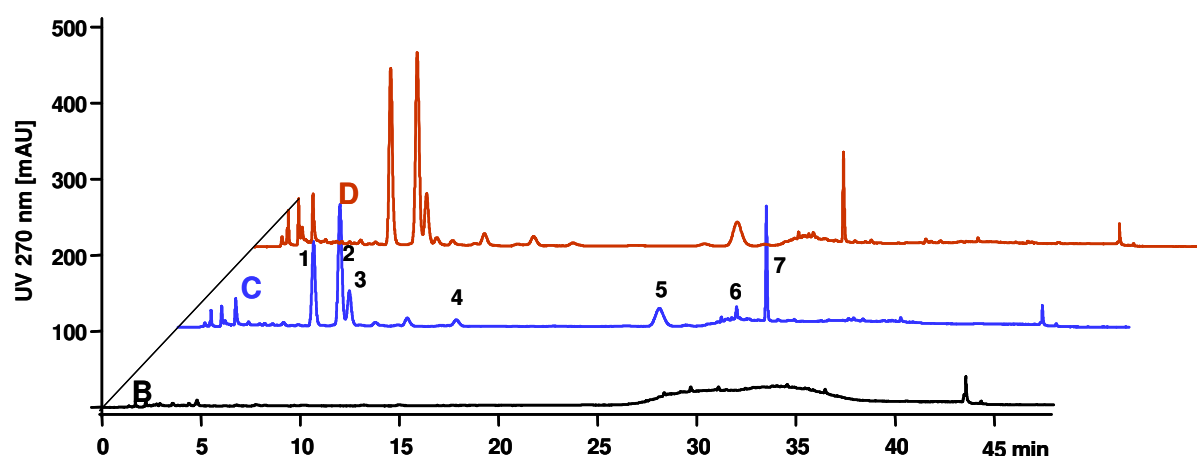


Figure 5.7: UV chromatograms of sample 6 (group extraction 3 repeated). Identification of chromatograms and peaks refer to Figure 5.6.

Figures 5.8, 5.9 and 5.10 depict the analysis of three samples extracted consecutively in 4 steps according to Table 5.2 (group extraction 4). The extracts from sample 9 were collected in amber vials.

The chromatograms from all samples showed a similar pattern for the individual steps. However, the peak areas of the substances from the samples extracted using identical methods were different. Peaks of substances of the extracts from sample 8 were significantly higher than from other samples, although the extracts from sample 9 were collected in amber vials. No peak was found in all hexane and dichloromethane extracts (chromatogram A). Substance quercetin was not found in all extracts. The peaks of rutin, hyperoside and isoquercitrin in the ethyl acetate extract were smaller than in the ACN extract, except in sample 8. However, biapigenin peaks in all ethyl acetate extracts was higher than in the ACN extract.

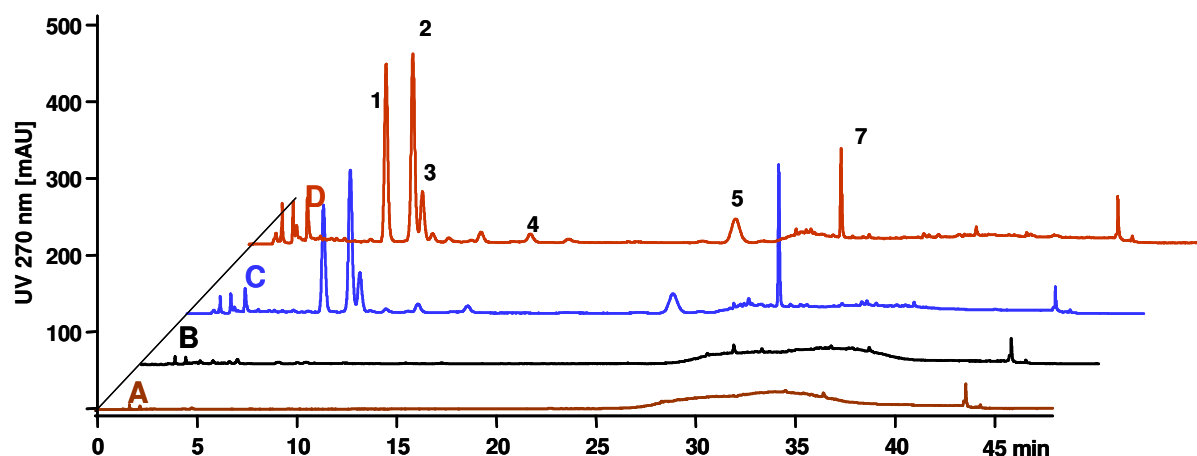


Figure 5.8: UV chromatograms of sample 7 (group extraction 4). A, B, C, and D refer to extraction method 4 (hexane), 1 (dichloromethane), 2 (ethyl acetate) and 3 (acetonitrile). Peak identification: (1) rutin, (2) hyperoside, (3) isoquercitrin, (4) quercitrin, (5) protohypericin, (6) quercetin, (7) biapigenin.

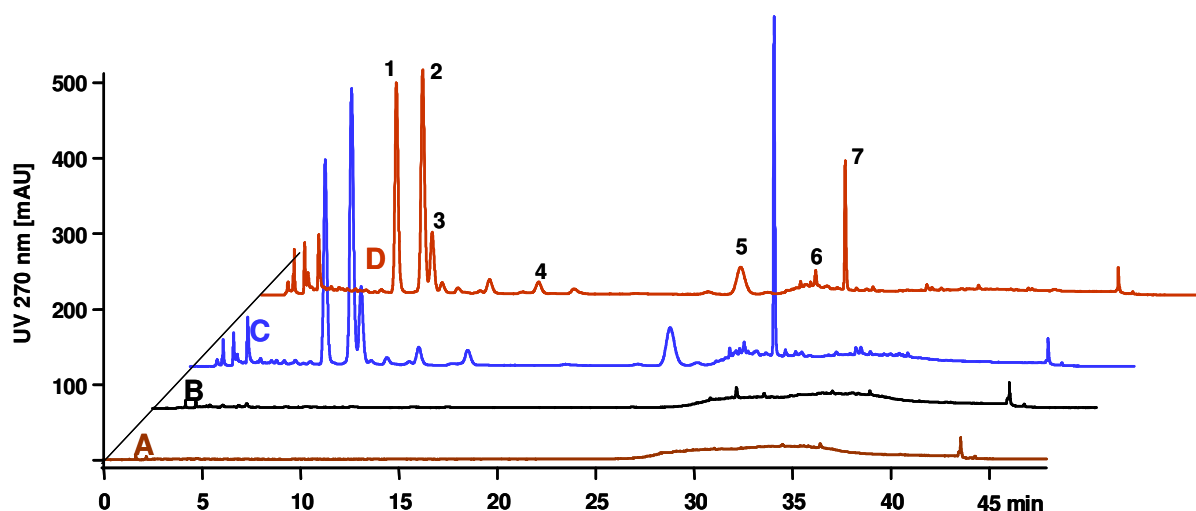


Figure 5.9: UV chromatograms of sample 8 (group extraction 4 repeated). Identification of chromatograms and peaks as in Figure 5.8.

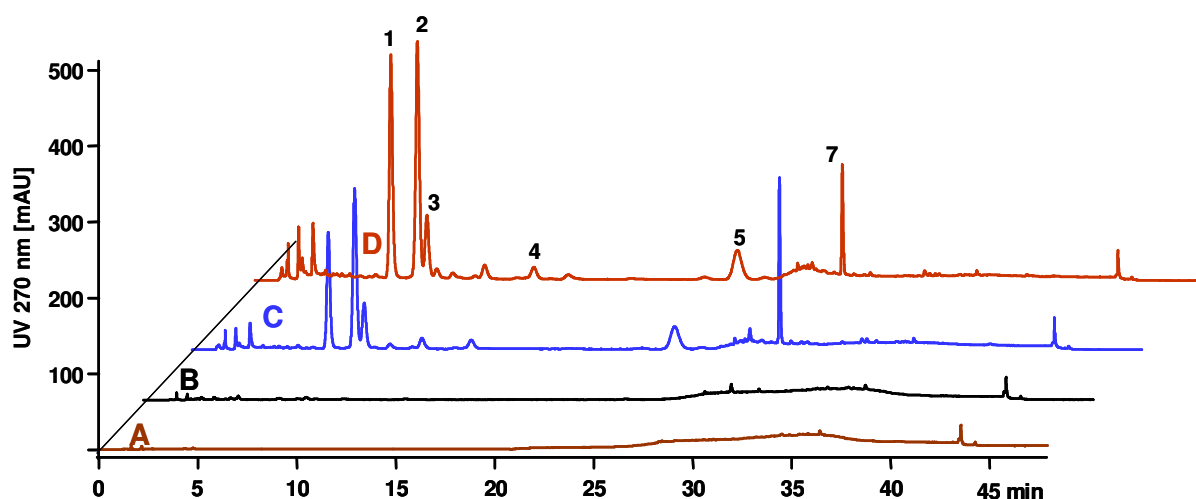


Figure 5.10: UV chromatograms of sample 9 (group extraction 4 repeated in amber vials). Identification of chromatograms and peaks as in Figure 5.8.

5.3.3 Quantification of the extraction yields

This section presents a discussion on the differences between the individual applied ASE procedures and the general ASE repeatability on a more quantitative basis.

The dry mass of the extracts from individual extraction steps and the total extract mass are shown in Figure 5.11. The total extract dry mass was similar for almost all extraction procedures, except for extraction 1 and the repeated procedure. Except for extraction group 3, the dry mass from individual steps varied within repeated

extraction procedures. However, the pattern for three repeated extraction procedure for extraction group 4 was similar.

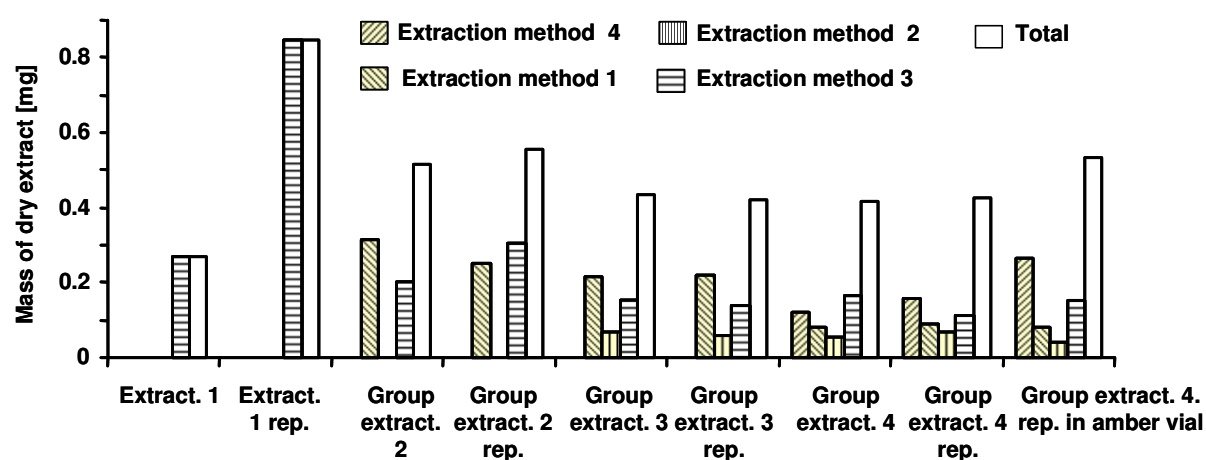


Figure 5.11: Mass of ASE extracts in individual extraction steps and the total weight for each sample.

Table 5.5 shows the comparison of the total extract weight normalized by plant material weight and rutin content obtained from different ASE procedures. Rutin content in the extracts was determined by calibration of the peak areas using rutin standard substance. The obtained total extract dry mass per gram plant material except for extraction 1 was similar, as also depicted in Figure 5.11 for absolute total extract weight. However, these normalized values (between 84 and 111 mg/g plant material) were less than 50% of the value obtained using extraction solvent methanol (40 °C, 100 bar) as reported by Smelcerovic et al. [8] (Table 5.5 last row).

Similar total rutin content within the repeated extraction procedures was observed in extraction 1 and group extraction 3, but not in other extraction procedures (Table 5.5 third column). Total rutin contents normalized by plant material weight and by extract dry mass are depicted in Table 5.5 fourth and fifth columns, respectively. These values were normalized in order to compare these from different ASE extraction procedures and to compare these ASE procedures to the value obtained in the literature and obtained by analysis of a commercial extract. Total rutin contents per gram plant material were similar within the repeated extraction procedures, except in group extraction 2 and in one repeat in group extraction 4. The difference in rutin content normalized by extract weight is due to the inconsistency of the extract weight

from individual steps, as shown in Figure 5.11. As can be seen in Table 5.5, the highest total rutin content was achieved by ASE procedures from group extraction 4. Smelcerovic et al. reported results of active compound contents in St. John's wort extracts obtained using different extraction devices [7]. They found that the highest amount of active compounds was achieved by using direct sonication. The results obtained by ASE using only methanol as extraction solvent (40°C, 100 bar) were comparable to that by Soxhlet extraction. However, Soxhlet extraction needs significantly longer extraction time (20 min by ASE compared to 24 h by Soxhlet). Rutin content obtained by ASE reported by Smelcerovic et al. [7] was 2.0 mg/g plant material. This value is 25% higher than that obtained in this study.

Comparing rutin content from ASE to that from a commercial St. John's wort extract obtained as a coating tablet containing 600 mg extract (Neuroplant 1x1, Schwabe Arzneimittel, Karlsruhe, Germany) (Table 5.5 before last row), it is obvious that rutin amount per 1 gram extract in Neuroplant was comparable with the highest content obtained in one of group extraction 4. However, the amount from ASE was not reproducible.

Table 5.5: Total extract dry mass and rutin content obtained using different ASE procedures compared to literature results and a commercial St. John's wort extract.

	Total extract (mg/g plant material)	Total rutin content (μ g)	Rutin content (mg/g plant material)	Rutin content (mg/g extract)
Extraction 1	53	2920	0.6	10.9
Extraction 1 repeated	169	2762	0.6	3.3
Group extraction 2 ^{a)}	103	1518	0.3	3.0
Group extraction 2 repeated	111	4213	0.8	7.6
Group extraction 3 ^{a)}	87	4556	0.9	10.5
Group extraction 3 repeated	84	4933	1.0	11.8
Group extraction 4	84	5346	1.1	12.8
Group extraction 4 repeated	85	7872	1.6	18.6
Group extraction 4 repeated in amber vials	107	6414	1.3	12.0
Neuroplant 1x1 (600 mg extract)	-	9860	-	16.4
ASE extraction using methanol [7]	240		2.0	

^{a)} Acetonitrile extract (extraction method 3) from these groups was re-constituted in acetonitrile

Because only rutin was available as reference substance for the calibration of the analytical HPLC method, peak areas for five compounds of interest (rutin, hyperoside, isoquercitrin, protohypericin, biapigenin) were monitored for the two extraction steps (methods) in all extraction sequences (group extractions) that yielded analyzable amounts of the mentioned substances. These methods comprised ethyl acetate (method 2) or acetonitrile (method 3) as extraction solvents. The peak areas are given in bar charts and depict the results from the two individual extraction steps (if both were applied). The third bar chart shows the sum of peak areas from

these two steps to monitor the total extraction yield of a distinct sequence. The asterisks mark the two cases where the extracts were re-constituted with acetonitrile instead of methanol. Below each figure of this type, a second bar chart is given to monitor the peak areas normalized to the extract dry mass of the individual extraction steps (see Table 5.2 and Figure 5.11). This additional representation was made since marked differences of the absolute extraction yields were observed, even for group extraction repetitions (lower extraction amounts should result in smaller peak areas). From Figures 5.12 to 5.21 it can be concluded that both the total extraction yield of each individual substance and the ratio between the extraction yields with ethyl acetate and acetonitrile varied when experiments were repeated. The variations in the total yield are still observed when normalized peaks areas are displayed (see extraction 1 and group extraction 4). However, with the normalized diagrams the pattern (ethyl acetate yield – acetonitrile yield – total yield) was copied in the repetitive experiments for all selected ingredients.

With respect to the comparison of methanol and acetonitrile to re-constitute the dried extracts (see asterisks), no consistent results were obtained. Whilst acetonitrile yielded smaller normalized peak areas for rutin, hyperoside and isoquercitrin, protohypericin and similar peak areas for biapigenin with group extraction 3, the normalized peak areas with group extraction 2 were smaller from the methanol solution for all substances except for rutin. For chromatographic reasons, the general preference given to methanol was mainly motivated by the better peak shapes obtained for the early eluting compounds (see chromatograms C and D in Figure 5.6) due to the solubility of these substances in methanol.

When the different ASE procedures are compared for their total extraction yield, the most advantageous protocol was group extraction 4 (hexane, dichloromethane, ethyl acetate, acetonitrile) followed by group extraction 3 (dichloromethane, ethyl acetate, acetonitrile). The single acetonitrile extraction yielded smaller extracted amounts than the two step protocol dichloromethane and acetonitrile. The obvious reason for the success of a protocol starting with a non-polar extraction step could be a kind of pre-washing effect. The non-polar solvents extract the hydrophobic ingredient (e.g. lipids) from the sample and improve the wetting of the plant material surface by the polar solvents ethyl acetate and acetonitrile.

Comparing the extraction yield ratio of ethyl acetate and acetonitrile, it can be seen that ethyl acetate resulted in higher normalized peaks for all substances. This could

be attributed to the fact that the ethyl acetate step was always prior to the acetonitrile step and both solvents seem to be appropriate to extract the compounds of interest. In other words, the compounds were mostly, but not completely extracted with ethyl acetate. However, the predominance of the normalized peak areas from the ethyl acetate extract increased from rutin to biapigenin with increasing hydrophobicity of the compounds. Ethyl acetate solubility relative to acetonitrile solubility increases with the hydrophobicity of the solute.

It can be concluded that ASE should be carried out with the protocol of group extraction 4; the dried extracts should be re-constituted in methanol for re-injection into the APS. They could be combined from the ethyl acetate and the acetonitrile extract, since both chromatograms turned out to be very similar (see Figures 5.8 to 5.10). However, the ASE method reproducibility appeared to be not very satisfying, as can be seen in the variation in dry mass and HPLC results for repetitive ASE experiments.

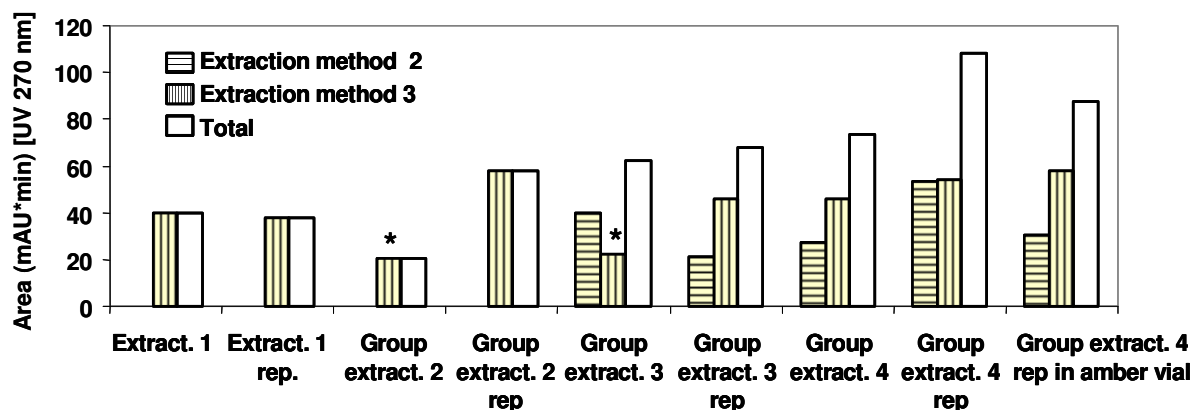


Figure 5.12: The rutin content in all samples. (*) re-constituted in ACN.

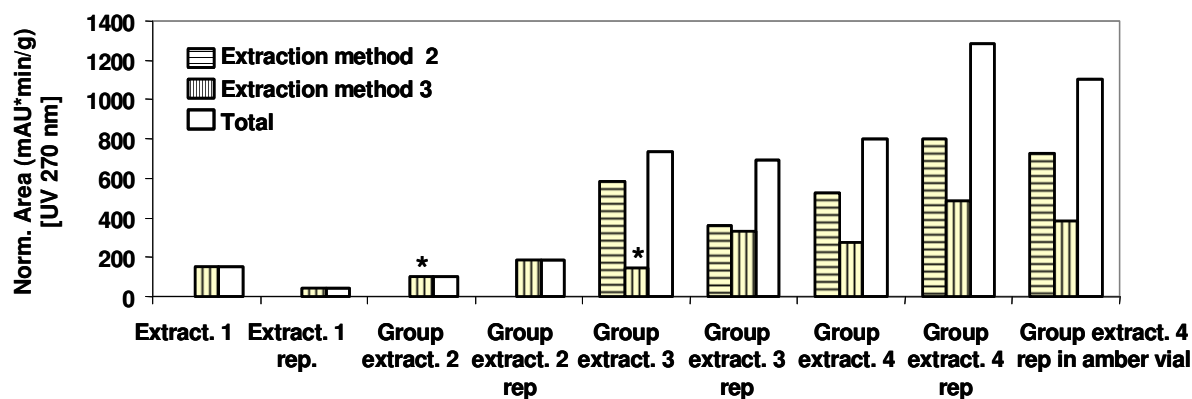


Figure 5.13: The content of rutin in all samples, normalized by the dry mass. (*) re-constituted in ACN

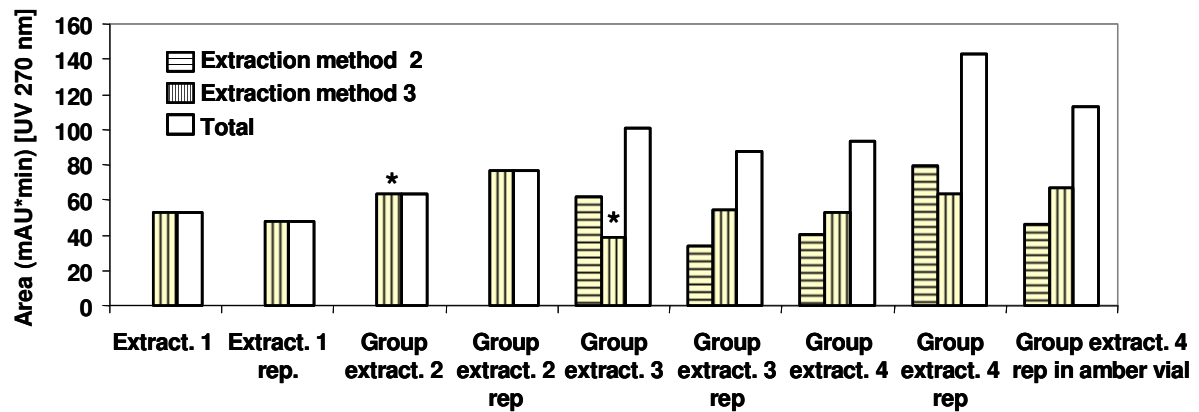


Figure 5.14: The hyperoside content in all samples. (*) re-constituted in ACN

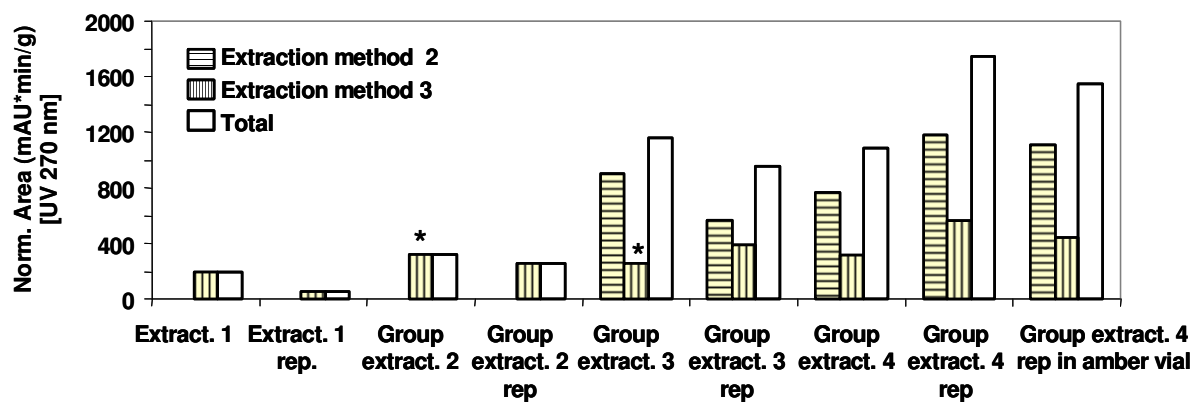


Figure 5.15: The normalized yield of hyperoside in all samples. (*) re-constituted in ACN

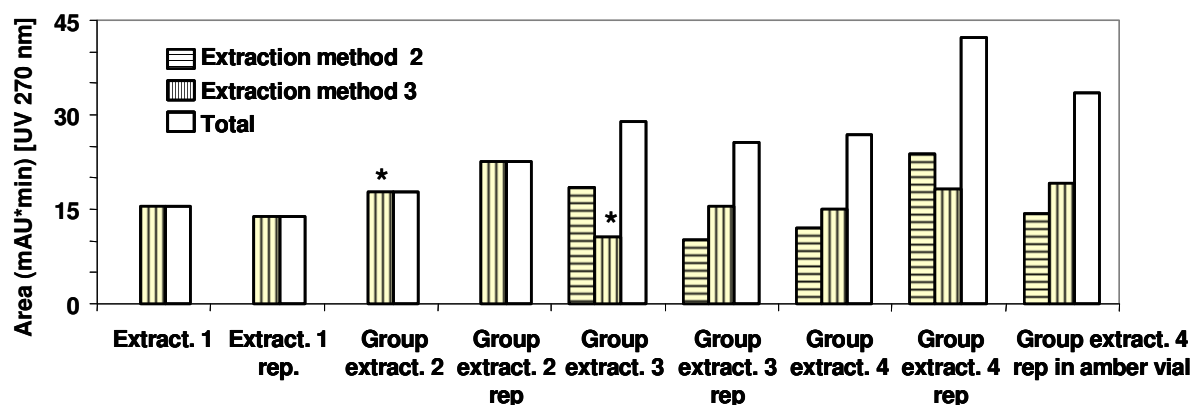


Figure 5.16: The isoquercitrin content in all samples. (*) re-constituted in ACN

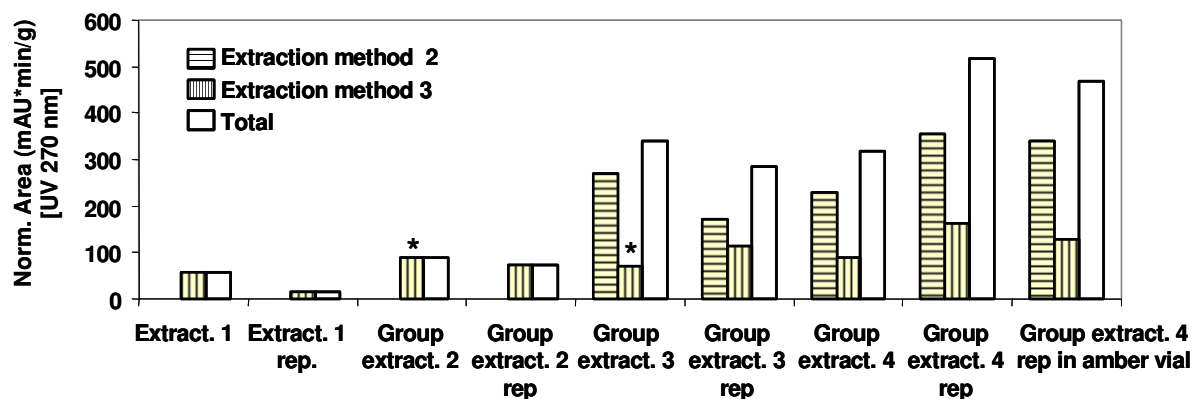


Figure 5.17: The normalized isoquercitrin content in all samples. (*) re-constituted in ACN

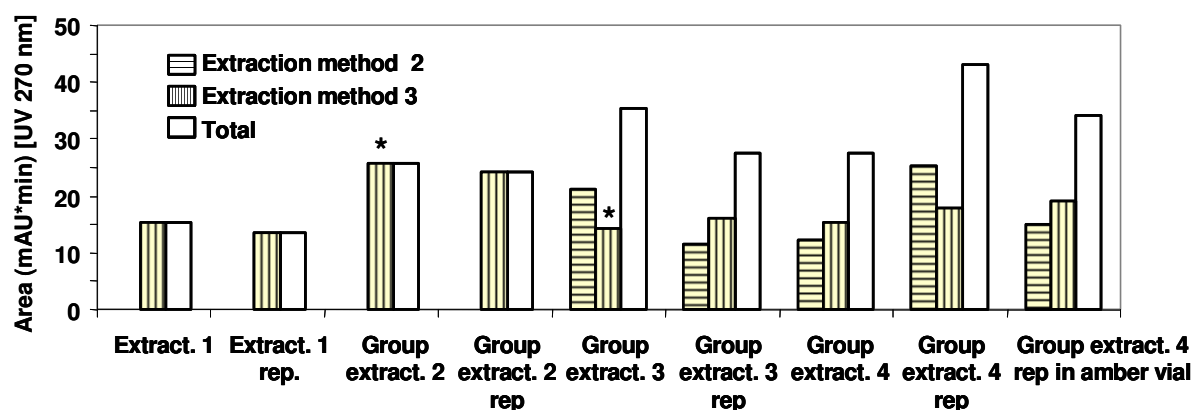


Figure 5.18: The content of protohypericin in all samples. (*) re-constituted in ACN

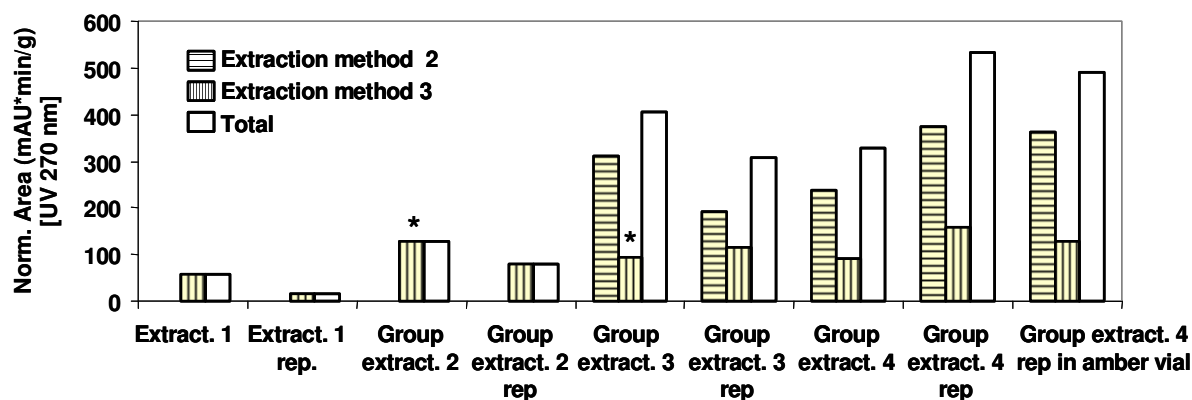


Figure 5.19: The yield of protohypericin in all samples normalized by the dry mass. (*) re-constituted in ACN

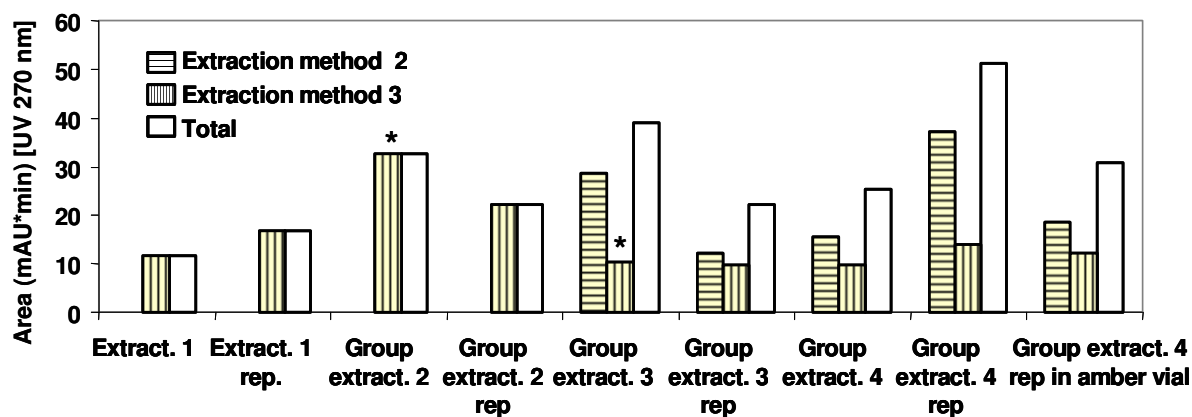


Figure 5.20: The content of biapigenin in all samples. (*) re-constituted in ACN

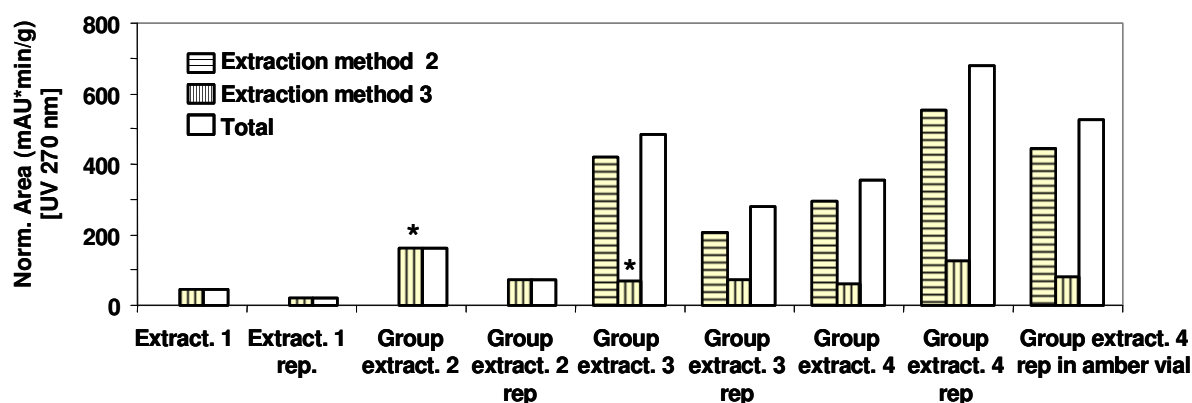


Figure 5.21: The yield of biapigenin in all samples normalized by the dry mass. (*) re-constituted in ACN

5.3.4 Comparison of the Luna and Acclaim columns

Figure 5.22 shows the UV chromatograms and gradient profile in Luna and Acclaim columns. Comparing both analytical columns, under identical conditions no pronounced difference was encountered. However, Acclaim exhibited more retention due to its higher hydrophobicity, as proved by Engelhardt test for both columns (substances toluene and ethylbenzene eluted in Acclaim later than in Luna).

The sharp peak of protohypericin on Acclaim compared to Luna is due to the elution of the peak in a steep gradient in the case of Acclaim, whilst in the flat part of the gradient in the case Luna. Considering the selectivity of small peaks between 5 and 17 minutes (Figure 5.23) in Luna and Acclaim, it turned out that peaks 3, 5 and 6 were better resolved with Luna, whilst peak 2 and 8 were better resolved with Acclaim.

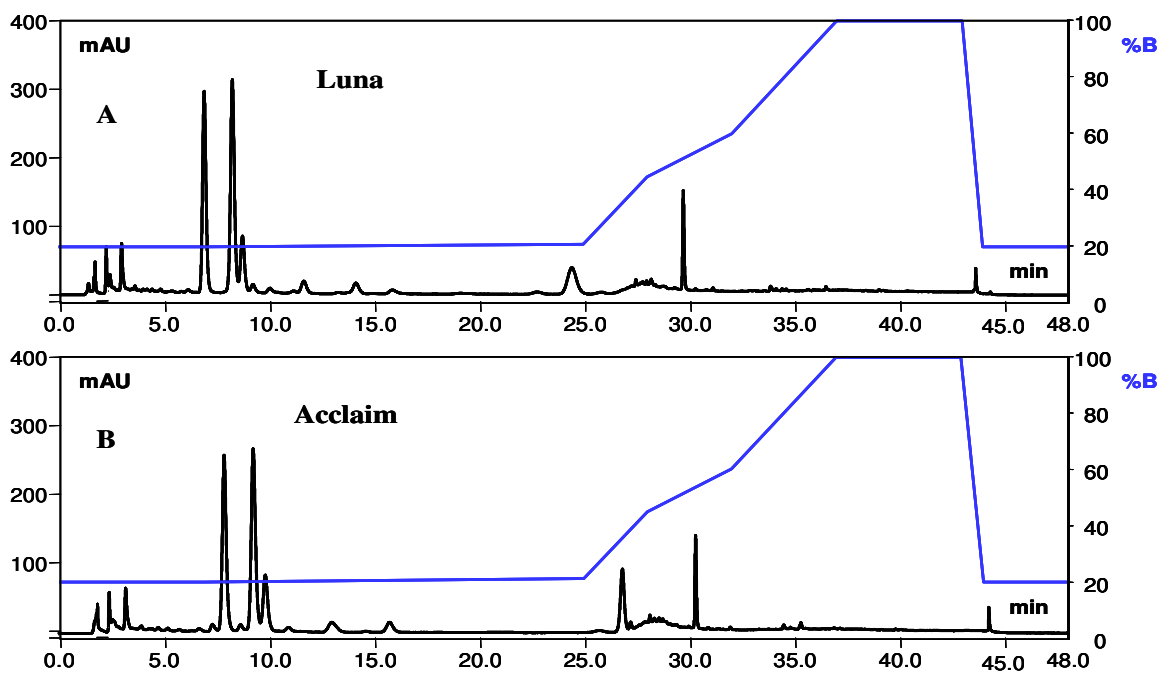


Figure 5.22: UV Chromatograms and gradient profile in between Luna (A) and Acclaim (B) columns.

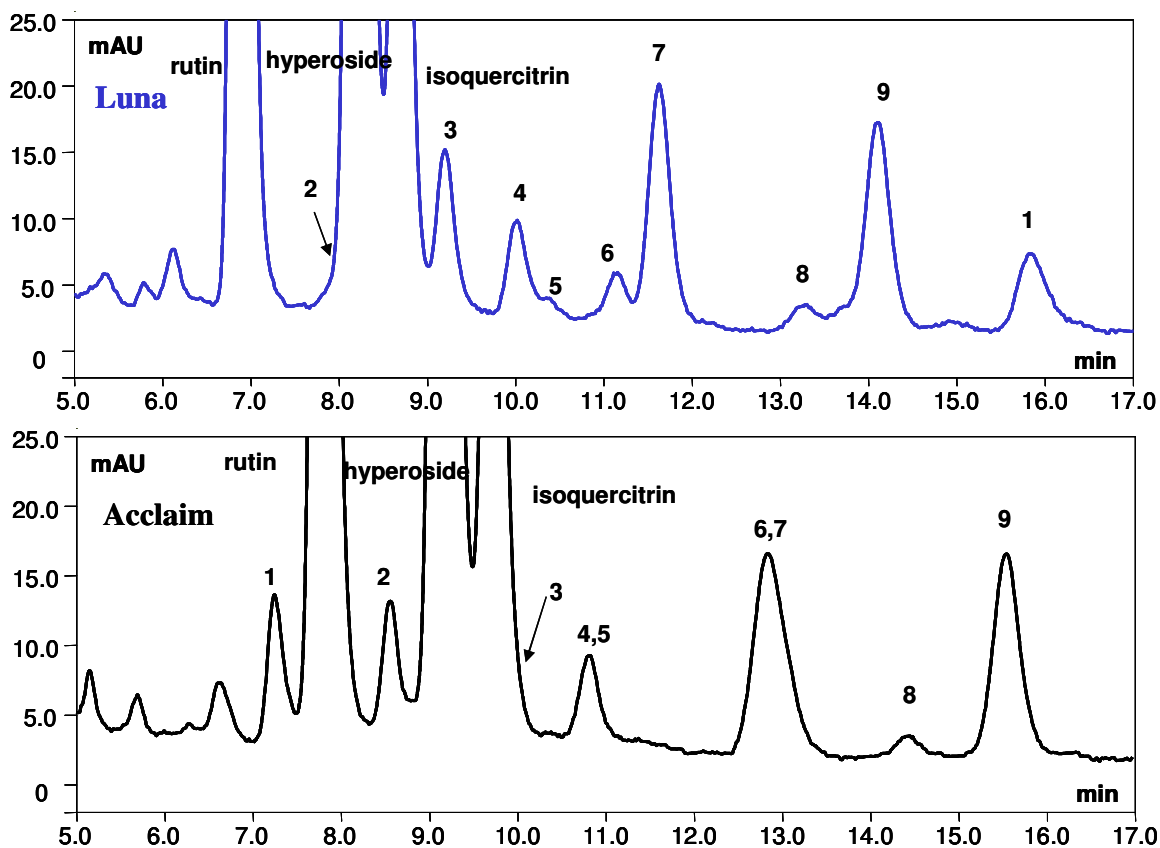


Figure 5.23: Zoomed chromatograms between 5 and 17 minutes.

5.4 Conclusions

St. John's wort extracts obtained from ASE applying different extraction protocols using the extraction solvents dichloromethane, ethyl acetate, acetonitrile and n-hexane were identified, characterized and quantified. Different samples of plant material were extracted either by one single extraction step or several times applying a sequence of extraction methods.

The active substances of St. John's wort rutin, hyperoside, isoquercitrin, quercitrin, quercetin, protohypericin and biapigenin could be identified by HPLC analysis using UV and MS detectors. The two isomers hyperoside and isoquercitrin could not be completely resolved nor with Acclaim, neither with Luna column. In general, the resolution of the whole spectrum of ingredients was satisfying. However, not all St. John's wort ingredients reported in literature could be traced. Quercetin was detected in a considerable quantity only in 2 ASE extracts, whilst hyperforin might be lost during or after the extraction due to its sensitivity against high temperature and light.

Accelerated solvent extraction should be carried out with the protocol of group extraction 4: four consecutive extractions applying hexane, methylene chloride, ethyl acetate, and acetonitrile. It appears that extraction with non-polar solvents such as hexane and methylene chloride initially removed the matrices from the plant material notably the lipophilic substances, but did not extract the desired biologically active ingredients. The dried extracts should be re-constituted in methanol for analysis using HPLC or for fractionation applying APS. However, the ASE method reproducibility appeared to be not very satisfying, as can be seen in the variation in dry mass and HPLC results for repetitive ASE experiments.

Comparing the Acclaim and Luna analytical columns, both columns were generally comparable under identical conditions. No pronounced difference was encountered, except that Acclaim exhibited more retention than Luna.

References

- [1] Morf, S., Debrunner, B., Meier, B., Kurth, H. (1998) Automatische Probenvorbereitung von pflanzlichen Arzneimitteln. Ein Vergleich mit der konventionellen Methode am Beispiel Johanniskraut. *LaborPraxis*, **22**, 56, 59-60, 62.

- [2] Mannila, M., Kim, H., Isaacson, C., Wai, C.M. (2002) Optimisation of supercritical fluid extraction for the separation of hyperforin and adhyperforin in St. John's wort (*Hypericum perforatum* L.). *Green Chem.*, **4**, 331-336.
- [3] Roempp, H., Seger, C., Kaiser, C. S., Haslinger, E., Schmidt, P. C. (2004) Enrichment of hyperforin from St. John's Wort (*Hypericum perforatum*) by pilot-scale supercritical carbon dioxide extraction. *Eur. J. Pharm. Sci.*, **21**, 443-451.
- [4] Seger, C., Roempp, H., Sturm, S., Haslinger, E., Schmidt, P.C., Hadacek, F. (2004) Characterization of supercritical fluid extracts of St. John's Wort (*Hypericum perforatum* L.) by HPLC-MS and GC-MS. *Eur. J. Pharm. Sci.*, **21**, 453-463.
- [5] Cui, Y., Ang, C.Y.W. (2002) Supercritical Fluid Extraction and High-Performance Liquid Chromatographic Determination of Phloroglucinols in St. John's Wort (*Hypericum perforatum* L.) *J. Agric. Food Chem.*, **50**, 2755-2759.
- [6] Mannila, M., Wai, C.M. (2003) Pressurized water extraction of naphthodianthrones in St. John's wort (*Hypericum perforatum* L.). *Green Chem.*, **5**, 387-391.
- [7] Smelcerovic, A., Spiteller, M., Zuehlke, S. (2006) Comparison of methods for the exhaustive extraction of hypericins, flavonoids, and hyperforin from *Hypericum perforatum* L. *J. Agric. Food Chem.*, **54**, 2750-2753
- [8] Liu, F.F., Ang, C.Y.W., Springer, D. (2000) Optimisation of extraction conditions for active components in *Hypericum perforatum* using response surface methodology. *J. Agric. Food Chem.*, **48**, 3364-3371.
- [9] Tolonen, A., Hohtola, A., Jalonen, J. (2003) Fast High-performance Liquid Chromatographic Analysis of naphthodianthrones and phloroglucinols from *Hypericum perforatum* extracts. *Phytochem. Anal.*, **14**, 306-309.
- [10] Liu, F.F., Ang, C.Y.W., Heinze, T.M., Rankin, J.D., Beger, R.D., Freeman, J.P., Jackson, O.L. (2000) Evaluation of major active components in St. John's Wort dietary supplements by high performance liquid chromatography with photodiode array detection and electrospray mass spectrometric confirmation. *J. Chromatogr. A*, **888**, 85-92.
- [11] Erdelmeier, C.A.J. (1998) Hyperforin, possibly the major non nitrogenous secondary metabolite of *Hypericum perforatum* L. *Pharmacopsychiatry*, **31S**, 2-6.
- [12] Orth, H.C.J., Rentel, C., Schmidt, P.C. (1999) Isolation, purity analysis and stability of hyperforin as a standard material from *Hypericum perforatum* L. *J. Pharm. Pharmacol.*, **51**, 193-200.
- [13] Fuzzati, N., Gabetta, B., Streponi, I., Villa, F. (2001). High performance liquid chromatography-electrospray ionisation mass spectrometry and multiple mass spectrometry studies of hyperforin degradation products. *J. Chromatogr. A*, **926**, 187-198.

Chapter 6

Method Development for the Analysis and Quantification of Polycyclic Aromatic Hydrocarbons (PAHs) and Small Phenols in Road Asphalts Containing Tar

6.1 Introduction

In the industrialized countries the quality of the infrastructure for the road traffic is very important. Over the last 50 years many new roads and highways have been constructed. Road pavements contain approx. 95% aggregate and 5% binder. In the past years coal tar pitch was used as binder for road pavement or so-called asphalt pavement. Today the binder for asphalt pavements is served from bitumen.

Asphalt containing tar is classified as a hazardous waste [1]. This contains toxic and carcinogenic compounds at high concentration levels, especially polycyclic aromatic hydrocarbons (PAHs), e.g. benzo[a]pyrene and phenols, which are dangerous for the environment and health, and contaminate groundwater reservoir [1]. Asphalt containing tar should be distinguished from bitumen asphalt achieved from crude oil distillation [2, 3, 4]. Since 1983 a clear terminology is given by the German standard DIN 55946-1 [2] and DIN 55946-2 [3] to distinguish bitumen from tar. At the same time, the use of tar products for road construction materials was prohibited in many countries.

Although coal tar contains numerous hazardous substances at different and varying concentration levels, it has become common to analyse a set of representative PAHs and phenols for quantitative chemical analyses. A frequently used set of compounds has been proposed by the US Environmental Protection Agency (US-EPA) [5].

The aim of this work was to develop sample preparation and HPLC methods for the quantification of polycyclic aromatic hydrocarbons (PAHs) and small phenols in road asphalts containing tar. In addition to a successful extraction of the hazardous substances from the asphalt, an effective sample preparation considering the matrix was essential.

6.2 Experimental

6.2.1 Materials and Chemicals

The original road surface sample was crushed to 0/25 and reduced according to EN932-2 (prepared by Juchem Company, Niederwörresbach, Germany). An aliquot of this sample was milled to a fine powder. All chemical used were of analytical grade. A standard reference mixture of 16 EPA-PAHs was purchased from Supelco (Pennsylvania, USA).

The column used for the PAH analysis was a Nucleodur C18 Gravity, 5 μm , 150 x 4.0 mm i.d. (Macherey & Nagel, Düren, Germany). A ProntoSil C18 ACE EPS column (120Å, 3 μm , 150 x 4.0 mm id) from Bischoff Chromatography (Leonberg, Germany) was used for phenol analysis.

6.2.2 HPLC Apparatus and Elution Conditions

HPLC analysis for PAHs was performed using a Waters Alliance system (Waters, Germany). Phenol analysis was carried out using a Dionex Summit system (Dionex, Germering, Germany). Both systems were equipped with a diode array detector.

Elution conditions for PAHs analysis were as follows:

Mobile phase: (A) water, (B) acetonitrile; gradient method: 0-3 min 60% B isocratically, 3-30 min 60-100% B, 30-32 min 100% B, 32-35 min 100-60% B, 35-40 min 60% B; injection 10 μL ; flow rate: 1.0 mL/min; temperature: 38 °C, detection: UV at 220 nm and UV spectra.

Elution conditions for phenol analysis were as follows:

Mobile phase: (A) water, (B) acetonitrile; 0-20 min 35% B isocratically, 20-22 min 35 - 100% B for cleaning the column, 22-25 min 100%-35% B, 25-30 min 35% B; injection 20 μL ; flow rate: 1.7 mL/min; temperature: 38 °C, detection: UV at 215 nm and UV spectra.

6.2.3 Procedure of Extraction by Sonication of the Raw Sample for Phenol Analysis

Extraction of the coarse material:

80 g coarse sample were 3x sonicated with 80 mL CH_2Cl_2 each. Separation of the liquid was done by decantation. The total volume was concentrated to 133 mL.

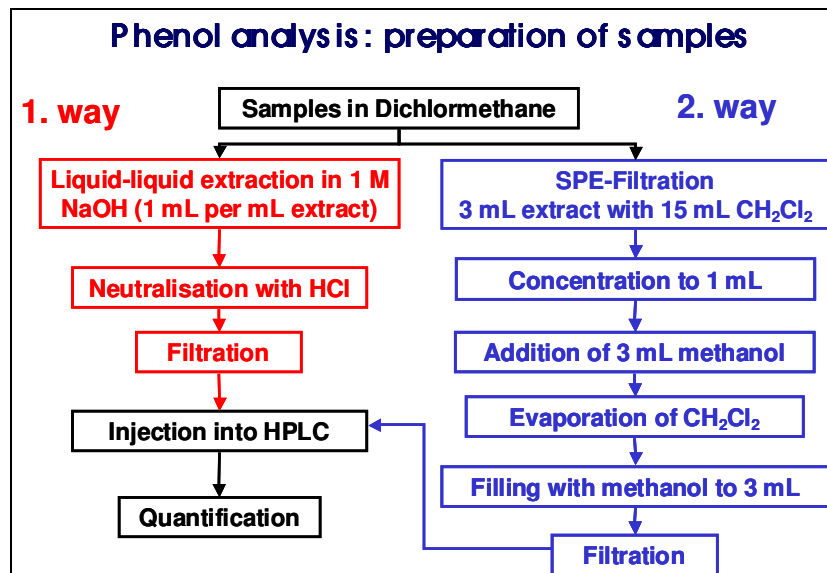
Extraction of the fine material:

30 g of powdered sample were 3x sonicated with 40 mL CH_2Cl_2 each. The total extract was concentrated to 80 mL.

The stones of both samples were dried overnight at room temperature.

6.2.4 Procedure for the Sample Preparation for Phenols prior to HPLC Analysis

The CH_2Cl_2 extract was prepared for the phenol analysis in two different ways as depicted in the following scheme:



Preparation of the SPE:

0.8 g of silica (40 μm , DuPont) was packed into SPE cartridge. The cartridges were fitted in the SPE vacuum apparatus (JT Backer). Before elution of samples the cartridges were washed 2 times with 1.5 mL CH_2Cl_2 .

6.3 Results and Discussion

6.3.1 Analysis of PAHs

6.3.1.1 Development of the Gradient HPLC Method for PAH Analysis

The list of 16 representative hazardous PAHs proposed by US EPA is depicted in Figure 6.1. For the separation of PAHs in reversed phase chromatography, special features of the stationary phase are required in order to separate solutes that are similar in their molecular structure. This essential property is called molecular recognition or shape selectivity. It is usually obtained on C18 phases with wide pores (>15nm) and high alkyl chain density, preferably polymer modified. Other special phases (e.g. C30) also provide that property. Because no special PAH columns were available, two potentially appropriate standard columns were investigated (Nucleodur C18 Gravity, 5 μm , 150 x 4 mm from Macherey & Nagel, Düren, Germany and YMC Pro-C18, 120 \AA , 3 μm , from YMC Inc. USA). Both columns were evaluated for the analytical task and the Nucleodur column proved to be clearly superior.

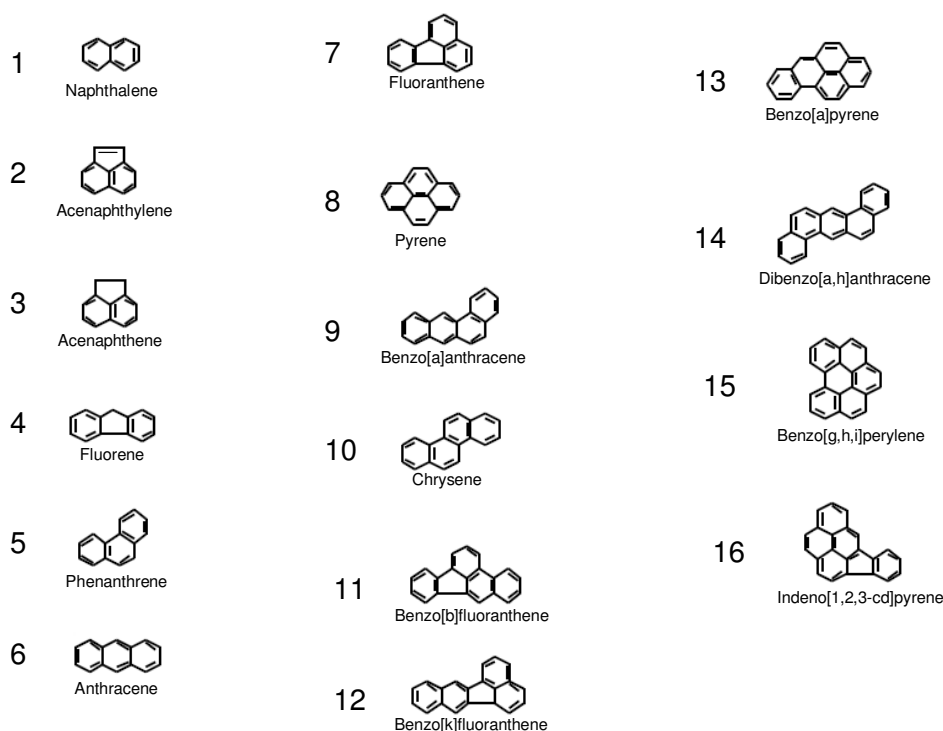


Figure 6.1: Structures of the 16 EPA PAH and numbers for peak assignment.

The obtained separation is depicted in Figure 6.2 with a 5 ppm standard of 13 PAHs, the peak assignment is according to Figure 6.1. Indeno(1,2,3-cd)pyrene, dibenzo(a,h)anthracene and benzo(g,h,i)perylene were not available as individual compounds and are missing in this standard chromatogram. It can be seen, that acenaphthene and fluorene could not be separated, the 2 pairs chrysene and benzo[a]anthracene as well as benzo[b]fluoranthene and benzo[k]fluoranthene are only partly resolved.

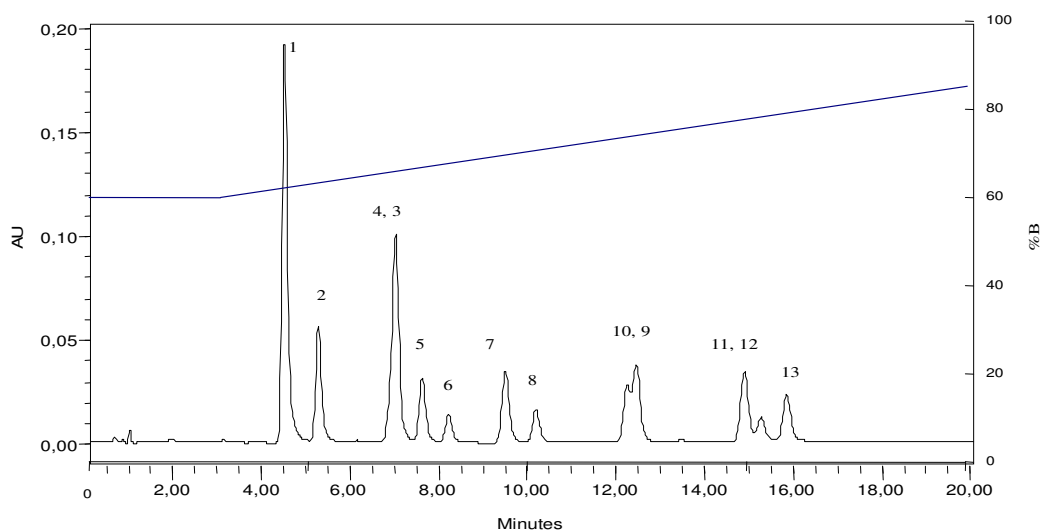


Figure 6.2: PAH separation on Nucleodur C18 Gravity, 5 μ m, 150 x 4 mm (Macherey&Nagel), detection 220 nm.

6.3.1.2 PAH Detection

From the photodiode array detector, UV spectra of each peak in the chromatogram can be extracted (Figure 6.3). The spectra of those solutes causing poorly resolved peak pairs on the column used, namely (10, 9) and (11, 12), can be seen. It can be deduced, that peak identity can unambiguously be verified from the significantly different spectra. Moreover a tuning of the detection wavelength would partially allow discrimination between the compounds that compose a purely resolved peak pair.

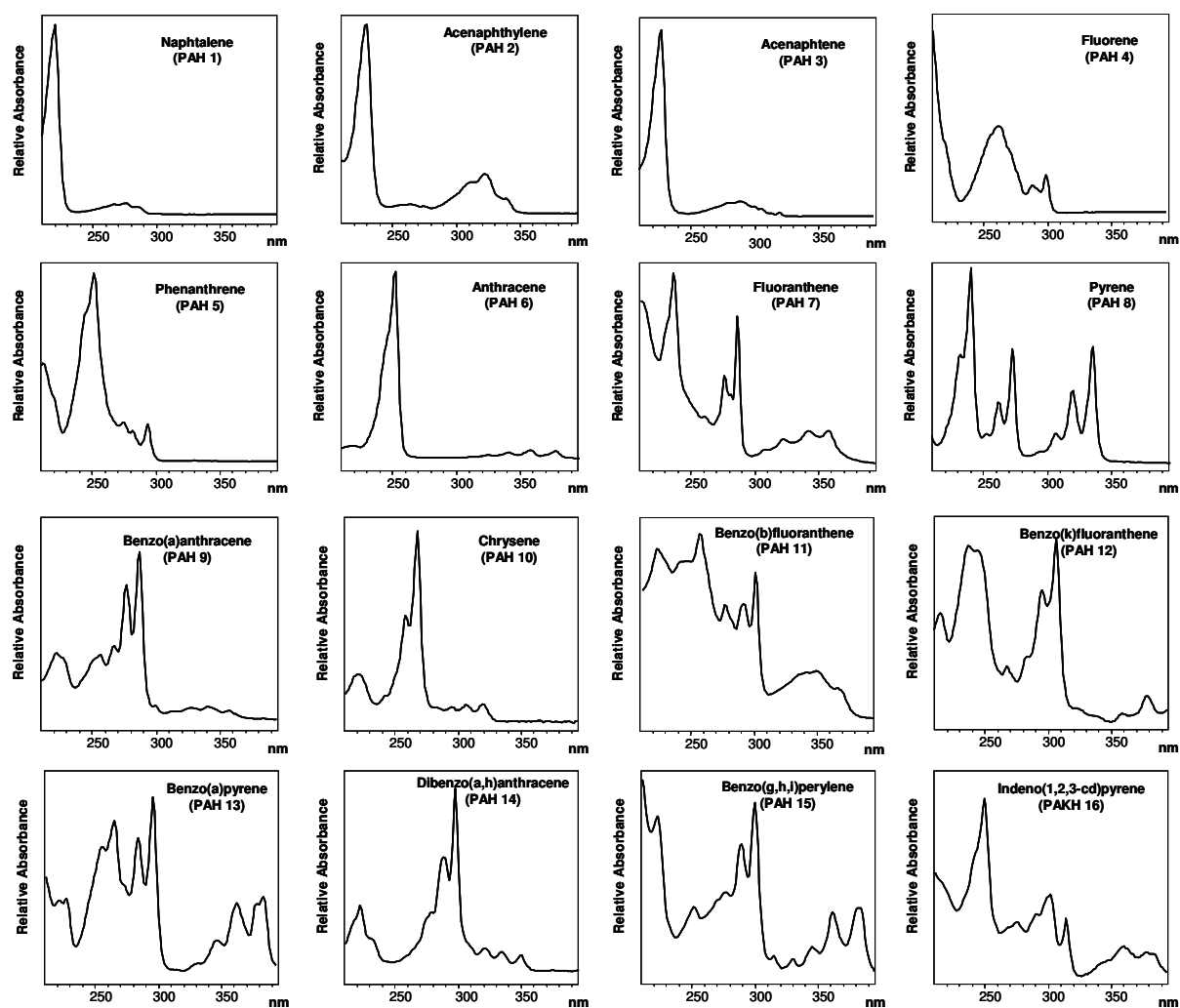


Figure 6.3: Peak UV spectra taken from single injections of the PAH.

6.3.1.3 Calibration for PAH Analysis

The developed method was calibrated for quantification with external standard solutions. The calibration solution for most analytes with the exception of phenanthrene (5) and benzo[k]fluoranthene (12) were prepared by diluting a 2000 ppm stock solution in CH_2Cl_2 (purchased from Supelco) with methanol to concentrations between 5 and 50 ppm, which is appropriate for the analysis of an asphalt containing tar extract after dilution by factor 20 (low abundance PAHs are quantified by extrapolation). It was verified that the residual 5% CH_2Cl_2 had no impact on the quality of the chromatogram. Figure 6.4 shows a chromatogram from the 10 ppm solution of the mixture. Peak B is 2-bromonaphthylene, which is included from the manufacturer for internal calibration but could not be resolved from the phenanthrene peak by the applied method. Hence, phenanthrene and the missing

PAH 12 were calibrated from individually prepared solutions in methanol (corresponding to chromatogram in Figure 6.2). All calibration curves were recorded at the same detection wavelength (220 nm) and are depicted in Figure 6.6. For the non resolved peak pairs PAHs 3 and 4, PAHs 9 and 10 and PAHs 14 and 16, a sum value was calibrated, neglecting the differences in the absorption coefficients.

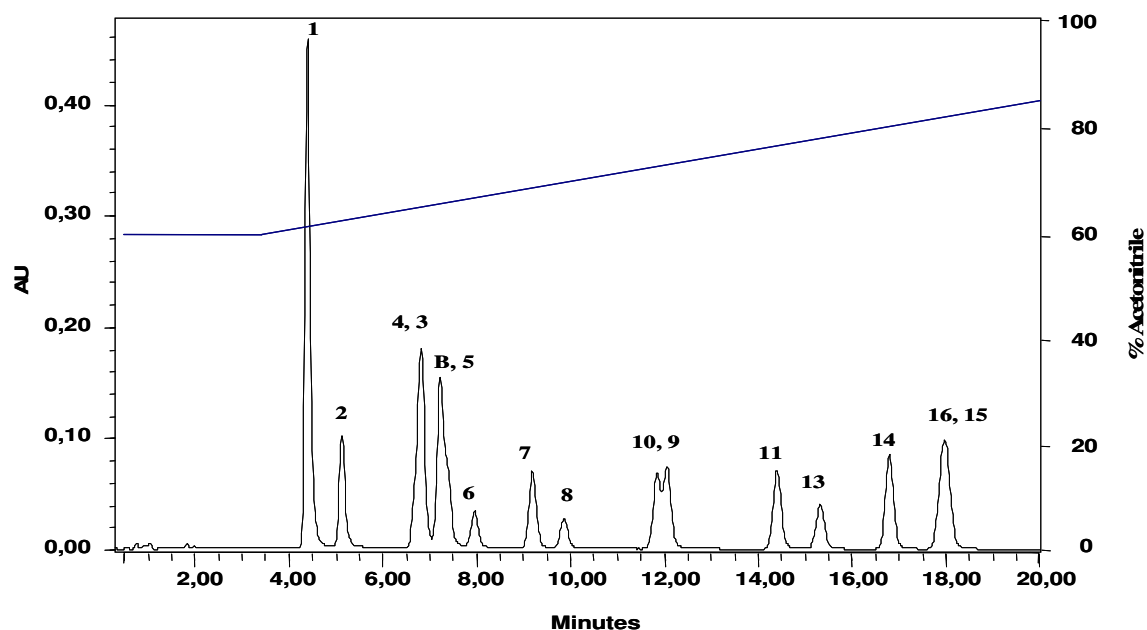


Figure 6.4: Separation of the diluted Supelco mixture (10 ppm), conditions as in Figure 6.2, peak B is 2-bromonaphtylene.

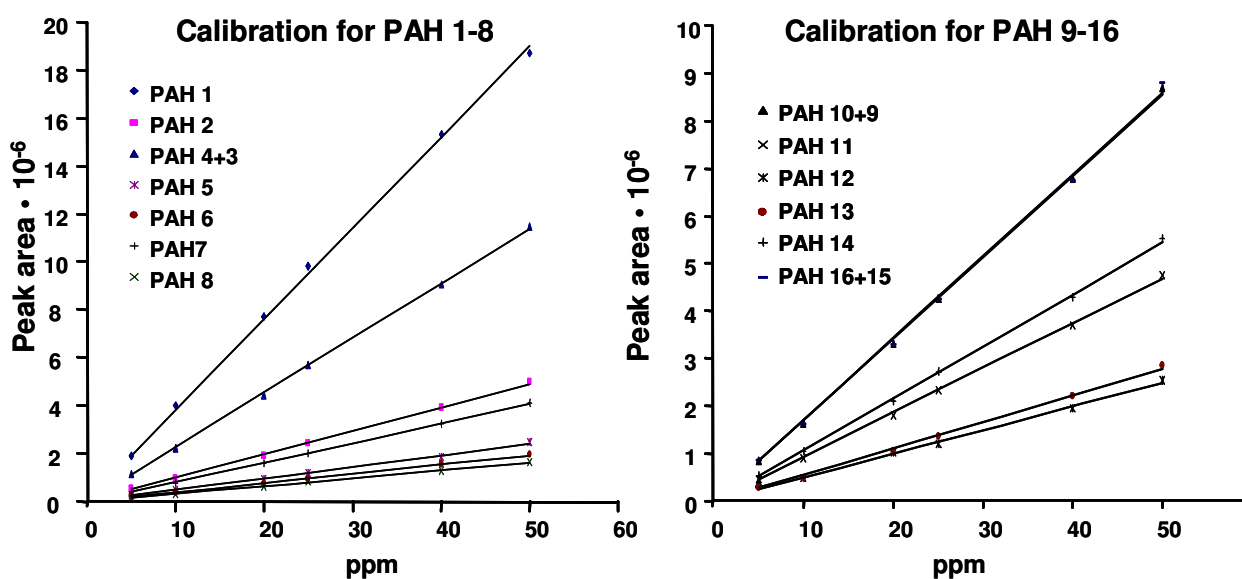


Figure 6.5: PAH calibration curves for peak areas.

6.3.1.4 Extraction Procedure for Asphalts Containing Tar

The raw sample of road asphalt containing tar was extracted by two different methods. The first extraction method was the Soxhlet technique using 2 mL CH_2Cl_2 per g sample. This method was applied to the coarse and powdered samples. From the extraction procedure on the fine, powdered the sample Soxhlet aliquots of 10 mL were taken after 4 h and after 8 h. The extraction was terminated after 24 h. From the coarse sample a 10 mL aliquot was taken after 4 h and the extraction was also terminated after 24 h. The extracts were subjected to a clean-up procedure described in the following paragraph. The other extraction method was a cold extraction. This extraction was carried out with dichloromethane in a closed vessel stored for 24 h in a refrigerator. This extraction method was used by a laboratory for road authority in Luxemburg.

6.3.1.5 Sample Preparation for HPLC

It is obvious that the dark brownish CH_2Cl_2 extracts from Soxhlet contain high amounts of resin-like substances acting as the effective binder in the asphalt. When the CH_2Cl_2 volume was decreased from 10 mL to 3 mL by evaporation, an almost black resin-like residue was obtained, which could not be dissolved or not even be wetted by methanol (reason and context in following paragraph). To separate the PAH from this matrix and to obtain an HPLC compatible sample, a column liquid chromatography on bare silica was carried out. 0.5 g of silica (Impaq, 20 μm , DuPont) was filled into a modified Pasteur pipette (the long narrow tip was cut off to reduce the dead volume) and the silica bed was retained with glass wool at both ends. This column was rinsed with 5 mL CH_2Cl_2 to clean the silica from impurities. 1 mL CH_2Cl_2 extract was poured onto this column. The PAH fraction was eluted with further CH_2Cl_2 until the effluent became clear or slightly yellow (approx. 5 mL required).

It is not possible to inject a CH_2Cl_2 solution directly onto a C18 reversed phase HPLC column. Due to the strong elution power of this solvent on reversed phases, tremendous peak distortion and shift of retention times would occur. Hence, a transfer to a RP-HPLC compatible solvent like methanol was mandatory. Therefore, the 5 mL CH_2Cl_2 effluent was reduced to 1 mL in a Rotavapor at 550 mbar and ambient temperature. To this concentrate, methanol was added to a volume of

10 mL. The solution became turbid and suspension-like. Then the residual CH_2Cl_2 was evaporated from this solution by rotating it again under 200 mbar to a volume of approx. 7 mL. The resulting solution was exactly filled up to 10 mL with methanol, filtered through a 0.45 μm hydrophilic PTFE membrane filter and directly injected into the HPLC. 1 mg/L PAH concentration in this solution corresponds to 20 mg PAH in 1 kg asphalt containing tar (neglecting the incomplete recovery).

6.3.1.6 Recovery of the Sample

For the recovery studies, a 10 ppm solution in CH_2Cl_2 diluted from the Supelco mixture was applied. For PAH 5 and 12, an individual 10 ppm solution was prepared. These solutions were subjected 3 times to the described evaporation procedure for the solvent change from CH_2Cl_2 to methanol, as well as to the complete sample preparation procedure (silica fractionation). The peak areas measured from the direct dilution of the 2000 ppm mixture were taken as reference values. Those peak areas measured after transferring the 10 ppm solution to methanol, or after applying the silica chromatography with subsequent transfer to methanol, were taken to calculate a recovery for the procedure. The precision determined from the obtained results was not very satisfying, since the relative standard deviation was up to 25 % (varying for individual compounds). For both the solvent change and the complete procedure, the second attempt yielded the most plausible and consistent recovery values. The recovery rates for the individual PAHs and the non-resolved peak pairs are given in Table 6.1. For calculating the PAH contents in the real samples, the recovery rates of the right column in Table 6.1 were taken into account.

Table 6.1: Recovery of the reconstitution in methanol after CH₂Cl₂ evaporation and of the column chromatography clean-up with subsequent solvent transfer.

PAH	Recovery of solvent change	Recovery of complete procedure
PAH 1	86 %	81 %
PAH 2	95 %	94 %
PAH 4+3	94 %	94 %
PAH 5	99 %	99 %
PAH 6	89 %	90 %
PAH 7	95 %	95 %
PAH 8	95 %	97 %
PAH 10	91 %	93 %
PAH 9	93 %	91 %
PAH 11	94 %	94 %
PAH 12	95 %	94 %
PAH 13	99 %	99 %
PAH 14	94 %	93 %
PAH 16+15	95 %	95 %

6.3.1.7 HPLC Analysis of the Sample for PAH Content

When real asphalt sample extracts are injected, in spite of the foregoing clean-up procedure, it is mandatory to use a pre-column to protect the separation column. The complete sample preparation method was applied to different Soxhlet extracts from the aliquots (powder and coarse) of the sample.

Figure 6.6 shows the chromatogram obtained from the 4 h extract of the sample milled to a fine powder. The method was applied to the Soxhlet extract of the powder and the coarse sample as well as to the CH₂Cl₂ cold extract. The non resolved peaks of PAH 3, 4, 9, 10 and 14, 16 were quantified as approximate sum content by using the averaged calibration function of both compounds. For these three samples, the PAH concentrations are given in Table 6.2. A possible small peak of acenaphthylene would be overlaid by another co-eluting substance that could be clearly distinguished by the UV spectrum. Therefore this could not be determined. However, it could be present at the lower or sub ppm level.

When the extracted amounts between the fine and the coarse sample are compared, it becomes obvious that by 18 % more PAH could be extracted from the powder sample, a trend that was to be expected. The PAH pattern of both sample forms was similar, but not identical.

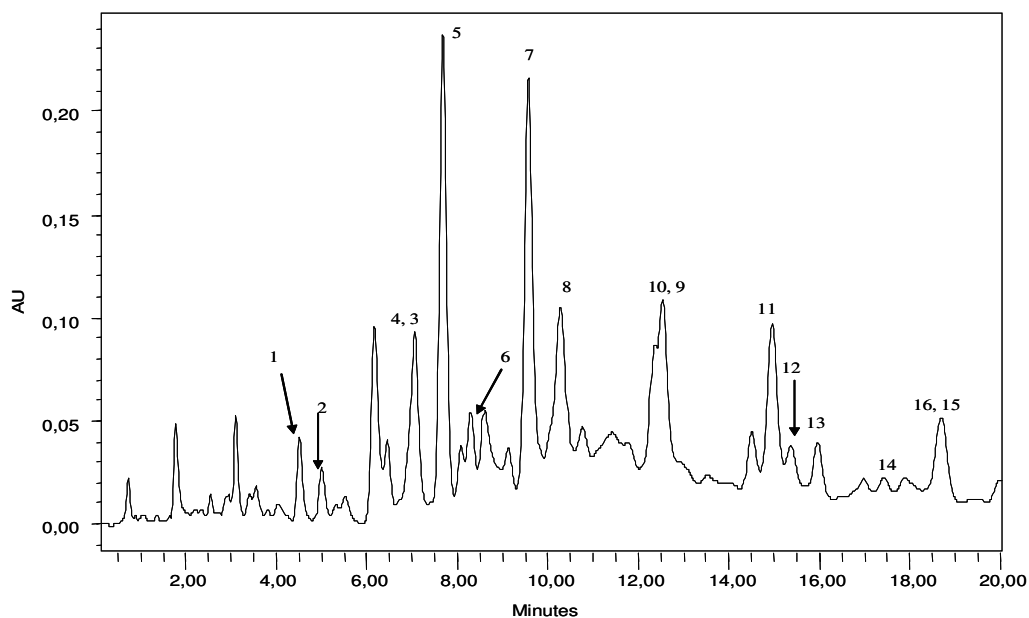


Figure 6.6: Analysis of powder sample after 4 h extraction on Nucleodur C18 Gravity, detection at 220 nm.

Table 6.2: PAH amounts in the sample (in mg/kg solid material).

Compound	4 h Soxhlet extract from powder	4 h Soxhlet extract from coarse sample	Cold extract
PAH 1	25	29	14
PAH 2	not found	not found	not found
PAH 4,3	128	129	71
PAH 5	1088	1107	611
PAH 6	341	309	169
PAH 7	730	624	334
PAH 8	1314	932	455
PAH 10,9	414	248	111
PAH 11	310	286	164
PAH 12	164	145	86
PAH 13	141	134	75
PAH 14	40	41	22
PAH 16+15	100	92	52
Sum of all	4794	4075	2164

6.3.1.8 Comparison of the Powder and Coarse Sample Extraction Kinetics

Both forms of the sample were extracted for 24 h and aliquots after 4 and 8 h were taken. For the sake of clarity, only the sum contents of the PAHs analyzed in the extracts after different Soxhlet extraction times are presented in Figure 6.7. It can be deduced that the sum amount decreased with increasing extraction time. The reason is a drop of the concentration of the higher PAHs which might be due to a thermal decomposition or any kind of conversion of these compounds. This effect might be an essential disadvantage of the Soxhlet technique, were the analytes are subjected to the boiling dichlormethane (40 °C) for several hours or even to higher temperatures when dried out at the inner glass surface above the solvent level in close contact to the heating device.

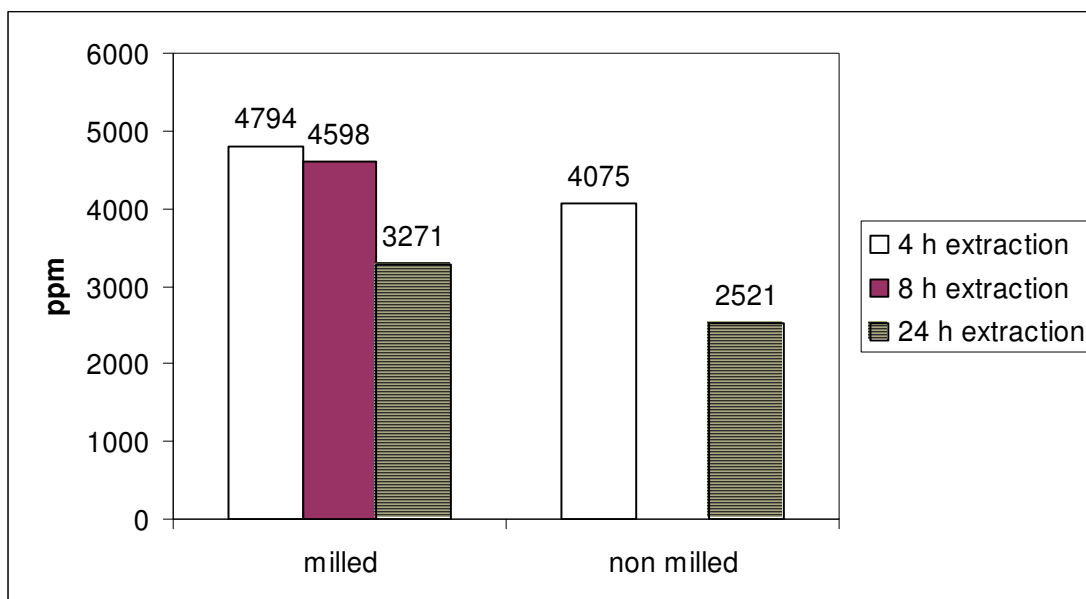


Figure 6.7: Sum amount of PAH in the fine and the coarse the sample after different times of Soxhlet extraction.

6.3.1.9 Optimization of Detection Wavelength for HPLC Analysis of PAHs

It is obvious that the UV detection at 220 nm is a non-selective detection, especially in presence of a very complex matrix. Hence, it was evaluated whether wavelength optimization in UV detection enables a more selective detection and thus more accurate analysis results. Figure 6.8 illustrates a detection optimization approach for the example of the poorly resolved peaks from the PAHs chrysene (11.42 min) and benzo[a]anthracene (11.62 min). Besides the use of a selective wavelength, a calibration via peak heights should be less sensitive to matrix bias than peak area calibration, since it is more likely that the peak edges incorporate significantly contributing impurities than this is the case for the peak apex.

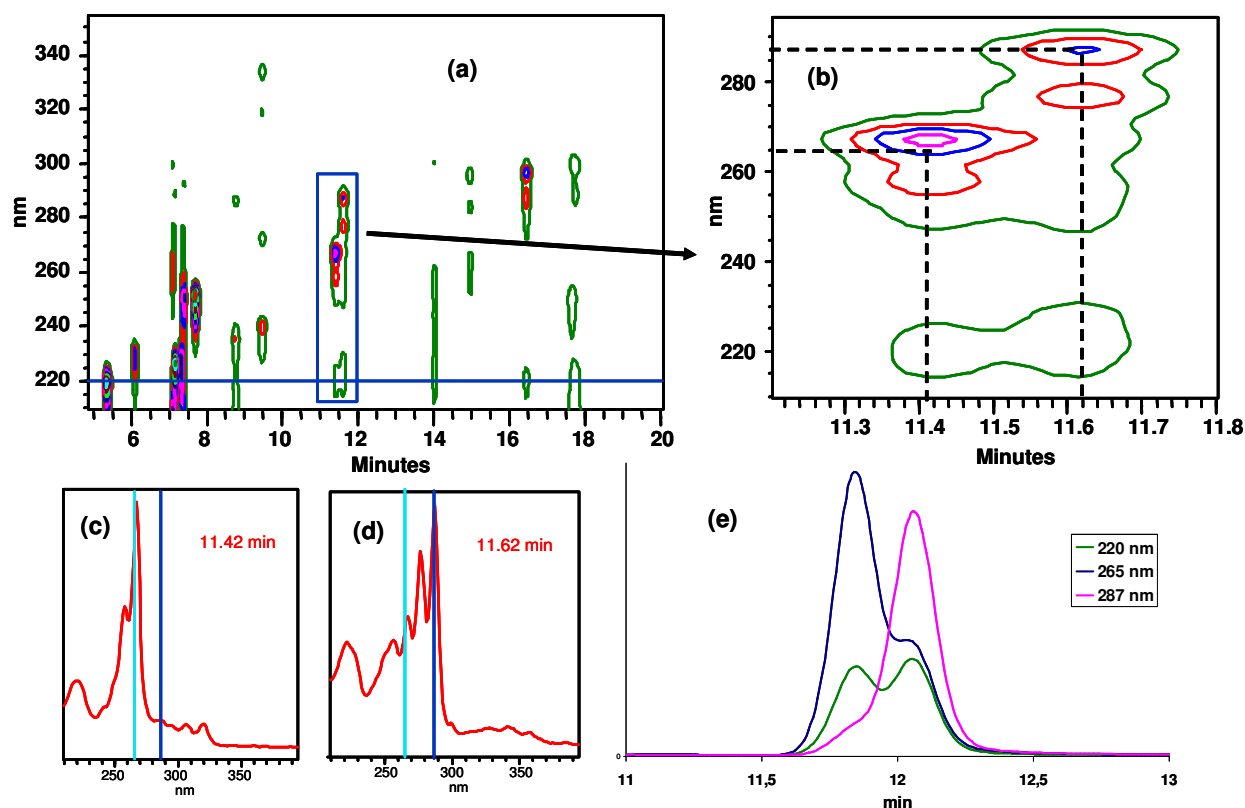


Figure 6.8: UV photodiode array contour chromatogram of PAH separation (a) (b) and UV peak spectra of chrysene and benzo[a]anthracene (c) (d). The chromatogram overlay (e) compares the non-selective detection at 220 nm, chrysene selective detection at 265 nm and benzo[a]anthracene selective detection at 287 nm.

The calibration data from 3-dimensional chromatograms were re-calculated for peak heights with optimized detection wavelengths and the PAH quantification in the sample was corrected based on these calibration curves. Optimal detection wavelengths for the 16 compounds are given Table 6.3.

Table 6.3: Detection wavelengths for optimized selectivity in PAH analysis.

PAH	UV detection wavelength [nm]
Naphthalene	220
Acenaphthylene	229
Acenaphthene	227
Fluorene	262
Phenanthrene	252
Anthracene	252
Fluoranthene	235
Pyrene	240
Benzo[a]anthracene	287
Chrysene	265
Benzo[b]fluoranthene	256
Benzo[k]fluoranthene	306
Benzo[a]pyrene	296
Dibenzo[a,h]anthracene	297
Benzo[g,h,i]perylene	209.5
Indeno[1,2,3-cd]pyrene	245.5

Using the selective detection wavelengths for PAH (given in Table 6.3) and calibrating the method via peaks heights instead of peak areas, the HPLC analysis results of the fine sample by 4 h Soxhlet extraction were recalculated. The obtained PAH concentrations are summarized in Table 6.4.

Table 6.4: Concentration of PAHs quantified by selective detection results in the sample. All concentrations in mg/kg in solid sample.

PAH	Concentration in mg/Kg selective detection
Naphthalene	19
Acenaphthylene	-
Acenaphthene	78
Fluorene	104
Phenanthrene	874
Anthracene	164
Fluoranthene	661
Pyrene	436
Benzo[a]anthracene	265
Chrysene	195
Benzo[b]fluoranthene	210
Benzo[k]fluoranthene	226
Benzo[a]pyrene	124
Dibenzo[a,h]anthracene	19
Benzo[g,h,i]perylene	60
Indeno[1,2,3-cd]pyrene	63
Sum of PAHs	3499

To discuss some of these deviations more in detail, Table 6.5 compares results of HPLC at universal detection wavelength and at optimized detection wavelength with the quantitative data obtained with GC-FID and GC-MS for three representative compounds. For fluorene, the difference between peak area and peak height quantification is depicted. Moreover, an optimized detection protocol even enables quantification of compounds with poorly resolved peaks in the chromatogram. The fluorene quantification via peak height and the selective detection of chrysene yielded concentrations close to the values determined with GC-FID. Nevertheless, the HPLC results for benzo[a]anthracene showed that no reliable quantification with HPLC-UV is possible, even with optimized detection.

Table 6.5: Influence of the separation-, detection- and calibration method on quantitative PAH results in the sample. All concentrations in mg/kg solid sample.

PAH	HPLC UV 220 nm peak area	HPLC peak height (λ)	GC-FID	GC-MS
Fluorene	730	673 (220 nm)	648	550
Chrysene (Chr)	-	195 (265 nm)	181	129
Benzo[a]anthracene (BaA)	-	265 (287 nm)	208	136
Chr+BaA	414	470 (265, 287 nm)	389	265

6.3.2 Analysis of Phenols

Small phenols were extracted from the raw sample applying both Soxhlet extraction and sonication. 10 small phenols as depicted in Figure 6.9 should be monitored as representatives of elutable hazardous substances in asphalt containing tar. To separate the weakly acidic phenols from the CH₂Cl₂ extract of the asphalt, either a liquid-liquid extraction into sodium hydroxide solution or solid phase extraction (SPE) was carried out.

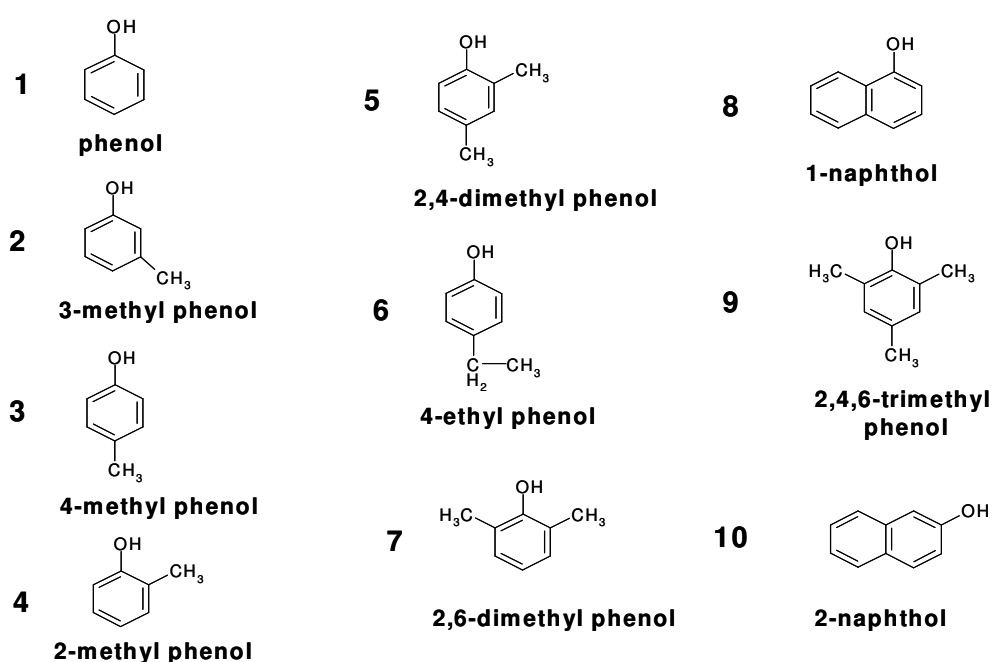


Figure 6.9: Structures of 10 small phenols.

6.3.2.1 Development of the HPLC Method for Phenol Analysis

It was not possible to develop an appropriate method applying the Nucleodur HPLC column, which was used for the PAH analysis. Several available columns were tested with isocratic elution using non buffered eluents of water/methanol or water/acetonitrile and also the addition of 10 mM phosphate buffer at pH 3 was elaborated. A polar embedded C18 Phase ProntoSil C18 ACE EPS 120Å, 3 µm (Bischoff, Leonberg) in a 150 x 4.6 mm column provided the best selectivity and required no buffer addition to obtain excellent peak shapes. However, it was not possible to separate 3- and 4-methylphenol. A pre-column was mounted to protect the separation column from matrix compounds when real samples are injected.

The obtained separation is depicted in Figure 6.10 with a 5 ppm standard of 10 phenols dissolved in methanol. The 150 mm column packed with 3 µm particles provides high separation efficiency, which is mandatory for the complex matrix and the expected low concentration range of the analytes.

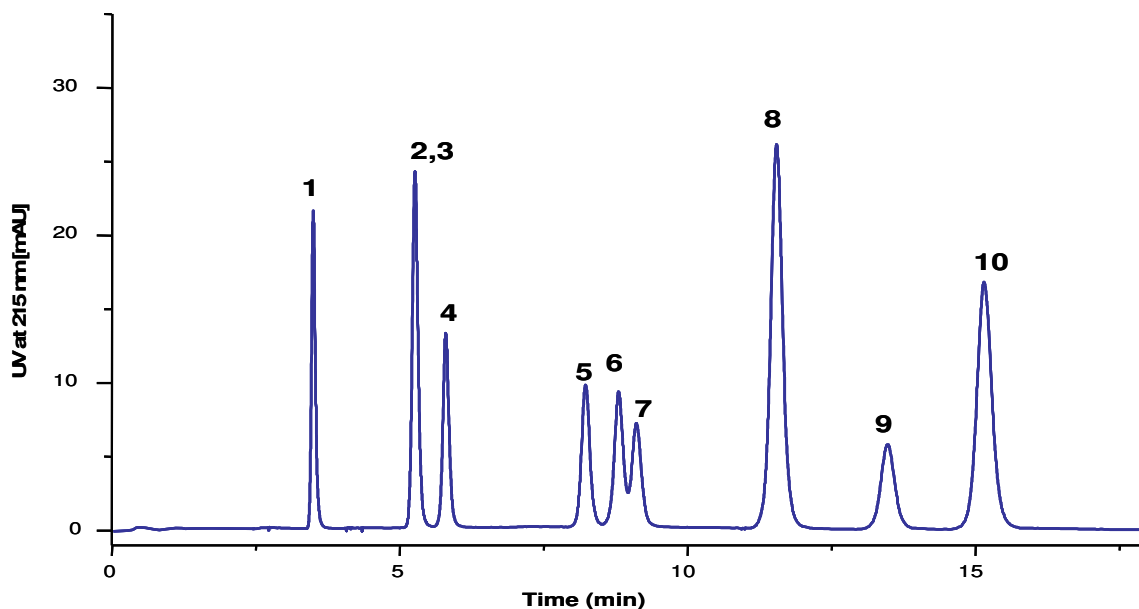


Figure 6.10: PAH separation on ProntoSil C18 ACE EPS 120Å, 3 µm (Bischoff, Leonberg), 150 x 4 mm column), detection at 215 nm, Peaks: 1, phenol; 2, 3-methylphenol; and 3, 4-methylphenol 4, 2-methylphenol; 5, 2,4-dimethylphenol, 6 4-ethylphenol; 7, 2,6-dimethylphenol: 8, 2-naphthol; 9, 2,4,6-trimethylphenol; 10, 1-naphthol, 5 ppm each phenol.

UV peak spectra were recorded with the photodiode array detector. Unlike the PAH UV spectra, they exhibit no pronounced differences between the individual alkyl phenols. However, the spectra were helpful to distinguish phenol or naphthol peaks from other matrix compounds in the real samples. Figure 6.11 shows the UV spectra of the phenols.

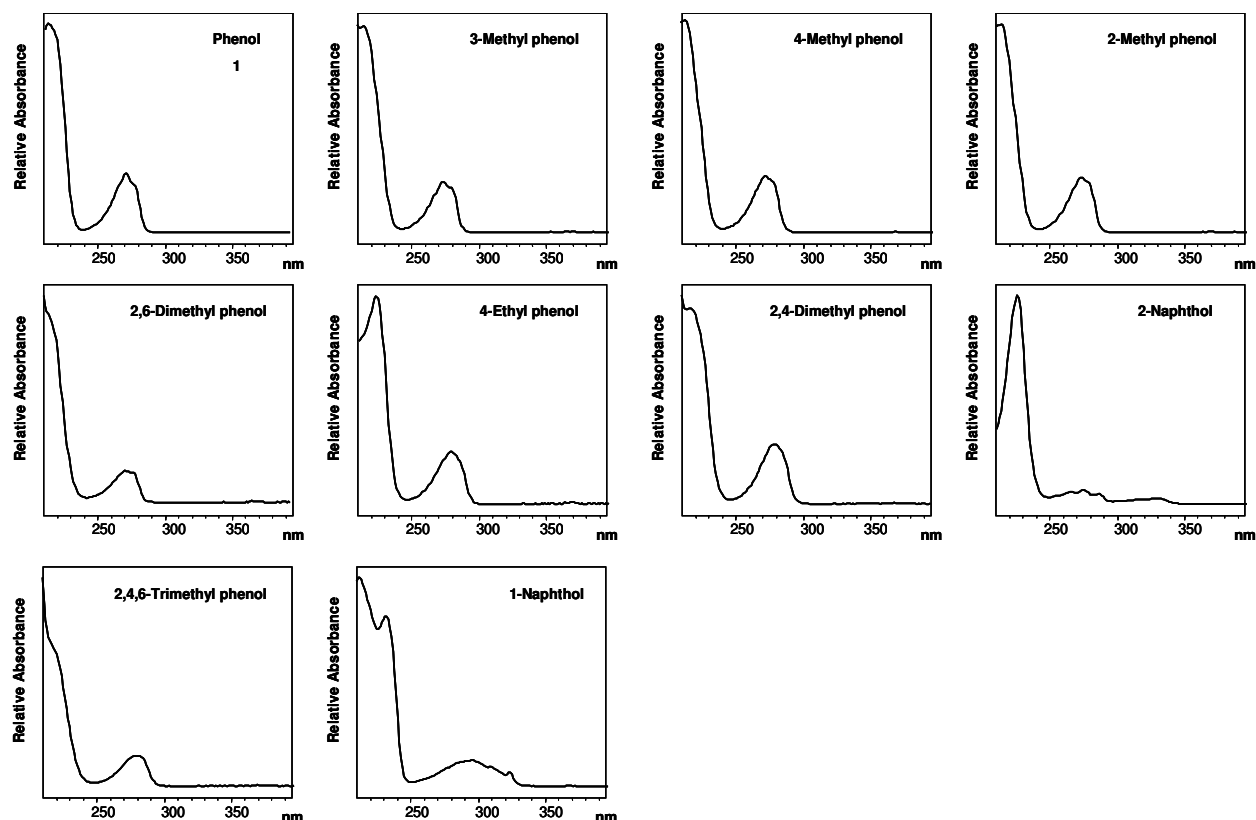


Figure 6.11: UV spectra of the phenols.

6.3.2.2 Calibration for Phenol Analysis

The developed method was calibrated for quantification with external standard solutions. They were prepared as a mixture of 10 phenols dissolved in methanol/water 1/1 (v/v). The concentration range was between 1 and 5 ppm, as the phenol concentrations in the extracts were in the low ppm range and it was not possible to determine sub ppm levels accurately due to matrix influence and precision of the extraction procedure. All calibration curves are given in Figure 6.12.

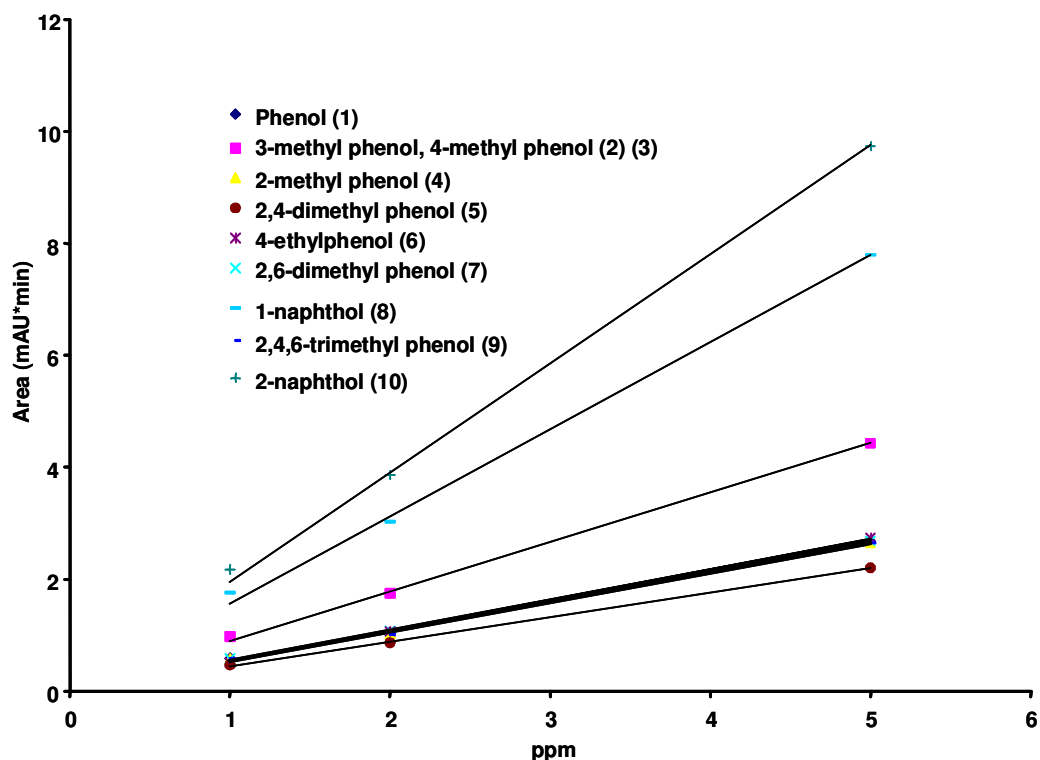


Figure 6.12: Calibration curves for peak areas of phenols.

6.3.2.3 Sample Preparation for Phenols and Recovery Rate of Alkaline Aqueous Extraction from CH_2Cl_2

A liquid-liquid extraction into sodium hydroxide solution was carried out to separate the weakly acidic phenols from the CH_2Cl_2 Soxhlet extract of the asphalt. The alkaline extract was neutralized with HCl solution of factor 10 higher concentration, because strongly basic solutions can damage the silica based HPLC packing. It was verified that the resulting NaCl content in the sample solution (up to 1.8 mol/L) had no impact on the chromatographic separation. The neutralized solution was filtered through a 0.45 μm PTFE membrane filter and 10 μL injected into the HPLC system. The dilution due to the neutralization with HCl was considered in the quantification calculation.

To optimize the pH in the extraction solvent, the recovery rate for the extraction of all 10 phenols at 25 ppm concentration into aqueous NaOH solution of 10 mM, 100 mM, 500 mM, 1000 mM and 2000 mM was determined. To assess the influence of the matrix on the extraction constant, the same experiment was performed with a 25 ppm spiked solution of the 24 h Soxhlet extract of the powder from asphalt containing tar the sample. The 24 h extract was selected, because sufficient volume from the 4 h or

8 h extracts was not available. The spiking was performed by dosing 1000 ppm stock solution of the 10 phenols dissolved in dichloromethane to the extract. Because of the high spiking level of 25 ppm relative to actual phenol content of the sample, this original phenol content was not considered. Regarding the general accuracy of the results, the possible resulting error (<5 %) appears to be justifiable. A chromatogram of the spiked sample is depicted in Figure 6.13.

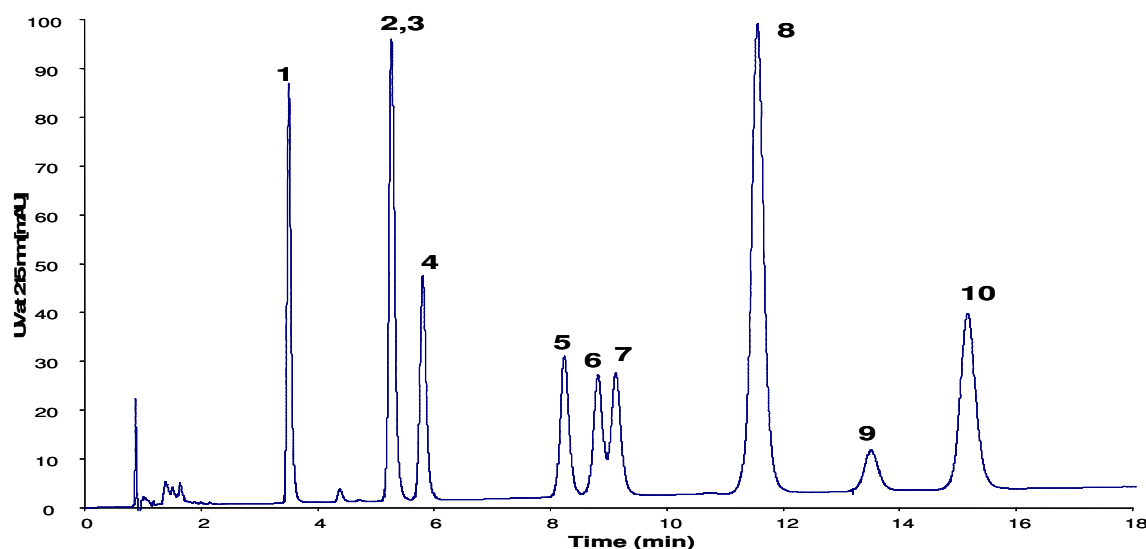


Figure 6.13: Soxhlet extract (24 h) of the sample (powder) spiked with phenols to 25 ppm. For peak identification see Figure 6.9.

Figure 6.14 shows the Influence of the NaOH concentration on the extraction constant expressed as a recovery rate in % for both series. It became obvious that, except for phenol itself, the NaOH content of 100 mM or below was insufficient to obtain a satisfying extraction yield. The reason is the decreased acidity due to the inductive effect of the alkyl groups, besides the poor water solubility of the naphthols. At 500 mM NaOH, appropriate extraction was yielded for all substances except ethyl phenol and trimethyl phenol. An increase to 2000 mM NaOH could not markedly improve the recovery. When both graphs in Figure 6.14 are compared, it becomes obvious that there is a matrix influence on the recovery, which increases with increasing analyte hydrophobicity. It must be considered that the aqueous alkaline extract is taken from the CH_2Cl_2 Soxhlet extract without further purification. This raffinate is a deeply brownish and colloidal broth which contains resinlike substances that can adsorb or occlude the hydrophobic phenols.

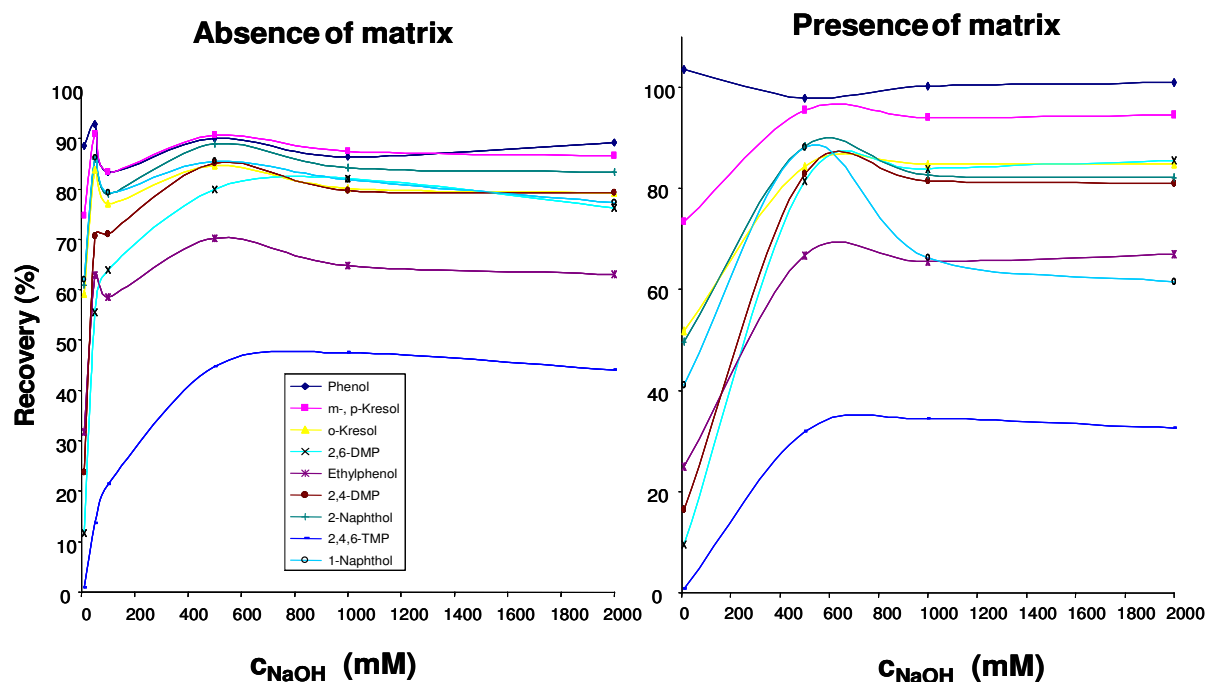


Figure 6.14: Recovery rate for phenols for extraction from CH_2Cl_2 using extraction solvents with different NaOH concentrations.

It was decided to work with the 1000 mM NaOH extracts. Table 6.6 presents the recovery rates calculated from the ratio of the peak areas (extract to methanol-water standard solution) for the extraction from 25 ppm CH_2Cl_2 solutions and from the spiked extracts from the sample (as shown in Figure 6.13). The higher recovery rates of the more hydrophilic phenols in presence of the matrix may be due to a solvophobic effect caused by the apolar matrix compounds.

Table 6.6: Recovery of the 1000 mM NaOH aqueous extraction from CH₂Cl₂ in absence and presence of asphalt matrix at a phenol level of 25 ppm.

Substance	Recovery in absence of matrix	Recovery in presence of matrix
Phenol	86 %	100 %
3-, 4-MP	87 %	94 %
2-MP	80 %	85 %
2,6-DMP	82 %	84 %
4-Ethyl phenol	65 %	67 %
2,4-DMP	80 %	81 %
2-Naphthol	84 %	83 %
2,4,6-TMP	48 %	34 %
1-Naphthol	82 %	66 %

6.3.2.4 HPLC Analysis for Phenol Content

The above described sample preparation method (alkaline extraction, neutralization and filtration) was applied to the 4 h Soxhlet extracts from the finely milled sample. 10 µL of the filtrate were subjected to HPLC analysis following the protocol described above. The obtained chromatogram is shown in Figure 6.15, where the chromatogram of the spiked matrix is added to facilitate peak identification. Figure 6.16 depicts a direct overlay of the UV peak spectra recorded from the standard mixture and from the analysis of the asphalt containing tar sample. Most of the listed phenols could be identified by their spectra in addition to the matching retention times. Even for the very small peak 5 (ethyl phenol), the noisy spectrum was almost unambiguous. However, the noise dominated in the spectra of trimethyl phenol and the 2 naphthols. For the quantification peaks 1 through 9 were treated as identified and pure and the calibration shown in Figure 6.12 was applied. The obtained results (given in Table 6.7) were calculated using the recovery rate that considers the matrix influence (right column in Table 6.6). To calculate the content the solid sample, it must be considered that 1g material was extracted with 2 mL CH₂Cl₂. The subsequent liquid-liquid extraction was carried out with equal volumes of raffinate

and extract in 1 step. The sum amount for all 10 phenols in the asphalt was determined to be around 16 ppm.

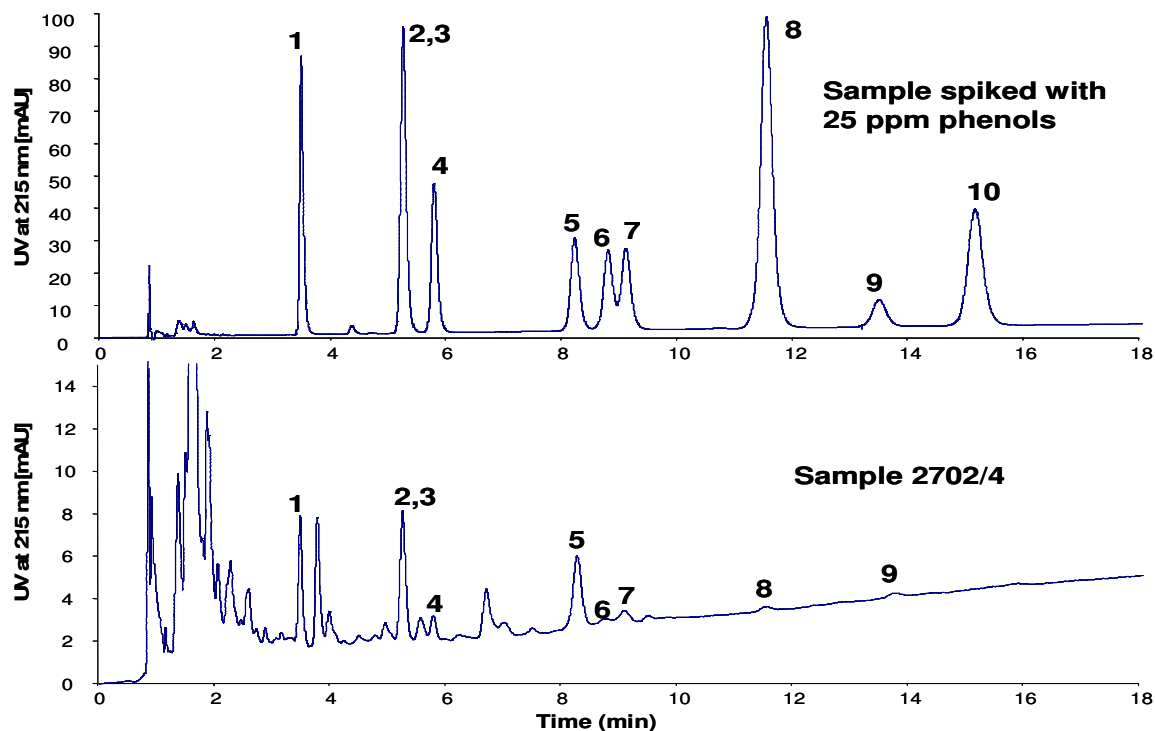


Figure 6.15: Analysis of 2702/4 powder sample after 4 h extraction using the method described in the text. The chromatogram of the 25 ppm spiked matrix is included for comparison.

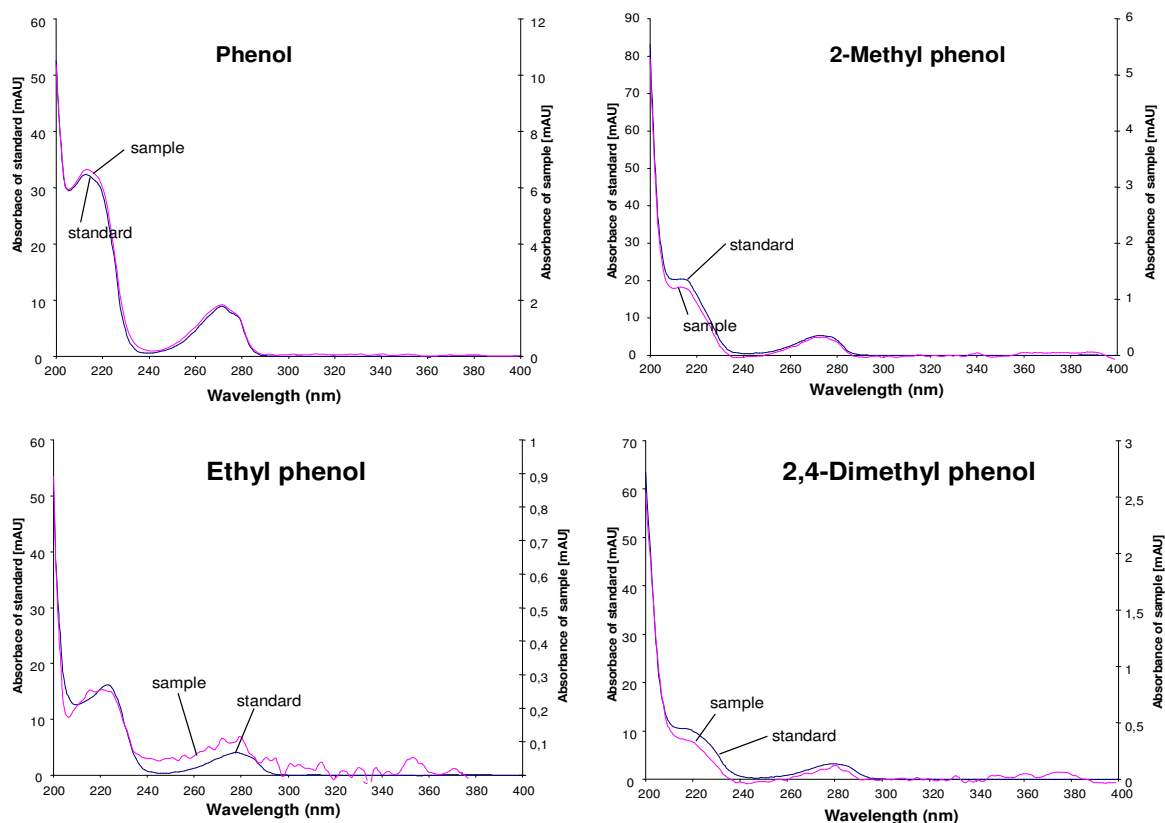


Figure 6.16: Peak UV spectra from analysis of the sample overlaid with spectra recorded from injection of standard.

Table 6.7: concentration of phenols determined with the 4 h Soxhlet extract from the sample (milled powder).

Substance	Concentration in the alcal. aqueous extract in mg/L	Concentration in the solid sample in mg/kg
Phenol	1.9	3.8
3-,4-Methyl phenol	1.6	3.2
2-Methyl phenol	0.5	1.0
2,6-Dimethyl phenol	2.6	5.2
4- Ethyl phenol	0.5	1.0
2,4-Dimethyl phenol	0.5	1.0
2-Naphthol	0.1	0.2
2,4,6-Trimethyl phenol	0.5	1.0
1-Naphthol	not found	not found
Sum of all phenols	8.2	16.4

6.3.2.5 Batch Extraction of the Raw Sample for Phenol Analysis Applying Sonication

The determination of phenol content from the raw sample using three successive batch extraction steps with CH_2Cl_2 under sonication (see details in experimental part) was carried out in order to compare this method with the Soxhlet extraction technique. The coarse and fine materials from the sample were simultaneously extracted by 3 successive steps under sonication. The solid material and supernatant were separated by decantation, since no centrifugation device at appropriate scale is available. Moreover, the remaining minerals were extracted with 1000 mM sodium hydroxide solution under sonication after CH_2Cl_2 extraction and this extract was also analyzed for phenols.

The analysis was carried out by HPLC. However, no phenols could be found neither in the alkaline extract from organic solvents nor in that from the stones (Figure 6.17), since none of the peaks observed in the chromatograms B through D exhibited identifiable UV-spectra. Consequently, the phenols must be still present in the organic phase (CH_2Cl_2), possibly adsorbed to fines from minerals and non-soluble asphaltenes generated under the influence of sonication. These fines are not likely to be present at a similar level when applying the Soxhlet procedure for extraction.

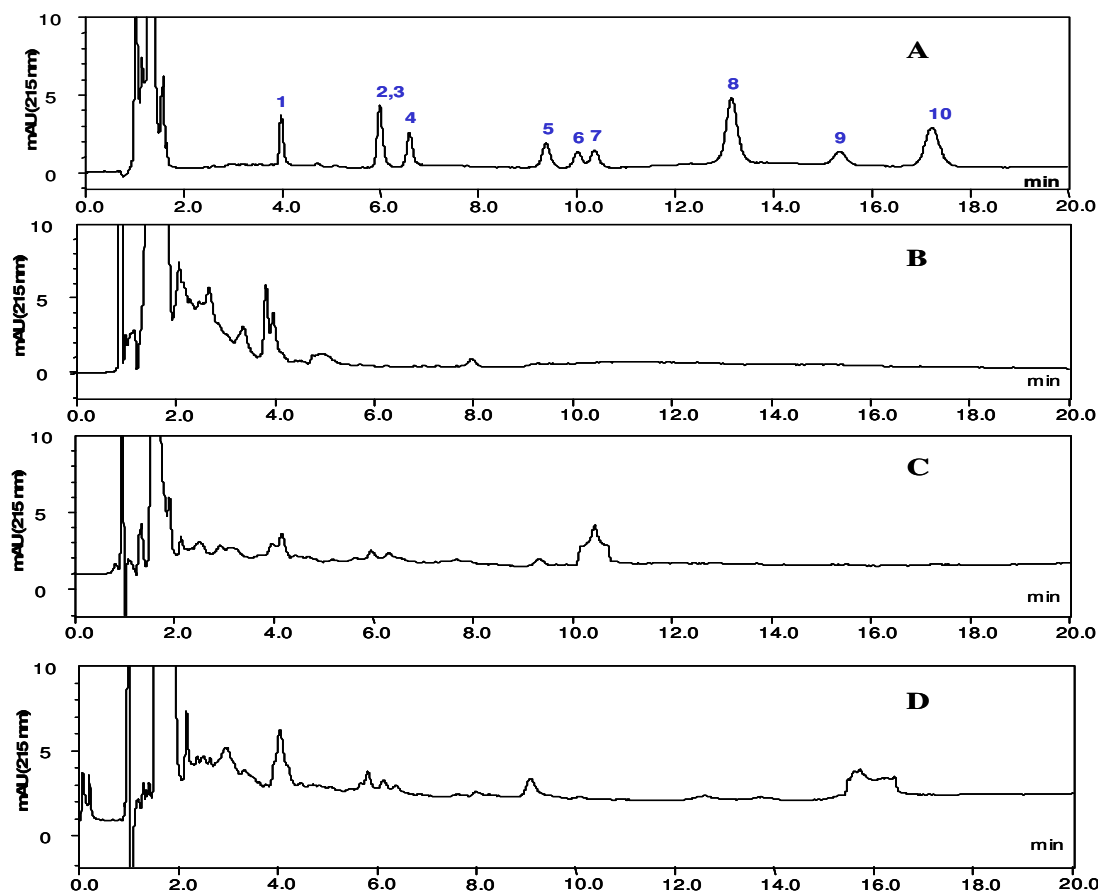


Figure 6.17: Chromatograms of 10 small phenols standard at 5 ppm (A) and alkaline aqueous extract from coarse stones 2702/4 after CH_2Cl_2 batch extraction (B), liquid-liquid extraction from CH_2Cl_2 batch extract of 2702/4 in coarse form (C) and in fine form (D). For peak identification see Figure 6.9.

At this stage of experiments it was obvious that the sonication batch extraction did not yield the same result like the Soxhlet technique. An adherence of phenolates to the stones and suppression of dichloromethane extraction, however, could not be verified. To elucidate the reason behind the ineffective aqueous extraction, further experiments were required.

6.3.2.6 Comparison of Liquid-liquid Extraction into Alkaline Aqueous Solution and SPE Clean-up of CH_2Cl_2 Extracts for Sample Preparation Prior to Phenol Analysis

It was discussed in the last section, that applying sonication batch extraction with CH_2Cl_2 , no phenols could be found after liquid-liquid extraction in the alkaline solution. Hence, the next task was to analyze the phenols in the CH_2Cl_2 extract.

Therefore this extract was cleaned by solid phase extraction (SPE) on a silica cartridge (see experimental part), since the percolation through a Pasteur pipette packed with the 20 μm silica was extremely slow when the sonicated extracts were applied. This observation already indicates a consistency different from that of the Soxhlet extracts. The cartridge was eluted with CH_2Cl_2 (5 times the sample loading volume). Then, the effluent was concentrated and the solutes transferred to methanol following the protocol developed for PAH analysis. Using this sample preparation, only 4 phenols at an approximate concentration of 1 ppm each were determined (Figure 6.18). Comparing the chromatograms in Figure 6.18 with those in Figure 6.17 C and D, it is obvious that numerous compounds of similar polarity like the selected phenols are present in the CH_2Cl_2 batch extract, which are not extractable into the alkaline solution with liquid-liquid extraction. These matrix compounds markedly biased the analysis of the phenols.

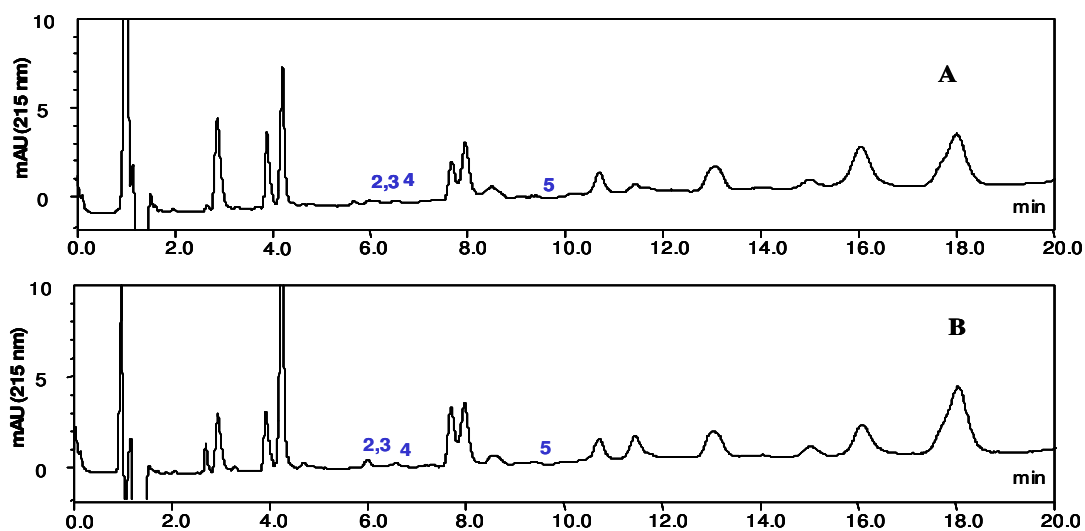


Figure 6.18: Chromatograms of CH_2Cl_2 extract of coarse (A) and fine (B) raw sample with SPE.

The possible reason why no equivalent amount of phenols compared to Soxhlet extraction could be found, could be again the impact of a differing matrix effect under influence of sonication, which obviously leads to fines from the original asphalt sample. The higher yield from the CH_2Cl_2 phase cleaned by SPE on silica relative to the liquid-liquid extraction sample preparation approach must be due to a more efficient phenol leaching from the fines under the percolation in the SPE-cartridge relative to single equilibrium step in the liquid-liquid system. Unfortunately, other disturbing matrix compounds were also leached from the SPE cartridge.

6.3.2.7 Phenol Analysis from Cold Batch Extraction on the Sample

To complete the characterization of the different extraction processes performed with the raw asphalt sample, a phenol determination was carried with the asphalt cold extract. The extraction was carried out with dichloromethane in a closed vessel stored for 24 h in a refrigerator. With this sample, significantly lower PAH extraction yields were already encountered.

The resulting phenol contents analyzed from this extract are listed in Table 6.8. The chromatogram is shown in Figure 6.19. Although the pattern resembles that obtained from the Soxhlet extract, the resulting concentrations were only at a 30% level relative to the exhaustive extraction technique. This result goes along with that obtained for the PAH analysis from the same extract. For both the PAHs and phenol, the cold batch extraction of asphalt with dichloromethane does not yield a representative extract for analysis.

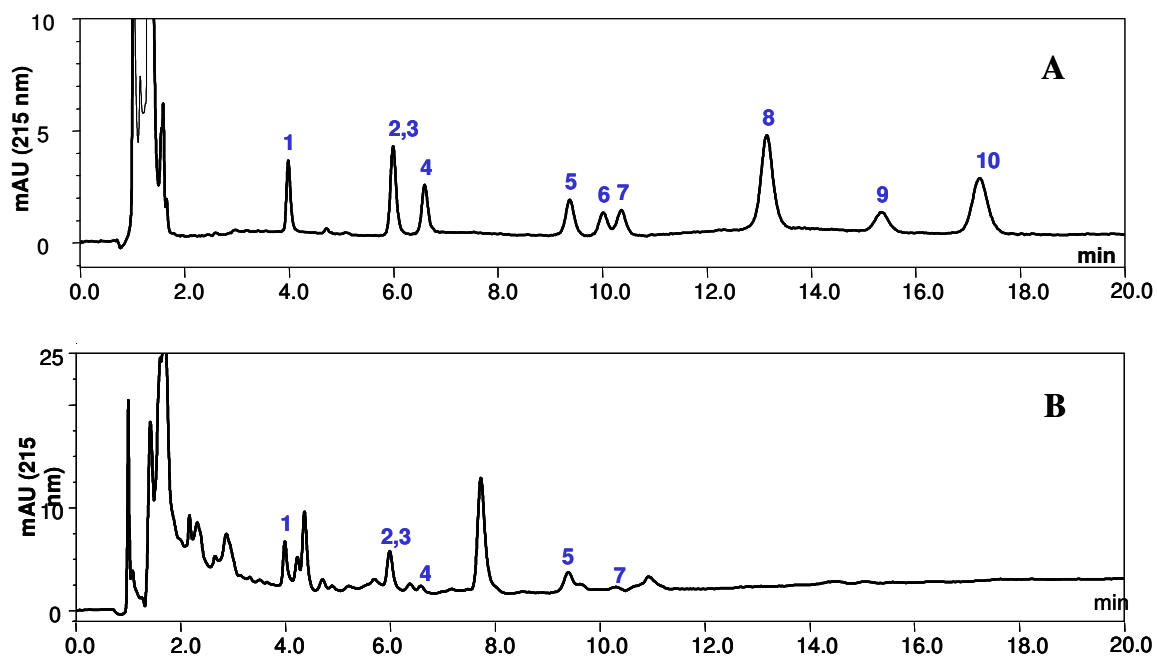


Figure 6.19: Chromatogram of standards with each 1 ppm phenols (A) and phenols from cold extraction (B).

Table 6.8: Phenol content from the cold extraction.

Substance	Concentration in the solid sample in mg/kg
Phenol	1.7
3-,4-Methyl phenol	1.0
2-Methyl phenol	0.2
2,6-Dimethyl phenol	1.1
4- Ethyl phenol	-
2,4-Dimethyl phenol	0.5
2-Naphthol	-
2,4,6-Trimethyl phenol	-
1-Naphthol	-
Sum of all phenols	4.5

6.4 Conclusions

Two individual HPLC methods with photodiode array detection and individual foregoing sample preparation procedures aligned to the demands of the present matrix were developed for the analysis of small phenols and polycyclic aromatic hydrocarbons (PAHs) in tar asphalt samples. For the PAH separation, gradient HPLC was required, whilst the phenol separation could be performed isocratically.

The extraction of PAHs and phenols were performed with CH_2Cl_2 by Soxhlet and by cold extraction. The extraction of the phenols was additionally evaluated for a triple batch extraction under sonication.

Two individual ways of sample preparation were developed for the phenol analysis. One comprised a liquid-liquid extraction from the CH_2Cl_2 extract into alkaline aqueous solution at $\text{pH}=13.0$, the other pursued a cleaning up of the CH_2Cl_2 extract by liquid chromatography on silica followed by a transfer to a methanol solution to inject into reversed phase HPLC. The sample preparation for the analysis of PAHs was carried out in a similar way by liquid chromatography on silica.

The developed analysis methods were applied to the coarsely and a finely milled aliquots of the sample. From the coarse sample, lower amounts of PAHs could be extracted and analyzed under the same conditions, which can rather be attributed to non representative aliquotation of the coarse sample than to less exhaustive extraction.

The phenol analysis resulted in a total content of small phenols at approx. 17 ppm, individual phenol concentrations were approx. 2 ppm. The Soxhlet CH_2Cl_2 extraction with following alkaline aqueous extraction turned out to be the preferred way. With both the sonication batch extraction and the sample preparation via chromatographic clean-up of the CH_2Cl_2 extract, problems were encountered. No significant differences in the determined phenol content were observed between the coarse sample and the milled sample.

References

- [1] Glet, W. (1992) Considerations relating to hazardous emissions from bitumen, asphalt, and older road construction materials. *Gefahrstoffe – Reinhalt. Luft*, **58**, 397-405.
- [2] Deutsches Institut für Normung e.V. (1983) Bitumen und Steinkohlenteerpech – Begriffe für Bitumen und Zubereitungen aus Bitumen. *DIN 55946-1 (Teil 1)*.
- [3] Deutsches Institut für Normung e.V. (1983) Bitumen und Steinkohlenteerpech – Begriffe für Steinkohlenteerpech und Zubereitungen aus Steinkohlenteer-Spezialpech. *DIN 55946-2 (Teil 2)*.
- [4] European Committee for Standardisation. (2000) Terminology and classification of coal tar and pitch based binders and related products. *EN 13847*.
- [5] Environmental Protection Agency (USA). (1992) Test method: Polynuclear Aromatic Hydrocarbons, Method 610.

Appendix

Chromeleon program for fractionation of TDS Sample

```
;PROGRAM TDS
  Log ComputerName
  Log LampIntensity

;Pump settings
  Pressure.LowerLimit = 5
  Pressure.UpperLimit = 120
  %A.Equate = "water + 0.02% TFA+5% ACN"
  %B.Equate = "100% ACN + 0.02% TFA"

;Sampler settings
  DispSpeed =                20
  DrawSpeed =                 20
  SampleHeight =             0.50
  SyringeDelay =              5
  UpSpeed =                   5.00
  DownSpeed =                 5.00
  RadialSpeed =               20.00

;Definition of MS channels and of the filter index
;for the channels MS_01 to MS_03. NOTE: programmed for M + 1 !

  Smoothing = Gaussian
  SmoothingPoints = 9

  MS_01.MinMass = 217.0+0.5
  MS_01.MaxMass = 217.0+1.5
  MS_01.FilterIndex = 1

  MS_02.MinMass = 331.0+0.5
  MS_02.MaxMass = 331.0+1.5
  MS_02.FilterIndex = 1

  MS_03.MinMass = 290.0+0.5
  MS_03.MaxMass = 290.0+1.5
  MS_03.FilterIndex = 1

;*****
;* Definition of triggers for fraction collection starts here.
;*****

  Trigger FracStart                FracStartDetected
  Valve                               = On
  EndTrigger

  Trigger TubeChange                FracTubeChange
  Valve =                             Off
  Tube =                               Tube + 1
  Valve                               = On
```

```

EndTrigger

Trigger FracEnd                               FracEndDetected
Valve                                           = Off
Tube =                                          Tube + 1
EndTrigger

;*****
;Definition of triggers for fraction collection ends here.
;*****

;Basic fraction collection parameters
CollectFractions =                            Yes
CollectOutsidePeaks =                         No
PumpDevice =                                   "Pump"
TubeMaxVolume =                               7.00
TotalNumberInstalled =                       144
MaxTubesPerFraction =                        Unlimited
TubeWrapping =                               No
DelayVolume =                                 1275
ChannelEvaluation =                           All

;Conditions for online peak recognition at program start:
DetectionChannel1.Name =                      "MS_01"
DetectionChannel1.PeakStartSlope =                               Off
DetectionChannel1.PeakEndSlope =              Off
DetectionChannel1.PeakStartThreshold =250000.00
DetectionChannel1.PeakEndThreshold = 150000.00
DetectionChannel1.ThresholdNoPeakEnd = 700000.00
DetectionChannel1.ThresholdDoNotResolve = 400000.00
DetectionChannel2.Name =                      "UV_Vis_1"
DetectionChannel2.PeakStartSlope =            3
DetectionChannel2.PeakEndSlope =              -2
DetectionChannel2.PeakStartThreshold =        4
DetectionChannel2.PeakEndThreshold =          2
DetectionChannel2.ThresholdNoPeakEnd =        50.00
DetectionChannel2.ThresholdDoNotResolve =     20.00
UV_VIS_1.Wavelength =                         205
UV_VIS_1.Bandwidth =                          1
UV_VIS_1.RefWavelength =                      600
UV_VIS_1.RefBandwidth =                      1
UV_VIS_1.Step =                              Auto
UV_VIS_1.Average =                           On

3DFIELD.RefWavelength =                      600.0
3DFIELD.RefBandwidth =                       1.9
3DFIELD.Step =                               0.5
3DFIELD.MinWavelength =                     200.0
3DFIELD.MaxWavelength =                     400.0
3DFIELD.BunchWidth =                        1.9

0.000 Flow =                                5.700 [ml/min]
      %B =                                  7.5 [%]
      AuxFlow =                             0.20 [mL/min]
      Autozero
      Wait Sampler.Ready and MS.Ready

```

```
Inject
UV_VIS_1.AcqOn
Pump_Pressure.AcqOn
3DFIELD.AcqOn
MS_01.AcqOn
MS_02.AcqOn
MS_03.AcqOn
5.000 %B = 7.5 [%]
7.200 DetectionChannel1.Name = "MS_02"
9.000 DetectionChannel1.Name = "MS_03"
AuxFlow = 0.30 [mL/min]

11.000 AuxFlow = 0.20 [mL/min]
12.000 %B = 19.0 [%]
13.500 %B = 50.0 [%]
14.500 %B = 7.5 [%]
19.000 UV_VIS_1.AcqOff
Pump_Pressure.AcqOff
3DFIELD.AcqOff
MS_01.AcqOff
MS_02.AcqOff
MS_03.AcqOff
Flow = 5.700 [ml/min]
%B = 7.5 [%]
19.100 End
```